Nonlinear Low Frequency Wave Phenomena in Space Plasmas

by

Rufai Odutayo Raji

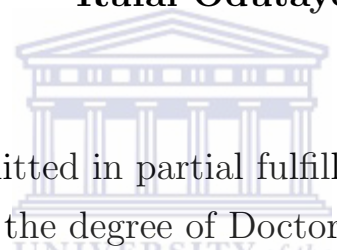

A thesis submitted in partial fulfillment of the requirements
for the degree of Doctor of Philosophy
in the
Department of Physics,
University of the Western Cape, Cape Town, South Africa.

Supervisor: **Prof. R. Bharuthram**
(University of the Western Cape)
Co-supervisors: **Prof. S. V. Singh,**
Prof. G. S. Lakhina
(*Indian Institute of Geomagnetism, Mumbai, India*)

November, 2013

Abstract

Space is endowed with a rich variety of electrodynamic phenomena. Much of known matter in the universe exists as plasmas. Plasmas occur naturally, predominantly occupy the Sun, Stars, Auroras and Interstellar space. The solar wind is a stream of energized, charged particles (i.e., electrons and protons, along with few heavier ions), flowing outward from the Sun, through the solar system at a very high speed and temperature. Once the solar wind has blown into space, the particles travel all the way past planet Pluto and do not slow down until they reach the termination shock within the heliosphere. Because of the author's interest in space electrodynamics phenomena, the focus of this thesis is " Nonlinear low frequency wave phenomena in space plasmas".

The fact that the space environment hosts nonlinear wave phenomena has attracted many researchers. Soliton formation and propagation is one of the most interesting nonlinear structures in space plasmas. S3-3, Viking, POLAR, FAST, FREJA, WIND, CLUSTER and GEOTAIL satellite observations have clearly indicated that solitary wave structures are frequently observed in different regions of the Earth's magnetosphere, e.g. the auroral acceleration region, the plasma sheet boundary layer (PSBL), the bow shock, the magnetopause and on cusp field lines, the Polar cap boundary layer, the auroral kilometric radiation (AKR) source region, the magnetosheath and Earth's foreshock region. Various theoretical models have been developed to describe the observed solitary wave structures at different regions of the Earth's magnetosphere.

In this thesis, using multispecies fluid plasma models, nonlinear electrostatic solitary wave fluctuations will be investigated in magnetized plasmas. The different models used for the investigation will be guided by the satellite observations in different regions of the Earth magnetosphere. These investigations will enable us to attempt theoretical explanations for the nonlinear potential structures observed in the satel-

lite data. Multispecies plasma consisting of cool and hot electrons with Maxwellian distributions and fluid ions will be considered to study low frequency solitons. The ions will be considered as magnetized. The study will be extended to include magnetized oxygen ions. The model will be modified for regions of the magnetosphere consisting of two ions having Maxwellian distributions and magnetized electrons. The nonthermal distributions of energetic hot electrons and the Maxwellian distributions of cool electrons with magnetized cold ions fluid will also be considered. For all the models, the effect of ion and electron densities, temperatures, magnetic field strenght and propagation angle will be studied during the investigation of soliton structures. In all the above mentioned studies, arbitrary amplitude theory is carried out by the Sagdeev pseudo-potential method. Further investigations on the charateristics and existence domains of the solitons is found both analytically and numerically, using satellite data where applicable.

Declaration

I declare that the thesis *Nonlinear low frequency wave phenomena in space plasmas* is my own work, and that it has not been submitted for any degree or examination at this or any other university. All the sources I have used or quoted have been indicated and duly acknowledged as complete references.

Rufai Odutayo. R November 2013

Signed.....

Acknowledgments

In the name of Allah, the Beneficent and the Merciful. I would like to express my sincere appreciation and gratitude to the following people, departments and institutions, without whose involvement this work would not been possible.

- My supervisor, Prof. Ramesh Bharuthram for his expert guidance, fatherly advice and encouragement.
- My co-supervisors, Prof. S. V Singh and Prof. G. S Lakhina of the Indian Institute of Geomagnetism, Mumbai, India for their contributions to the collaborative work.
- Mrs Gasfa Davids and Dr. Vanessa Brown of the Deputy Vice Chancellors: academic's, University of the Western Cape.
- The Division of Postgraduate Studies, University of the Western Cape.
- South Africa National Space Agency (SANSA).
- Dr. S. K Maharaj and Research students of the South Africa National Space Agency (SANSA).
- Lagos State University, Ojo, Lagos, Nigeria, and the entire staff member of the Department of Mathematics .
- Special thanks to Prof. E. Mwambene, Prof. P. Witbooi and all members of the Department of Mathematics and Applied Mathematics, University of the Western Cape.
- The Department of Physics, University of the Western Cape.
- All my teachers, Mallams, Lecturers and Professors.

- Muslim Dua (Prayer) Forum, Cape Town, South Africa.
- Nigerian Community, University of the Western Cape, South Africa.
- Friends and Well-wishers.
- My entire family for their untiring encouragement, support and understanding throughout the challenging period of my study.

Above all, I am deeply grateful to Almighty Allah, Al-Rahman, Al-Roheem, Robuli-Alamin, may his blessing continue to be upon the prophet of Islam, Mohammed (S.A.W), his household and followers. May his mercy and guidance be upon me, my family and those who assisted in achieving my dream (Ameen).

List of included papers

This thesis is based on the following papers:

(i) Rufai, O. R., Bharuthram, R., Singh, S. V., and Lakhina, G. S.,
Low frequency solitons and double layers in a magnetized plasma with two temperature electrons, *Physics of Plasmas*, **19**, 122308, 2012.
http://dx.doi.org/10.1063/1.4771574.

(ii) Rufai, O. R., Bharuthram, R., Singh, S. V., and Lakhina, G. S.,
Effect of hot ion temperature on obliquely propagating ion-acoustic solitons and double layers in an auroral plasma, *Comm. Nonlin. Sci. Numer. Simulat.*, **19**, 1338-1346, 2014. http://dx.doi.org/10.1016/j.cnsns.2013.09.024.

(iii) Rufai, O. R., Bharuthram, R., Singh, S. V., and Lakhina, G. S.,
Ion-acoustic solitons and double layers in a magnetized plasma with nonthermal hot electrons and Boltzmann cool electrons (Submitted).

(iv) Rufai, O. R., Bharuthram, R., Singh, S. V., and Lakhina, G. S.,
Finite amplitude ion-acoustic solitary waves in a magnetized two ion-species plasma (Manuscript).

(v) Rufai, O. R., Bharuthram, R., Singh, S. V., and Lakhina, G. S.,
Ion-acoustic solitons and double layers in magnetized four-component space plasmas (Manuscript).

Contents

List of Tables

List of Figures

Chapter 1

General introduction

The subject of this thesis is nonlinear low frequency wave phenomena in space plasmas. Plasma is known as the fourth state of matter, which is in the form of an electrified gas with charged particles (i.e. the atoms dissociate into positive/negative ions and negative electrons, such that the overall charge of a plasma is roughly zero). Plasma, unlike other classes of matter, forms unique structures such as filaments, beams, solitons and double layers, under the influence of a magnetic field. It is generally known that more than 99 percent of the universe is in a plasma state. Plasma occurs naturally, predominantly in the sun, stars, auroras and interstellar space. Plasma can also be created when a gas is brought to a temperature that is comparable to or higher than that in the interior of stars. It exists in neon and fluorescent tubes, in the sea of electrons that moves freely with energy bands in the crystalline structure of metallic solids, and in many other objects (Parks, 1991; Peratt, 1991).

The motivation behind the studies presented in this thesis is an attempt to explain certain satellite observations of nonlinear electrostatic fluctuations in different regions of the Earth's magnetosphere.

Space plasma was first observed in space by USSR Sputnik satellite on October 4, 1957, and then by Explorer I of USA on January 31, 1958. Then space became accessible and more satellites were instrumented to study the Earth's environment (Parks, 1991; Moolla, 2004).

Satellite observations in auroral regions revealed that space is endowed with a rich variety of electrodynamic phenomena. The knowledge acquired from our solar system plasmas can be generally applied to other plasmas in the universe. This is premised

on the fact that our solar electrodynamic system exemplifies similar dynamics that occur in other planets, magnetosphere and solar systems (Parks, 1991).

1.1 Solar wind

The solar wind is a stream of energized, charged particles (i.e., electrons and protons, along with few heavier ions), flowing outward from the sun, through the solar system at a very high speed of $900km/s$. The temperature reaches about $1,000,000^oC$. It is completely made of plasmas. Once the solar wind is blown into space, the particles travel all the way past planet Pluto and do not slow down until they reach the termination shock within the heliosphere. The source of the solar wind is the Sun's hot corona. The Sun consists of several ions species of about 90% hydrogen, 10% helium, and 0.1% of other minor constituents, such as carbon, nitrogen, and oxygen. Solar wind has a large influence on our planet, particularly on the ionosphere, the Earth's magnetic field, on Earth's auroras and on telecommunication systems (Parks, 1991).

1.2 Magnetosphere

A magnetosphere is the region surrounding a planet, where the planet's magnetic field dominates, and comprises the following parts: the bow shock, magnetosheath, boundary layer, magnetotail, plasmasheet, lobes, plasmasphere, radiation belts, polar wind, magnetopause and many electric currents. The magnetosphere prevents most of the solar wind particles coming from the sun from hitting the Earth. It is composed of charged particles and magnetic flux. These particles are responsible for many wonderful natural phenomena such as the auroral and radio emissions. It even generates storms (NASA). Figure 1.1 shows the Sun and Earth's connection to solar wind plasma.

In the case of magnetized bodies such as Mercury, Jupiter, Earth, Saturn, Uranus and Neptune the magnetosphere formed around each of these bodies and the interaction between them induces large-scale currents that can almost confine the planetary magnetic field. Unlike unmagnetized bodies such as Mars, Venus and the comets, the solar wind interacts with the ionized particles of their atmospheres and induces

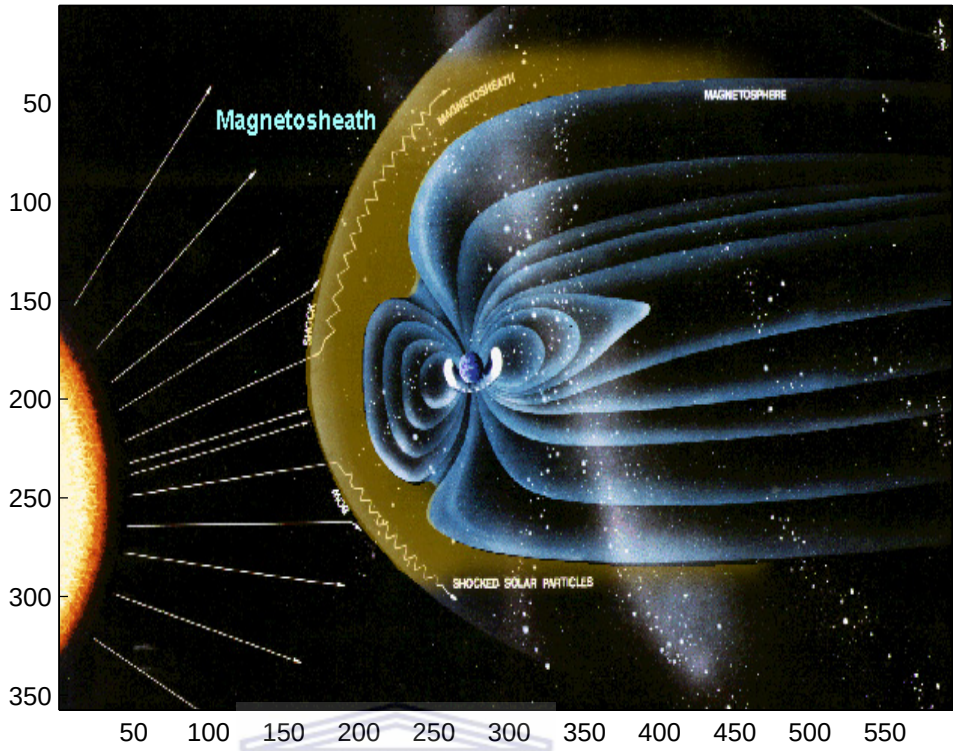

Figure 1.1: Sun-Earth's Magnetosphere connection with solar wind plasma (David, 2008)

currents whose magnetic fields then divert the solar wind around them (Parks, 1991).

The motivation behind this thesis is to theoretically describe the natural phenomena that occur in different regions of the Earth's magnetosphere . In particular, our focus will be more on the nonlinear electrostatic solitary waves and double layers (see Section 1.3) which have been observed by satellite missions at the low frequency regions of the Earth's magnetosphere.

1.3 Nonlinear structures

The nonlinearities in space plasma contribute to the localization of waves leading to different types of coherent structures in the Earth's magnetosphere, namely solitary waves (solitons), double layers, shock waves and vortices etc. These structures are very important both in the laboratory experiments and theoretical analysis. The

nonlinear structures can be responsible for turbulent flows and also play an important role in energy transport in plasmas.

1.3.1 Solitons

Solitons are nonlinear waves. As a preliminary definition, a soliton is a single, well-defined non-dissipative wave that can travel for a long distance without depreciating in size or form (shape)(Mahmood, 2007). We can also say that a soliton is a nonlinear fluctuation that propagates long distance without losing its originality. They have the following unique properties:

- They are nonlinear localized structures which travel with permanent form and constant velocity (Drazin and Johnson, 1989).
- They are robust against perturbations and can cross each other without change in their shapes and velocities (Mahmood, 2007).

A solitary wave is a hump or dip shaped nonlinear wave of relatively stable profile, which preserves its shape. It is formed due to the balance between the effects of the nonlinearity and the dispersion.

The history of solitary waves dates back to the report of the observations by John Scott Russell at the meeting of the Society for the Advancement of Science in 1834. Here is an extract from the original reports:

> *I was observing the motion of a boat which was rapidly drawn along a narrow channel by a pair of hoses, when the boat suddenly stopped-not so the mass of water in the channel which it had put in motion; it accumulated round the prow of the vessel in a state of violent agitation; then suddenly leaving it behind, rolled forward with great velocity, assuming the form of a large solitary elevation, a rounded, smooth and well defined heap of water, which continued its course along the channel apparently without change of form or dimension of speed. I followed it on horseback, and overtook it still rolling on at a rate of some eight or nine miles an hour, preserving its original figure some thirty feet long and a foot to foot and half in height. Its height gradually diminished, and after a chase of one or two miles I lost*

it in the windings of the channel. Such, in the month of August 1834, was my first chance interview with that singular and beautiful phenomenon which I have called the Wave of Translation a name which it now very generally bears." (J. Scott Russell, 1844)

Later in 1895, the Korteweg-de Vries (KdV) equation was derived, to describe the (unidirectional) propagation of waves on the surface of the shallow channel with exact soliton solution (Scott et al. 1973, Drazin, 1984, Baboolal, 1988). In 1957, Bernstein, Green, and Kruskal (Scott et al. 1973, Drazin, 1984, Baboolal, 1988) predicted the existence of a broad class of nontrivial wave solutions of the Vlasov-Poisson equations in space plasma. The model is strongly related to the existence of trapped particles in the self-consistent electrostatic potential. The properties of the KdV equation have been investigated extensively by a number of researchers in terms of ion-acoustic waves (Gardner and Morikawa, 1965; Zabusky and Kruskal, 1965; Washimi and Taniuti, 1966). Using fluid equations, Sagdeev (1969) described properties of solitons in a plasma consisting of hot isothermal electrons and cold ions. More extensive investigations by laboratory experiments (Ikezi et al. 1970; Ikezi, 1973) and theoretical analysis (Block, 1972; Tagare, 1973) have been done on the existence and behaviors of the ion-acoustic solitary waves in various plasmas. Experimental and theoretical investigation of ion-acoustic wave (IAW) propagation in a plasma with the electron velocity distribution of which may be represented by the superposition of two Maxwellian, has been done by Jones et al. (1975). Later experiments were done in double-plasma devices (Nakamura, 1987a, 1987b) and in conducting polymers (Heeger et al. 1988). Observations of solitons have been made in several regions of the Earth's magnetosphere, e.g., auroral field lines (Temerin et al. 1982; Mozer and Temerin 1983; Temerin and Mozer, 1984; Boström et al. 1988; Mozer et al. 1997; Ergun et al. 1998; Bounds et al. 1999), the bow shock (Bale et al. 1998), magnetopause and on cusp field lines (Franz et al. 1998; Cattel et al. 1999), Polar cap boundary layer (Tsurutani et al. 1998), plasma sheet boundary layer (PSBL) (Matsumoto et al. 1994; Omura et al. 1994, 1999), auroral kilometric radiation (AKR) source region (Pottelette et al. 1999) and magnetosheath (Pickett et al 2003, 2005). The Rossby soliton has been proposed to explain Jupiter's great red spot (Antipov et al. 1985) and soliton models are proposed in descriptions of solid state devices (Scott et al.1973) and in nuclear structure theories (Gavin et al. 1987).

These fundamental space plasma phenomena continue to interest both experimentalists and theoreticians alike and have been the subject of intense reviews (Scott et al. 1973; Block, 1978; Watanabe, 1978; Tran, 1979; Buti, 1980; Nishihara and Tajiri, 1981; Smith, 1982; Shukla, 1983; Borovsky, 1984; Pecesli, 1985; Bharuthram and Shukla, 1985, 1986; Mälkki et.al., 1989; Baboolal et al. 1990; Pottelette et.al. 1990; Yadav and Sharma, 1990; Mace et al. 1991; Reddy and Lakhina, 1991; Reddy et.al. 1992; Cairns et al. 1995; Mamun, 1997; Malka et al. 1997; Berthomier et al. 1998; Yadav et al. 1995; Ghosh et.al. 1996; Ghosh and Iyengar, 1997, 2002; Singh et al. 2001; Bharuthram et al 2002; Kourakis and Shukla, 2003; Singh and Lakhina, 2004; Gill et al. 2006; Verheest et al. 2007, 2008; Lakhina et al. 2008 a and b, 2009, 2011).

1.3.2 Double layers

A double layer is a unique structure in space plasmas. It consists of two space-charge regions ("layers") in close proximity, with a strong electric field between the positive charge and the negative charge. In general, double layers (which may be curved rather than flat) separate regions of plasma with quite different characteristics. In other words, the potential drop across the double layer is essentially monotonic and is greater than or of the order of the electron thermal energy. It occurs over a localized region of the plasma with dimensions, given in terms of the electron Debye length, small in comparison with the system length. Double layers are found in a wide variety of plasmas, from discharge tubes to space plasmas to the Birkeland currents supplying the Earth's aurora. They are especially common in current-carrying plasmas.

In the 1920s, double layers were known as plasmas that have a limited capacity for current maintenance, before the observations of Langmuir in 1929 in the laboratory, when he was investigating the cathode sheath formations in the diode. More observations of double layers have been reported in the laboratory (Coakely et al. 1979, Sato 1982, Ameniya and Nakamura 1986), in laser plasma (Ludmirsky et al. 1985), in the auroral region (Temerin et al. 1982; Mozer and Temerin 1983; Boehm et al. 1984), and in the magnetosphere (Mozer et al. 1985). At the moment many groups are working on numerical simulation and theoretical models (Sato and Okuda 1980, 1981; Baboolal et al. 1988, 1990; Verheest et al. 2005, 2008; Lakhina et al. 2010, 2011).

1.3.3 Shock waves

A shock wave is a propagating disturbance where there is sharp transition in a dynamic property (typically density) over a relatively small temporal or spatial interval. Such waves of course would include double layers as special cases. Like an ordinary wave, it carries energy and can propagate through a medium or, in some cases in the absence of a material medium, through a field such as the electromagnetic field. (Anderson, 1984)

The universe is woven through by plasmas in motion. Between the planets, the stars and the galaxies there are flows of plasma and field energy, and wherever these flows exceed the speed of sound and the Alfven speed (Shukla and Stenflo, 1997), there will also be shock waves (Schwartz et al. 2004). In the solar system there are shocks in front of all the planets, in their magnetotails, and in the solar corona and solar wind. Shock waves are widely studied in space and astrophysics plasmas. They are places where the plasma and field go through dramatic changes: changes in density, temperature, field strength and flow speed. These changes, combined with the collisionless nature of space plasmas and the wide variety of wave modes, produce a rich collection of different shock types (Schwartz et al. 2004).

Shock waves have been studied in different aspects of space plasma, in supernovae shock waves or blast waves through the interstellar medium (Giacobbe 2005), and in the bow shock caused by the Earth's magnetic field colliding with the solar wind (Kivelson and Russell 1995).

1.3.4 Vortices

Vortices are spinning, often turbulent, flows of fluid. A polar vortex is a persistent, large-scale cyclone located near one or both of a planet's geographical poles. On Earth, the polar vortices are located in the middle and upper troposphere and the stratosphere. They surround the polar highs and are part of the polar front (Ting, 1991).

Coherent vortices appear in two-dimensional fluids and magnetized plasmas. In simplest possible scenario, the vortex dynamics is governed by the Naiver Stock equation, which admits a monopolar vortex (Hasegawa 1985). However, in magnetized dusty plasma, we have the possibility of vortices comprising a bipolar (Bharuthram

and Shukla 1992b), a tripolar, and a chain (Vranjeŝ et al 2001). Here the vortices are associated with nonlinear dispersive waves that possess at least a two-dimensional character. When the velocity of the fluid (or plasma particles) motion associated with the dispersive waves becomes locally larger than the wave phase velocity because of the nonlinear effects, one encounters a curving of the wave front, which leads to the formation of a two-dimensional traveling vortex structure (Shukla and Mamum 2002).

The so-called "dipole" is probably the most observed shape, but transitions to a tripole and to a fairly circular shape are also likely. This structure has been studied in Earth's magnetosphere by many authors, like Kaladze and Tsamalashvili (1997), Sreenivasan and Jones (2005), Olson and Amit (2006).

1.4 Thesis structure

The thesis is structured as follows:

In the present chapter, the basic concepts are introduced and the scope of the present work is outlined.

In Chapter Two, we survey the literature on nonlinear structures in the Earth's magnetosphere, such as space observations and theoretical models of nonlinear electrostatic fluctuations in auroral regions.

In Chapter Three, we provide an explanation for the low-frequency electrostatic fluctuations observed by the spacecraft missions (e.g. S3-3, FAST, POLAR, WIND, FREJA, Viking, CLUSTER, GEOTAIL) in the auroral regions of the Earth's magnetosphere. Using quasi-neutrality conditions, evolution of solitons and double layers are studied in a three-component plasma model consisting of ions and two electrons species. The conditions under which the solitary waves and double layers can exist are found both analytically and numerically for the plasma models. We show the existence of negative potential solitary waves and double layers. Our calculations show good agreement with Viking satellite observations of the electric field structures in the auroral region of the magnetosphere. (The input parameter values were taken from satellite data). This chapter is composed of three models, Model 1: Magnetized plasma with a cold ions and two-Boltzmann electrons; Model 2: Magnetized plasma with adiabatic ions and two-Boltzmann electrons and Model 3: Magnetized plasma with cold ions, cool electrons and hot nonthermal electron species.

Recent observations (FAST satellite measurements) have clearly indicated that the auroral plasma is fully composed of several ions species (i.e. multi-ion-component) (Cattel et al., 1998; Crumley et al., 2001). The most abundant ion components, which comprise over 95% of the total ion density in the low auroral region, are hydrogen and oxygen ions. In Chapter 4 we provide the theoretical explanations for the nonlinear electrostatic structures with multi-ion species observed in the Earth's magnetosphere. In multi-component plasma models, nonlinear electrostatic structure are studied using Sagdeev pseudo-potential technique. The present investigation concurs with satellite observations in the auroral zone of the Earth's magnetosphere. The chapter is composed of three plasma models, Model 1: Magnetized plasma with cold oxygen ions and Boltzmann distribution of hot protons and cool electrons; Model 2: Magnetized plasma with cold oxygen ion beam and Boltzmann distribution of hot protons and cool electrons and Model 3: Magnetized plasma with cold oxygen ions, Maxwellian ions and two-Boltzmann electrons.

We shall present the summary of the thesis in Chapter 5.

Chapter 2

Nonlinear structures in the Earth's magnetosphere

As mentioned in the previous chapter, the Earth's magnetosphere is characterized by linear and nonlinear wave phenomena. In this chapter a brief overview will be provided of spacecraft observations of nonlinear fluctuations in the Earth's magnetosphere. In doing so, theoretical concepts and models developed to explain the observations will also be discussed.

2.1 Observations of nonlinear fluctuation phenomena in space plasmas

Nonlinear electrostatic solitary waves traveling parallel to the background magnetic field, which can be identified by their bipolar electric field structure parallel to the magnetic field, have been observed in several parts of the magnetosphere (Temerin et al. 1982). The first observations of such phenomena in the auroral acceleration region were reported by the S3-3 satellite mission in 1982 (Temerin et al. 1982). These nonlinear electrostatic structures have been sighted in several regions along the magnetic field line of the magnetosphere, including the auroral kilometric radiation, cusp field lines, plasma sheet boundary layer, polar cap boundary layer, the bow shock, magnetosheath, magnetotail and the Earth's foreshock region. The observations of electrostatic solitary waves in the auroral region of the magnetosphere are categorized into two classes by Ergun et al. (1998), either connected with ion or electron beams.

Solitary waves in connection with ion beams may be liable to have lower speeds than those in association with electron beams (i.e. electrons propagate at higher speeds than ions)(Crumley et al. 2001). Viking satellite (Bostrom et al. 1988) later reported similar observations of solitary waves propagating with background ion beams in the auroral acceleration region. Not long ago, by the FAST (Fast Auroral Snapshot) satellite (McFadden et al. 1999a) follow by the Polar satellite (Mozer et al. 1997; Bounds et al. 1999). Geotail satellite were the first to announce the solitary wave structures associated with electrons in the auroral region (Matsumoto et al. 1994), and later by the Fast Auroral Snapshot satellite (Ergun et al. 1998), WIND satellite (Bale et al. 1998), and POLAR satellite (Franz et al. 1998; Cattell et al. 1999).

The S3-3 spacecraft measurements between the altitudes of about 6000 and 8000 km, reported the observations of small-amplitude solitons and double layers comprising of magnetic and electric field components in the auroral region (Temerin et al. 1982). Observed solitary waves in the ion beam region were estimated to be propagating along the magnetic field line with velocity greater than 50 kms^{-1}, with widths corresponding $\sim 40\lambda_D$. Their electric field is about 15 mV/m, their electrostatic polarization relative parallel to the magnetic field and the duration of about 2-20 ms for the double layer (Temerin et al. 1982).

Swedish Viking satellite measurements (Bostrom et al. 1988) at lower altitude, of about $\sim$ 7000 km, detected small-scale, large-amplitude solitary waves with negative potential, moving upwards along the magnetic field lines. Dombeck et al. (2001) reported the solitary waves of 5-50 km s^{-1} speed with the potential of about 2-3 V and the scale sizes of about 50-100 m, which is equivalent to $\sim 10\lambda_D$, with a cold electron species. The temperature and density are 5 eV and 5 cm^{-3} respectively (Bostrom et al. 1988; Koskinen et al. 1990; Malkki et al. 1993). Viking observations in the auroral magnetic zone of the magnetosphere also revealed the solitary structures associated with both density peaks and density depression (Cairns et al. 1995).

Spacecraft data from the Polar satellite at altitudes of $\sim$ 6000 - 7000 km revealed ion-related solitons in the auroral zone of the magnetosphere (Dombeck et al. 2001). Bounds et al. (1999) recorded the solitary waves with potentials of 10-100 V, between the hydrogen H^+, and oxygen O^+ beam speeds, within the range of 75-300 km s^{-1}, the scale size of $\sim 10 - 20\lambda_D$ in the parallel direction with about $\sim$ 200 m of the Debye length (Crumley et al. 2001). Bounds et al. (2000) showed that the ion acoustic solitary waves were propagating in connection with up-flowing ion beams, while the

electron acoustic solitary waves travel with down-flowing electron beams (Cattell et al. 2001). Recent observations by Polar satellite at the low altitude regions of the auroral zone (Dombeck et al. 2001), recorded solitary waves with a velocity of lower amplitude near the oxygen beam velocity and higher near the hydrogen beam velocity.

Exploiting spacecraft measurements from the FAST satellite, Ergun et al. (1998) reported the observations of fast solitary waves propagating along the magnetic field line. These waves were associated with cold electron beams with background downward electric current zone of the auroral plasma, which propagate upward at $\sim$ 4500 km/s. The amplitude is very large (up to 2.5 V/m), propagates at very high frequency above ion acoustic speed and has potential of about $\sim$ 100 Volts. These large amplitude waves have an electromagnetic signature (electron holes) traveling anti-earthward. Later, FAST satellite mission data in the upward ion beam region indicated that cold plasma densities are insignificant in the upward ion beam region (Strangerway et al. 1998; McFadden et al. 1999c).

Observations made by the Freja satellite mission (Dovner et al. 1994) reported that electrostatic solitary structures involving density depletions of the order of 10%, associated with electric fields, were detected in the upper ionosphere in the auroral zone.

2.2 Theoretical studies of nonlinear fluctuation phenomena

Solitons are nonlinear restricted symmetric (asymmetric) electric potential structures with no net potential drop, which have been observed in different regions of the auroral magnetosphere (Lakhina et al. 2003). These observations has been described by a number of authors in terms of low frequency solitons, both in magnetized (Lee and Kan 1981; Hudson et al. 1983; Bharuthram and Shukla 1986; Qian et al., 1988; Reddy et al., 1992) and unmagnetized plasmas (Kuehl and Imen 1985; Bharuthram and Shukla 1986; Baboolal et al. 1990; Sayal et al. 1993). Using the Poisson equation, Bharuthram and Shukla (1985) described the propagation of the solitary waves and double layers in a magnetized plasma consisting of a cold ions fluid with two distinct groups of Maxwellian electron species. They used a reductive perturbation technique to derive a general three-dimensional differential equation for the small amplitude

potential structures. Berthomier et al. (1998) described the characteristics of ion acoustic solitary waves and weak double layers observed by the Viking satellite in auroral region. Using an unmagnetized plasma model consisting of a two Boltzmann electron temperature with hot background ions.

The space plasma in the auroral zone of the Earth's magnetosphere is distinguished by multi-ion beams such as hydrogen H^+, oxygen O^+, helium He^+ and two temperature electron species (Koskinen et al. 1990, Lakhina et al. 2003). Reddy et al. (1992) presented a plasma model to describe small amplitude low frequency solitons and double layers in a magnetized plasma for any charge ion beam population, together with two distinct group of electron species. On the other hand, in the high frequency regime, theoretical models have been developed to explain the linear and nonlinear features of broadband electrostatic noise (BEN), observed in the Earths magnetosphere, through electron-acoustic waves (Singh and Lakhina, 2000; Singh et al. 2001; Singh and Lakhina, 2004; Tagare et al., 2004; Kakad et al. 2007; Ghosh et al. 2008; Lakhina et al. 2008, 2009).

In the low frequency regime, an analytical model of the coupled nonlinear ion cyclotron and ion-acoustic waves has been developed by Reddy et al. (2002, 2006), which could describe the FAST satellite observations in auroral region presented by Ergun et al. 1998. Lately, Lakhina et al. (2011) investigated the properties of low and high frequency solitary waves and double layers in an unmagnetized plasma composed of four species: core electrons, counter-streaming electron beams and ion species. Their model predicted the existence of three types of solitons: ion-acoustic, slow and fast electron-acoustic modes. Furthermore, it was stated that the three modes can coexist in different Mach number regimes or differently, depending upon the plasma parameters.

2.2.1 Two-electron temperature plasmas

Various theoretical models have been developed to study the low frequency solitary waves in the auroral plasma. Lee and Kan (1981) studied nonlinear low-frequency waves in magnetized electron-ion plasma and showed, that depending upon the speed of soliton, there are three types of nonlinear waves: periodic ion-cyclotron, periodic ion-acoustic and ion-acoustic solitons. Bharuthram and Shukla (1985) discussed the dynamics and structure of multi-dimensional ion acoustic solitons and double layers

in a magnetized plasma consisting of two electron species. Incorporating the departures from quasi-neutrality, they used a reductive perturbation technique to derive a general three-dimensional differential equation for the potential for small amplitude perturbations. In a later paper, Bharuthram and Shukla, (1986) presented the Sagdeev potential model for an unmagnetized plasma with cold ions fluid and two Boltzmann distributed electron species and obtained the conditions for the existence of small and large amplitude double layers. They derived a perturbation technique to obtain a modified Korteweg-de Vries (MKdV) equation which controls the dynamics of a weak double layer. Baboolal et al. (1990) have shown the cut-off conditions and existence domains for arbitrary amplitude ion-acoustic solitary waves and double layers in unmagnetized fluid plasmas. The plasma was composed of two Boltzmann electrons temperature and a stationary cold ion fluid background. Below an electron temperature ratio point, they found the existence of both positive potential solitons and negative-potential solitons limited by double layer solutions.

Motivated by the Viking satellite observations of the solitary structures with negative potentials, many theoretical models using multi-component plasmas have been developed to study nonlinear ion-acoustic waves (Pottelette et al., 1990; Yadav and Sharma, 1990; Mace et al., 1991; Reddy and Lakhina, 1991; Reddy et al. 1992; Yadav et al, 1995, Ghosh et al. 1996; Ghosh and Iyengar, 1997, 2002; Das et al. 1998; Ghosh and Lakhina, 2004; Eliasson and Shukla, 2006). Berthomier et al. (1998) studied low frequency solitons and weak double layers in two-temperature electron component unmagnetized plasma. They showed that the velocity, width, and amplitude of these structures are in agreement with the Viking observations in the auroral region. Lakhina et al. (2008a,b) studied finite amplitude low and high frequency (ion- and electron-acoustic) solitary waves in an unmagnetized auroral plasma, made up of cold electrons and cold ions, hot background electron beam and ion beam using the Sagdeev pseudo-potential approach. They found slow ion-acoustic, ion-acoustic and electron-acoustic solitary waves. Recently, Baluku et al. (2010) studied the ion acoustic solitary waves in two-temperature electron unmagnetized plasmas. They have reported finite-amplitude results and showed that positive (compression) double layers may be found for a limited range of cool-electron densities, in addition to positive potential ion acoustic solitary wave structures. They have further shown, by deriving the third derivative of the Sagdeev potential, that positive-potential double layers can form below a critical density ratio.

2.2.2 Nonthermal velocity distributions

Spacecraft observations (Boström et al. 1988, 1992; Dovner et al. 1994), laboratory experiments (Malka et al. 1997; Sarri et al. 2010) and theoretical models (Mälkki et al. 1989; Cairns et al. 1995) have provided evidence of the occurrence of abnormal energetic particles present in the Earth's magnetosphere. Plasmas with thermal equilibrium (Maxwellian) velocity distributions have been studied over several years (Bharuthram et al. 1985, 1986, 1987; Mahmood et al. 2003; Deng et al. 2006; Pickett et al. 2008; Baluku et al. 2010; Barman and Talukdar, 2010). In recent times, consistent attempts have been made to study the excess energetic particles effects through Cairn's nonthermal distribution model (Cairns et al. 1995; Mamun, 1997; Singh and Lakhina, 2004; Bahamida et al. 2007; Djebli and Marif, 2009; Choi et al. 2010; El-Labany et al. 2010; Ali-Fedela et al. 2010; Massood and Rizvi, 2011; Pakzad, 2011), as well as through the Kappa's distribution model (Hellberg et al. 2009; Sultana et al. 2010; Jung and Hong, 2011; Danetikar et al. 2011; Sahu, 2011).

Cairns et al. (1995) proposed a nonthermal distribution model for the electron species with excess energy in order to explain the observations made by the FREJA and Viking satellites in auroral regions of the Earth's magnetosphere. Later, Mamun, (1997) investigated the effects of adiabatic ion temperature and the contributions of nonthermal distribution of electron species on arbitrary amplitude ion acoustic solitons, using the pseudo-potential technique for a two component unmagnetized plasma. Their results are within the spacecraft captured data. Gill et al. (2004) used the reductive perturbation method to derive the KdV and m-KdV equations, which govern the dynamics of ion acoustic solitons and double layers for the plasma consisting of unmagnetized warm positive and negative ions with different masses and charged states, and nonthermal distribution of electron species. Also, Bahamida et al. (2007) presented a three component plasma model consisting of unmagnetized positively charge ions, nonthermal distribution electrons and Boltzmannian positrons to investigate the properties of arbitrary amplitude ion acoustic solitons observed at different regions of the Earth's magnetosphere. Verheest and Hellberg, (2010) studied the characteristics of compressive and rarefactive ion acoustic solitary waves in a plasma consisting of positive ions and nonthermal electrons. Rarefactive solitary waves and double layer structures were obtained when the electron nonthermality exceeded a certain minimum. Jung and Hong, (2011) deviated from the standard Maxwellian plasmas by considering a Lorentzian plasma. They investigated nonthermal effects on the propagation of the ion acoustic solitons in generalized Lorentzian

electron-ion plasmas. Their analyses were done by obtaining the Korteweg-de Vries (KdV) equation as a function of the spectral index in generalized Lorentzian plasmas. Jilani et al. (2013) studied the properties of nonlinear ion acoustic solitary waves in an unmagnetized and collisionless pair-ion plasma with a nonthermal distribution of electron population. Using the reductive perturbation technique, they obtained the nonlinear Korteweg-de Vries (KdV) equation for the soliton structures.

2.2.3 Multi-ions plasmas

Many theoretical analyses have been done to explain the soliton structures observed in various regions of the Earth's magnetosphere, which posed a lot of challenges in the past (e.g, Temerin et al. 1982; Lotko, 1983, 1986; Lotko and Kennel, 1983; Bharuthram and Shukla, 1985, 1986; Qian et al. 1988, 1989; Bergmann et al. 1988). M*ä*lkki et al. (1989) presented a theoretical explanation of the Viking satellite observations of nonlinear phase space ion hole instability in the Earth's auroral magnetosphere in the presence of hydrogen and oxygen ion beam population. Reddy et al. (1992) predicted the excitation of fast and slow hydrogen (as well as oxygen) beam acoustic modes, which can be either rarefactive double layers, or rarefactive or compressive solitons. The auroral plasma composed of isothermal cold and hot electrons with only a $H^+ - O^+$ ion beam. Nakamura (1999) investigated one-dimensional electrostatic solitary waves in a positive ion-beam and a quasi-neutral three component plasma system consisting of electrons, positive ions and negative ions, using a Korteweg-de Vries (KdV) equation.

The studies of low frequency nonlinear broadband electrostatic noise in the Earth's auroral regions has attracted much attention during the last decade (Lakhina, 1987; Koskinen et al., 1990; Berthomier et al. 1998; McFadden et al. 2003) due to its frequent occurrence in space magnetosphere. Recent observations have clearly indicated that the auroral plasma is fully composed of several ions species (i.e. multi-ion-component) (Cattel et al. 1998; Crumley et al. 2001). The most abundant ion components, which comprise over 95% of the total ion density in the low auroral region, are hydrogen and oxygen ions. Many theoretical models have been proposed to describe the multi-ion plasmas observed in different regions of the magnetosphere (Wang et al. 1998; Wang and Huang, 2001; Lakhina et al. 2003, 2008), particularly in the auroral zone where oxygen ions are the dominant ion species. Motivated by the FAST satellite observations of waves near the cyclotron frequencies of H^+, O^+ and

He^+, and the associated ion beams and field-aligned currents in the auroral region of the Earth's magnetosphere, reported by Cattell et al. 1998, several theoretical analysis have been presented to study the nonlinear low-frequency electrostatic waves in a magnetized oxygen ion beam plasma (Bharuthram et al. 2002; Reddy et al., 2006; Moolla et al. 2010).

Sauer et al. (2003) described the plasma behaviors in the low-frequency range with multi-fluid equations for protons and electrons obliquely propagating to the magnetic field. The study was based on modifying the Hall-MHD equations in single-ion plasma by the inclusion of a second ion population, which leads to the appearance of a new type of stationary nonlinear wave solution called an "oscilliton". Lakhina et al. (2003) proposed a theoretical explanation in terms of soliton models or BGK modes/phase space holes to the solitary pulses associated with bipolar electric field structures observed by several satellite missions in different regions of the magnetosphere, for the auroral plasma parameters with oxygen and hydrogen ion beam species. Ghosh and Lakhina, (2004) presented a theoretical explanation for POLAR satellite observations (Dombeck et al. 2001)) at low altitude region. Their analytical model showed the anomalous width variations of rarefactive large amplitude structures in the auroral plasmas. Choi et al. (2006) studied nonlinear ion acoustic solitary waves and double layers in solar wind plasma consisting of Boltzmann electron and magnetized ion fluid. In their model, they obtained new solitary wave solutions for higher order expansions of the Sagdeev potential. Verheest et al. (2007) discussed the necessary conditions and existence ranges for the generation of acoustic solitons (ion- and electron-acoustic) in space plasmas with one or more ion species which are hotter than some or all of the electron species. Recently, Moolla et al. (2010) extended the work of Reddy et al. (2006) by including the Poisson equation, which allows the charge separation effect rather than the quasi-neutrality condition. They revealed that the inclusion of charge separation tends to increase the oscillation of the wave structures. Lakhina et al. (2011) presented a model for ion- and electron-acoustic solitons and double layers in a multi-component unmagnetized plasma, consisting of background core electrons, two electron beams and ions. Using the Sagdeev pseudo-potential techniques, the model predicts the existence of three types of solutions, namely, ion-acoustic, slow and fast electron-acoustic soliton/double layer. More recently, Das (2012) studied the effect of ion temperature on small-amplitude ion acoustic solitons in a magnetized ion-beam plasma in the presence of electron inertia. Using the Korteweg-de Vries (KdV) equation for a plasma model consisting of ions, electrons and ion beams, they showed

that though both compressive and rarefactive solitons exist for the slow mode, only compressive solitons exist for the fast mode.

2.3 The physics of solitons and double layers

Extensive investigations on laboratory experiment (Ikezi et al. 1970; Ikezi, 1973) and the theoretical analysis (Tagare 1973; Gell and Roth 1977; Abrol and Tagare 1980; 1981) have been done on the existence and behaviors of nonlinear low frequency soliton and double layer structures propagating in various plasmas.

The theoretical studies of solitons and double layers were classified into two categories (Baboolal, 1988), namely; small and large (finite) amplitude. In addition, one could further sub-classify them according to whether they are stationary or time-dependent, fluid or kinetic, analytical or numerical simulations. In all these classifications one common theme is that such structures are essentially nonlinear and thus linear theory fails.

In the small amplitude regime, various evolutionary equations of the Korteweg-de Vries (KdV) or modified Korteweg-de Vries (MKdV) type have been derived for solitons and double layers. A standard way of obtaining such equations is to employ the reductive perturbation technique (RPT) of Washimi and Taniuti (1966). In the reductive perturbation technique (RPT) one expands the wave amplitudes in powers of some small expansion parameters, and together with a transformation ("coordinate stretching") appropriate to the length and time scales in the problem, one obtains relations in the expanded quantities, with each relation corresponding to a respective order of the expansion parameter, and from these follows the required evolutionary equation. Perturbation techniques have been used by many authors to investigate the nonlinear ion-acoustic solitons and double layers in the auroral plasmas (e.g. Washimi and Taniuti, 1966; Zakharov, 1972; Yu, 1977; Schamel, 1982a, 1982b; Bharuthram and Shukla, 1986; Mann, 1986; Mishra et al. 1994; Tagare, 2000; Singh et al. 2005; Shah et al. 2010; Jilani et al. 2013).

In most real situations the amplitudes of these nonlinear structures are much larger than can be accounted for by means of small amplitude theories. In this connection, Baboolal et al. (1988a, 1988b) have showed that unless the amplitudes are small the KdV and MKdV can give erroneous results. In fully nonlinear large

amplitude theory, one bases the model on the full set of fluid and Poisson equations or Vlasov-Poisson system or a combination of such equations. Even in the time-independent or stationary situation the solution of the general case can be quite formidable, and, except in certain simple cases, can only be solved numerically. For low frequency fluctuations, the system of equations can be closed with quasi-neutrality conditions instead of using the full Poisson equation. In this case, we assume that the characteristic length is much larger than the Debye length λ_D. This assumption allows the charge neutrality condition. The study of the ion-acoustic waves in a magnetized plasma has been the focus of many authors recently (e.g. Bharuthram et al. 2002; Ghosh and Lakhina, 2004; Reddy et al. 2005; Barman and Talukdra, 2010; Rufai et al. 2012, 2014).

2.3.1 The Sagdeev pseudo-potential technique

In the finite amplitude analysis one looks for soliton structures that propagate undiminished. Introduce a stationary frame which co-moves with the nonlinear localized structure, then all basic equations will reduce to the first order ordinary differential equations (ODE) (Verheest et al. 2005).

Solving the problem in a stationary frame is to reduce the system equations to a single "equation of motion" of a "pseudo-particle" in the conservation field of a "pseudo-potential". The technique has been well formalized by Sagdeev (1966) after whom the original and more generalized pseudo-potential is named (Nishihara and Tajiri, 1981; Smith, 1982; Bharuthram and Shukla, 1986; Baboolal, 1988).

In the traditional pseudo-potential analysis (Sagdeev, 1966), the system reduced to an energy-type integral of the form

$$\frac{1}{2}\left(\frac{d\psi}{d\xi}\right)^2 + V(\psi, M) = 0 \tag{2.1}$$

where $V(\psi, M)$ is the pseudo- or Sagdeev potential, $d\psi/d\xi$ is the velocity of the pseudo-particle, $\psi(\xi)$ is the potential, and ξ is the "spatial" coordinate.

Solving equation (2.1), we obtain

$$\xi = \int \frac{d\psi}{\sqrt{-2V(\psi, M)}} \tag{2.2}$$

which can yield the solution in the form of solitary pulses. The arbitrary amplitude solitary wave solutions can be obtained by solving equation (2.2) numerically. (The curves in Figure 2.2 and 2.4 show the soliton and double layer potential).

2.3.2 Existence conditions for solitons and double layers

For the existence of the soliton solutions one requires the Sagdeev potential $V(\psi, M)$ in equation (2.1) to satisfy the following conditions, as stated by many authors (Bharuthram and Shukla, 1986; Ghosh and Lakhina, 2004; Lakhina et al. 2011); $V(\psi, M) = 0$, $d\psi/d\xi = 0$, and $dV(\psi, M)/d(\psi) = 0$ at $\psi = 0$, $d^2V(\psi, M)/d(\psi)^2 < 0$ at $\psi = 0$; $V(\psi, M) = 0$ at $\psi = \psi_m$ (some maximum/minimum value of ψ), $dV(\psi, M)/d(\psi) < (>)\ 0$ at $\psi_m < (>)\ 0$. Then, for the formation of a double layer, the last condition changes to $\frac{dV(\psi,M)}{d\psi}|_{\psi=\psi_m} = 0$ (Bharuthram and Shukla 1986; Lakhina et al. 2009; Singh et al. 2011).

For soliton solution, Figure 2.1 and 2.2 show the Sagdeev potential $V(\psi, M)$ and electrostatic potential ψ structures. As shown from the equilibrium it moves away from the initial conditions at $\psi = 0$ and ψ reached a maximum or minimum point at ψ_m, which is not a rest point, and it reflected by the potential back to its initial point.

For the case of double layer shows in Figure 2.3 and 2.4, the pseudo-particle trace a path starting from the equilibrium point $\psi = 0$ at $\xi = +\infty$, fall into the potential deep and reaches a maximum or minimum value $\psi = \psi_m$ at $\xi = -\infty$, which is another rest point from which it cannot return to its starting point.

In our work here this pseudo-potential technique will be used to study finite amplitude solitary waves and double layers in a magnetized multi-species plasma.

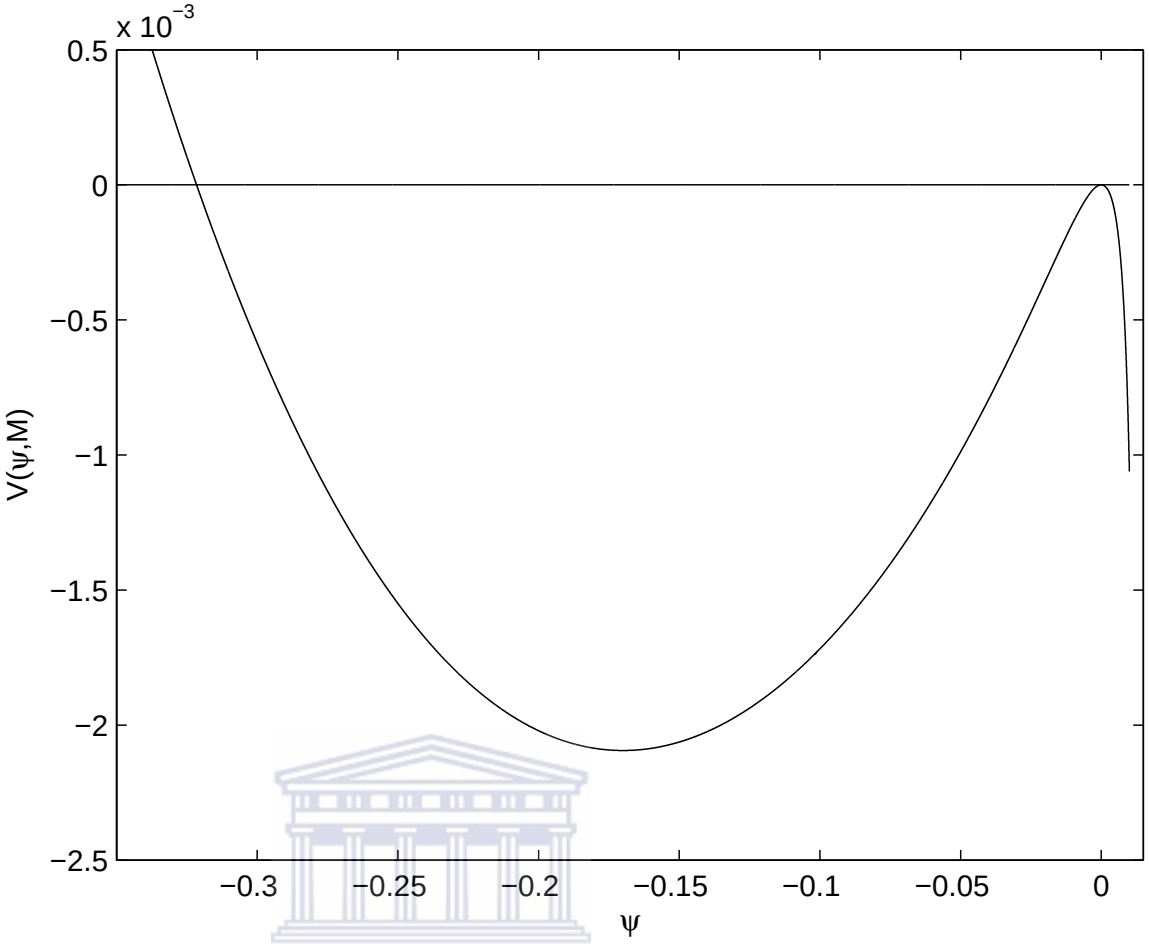

Figure 2.1: Typical shape of a Sagdeev potential $V(\psi, M)$

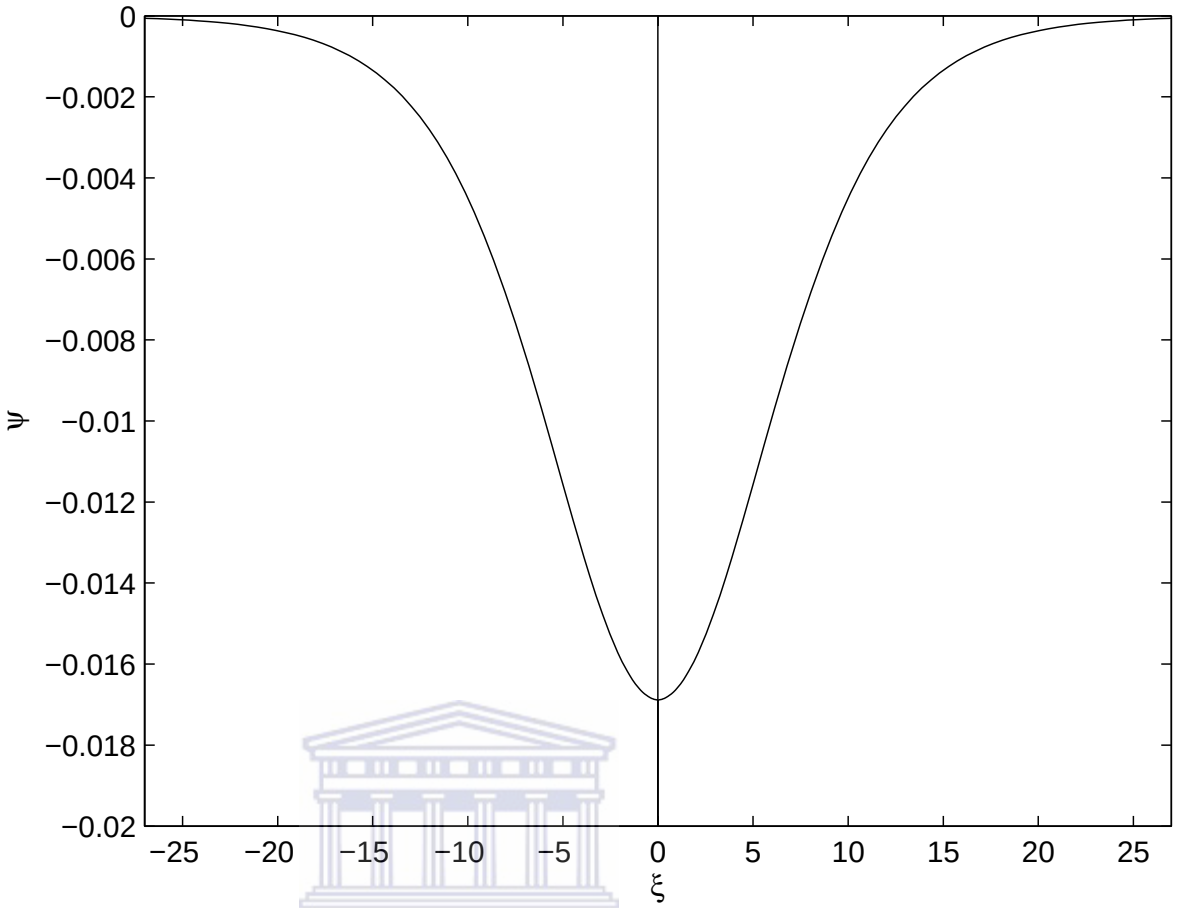

Figure 2.2: Soliton potential profile corresponding to $V(\psi, M)$ in Figure 2.1

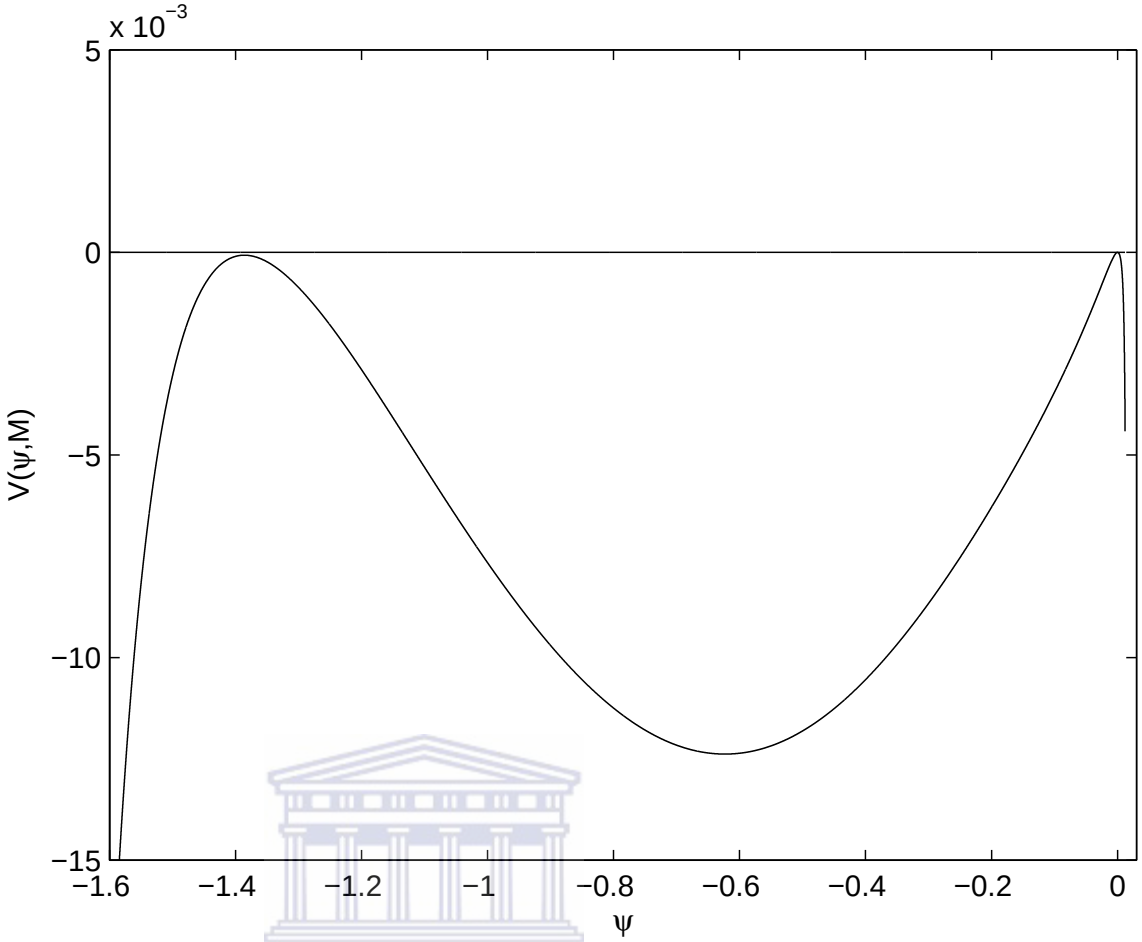

Figure 2.3: Typical shape of double layer Sagdeev potential $V(\psi, M)$

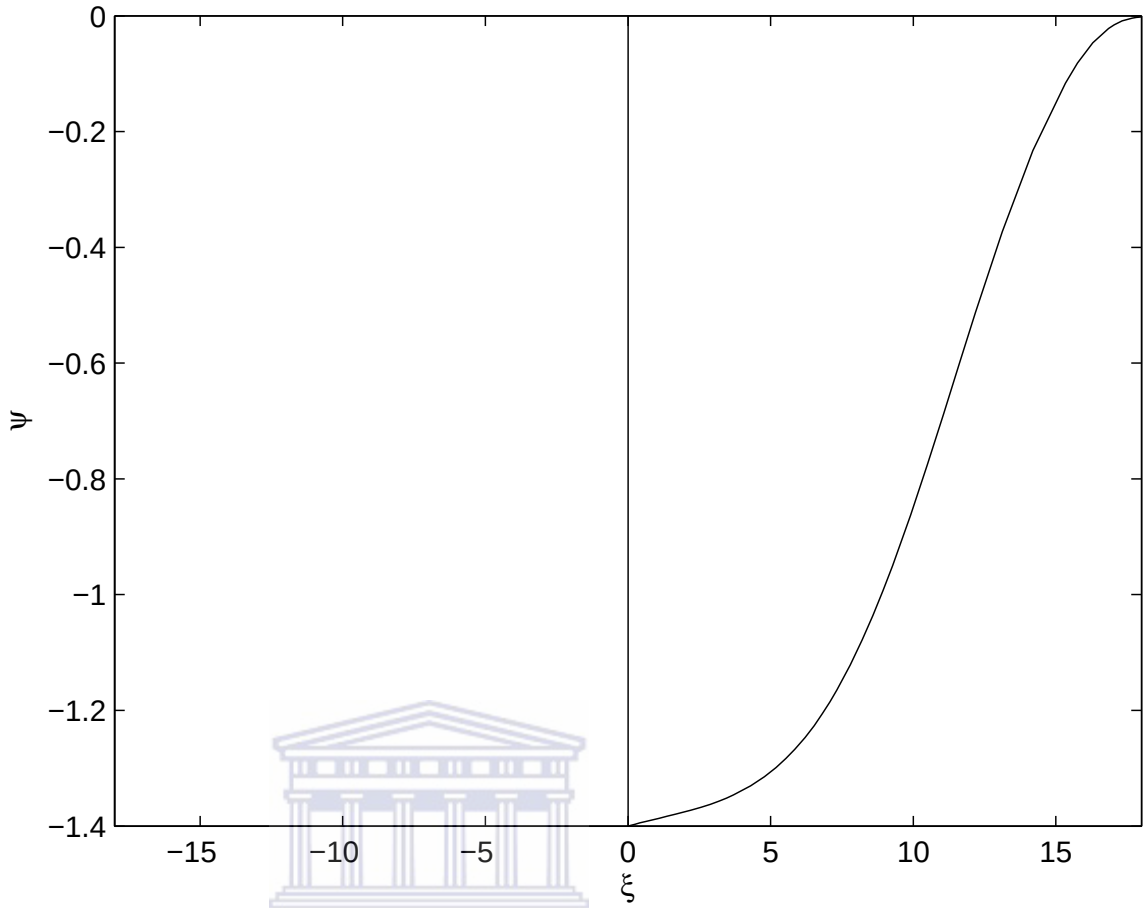

Figure 2.4: Double layer potential ψ corresponding to $V(\psi, M)$ in Figure 2.3

Chapter 3

Low frequency electrostatic fluctuations model

In Chapter 2 the importance of the study of nonlinear fluctuations in space environments was discussed and related to satellite observations. The physical mechanisms for the generation of soliton and double layer structures were also explained. In Section 2.3 the Sagdeev pseudo-potential technique for the generation of solitons and double layers was also presented. In this chapter, we shall use the technique to study finite amplitude, low frequency electrostatic fluctuations in the space plasmas. The conditions under which nonlinear structures such as solitons and double layers can exist shall be investigated both analytically and numerically.

3.1 Model 1: Magnetized plasma with a cold ions and two-Boltzmann electrons

In this model, finite amplitude non-linear ion-acoustic solitary waves are studied in a magnetized plasma consisting of a cold ion fluid and two distinct groups of Boltzmann electrons, using the Sagdeev pseudo-potential technique.

3.1.1 Basic equations

The collisionless, magnetized plasma consists of cold ions and two distinct groups of electrons, cool electrons (N_c, T_c) and hot electrons (N_h, T_h) (where $N_{c,h}$ are cool and hot electron density and $T_{c,h}$ are cool and hot temperature). We assume that the plasma is embedded in a uniform external magnetic field $\mathbf{B}_o = B_o\hat{\mathbf{z}}$, where $\hat{\mathbf{z}}$ is the unit vector along the $\mathbf{z}$ - axis. Further, we assume that the waves are propagating in the (x, z) plane obliquely to the magnetic field. The Boltzmann distribution is assumed for the densities of the cool (N_c) and hot (N_h) electron species and are given as follows:

$$N_c = N_{c0} \exp\left(\frac{e\phi}{T_c}\right) \tag{3.1}$$

$$N_h = N_{h0} \exp\left(\frac{e\phi}{T_h}\right) \tag{3.2}$$

where ϕ is the electrostatic potential and N_{c0} (T_c), and N_{h0} (T_h) are the equilibrium densities (temperature) of the cool and hot electrons, respectively. The assumption of the Boltzmann distribution means that the electrons are in thermal equilibrium, which is a valid assumption for low frequency phenomena, well below the electron plasma frequency. The dynamic of the cold ions are described by the fluid equations, namely, the continuity and the momentum equations:

$$\frac{\partial N_i}{\partial t} + \nabla(N_i V_i) = 0, \tag{3.3}$$

and

$$\left(\frac{\partial}{\partial t} + \mathbf{V_i}.\nabla\right)\mathbf{V_i} = -\frac{e\nabla\phi}{m_i} + e\frac{\mathbf{V}_i \times \mathbf{B}_o}{m_i c}, \tag{3.4}$$

where N_i, m_i and V_i are the number density, mass and the fluid velocity of the ions, respectively, e is the magnitude of the electron charge and c is the speed of light in vacuum.

We begin with a linear analysis of the above set of equations. For harmonic oscillations varying as $e^{i(kz-\omega t)}$, i.e. propagating along the magnetic field $\mathbf{B}_o$, then $\frac{\partial}{\partial t} \to -i\omega$, $\nabla \to ik$. From the continuity equation (3.3), we then have

$$-i\omega N_i + ikN_o V_i = 0$$

$$V_i = \frac{\omega N_i}{N_o k} \tag{3.5}$$

At equilibrium, we have

$$N_{io} = N_{co} + N_{ho} = N_o,$$

from which

$$\frac{N_{ho}}{N_o} = 1 - \frac{N_{co}}{N_o} = 1 - f,$$

where $f = \frac{N_{co}}{N_o}$.

Then

$$n_c = \frac{N_c}{N_o} = f \exp\left(\frac{e\phi}{T_c}\right),$$

$$n_h = \frac{N_h}{N_o} = (1-f) \exp\left(\frac{e\phi}{T_h}.\frac{T_c}{T_c}\right),$$

$$n_h = (1-f) \exp\left(\frac{e\phi}{T_c}.\tau\right),$$

where $\tau = \frac{T_c}{T_h}$. Using the quasi-neutrality condition, we have

$$n_i = \frac{N_i}{N_o} = \left[f \exp\left(\frac{e\phi}{T_c}\right) + (1-f) \exp\left(\frac{e\phi}{T_c}.\tau\right)\right]$$

then, we can expand the exponential in a Taylor series for $|e\phi/T_c| \ll 1$,

$$\exp\left(\frac{e\phi}{T_c}\right) = \left[1 + \frac{e\phi}{T_c} + \frac{1}{2}\left(\frac{e\phi}{T_c}\right)^2 + ...\right] \simeq 1 + \frac{e\phi}{T_c}.$$

Therefore, neglecting the higher order terms in the expansion we have

$$n_i = \left(f\left(1 + \frac{e\phi}{T_c}\right) + (1-f)\left(1 + \frac{e\phi}{T_c}.\tau\right)\right) = 1 + n_{i1},$$

from which

$$n_{i1} = (f + (1-f)\tau)\left(\frac{e\phi}{T_c}\right).$$

This implies

$$e\phi = \frac{T_c n_{i1}}{(f + (1-f)\tau)}.$$

From the momentum equation (3.4), we have

$$-i\omega V_i = -\frac{eik\phi}{m_i}. \tag{3.6}$$

Using (3.5) we have

$$\omega\left(\frac{\omega n_{i1}}{k}\right) = \frac{k}{m_i}\left(\frac{T_c n_{i1}}{(f+(1-f)\tau)}\right).$$

Therefore,

$$\frac{\omega^2}{k^2} = \frac{1}{m_i}\left(\frac{T_c}{f+(1-f)\tau}\right),$$

for which

$$\frac{\omega}{k} = \left(\frac{T_{eff}}{m_i}\right)^{1/2} \equiv c_s$$

is the ion acoustic phase speed, where $T_{eff} = \frac{T_c}{f+(1-f)\tau}$ is the effective electron temperature.

We present next the governing equations in normalized form: the densities are normalized with respect to the total ion equilibrium density $N_{i0} = N_{c0} + N_{h0} = N_0$, velocities by the effective ion-acoustic speed $c_s = (T_{eff}/m_i)^{1/2}$, distance by the effective ion Larmor radius, $\rho_i = c_s/\Omega$, time by the inverse of ion gyro-frequency Ω^{-1}, where $\Omega = eB_0/m_i c$ and potential ϕ by T_{eff}/e. Here $\tau = T_c/T_h$ is the cool to hot electron temperature ratio, $f = N_{c0}/N_0$ is cool to hot electron density ratio, $T_{eff} = T_c/(f+(1-f)\tau)$ is an effective electron temperature $\alpha_c = T_{eff}/T_c$, $\alpha_h = T_{eff}/T_h$, $\alpha = \sin\theta$, $\gamma = \cos\theta$; θ is the angle between the direction of wave propagation and the magnetic field and $\psi = e\phi/T_{eff}$.

Thus, the equations (3.1) - (3.4) in normalized form can be written as

$$n_c = f\exp(\alpha_c\psi). \tag{3.7}$$

$$n_h = (1-f)\exp(\alpha_h\psi). \tag{3.8}$$

$$\frac{\partial n_i}{\partial t} + \nabla.(n_i v_i) = 0. \tag{3.9}$$

$$\frac{\partial v_i}{\partial t} + v_i\nabla v_i = -\nabla\psi + \mathbf{v}_i \times \hat{\mathbf{z}}. \tag{3.10}$$

Further, the equations (3.9)-(3.10) in component form can be written as

$$\frac{\partial n_i}{\partial t} + \frac{\partial(n_i v_x)}{\partial x} + \frac{\partial(n_i v_z)}{\partial z} = 0. \tag{3.11}$$

$$\frac{\partial v_x}{\partial t} + \left(v_x\frac{\partial}{\partial x} + v_z\frac{\partial}{\partial z}\right)v_x = -\frac{\partial\psi}{\partial x} + v_y, \tag{3.12}$$

$$\frac{\partial v_y}{\partial t} + \left(v_x \frac{\partial}{\partial x} + v_z \frac{\partial}{\partial z} \right) v_y = -\frac{\partial \psi}{\partial y} - v_x, \tag{3.13}$$

$$\frac{\partial v_y}{\partial t} + \left(v_x \frac{\partial}{\partial x} + v_z \frac{\partial}{\partial z} \right) v_z = -\frac{\partial \psi}{\partial z} - v_z, \tag{3.14}$$

moving to a stationary frame using the transformation $\xi = (\alpha x + \gamma z - Mt)/M$, where $M = V/c_s$ is the Mach number, equations (3.11)-(3.14) become

$$\frac{d}{d\xi}(L_v n_i) = 0. \tag{3.15}$$

$$L_v \frac{dv_x}{d\xi} = -\alpha \frac{d\psi}{d\xi} + M v_y. \tag{3.16}$$

$$L_v \frac{dv_y}{d\xi} = -M v_x. \tag{3.17}$$

$$L_v \frac{dv_z}{d\xi} = -\gamma \frac{d\psi}{d\xi}. \tag{3.18}$$

where $L_v = -M + \alpha v_x + \gamma v_z$. Our system of equations is closed with the quasi-neutrality condition (which is justified in the study of low frequency phenomena)

$$n_i = n_c + n_h = f \exp(\alpha_c \psi) + (1 - f) \exp(\alpha_h \psi) \tag{3.19}$$

Solving the coupled equations (3.15)-(3.19) and using appropriate boundary conditions for solitary wave structures (namely, $n_i \to 1$, $\psi \to 0$, and $d\psi/d\xi \to 0$ at $\xi \to \pm\infty$), and eliminating v_x, v_y, and v_z, we can reduce (3.15)-(3.19) to an energy integral (see Appendix A for the details) given by

$$\frac{1}{2} \left(\frac{d\psi}{d\xi} \right)^2 + V(\psi, M) = 0 \tag{3.20}$$

where $V(\psi, M)$ is the Sagdeev potential (cf. Section 2.4), given by

$$V(\psi,M) = -\frac{1}{\left(1-M^2\left(\frac{\alpha_c f\exp(\alpha_c\psi)+\alpha_h(1-f)\exp(\alpha_h\psi)}{(f\exp(\alpha_c\psi)+(1-f)\exp(\alpha_h\psi))^3}\right)\right)^2}\left(-\frac{M^4}{2n_i^2}(1-n_i)^2\right.$$
$$-M^2(1-\gamma^2)\psi + M^2\left(\frac{f}{\alpha_c}(\exp(\alpha_c\psi)-1)+\frac{(1-f)}{\alpha_h}(\exp(\alpha_h\psi)-1)\right)$$
$$-\frac{\gamma^2}{2}\left(\frac{f}{\alpha_c}(\exp(\alpha_c\psi)-1)+\frac{(1-f)}{\alpha_h}(\exp(\alpha_h\psi)-1)\right)^2$$
$$\left.-M^2\gamma^2\left(\frac{\frac{f}{\alpha_c}(\exp(\alpha_c\psi)-1)+\frac{(1-f)}{\alpha_h}(\exp(\alpha_h\psi)-1)}{f\exp(\alpha_c\psi)+(1-f)\exp(\alpha_h\psi)}\right)\right). \tag{3.21}$$

The ion density n_i in the above equation is given by equation (3.19). Equation (3.20) can be regarded as an "energy integral" of an oscillating particle of unit mass, with the velocity $d\psi/d\xi$ and the position ψ in a potential $V(\psi, M)$. We now look for the solitary wave solutions of (3.20).

3.1.2 Soliton and double layers characteristics

In order to obtain soliton solutions of equation (3.21), the Sagdeev potential $V(\psi, M)$ must satisfy the soliton conditions (cf. Section 2.3.2): $V(\psi, M) = 0$, $d\psi/d\xi = 0$, $V(\psi, M) = 0$ and $dV(\psi, M)/d(\psi) = 0$ at $\psi = 0$. $d^2V(\psi, M)/d(\psi)^2 < 0$ at $\psi = 0$; $V(\psi, M) = 0$ at $\psi = \psi_m$, $dV(\psi, M)/d(\psi) < (>)\ 0$ at $\psi_m < (>)\ 0$. Then, for the formation of a double layer, one more additional condition must be satisfied, i.e, $\frac{dV(\psi,M)}{d\psi}|_{\psi=\psi_m} = 0$. It can be seen from (3.21) that $V(\psi, M) = dV(\psi, M)/d\psi = 0$ at $\psi = 0$.

The soliton condition $\mathrm{d}^2V(\psi, M)/\mathrm{d}\psi^2 < 0$ at $\psi = 0$ can be written as

$$\frac{d^2V(\psi,M)}{d\psi^2}|_{\psi=0} = \frac{M^2-M_0^2}{M^2-M_1^2} < 0 \tag{3.22}$$

where

$$M_0^2 = \frac{\gamma^2}{f\alpha_c+\alpha_h(1-f)} = \gamma^2. \tag{3.23}$$

is the critical Mach number and

$$M_1^2 = \frac{1}{f\alpha_c + \alpha_h(1-f)} = 1 \tag{3.24}$$

since $f\alpha_c + \alpha_h(1-f) = 1$.

For $\gamma \neq 0 : M_o^2 < 1(= M_1^2) \Rightarrow M_o < M_1$, then if $M > M_1 \Rightarrow M > M_0$ from which $M^2 - M_o^2 > 0$ and $M^2 - M_1^2 > 0$, consequently (3.22) is not satisfied.

Similarly, if $M < M_0 \Rightarrow M < M_1$ from which $M^2 - M_o^2 < 0$ and $M^2 - M_1^2 < 0$, once again (3.22) is not satisfied.

Therefore, (3.22) is satisfied only if

$$M_0 < |M| < M_1 \tag{3.25}$$

From equation (3.23) to (3.25), we obtain for oblique angles of propagation ($\theta \neq 0^o$) the condition

$$\gamma < |M| < 1 \tag{3.26}$$

which gives allowed values of Mach number M for a given angle of propagation of solitary waves for fixed values of plasma parameters f, α_c and α_h. It is interesting to note that in the magnetized plasma case, the ion-acoustic solitons and double layer can exist only in the subsonic Mach number region as seen from (3.26). On the other hand, for the case of unmagnetized plasma consisting of cold ions and two-temperature Boltzmann electrons, ion-acoustic solitons and double layers were found exist only in the supersonic Mach number regime (Berthomier et al. 1998), i.e., $M > 1$.

Next, we numerically solve the equation (3.20) with the Sagdeev potential $V(\psi, M)$ given by (3.21) for different parameters such as M, f, θ and τ. The figure 3.1 shows the Sagdeev potential $V(\psi, M)$ vs real potential ψ for different values of M for other fixed parameters namely, cool to hot electron temperature ratio, $\tau = T_c/T_h = 0.04$, cool electron number density, $f = N_{c0}/N_0 = 0.1$ and angle of propagation, $\theta = 15^o$. The corresponding soliton potential ψ against ξ, which has been obtained by numerically integrating equation (3.20) for the same parameters, are shown in Figure 3.2. As the Mach number increases, the soliton amplitude increase is accompanied by a decrease in soliton width. It is seen that the negative potential ion acoustic soliton amplitude ψ increases with increasing M. Further, our computation reveals that soliton solutions are not found for $M > 0.9994$. This conforms very well to the upper Mach number

limit $M < 1$ obtained analytically (cf. equation (3.26)). Only soliton solutions can be found, no double layer solution exists in the Mach number regime. Unlike the case of an unmagnetized plasma reported by Berthomier et al. 1998, negative potential solitons and double layers were found exist only in the supersonic Mach number regime. Also Baluku et al. 2010 found positive potential solitons and double layer solutions for $M > 1$.

Figure 3.3 shows the variation of the Sagdeev potential versus real potential ψ for different values of cool electron number density $f{=}N_{co}/N_o$. The other fixed parameters are $\tau = 0.04$, $\theta = 15^o$, and $M = 0.98$. It is observed that as the cold electron density increases (f increasing), the soliton amplitude increases. Numerical computations show that the soliton solutions are not possible beyond $f > 0.35$. This is consistent with Fig. 2(b) of Baboolal et al. 1990, where they showed that negative solitons and double layers exist for cold electron density ratio f roughly between 0.02 and 0.35. Figure 3.4 shows the soliton potential ψ against ξ, for the same parameters used in Figure 3.3. It is seen that as f increases, the ion-acoustic soliton potential amplitude increases and the width also increases. The latter variation is different from that for the Mach number M variation, where the amplitude increases but the width decreases with M. In the Mach number case the curves are reducing in the width.

The curves in Figure 3.5 show that as the angle of propagation θ increases (obliquity increases), the soliton amplitude increases. The effect of oblique propagation on electrostatic solitary waves have been studied in low frequency plasma extensively, using a single electron-ion plasma model (Bharuthram et al. 2002; Choi et al. 2006; Qureshi et al. 2010; Barman and Talukdar, 2010; Mushtaq, 2010), two electron temperature plasma model (Bharuthram and Shukla, 1985, 1986; Ghosh and Lakhina, 2003) and a dust plasma model (Farid et al. 2001). The chosen parameters are the normalized cool electron density $f = 0.1$, and the other parameters are the same as for Figure 3.3. It is interesting to note that at $\theta = 38.0425^o$ a double layer structure appears (cf. Section 1.3.2 and Section 2.4.1). For $\theta > 38.0425^o$ there are no soliton or double layer solutions. Thus the double layer potential represents the upper boundary for the range of possible soliton solutions. Figure 3.6 shows the corresponding real potential ψ against ξ, for the parameters used in Figure 3.5. It is seen from the curves that as we increase the propagation angle θ, the amplitude as well as width of the solitons increase until the double layer boundary, which is also plotted.

Figure 3.7 shows the variation of the Sagdeev potential with real potential ψ for different values of the cool to hot electron temperature ratio $\tau = T_c/T_h$ for $\theta = 15^0$. Other fixed parameters are the same as for figure 3.5. It is seen that the soliton amplitude increases with the increase in cool to hot electron temperature ratio, i.e. as the temperature of the cool electrons increase relative to the hot electrons. It must be pointed out that, in this case as well, a double layer solution as an upper bound has been found to exist for $\tau = 0.0877117$. Many authors have showed that no negative potential soliton and double layer solutions are possible for electron temperature ratio τ getting closer to 1 (Nishihara and Tajiri, 1981; Baboolal et al. 1990; Baluku et al. 2010). The corresponding ψ against ξ curves are shown in Figure 3.8. We observe that as the cool to hot electron temperature ratio τ increases, the amplitude as well as width of the soliton increases, until a double layer solution is found.

Figure 3.9 shows the variation of the Sagdeev potential with real potential correspond to the double layer solutions for different values of θ and M. Other fixed parameters are $f = 0.1$, and $\tau = 0.04$. The curves show all combinations of (θ, M) yield exactly the same value for the double layer amplitude. This corresponds to a "point" solution as found in a study by Djebli and Marif (2009). Figures 3.10 shows the existence domain of solitons and double layers for the fixed parameters in Figure 3.9. The curves show that a double layer solution is the upper bound for soliton solution as we increase the angle of propagation θ, for different M values. The maximum Mach number for negative potential solitons are bounded by those of the double layer solutions corresponding to a given θ value.

Figure 3.11 shows the variation of the Sagdeev potential $V(\psi, M)$ against the normalized potential ψ for different values of the cool to hot electron temperature ratio τ and the Mach number M for the fixed parameters $f = 0.1$ and $\theta = 15^o$. It is interesting to point out that the supersoliton (A new class of solitary waves known as super-nonlinear solitons reported by several authors, e.g. Dubinov and Kolotkov, 2012; Verheest et al. 2013; Maharaj et al. 2013) solution has been found to exist for $\tau = 0.095143$ and $M = 0.97$, $\tau = 0.0877117$ and $M = 0.98$, $\tau = 0.082394892$ and $M = 0.99$. In this case, a series of soliton solutions have an upper bound represented by a double layer, which is immediately coupled to a (super) soliton. In a recent paper by Verheest et al. 2013, they stated that the associated electric field signatures of supersolitons should be observable in available or future space and laboratory observations in three-component plasmas (e.g. Cluster spacecraft measurements (Pickett et al. 2004) shows a supersoliton electric field wedged between

two regular bipolar structures. Also, in the laboratory experiments, these should appear as "distorted" bipolar electric field forms, which may be resolved, e.g., via proton imaging (Romagnani et al. 2008), among other techniques). Figure 3.12 shows the existence domain of solitons, double layers and supersolitons for the same parameters in Figure 3.11. The curves were plotted for the variation of the maximum electrostatic potential ψ_{Max} against τ for different values of the Mach number M. In an unmagnetized plasma consisting of positive and negative ions and two electron temperature, Baboolal et al. (1990) showed the existence domain for compressive and rarefaction solitons bounded by negative potential double layer solutions. The reason for smaller amplitudes for larger $\tau=\frac{T_c}{T_h}$ can be seen from the expression for the effective temperature $T_{eff} = T_c/(f + (1 - f)\tau)$, which shows that for fixed f the normalization factor T_{eff} decreases with increasing τ so that the corresponding normalized potential ψ would linearly increase in magnitude. Similar behavior has been reported by Baboolal (1988).

3.1.3 Discussion

We have shown the existence of nonlinear ion-acoustic solitary waves and double layers in a magnetized plasma with two-temperature electron species and cold ions. The chosen plasma model supports negative potential ion-acoustic solitons and double layers, and they are found to exist only in the subsonic (i.e., $M < 1$) Mach numbers regime. In contrast, as shown by Berthomier et al. (1998), for the case of an unmagnetized plasma these negative potential nonlinear structures can exist only in the supersonic (i.e., $M > 1$) Mach number regime. We have shown that the amplitude of the ion-acoustic solitary waves increases with the Mach number, increased obliquity and cool electron number density.

In determining the relevance of our results to space plasmas, we apply our results to the negative potential ion-acoustic solitary waves observed by the Viking satellite in the auroral region of the Earth's magnetosphere. Berthomier et al. (1998) have reported ion-acoustic solitary structures in the auroral region with electric field amplitude of less than 100 mV/m, width of about 100 m, pulse duration of about 20 ms and soliton velocities in the range of $\approx 10 - 50$ km/s. For illustrative purposes we have taken the following parameters from the Viking observations (Berthomier et al 1998), namely, $n_c = 0.2$ cm^{-3}, $n_h = 1.8$ cm^{-3}, $T_c = 1$ eV, $T_h = 26$ eV which gives $T_{eff} \approx 7$ eV. The maximum electric field for $M = 0.98$, $\theta = 35^0$ for our model comes

out to be 49 mV/m and corresponding soliton width, pulse duration and speed comes out to be ≈ 270 m, 10 ms and 26 km/s, respectively. Thus, our results are in strong agreement with the Viking observations.

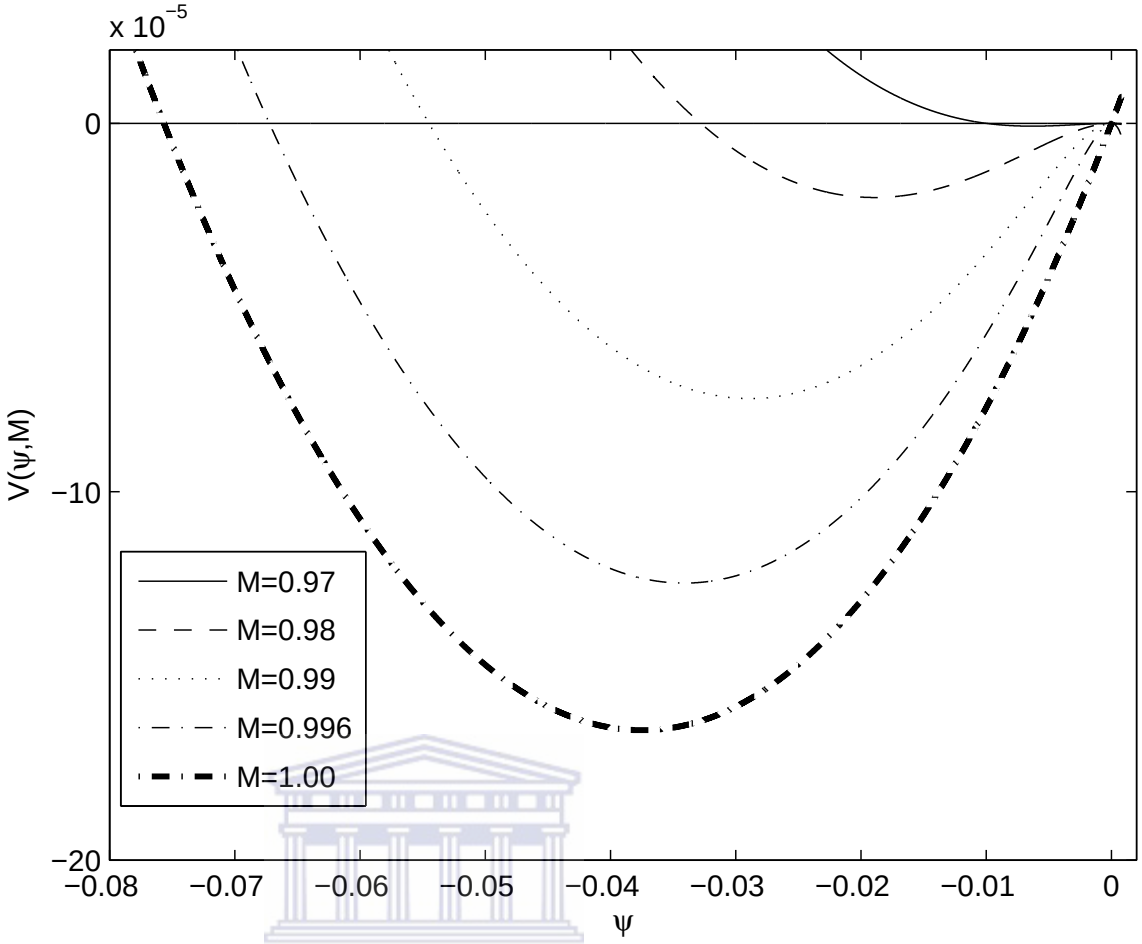

Figure 3.1: Sagdeev potential, $V(\psi, M)$ vs normalized electrostatic potential ψ. The parameters are τ= 0.04, f=0.1, θ=15^o and M= 0.97, 0.98, 0.99, 0.996, 1.00 (no solution).

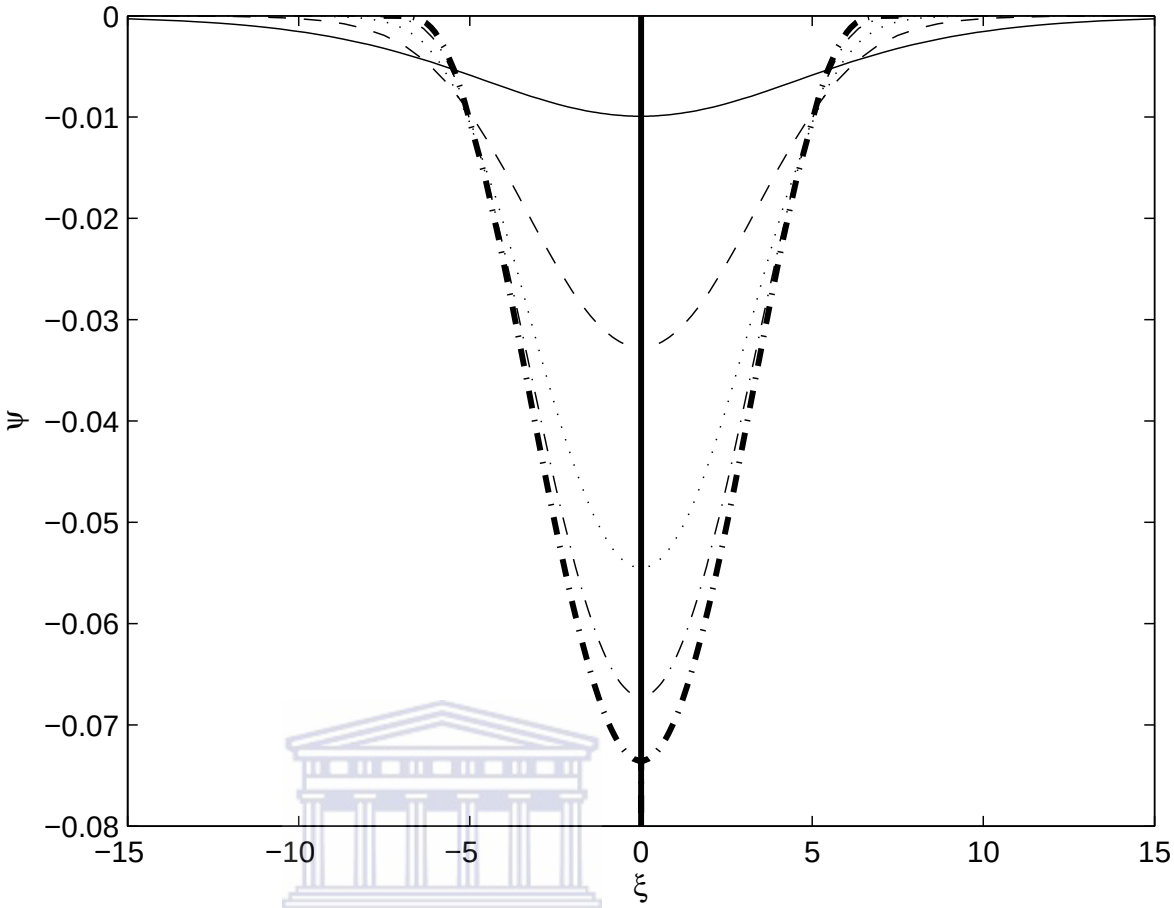

Figure 3.2: Electrostatic potential ψ vs ξ. The parameters of Figure 3.2 and M=0.97 (—), 0.98 (- - -), 0.99 (...), 0.996 (- . -) and 0.999 (—.—).

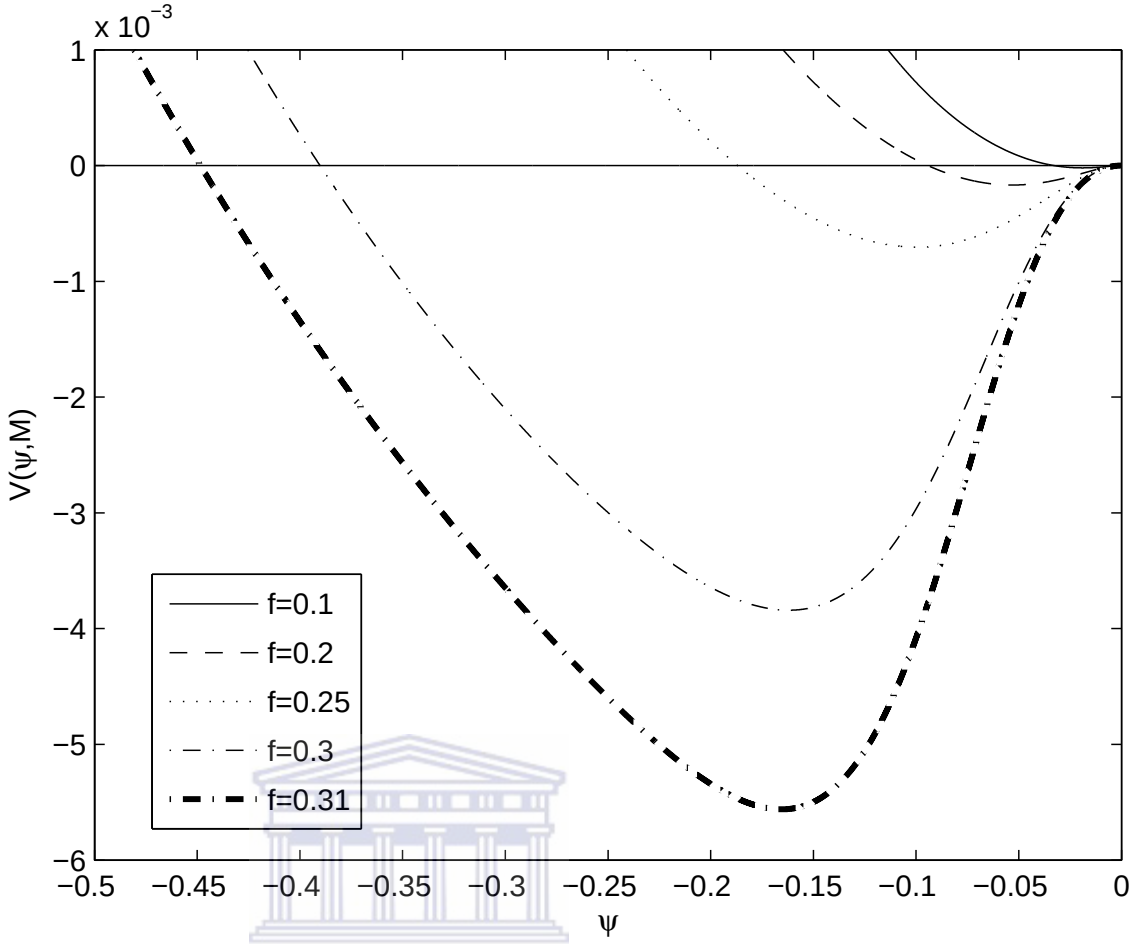

Figure 3.3: Sagdeev potential, $V(\psi, M)$ vs normalized electrostatic potential ψ. The parameters are τ= 0.04, θ=15^o, M=0.98 and f=0.1, 0.2, 0.25, 0.3, 0.31.

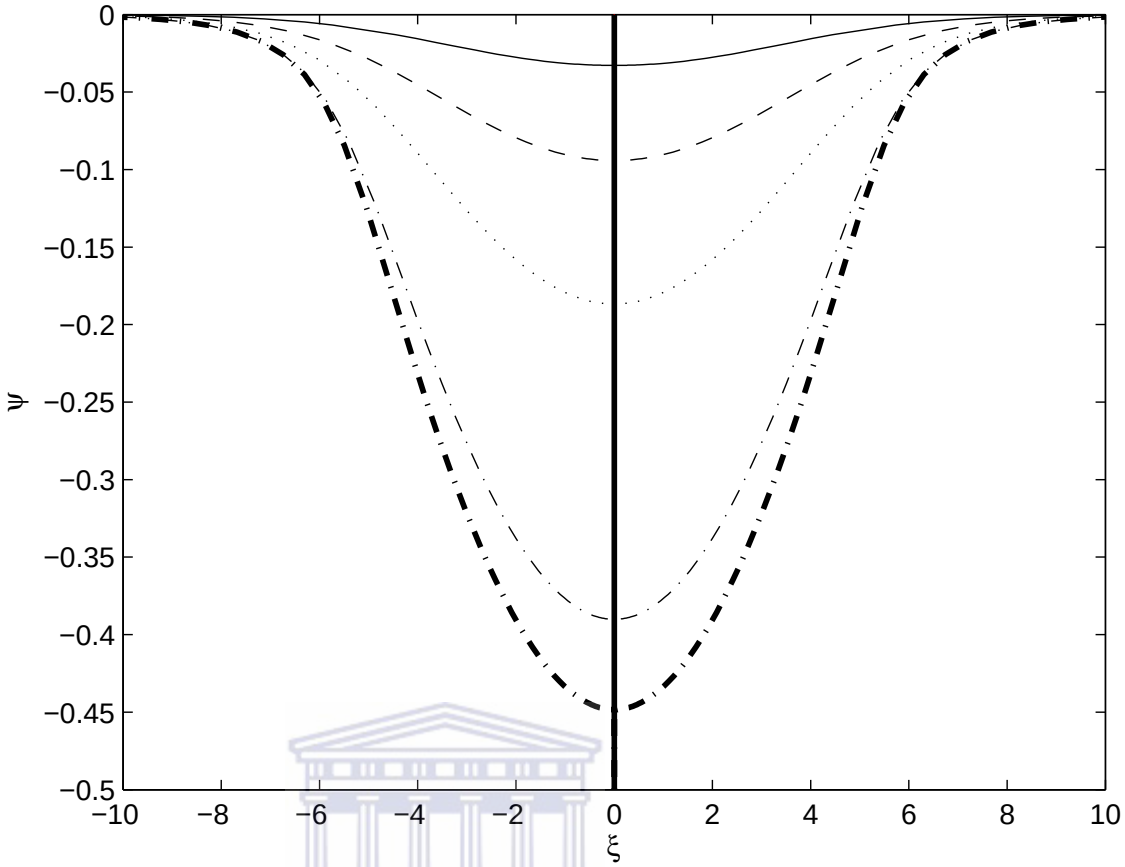

Figure 3.4: Electrostatic potential ψ vs ξ. The parameters of Figure 3.3 and f=0.1 (—), 0.2 (- - -), 0.25 (...), 0.3 (- . -) and 0.31 (—•—).

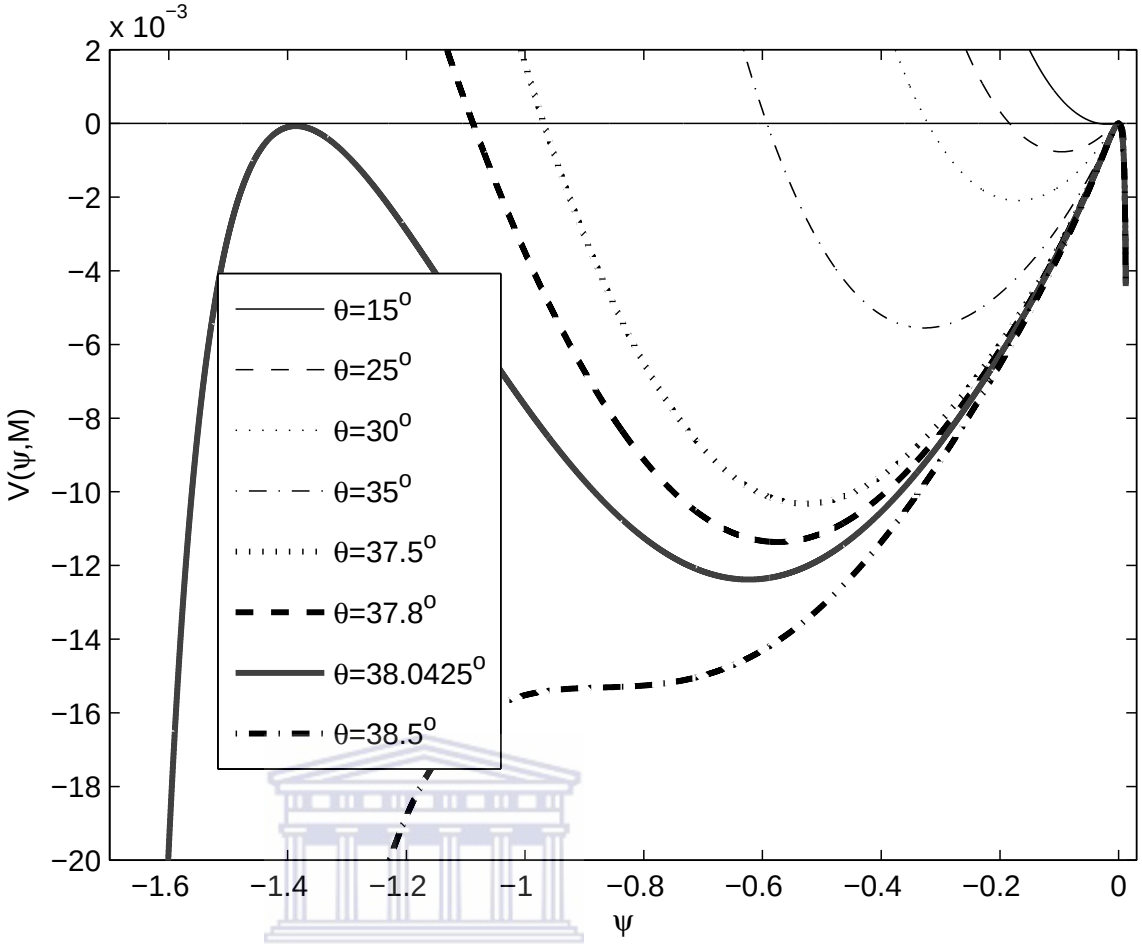

Figure 3.5: Sagdeev potential, $V(\psi, M)$ vs normalized electrostatic potential ψ. The parameters are τ= 0.04, f=0.1, M=0.98 and θ=15^o, 25^o, 30^o, 35^o, 37.5^o, 37.8^o, 38.0425^o(double layer), 38.5^o.

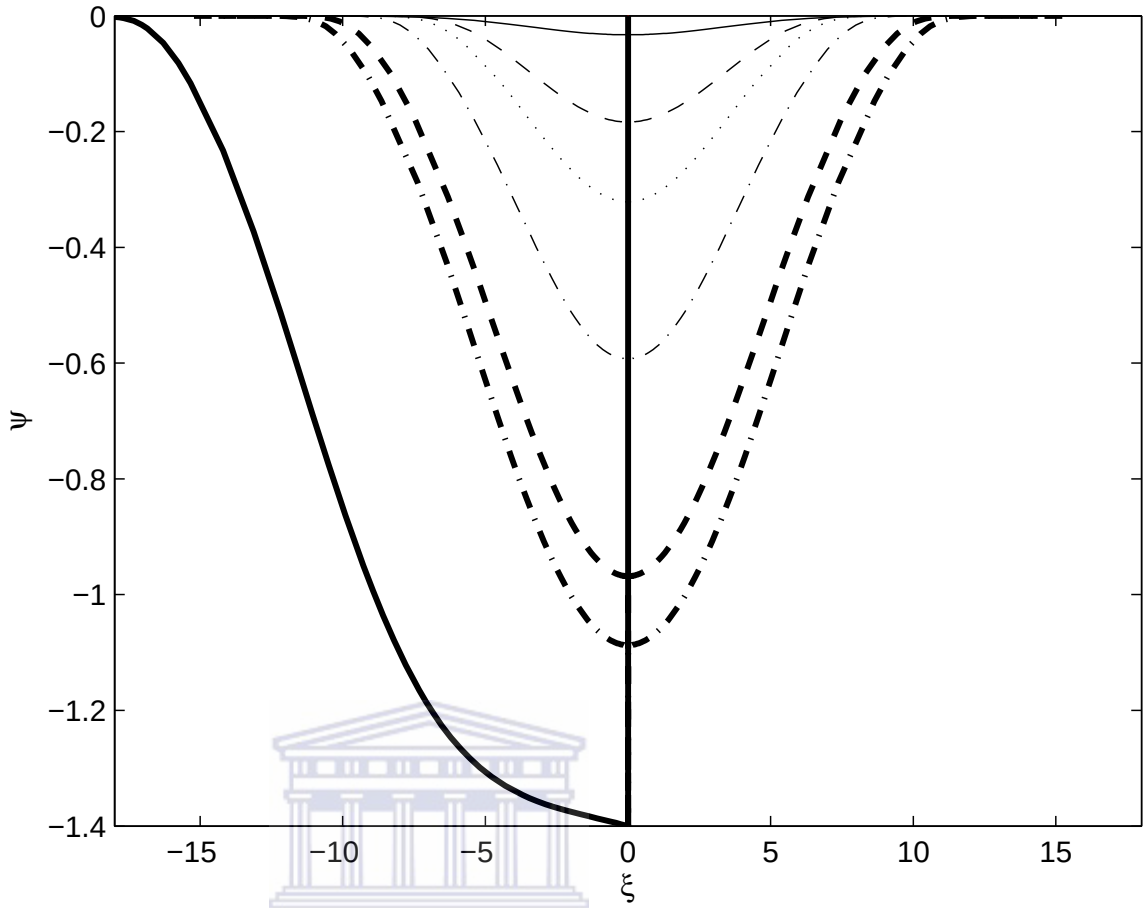

Figure 3.6: Electrostatic potential ψ vs ξ. The parameters of Figure 3.5 and θ=15^o (—), 25^o (- - -), 30^o (...), 35^o (- . -), 37.5^o (— — —), 37.8^o (—.—), 38.0425^o(—) for double layer .

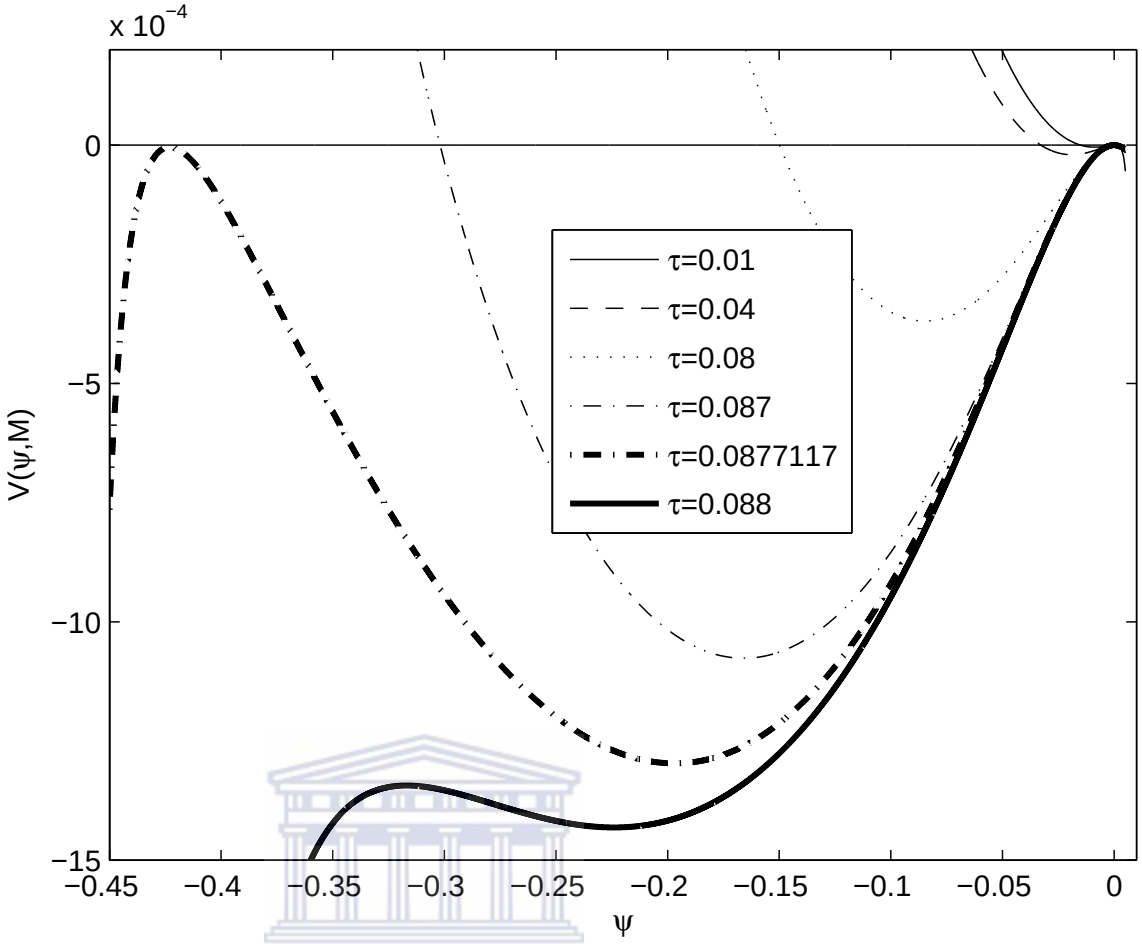

Figure 3.7: Sagdeev potential, $V(\psi, M)$ vs normalized electrostatic potential ψ. The parameters are f= 0.1, θ=15^o, M=0.98 and τ=0.01, 0.04, 0.08, 0.087, 0.0877117(double layer), 0.088.

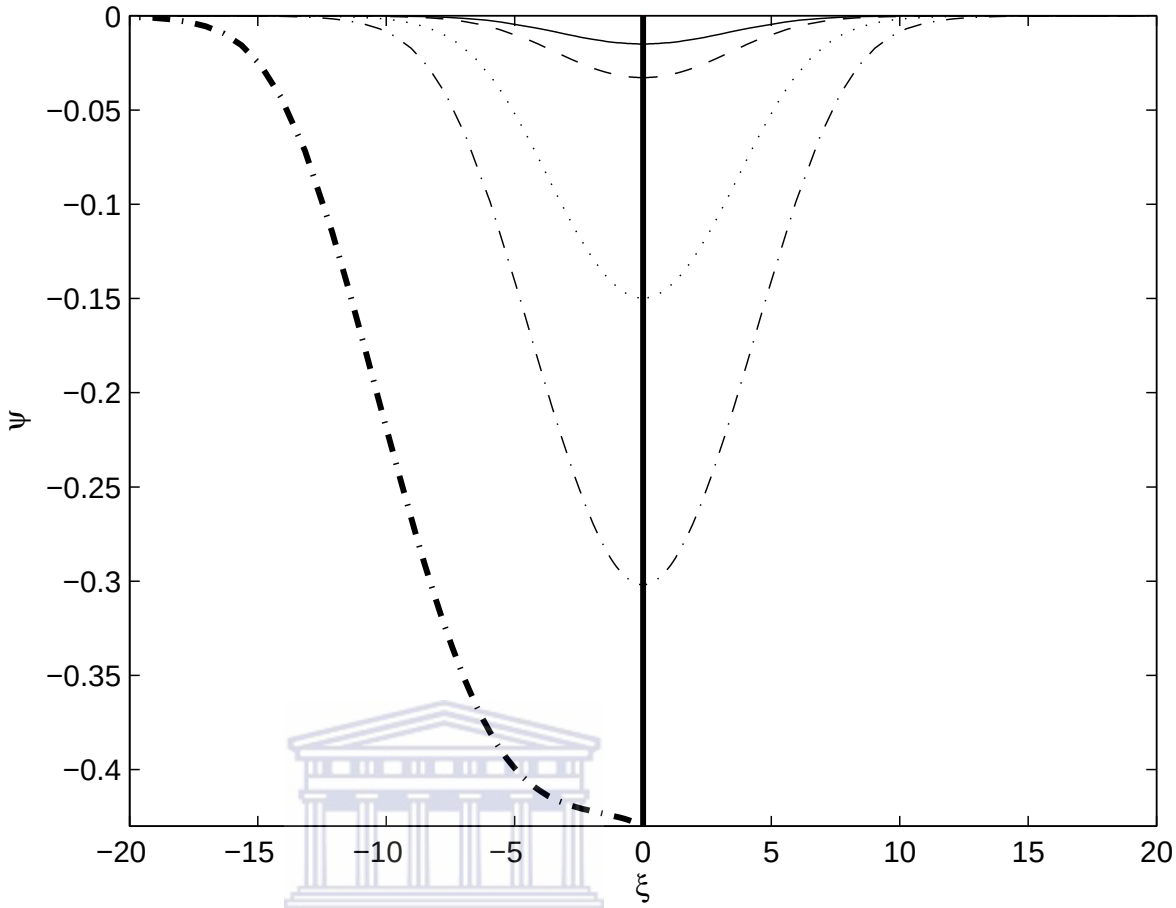

Figure 3.8: Electrostatic potential ψ vs ξ. The parameters of Figure 3.7 and τ=0.01 (—), 0.04 (- - -), 0.08 (...), 0.087 (- . -) and 0.0877117 (—.—).

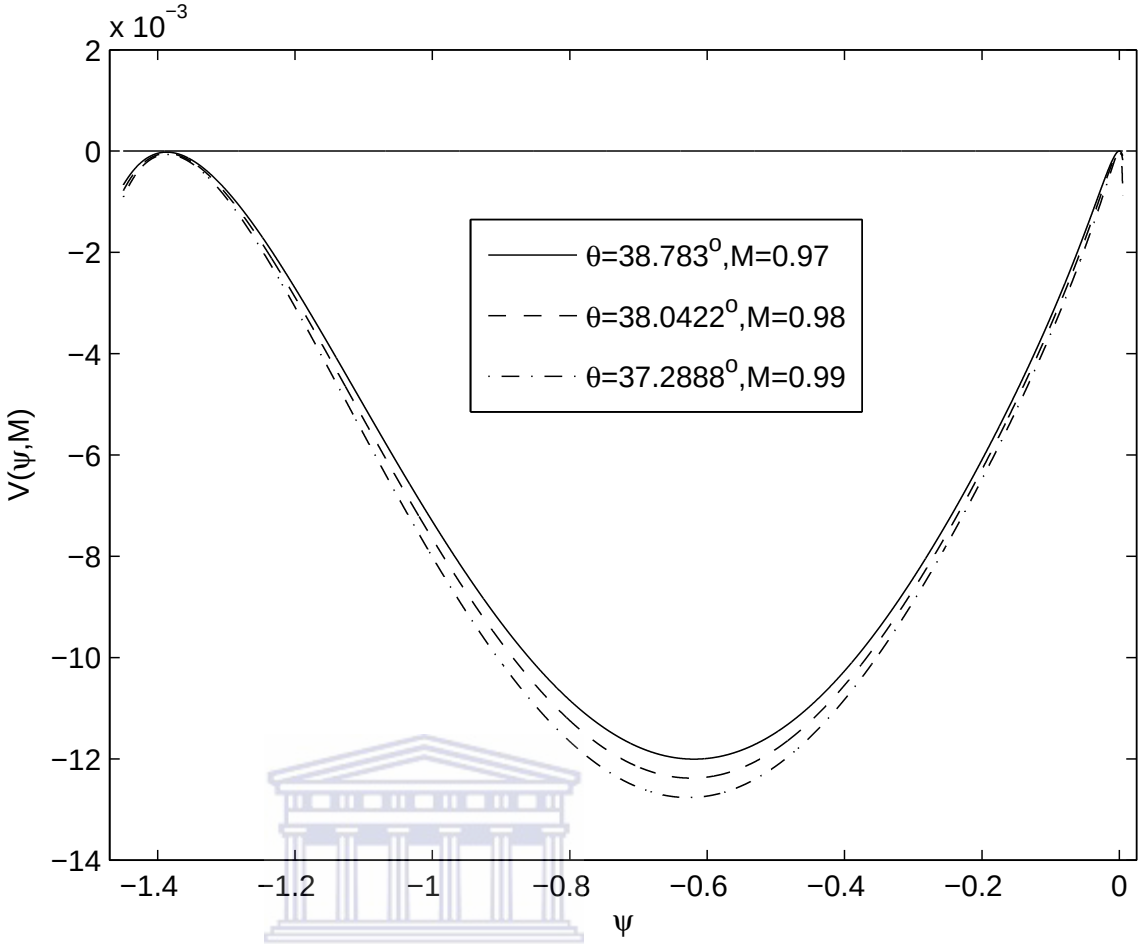

Figure 3.9: Sagdeev potential, $V(\psi, M)$ vs normalized electrostatic potential ψ. The fixed parameters are τ= 0.04, f=0.1 for θ=38.783^o and M=0.97, θ=38.0422^o and M=0.98, θ=37.2888^o and M=0.99.

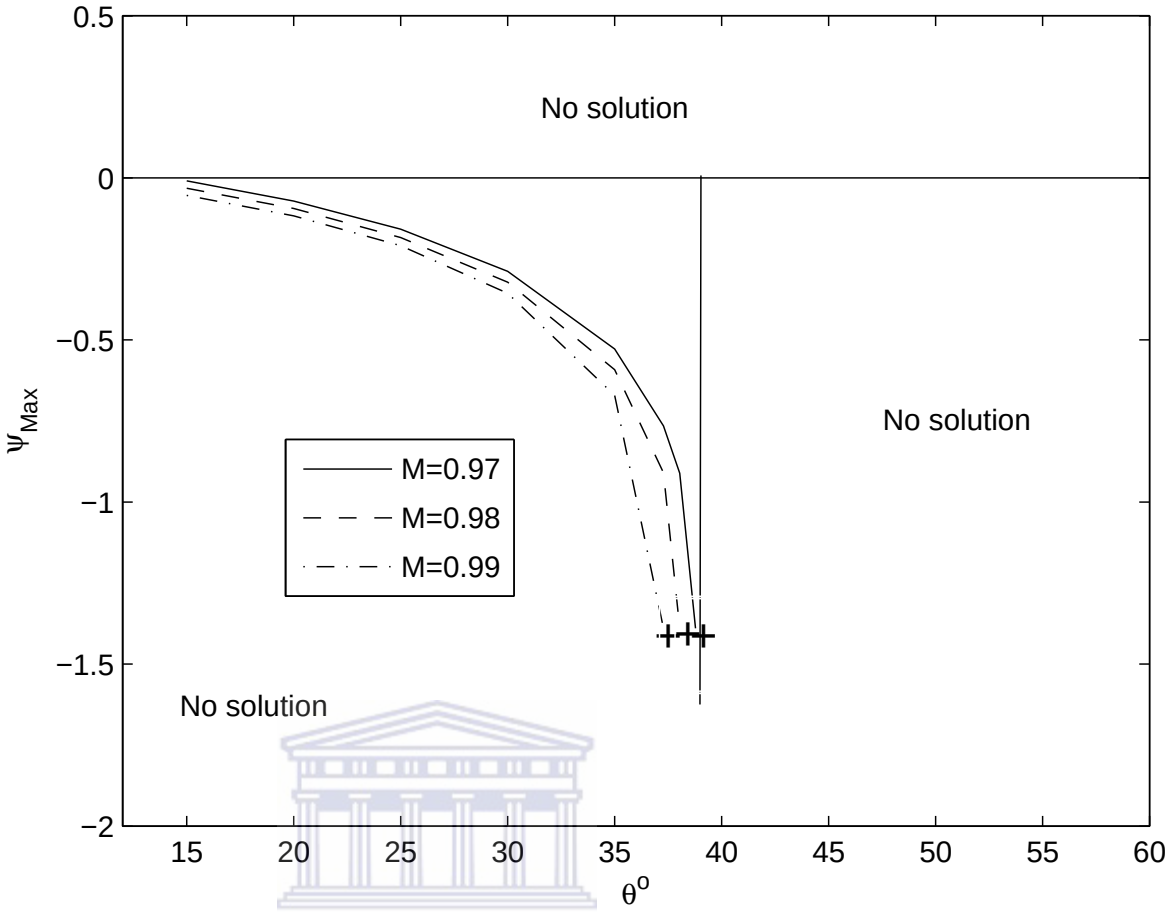

Figure 3.10: The existence domain of soliton for the parameters of Figure 3.9. The upper bound for soliton solution with increasing θ is a double layer, shown as an $''+$".

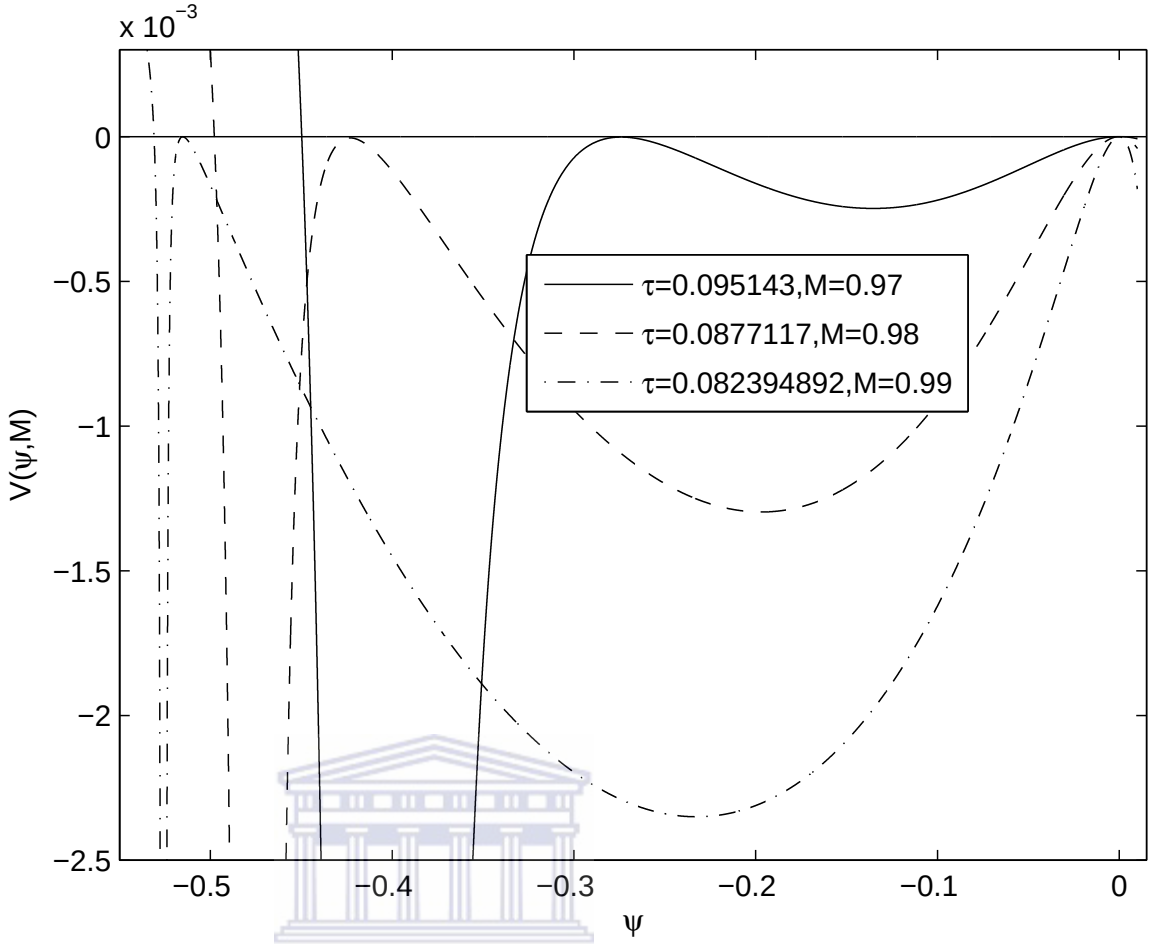

Figure 3.11: Sagdeev potential, $V(\psi, M)$ vs normalized electrostatic potential ψ. The fixed parameters are f= 0.1, θ=15^o for τ=0.095143 and M=0.97, τ=0.0877117 and M=0.98, τ=0.082394892 and M=0.99.

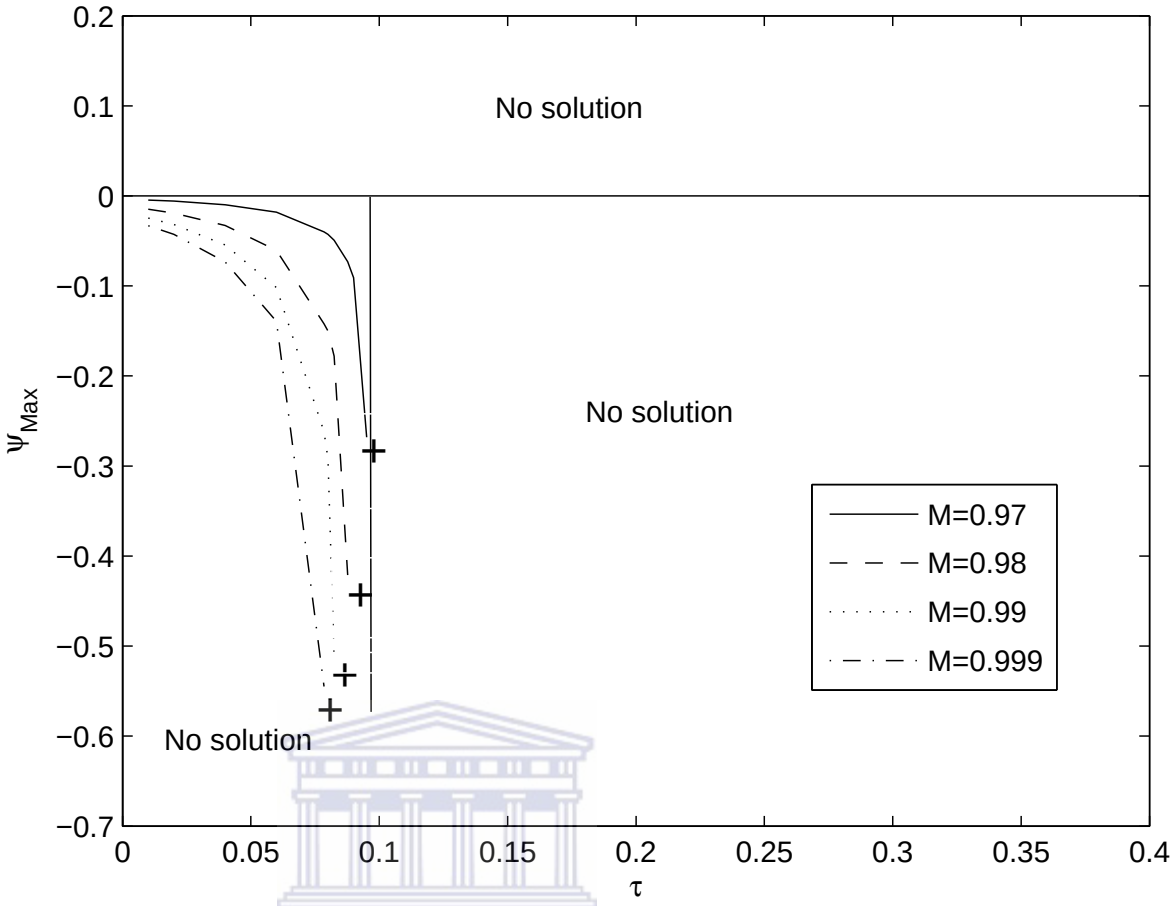

Figure 3.12: The maximum electrostatic potential ψ_{Max} against τ. The parameters of Figure 3.11 and τ=0.095143 and M=0.97, τ=0.0877117 and M=0.98, τ=0.082394892 and M=0.99.

This Section has been published in Physics of Plasmas.

O. R. Rufai, R. Bharuthram, S. V. Singh, and G. S. Lakhina
Low frequency solitons and double layers in a magnetized plasma with two temperature electrons, Physics of Plasmas, ***19****, 122308, 2012. http://dx.doi.org/10.1063/1.4771574.*

3.2 Model 2: Magnetized plasma with an adiabatic ions and two-Boltzmann electrons

In Model 1 we assumed the ions to be cold. In order to investigate the effect of temperature for the ions, we extend Model 1 to include a finite temperature of the ions. i.e. $T_i \neq 0$. This results in a modification to the momentum equation (3.4) as well as the inclusion of the ion pressure balance equation, as shown below.

3.2.1 Basic equations

Our basic set of equations for the inclusion of a finite ion temperature is identical to the set of equations (3.3) - (3.4), with a modification to equation (3.4) as given below

$$\left(\frac{\partial}{\partial t} + \mathbf{V_i}.\nabla\right)\mathbf{V_i} == -\frac{e\nabla\phi}{m_i} + e\frac{\mathbf{V}_i \times \mathbf{B}_o}{m_i c} - \frac{1}{n_i m_i}\nabla P_i. \tag{3.27}$$

In addition, we include the ion pressure balance equation

$$\frac{\partial P_i}{\partial t} + \mathbf{V}_i.\nabla P_i + \delta P_i \nabla \mathbf{V}_i = 0, \tag{3.28}$$

where n_i, $\mathbf{V}_i$ and m_i are the number density, fluid velocity and mass of the ions, e is the magnitude of the electron charge, c is the speed of the light in vacuum and the ion pressure P_i is given by the balance pressure equation (3.28). Further, ion pressure can be written as

$$P_i = P_{io}\left(\frac{N_i}{N_{io}}\right)^{\delta}, \tag{3.29}$$

where $\delta = \frac{(N+2)}{N}$ is the adiabatic index. N is the number of degrees of freedom. For magnetized adiabatic ions $N = 3$, hence $\delta = \frac{5}{3}$ and the ion pressure at equilibrium is $P_{io} = N_{io}T_i$.

For the three species of plasma, the quasi-neutrality condition at equilibrium is given by $N_{io} = N_{co} + N_{ho} = N_o$. We normalize the variables as we did in Model 1, with $T_{eff} = T_c/(f + (1-f)\tau)$ as the effective electron temperature, $\alpha_c = T_{eff}/T_c$, $\alpha_h = T_{eff}/T_h$, and $\sigma = T_i/T_{eff}$, where T_i is the ion temperature.

Then the normalized set of equations become,

$$n_c = f\exp(\alpha_c\psi). \tag{3.30}$$

$$n_h = (1-f)\exp(\alpha_h\psi). \tag{3.31}$$

$$\frac{\partial n_i}{\partial t} + \frac{\partial (n_i v_x)}{\partial x} + \frac{\partial (n_i v_z)}{\partial z} = 0. \tag{3.32}$$

$$\frac{\partial v_x}{\partial t} + \left(v_x\frac{\partial}{\partial x} + v_z\frac{\partial}{\partial z}\right)v_x = -\frac{\partial \psi}{\partial x} + v_y - \frac{\sigma}{n_i}\frac{\partial}{\partial x}.(n_i)^{5/3}, \tag{3.33}$$

$$\frac{\partial v_y}{\partial t} + \left(v_x\frac{\partial}{\partial x} + v_z\frac{\partial}{\partial z}\right)v_y = -\frac{\partial \psi}{\partial y} - v_x, \tag{3.34}$$

$$\frac{\partial v_z}{\partial t} + \left(v_x\frac{\partial}{\partial x} + v_z\frac{\partial}{\partial z}\right)v_z = -\frac{\partial \psi}{\partial z} - \frac{\sigma}{n_i}\frac{\partial}{\partial z}.(n_i)^{5/3}. \tag{3.35}$$

The above set of the equations is closed with the quasi-neutrality condition

$$n_i = n_c + n_h = f\exp(\alpha_c\psi) + (1-f)\exp(\alpha_h\psi). \tag{3.36}$$

3.2.2 Localized stationary solution

As before, for arbitrary amplitude treatment we look for soliton structures in a reference frame moving with the wave, i.e. with the Mach number. Assuming that all the dependent variables depend on a single independent variable ξ such that,

$$\xi = (\alpha x + \gamma z - Mt)/M \tag{3.37}$$

where $M = V/c_s$, and $V = \omega/k$ is the wave speed and $\alpha = \sin\theta$, $\gamma = \cos\theta$; θ is the angle of the wave propagation relative to $\vec{B}_0$.

Transforming the ion fluid equations in terms of the coordinate ξ and integrating with appropriate boundary conditions for solitary wave structure (namely, $n_i \to 1$, $\psi \to 0$, and $d\psi/d\xi \to 0$ at $\xi \to \pm\infty$), we obtain a single dimensionless nonlinear differential equation in terms of the ion density n_i and electrostatic potential ψ as,

$$\frac{d}{d\xi}\left(\frac{d\chi(\psi)}{d\xi}\right) = M^2(n_i-1)+\gamma^2\sigma n_i(1-n_i^{5/3})-\gamma^2 n_i\left(\frac{f}{\alpha_c}(e^{\alpha_c\psi}-1)+\frac{1-f}{\alpha_h}(e^{\alpha_h\psi}-1)\right), \tag{3.38}$$

where

$$\chi(\psi) = \left(\psi + \frac{M^2}{2n_i^2} + \frac{5}{2}\sigma n_i^{2/3}\right) \tag{3.39}$$

with n_i given by equation (3.37).

Now multiplying both sides of equation (3.38) by $d\chi/d\xi$ and integrating once with appropriate boundary conditions (see Appendix B for the details), we obtain

$$\frac{1}{2}\left(\frac{d\chi(\psi)}{d\xi}\right)^2 + V(\psi, M) = 0. \tag{3.40}$$

From equations (3.39) and (3.40), we obtain the following energy integral

$$\frac{1}{2}\left(\frac{d\psi}{d\xi}\right)^2 + V(\psi, M) = 0 \tag{3.41}$$

where $V(\psi, M)$ is the Sagdeev potential (cf. Section 2.4) and is given as

$$\begin{aligned} V(\psi, M) = &-\frac{1}{\left(1 - \frac{M^2}{n_i^3}\left(\alpha_c f e^{\alpha_c \psi} + \alpha_h(1-f)e^{\alpha_h\psi}\right) + \frac{5\sigma}{3n_i^{1/3}}\left(\alpha_c f e^{\alpha_c\psi} + \alpha_h(1-f)e^{\alpha_h\psi}\right)\right)^2} \times \\ &\left(-\frac{M^4}{2n_i^2}(1-n_i)^2 - M^2(1-\gamma^2)\psi + M^2 H(\psi) + M^2\sigma\left(n_i^{5/3} - \frac{5}{2}n_i^{2/3} + \frac{3}{2}\right)\right. \\ &+\gamma^2\sigma\left[H(\psi) + M^2\left(\frac{1}{n_i} + \frac{3}{2}n_i^{2/3} - \frac{5}{2}\right)\right] + \gamma^2\sigma^2\left(n_i^{5/3} - \frac{1}{2}n_i^{10/3} - \frac{1}{2}\right) \\ &\left.-\frac{\gamma^2}{2}H^2(\psi) - \frac{M^2\gamma^2}{n_i}H(\psi) - \gamma^2\sigma n_i^{5/3}H(\psi)\right) \end{aligned} \tag{3.42}$$

where n_i is given by (3.36) and

$$H(\psi) = \frac{f}{\alpha_c}(e^{\alpha_c\psi} - 1) + \frac{1-f}{\alpha_h}(e^{\alpha_h\psi} - 1). \tag{3.43}$$

In order to obtain the soliton solution from the energy integral equation (3.41), the Sagdeev potential given by (3.42) has to satisfy the soliton conditions in Section 2.3.2 (i.e. $V(\psi, M) = 0$, $d\psi/d\xi = 0$, $V(\psi, M) = 0$ and $dV(\psi, M)/d(\psi) = 0$ at $\psi = 0$. $d^2V(\psi, M)/d(\psi)^2 < 0$ at $\psi = 0$; $V(\psi, M) = 0$ at $\psi = \psi_m$, $dV(\psi, M)/d(\psi) < (>)\ 0$ at $\psi_m < (>)\ 0$. Then, for the formation of a double layer, one more additional condition must be satisfied, i.e, $\frac{dV(\psi,M)}{d\psi}|_{\psi=\psi_m} = 0$).

The condition $d^2V(\psi, M)/d\psi^2 < 0$ at $\psi = 0$ can be written as

$$\frac{d^2V(\psi, M)}{d\psi^2}|_{\psi=0} = \frac{M^2 - M_0^2}{M^2 - M_1^2} < 0 \tag{3.44}$$

where

$$M_o^2 = \gamma^2 \left(\frac{1}{f\alpha_c + \alpha_h(1-f)} + \frac{5\sigma}{3} \right) = \frac{\gamma^2(3+5\sigma)}{3} \tag{3.45}$$

is the critical Mach number and

$$M_1^2 = \frac{1}{f\alpha_c + \alpha_h(1-f)} + \frac{5\sigma}{3} = \frac{3+5\sigma}{3} \tag{3.46}$$

since $f\alpha_c + \alpha_h(1-f) = 1$.

Following the same analysis as in Section 3.1.2, i.e for $\gamma \neq 0 : \gamma^2 = \cos^2\theta < 1$; which implies $M_o < M_1$, then if $M > M_1 \Rightarrow M > M_0$ from which $M^2 - M_o^2 > 0$ and $M^2 - M_1^2 > 0$, consequently (3.44) is not satisfied.

Similarly, if $M < M_0 \Rightarrow M < M_1$ from which $M^2 - M_o^2 < 0$ and $M^2 - M_1^2 < 0$, once again (3.44) is not satisfied.

Therefore, (3.44) is satisfied only if

$$M_o < |M| < M_1. \tag{3.47}$$

From equation (3.45) and (3.46), the condition (3.47) can be written as

$$\gamma\sqrt{1 + \frac{5\sigma}{3}} < |M| < \sqrt{1 + \frac{5\sigma}{3}} \tag{3.48}$$

for $\theta \neq 0$, i.e. oblique angles of propagation to the magnetic field $\mathbf{B}_o$, which gives the Mach number range for fixed values of plasma parameters f, α_c, α_h and σ. It is noted that for cold ions, i.e. $\sigma = 0$, the conditions in equations (3.44 - 3.48) above, reduce to those in Model 1. In comparison to the earlier work, we observe from equation (3.46) that allowing for finite ion temperature ($\sigma \neq 0$) increases the upper limit of $|M|$ beyond 1, thereby allowing for supersonic solitons.

3.2.3 Numerical results

The Viking satellite has observed solitary potential structures with electric field amplitudes of ≈ 100 m V/m, width of about 100 m, pulse duration of about 20 ms, and potential solitary structures with a velocity range of $\approx 10 - 50$ km/s. For the numerical computation of equation (3.39), we choose plasma parameters of the dayside auroral zones corresponding to the observations which are as follows: cool electron density $n_{c0} = 0.2\ cm^{-3}$, hot electron density $n_{h0} = 1.8\ cm^{-3}$, cool electron temperature $T_c = 1$ eV, hot electron temperature $T_h = 26$ eV, then the effective temperature $T_{eff} \approx 7$ eV and $\sigma = T_i/T_{eff} = 0.01$ (Berthomier et al. 1998).

Table 3.1 shows the unnormalized values of the soliton velocity (V), electric field (E), soliton width (W), and pulse duration (τ^*) for various values of adiabatic index σ and the Mach number range M, respectively.

Table 3.1: Properties of ion-acoustic solitons, such as Soliton Velocity (V), Mach number range ($M_o < |M| < M_1$), Electric Field (E), Soliton Width (W) and Pulse Duration (τ^*), for various values of ion temperature (σ) with $\theta = 35^o$, Cool electron density $f = 0.1$, and Electron temperature $\tau = 0.04$

σ	$M_0 < \|M\| < M_1$	$V(kms^{-1})$	$E(mVm^{-1})$	$W(m)$	$\tau^*(ms)$
0.0	0.82 - 0.999	21.24 - 25.9	0.012 - 23.8	1435.2 - 227.2	67.57 - 8.77
0.05	0.854 - 1.0365301(DL)	22.12 - 26.84	0.029 - 20.13	1139.8 - 469.04	51.53 - 17.47
0.1	0.887 - 1.0536387(DL)	22.97 - 27.29	0.065 - 21.25	923 - 428.48	40.18 - 15.7
0.15	0.919 - 1.07063756(DL)	23.8 - 27.73	0.122 - 20.64	800.8 - 427.44	33.65 - 15.41
0.2	0.95 - 1.087547(DL)	24.61 - 28.17	0.21 - 20.97	702 - 410.28	28.52 - 14.51

Table 3.1 describes the behavior of the nonlinear structures for the angle of propagation, $\theta = 35^o$ and other plasma parameters being $f = 0.1$ and $\tau = 0.04$ respectively. It is clear from Table 3.1 that for the minimum Mach number M_o, the soliton velocity and electric field amplitude tend to increase with σ, but the soliton width and pulse duration decrease. Also, at the maximum Mach number of the range M_1, it is interesting to note that for $\sigma = 0.05$ and above, double layer solutions (DL) appear.

Figure 3.13 shows the range of Mach number values (see equation 3.48)) supported by the model for the existence of finite amplitude ion-acoustic solitons as a function of the ion temperature σ, for $\theta = 15^o$ implies that $\gamma = \cos\theta = 0.965925826$.

Figure 3.14 shows the variation of the Sagdeev potential $V(\psi, M)$ with real po-

tential ψ for different values of Mach number M as shown in the curves. The chosen fixed parameters are, $\tau = T_c/T_h = 0.04$, $f = 0.1$, $\theta = 15^o$ and ion temperature, $\sigma = T_i/T_{eff} = 0.01$. It is seen that the model supports solitons with (negative) amplitude ψ increasing with M- values. In this case, the solitons can only exist within the range of value $0.97 < M < 1.0056$, which is consistent with the condition in equation (3.48). In the case of cold ion in Mode 1, the range of values was $0.97 < M < 1.00$ for the same set of parameters. Our numerical computations also show that only soliton solutions are possible within this Mach number range, no double layer solutions are found, unlike the case of an unmagnetized plasma where both soliton and double layer solutions are reported (Berthomier et al. 1998; Baluku et al. 2010). Figure 3.15 shows the variation of real potential ψ vs ξ for the ion-acoustic solitons, which has been obtained numerically by integrating equation (3.42) for the same parameters as in Figure 3.14. As the Mach number increases, the amplitude increases and the width of ion-acoustic soliton decreases.

Figure 3.16 shows the variation of the Sagdeev potential with normalized electrostatic potential ψ for different ion temperature values (σ varying). The other fixed parameters are, $\tau = 0.04$, $f = 0.1$, $\theta = 15^o$ and $M = 0.98$. It was noticed that as the ion temperature increases, the ion-acoustic soliton amplitude decreases. For the selected parameter values, the solitary wave structures are possible only for ion temperature values in the range $0 \leq \sigma \leq 0.015$. We note that $\sigma = 0$ corresponds to the cold ions temperature in Model 1, curve corresponding $\sigma = 0.04$ in Figure 3.7. Baboolal et al. (1989) explained this effect as the result of a reduction in charge separation or decreasing wave dispersion with increasing ion temperature. Also, several earlier studies report similar behavior with temperature region (e.g Mahmood and Akhtar, 2008; Barman and Talukdar, 2010). Figure 3.17 shows the variation of the electrostatic potential ψ with ξ for the parameters in Figure 3.16. It is observed that as ion temperature increases (σ increasing), the amplitude decreases as well as the width of ion-acoustic soliton.

Figure 3.18 shows the variation of the Sagdeev potential versus the real potential ψ for different cool electron number density f, and for plasma parameters, $\tau = 0.04$, $\sigma = 0.01$, $\theta = 15^o$ and $M = 0.98$ respectively. The curves show that the solitary wave amplitude increases with an increase in cool electron density. Our computations show that the soliton solutions are not possible beyond $f > 0.34$, whereas for the cold ion case in Model 1 in section 3.1, the limit is $f > 0.35$ for the same set of parameters. Figure 3.19 shows the variation of real potential ψ vs ξ for the ion-acoustic solitons

for the same parameters in Figure 3.18. It seen that the soliton amplitude as well as the width increases as the cool electron density f increases.

Figure 3.20 shows the variation of the Sagdeev potential $V(\psi, M)$ versus the normalized electrostatic potential ψ for different propagation angles, with chosen parameters $f = 0.1$ and other fixed parameters of Figure 3.18. The curves show that as the angle of propagation θ increases, the soliton amplitude increases. At a propagating angle $\theta = 38.2885^o$ a double layer structures appears. For θ values above 38.2885^o there are no soliton or double layer solutions. It may be pointed out that for the cold ion case in Model 1 (section 3.1), the double layer appears at slightly lower angle of propagation, $\theta = 38.0425^o$ for the same set of parameters (Figure 3.5). It is important to note that for the unmagnetized case, several authors (Sayal et al. 1993; Berthomier et al. 1998; Tagare, 2000; Ghosh and Lakhina, 2004; Baluku et al. 2010) have studied the case for parallel propagation (i.e. $\theta = 0^o$). Figure 3.21 shows the variation of electrostatic potential ψ against ξ for ion-acoustic solitons and double layer for the parameters in Figure 3.20. The amplitude increases but width of ion-acoustic soliton decreases as the propagation angle increases, until a double layer appears as an upper bound.

Figure 3.22 shows the variation of the Sagdeev potential $V(\psi, M)$ with real electrostatic potential ψ for different values of the cool to hot electron temperature ratio, $\tau = T_c/T_h$ for propagation angle $\theta = 15^o$. The other fixed parameters are the same as in Figure 3.20. The ion-acoustic soliton amplitude increases with the increase in cool to hot electron temperature ratio. The double layer solution appears at cool to hot electron temperature ratio value $\tau = 0.092014$. Whereas for cold ion case in Model 1, the double layer solution is obtained at lower value of cool to hot electron temperature ratio, $\tau = 0.0877117$ for the same set of parameters. The cool to hot electron temperature ratio, τ plays a critical role in studying two-electron temperature space plasma phenomena. Its effect has been mentioned by a number of authors (e.g, Bharuthram and Shukla, 1986; Berthomier et al. 1998; Baboolal et al. 1990; Baluku et al. 2010). Figure 3.23 shows the variation of the electrostatic potential ψ against ξ for ion-acoustic solitons and double layer for the same parameters in Figure 3.22. The amplitude increases but width of ion-acoustic soliton decreases, as the propagation angle increases.

Figure 3.24 shows the variation of the Sagdeev potential $V(\psi, M)$ against the real electrostatic potential ψ for different values of Mach number M. The chosen

fixed parameters are, $\tau = T_c/T_h = 0.04$, $f = 0.1$, $\theta = 35^o$ and ion temperature, $\sigma = T_i/T_{eff} = 0.05$. It is interesting to note that at $M = 1.0365301$ a double layer appears, there are no solitons or double layer solutions above this value. It is emphasized here that the nonlinear solitary structures are possible for subsonic ($M < 1$) as well as double layer structures for supersonic ($M > 1$) for the current theoretical model, whereas for the cold ion case in Model 1, the soliton solutions are only possible for subsonic ($M < 1$) Mach number regime. Similar negative potential soliton and double layer structures for supersonic Mach number regime ($M > 1$) have been reported by Berthomier et al. 1998, for an unmagnetized plasma consisting of a finite ion temperature and two Boltzmann electrons. Figure 3.25 shows the variation of real potential ψ vs ξ for the ion-acoustic solitons and double layer for the same parameters in Figure 3.24. As the Mach number increases, the amplitude increases and the width of ion-acoustic soliton decreases

Figure 3.26 shows the variation of the Sagdeev potential $V(\psi, M)$ against the real electrostatic potential ψ for different values of the Mach number M and propagating angle θ. Other fixed parameters are $\tau = 0.04$, $f = 0.1$ and $\sigma = 0.01$. The curves show all combinations of (θ, M) yield exactly the same value for the double layer amplitude, similar to Figure 3.9 of Model 1. It also corresponds to a "point" solution as found by Djebli and Marif (2009). Figure 3.27 shows the existence domain of solitons and double layers for the fixed parameters in Figure 3.26. The curves show that a double layer solution is the upper bound for soliton solution as we increase the angle of propagation θ, for different M values. The maximum Mach number for negative potential solitons is bounded by those of the double layer solutions corresponding to a given θ value.

Figure 3.28 shows the variation of the Sagdeev potential $V(\psi, M)$ against the real electrostatic potential ψ for different values of Mach number M and cool to hot temperature ratio τ for the fixed parameters $\theta = 15^o$, $f = 0.1$ and $\sigma = 0.01$. As we mentioned in Model 1, the curves in Figure 3.28 show the existence of the supersoliton (Dubinov and Kolotkov, 2012; Verheest et al. 2013; Maharaj et al. 2013) solutions for $\tau = 0.092014$ and $M = 0.98$, $\tau = 0.0853963$ and $M = 0.99$, $\tau = 0.080429328$ and $M = 1.00$. Figure 3.29 shows the existence domain of solitons, double layers and supersolitons for the same parameters in Figure 3.28 and for the Mach number $M = 1.0055$. The curves were plotted for the variation of the maximum electrostatic potential ψ_{Max} against τ for different values of the Mach number M. The reason for smaller amplitudes for larger $\tau = \frac{T_c}{T_h}$ can be seen from the expression for the effective

temperature $T_{eff} = T_c/(f + (1-f)\tau)$, which shows that for fixed f the normalization factor T_{eff} decreases with increasing τ so that the corresponding normalized potential ψ would linearly increase in magnitude. For τ=0.078081 and M=1.0055 only soliton solitions can be found.

3.2.4 Discussion

We have studied the nonlinear propagation of arbitrary amplitude ion-acoustic solitary waves and double layers in magnetized auroral plasma consisting of two Maxwellian electrons and adiabatic ions. The present model extends the model presented in Model 1, by including an adiabatic ion temperature. The model predicts negative potential solitons and double layers in the auroral region of the Earth's magnetosphere, unlike the case reported by Berthomier et al. (1998), of two electrons temperature in an unmagnetized warm ion plasma, with positive potential and double layers. The Viking satellite measurements taken in the auroral zone reported an electric field amplitude of less than $100mV/m$, with the plasma parameters $n_c = 0.2cm^{-3}$, $n_h = 1.8cm^{-3}$, $T_c = 1eV$, $T_h = 26eV$, and $T_i = 0.07eV$ which gives $T_{eff} \approx 7eV$. The maximum electric field for the Mach number $M = 0.98$, $\theta = 35^o$ comes out to be $18mV/m$ and the corresponding soliton width, pulse duration and speed come out to be $\approx 223m$, $9ms$ and $25km/s$, respectively.

The effect of adiabatic ions temperature is found to decrease the soliton amplitude and increase the range values of Mach numbers for the existence of nonlinear structures, i.e. the ion temperature contribution pushes both the lower and upper limits of Mach number to the higher side for the existence of nonlinear structures. It gradually moved the Mach numbers regime to supersonic ($M > 1$). The model shows that the amplitude of ion-acoustic solitons increases with Mach number, cool electron density and propagating angle, but decreases with ion temperature. The present results are in agreement with the Viking satellite observations in auroral regions.

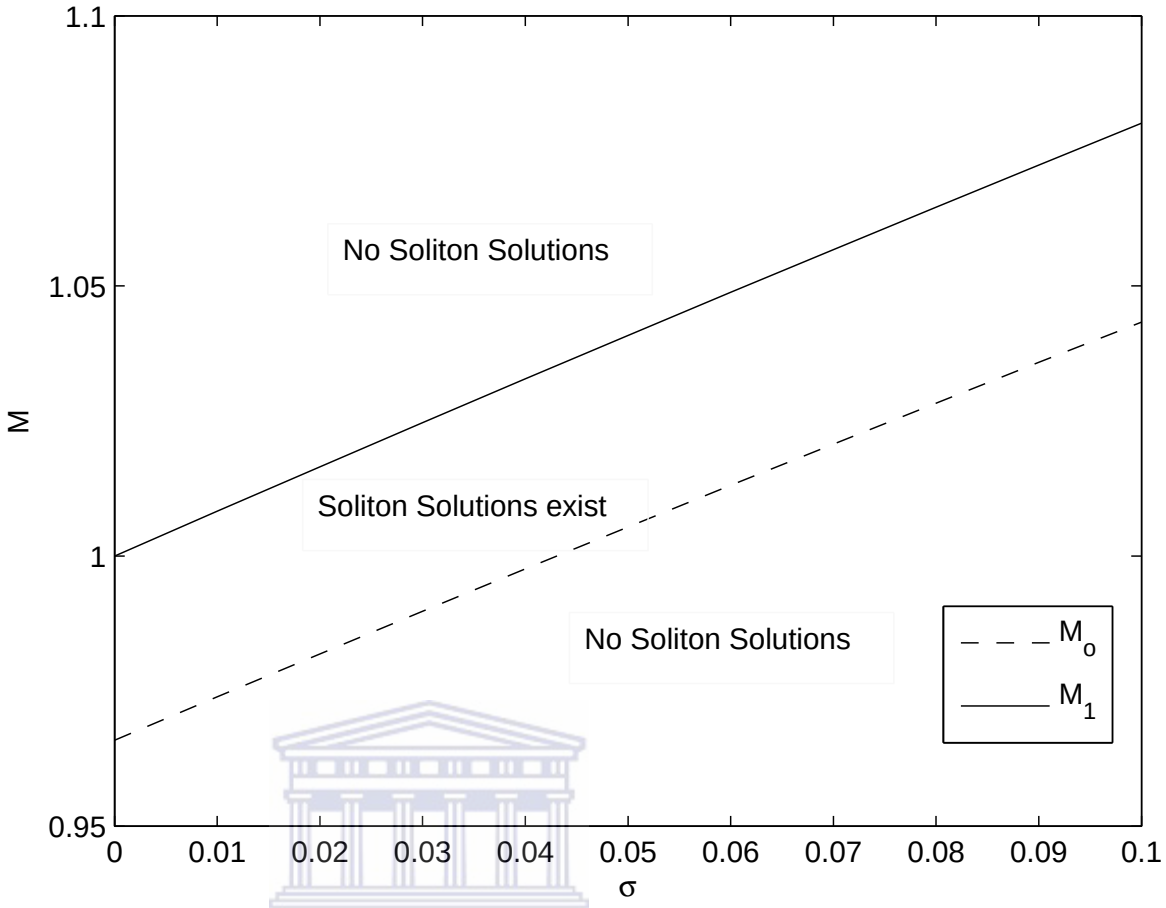

Figure 3.13: Existence domains of ion-acoustic solitons shown as a function of the normalized ion temperature σ. For $\gamma = \cos 15^o$, using equation (3.48).

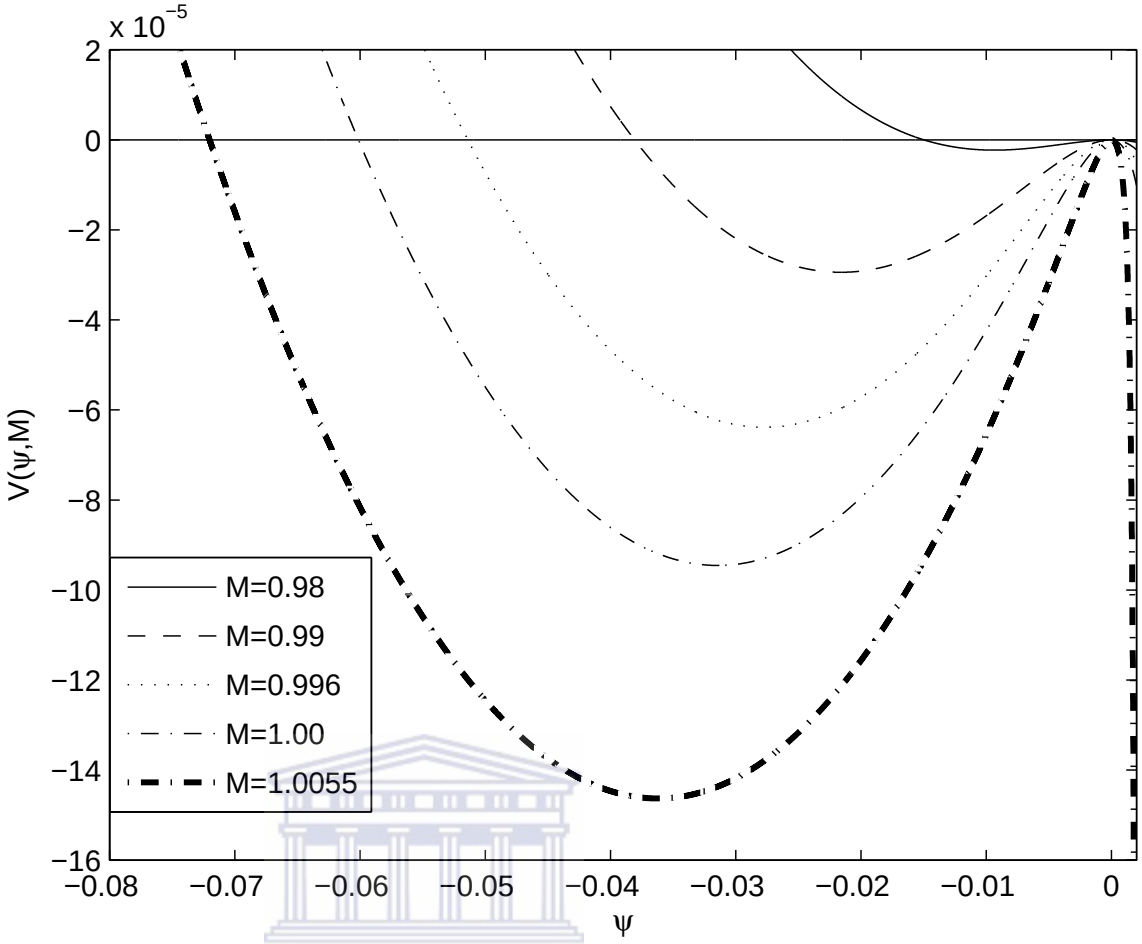

Figure 3.14: Sagdeev potential, $V(\psi, M)$ vs normalized electrostatic potential ψ. The fixed parameters are τ= 0.04, f=0.1, σ=0.01, θ=15^o and M = 0.98, 0.99, 0.996, 1.00 and 1.0055.

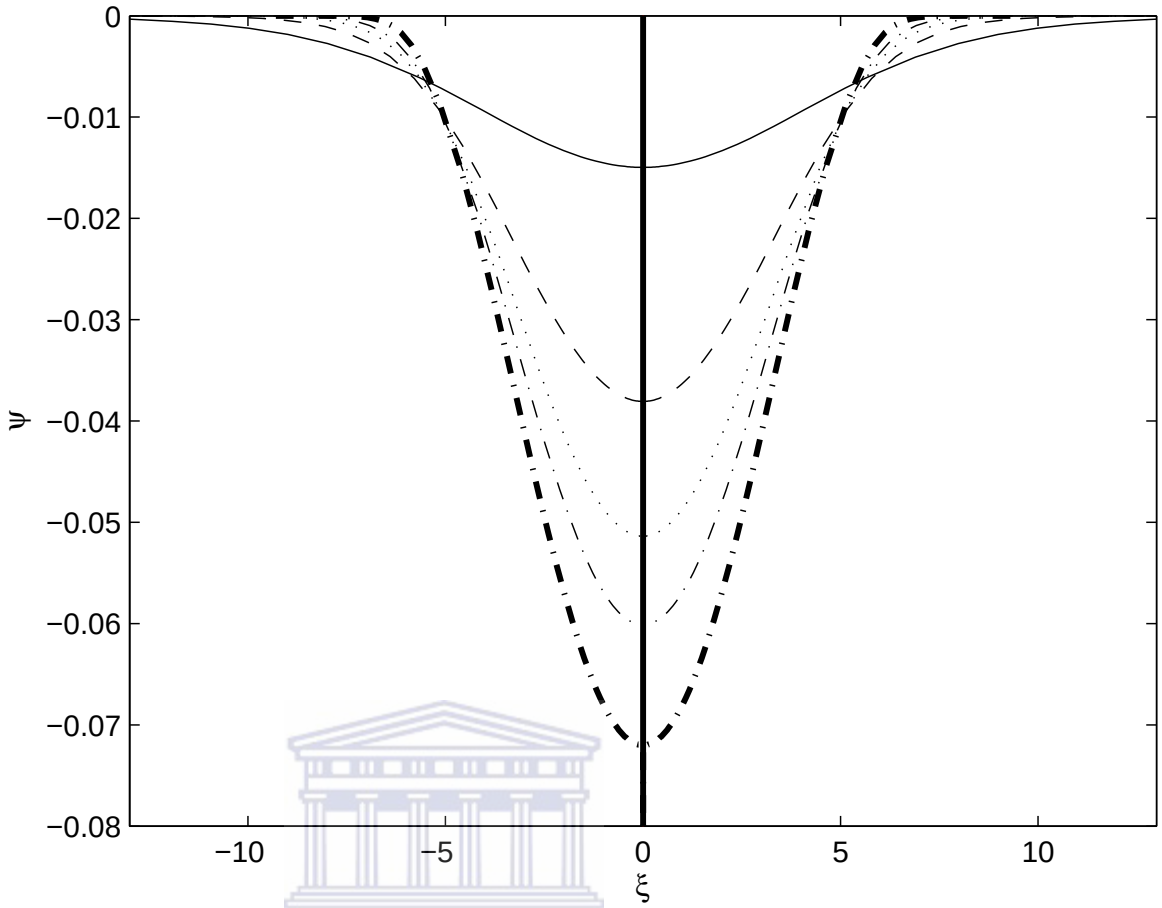

Figure 3.15: Electrostatic potential ψ vs ξ for the fixed parameters of Figure 3.14 and M=0.97(—), M=0.99 (- - -), $M = 0.996$ (...), M=1.00 (- . -) and M=1.0055(−.−).

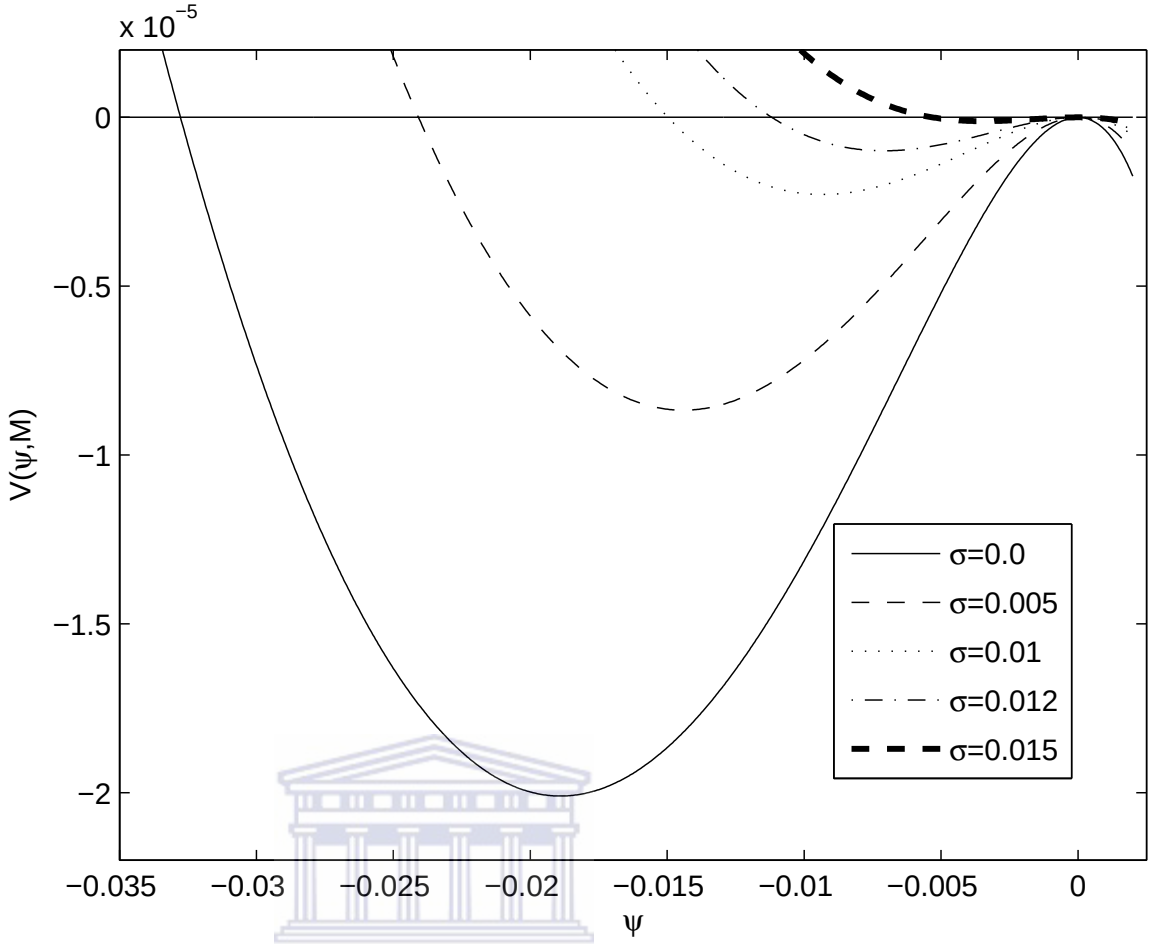

Figure 3.16: Sagdeev potential, $V(\psi, M)$ vs normalized electrostatic potential ψ. The fixed parameters are τ= 0.04, f=0.1, θ=15^o, M = 0.98 and σ=0.0, 0.005, 0.01, 0.012 and 0.015.

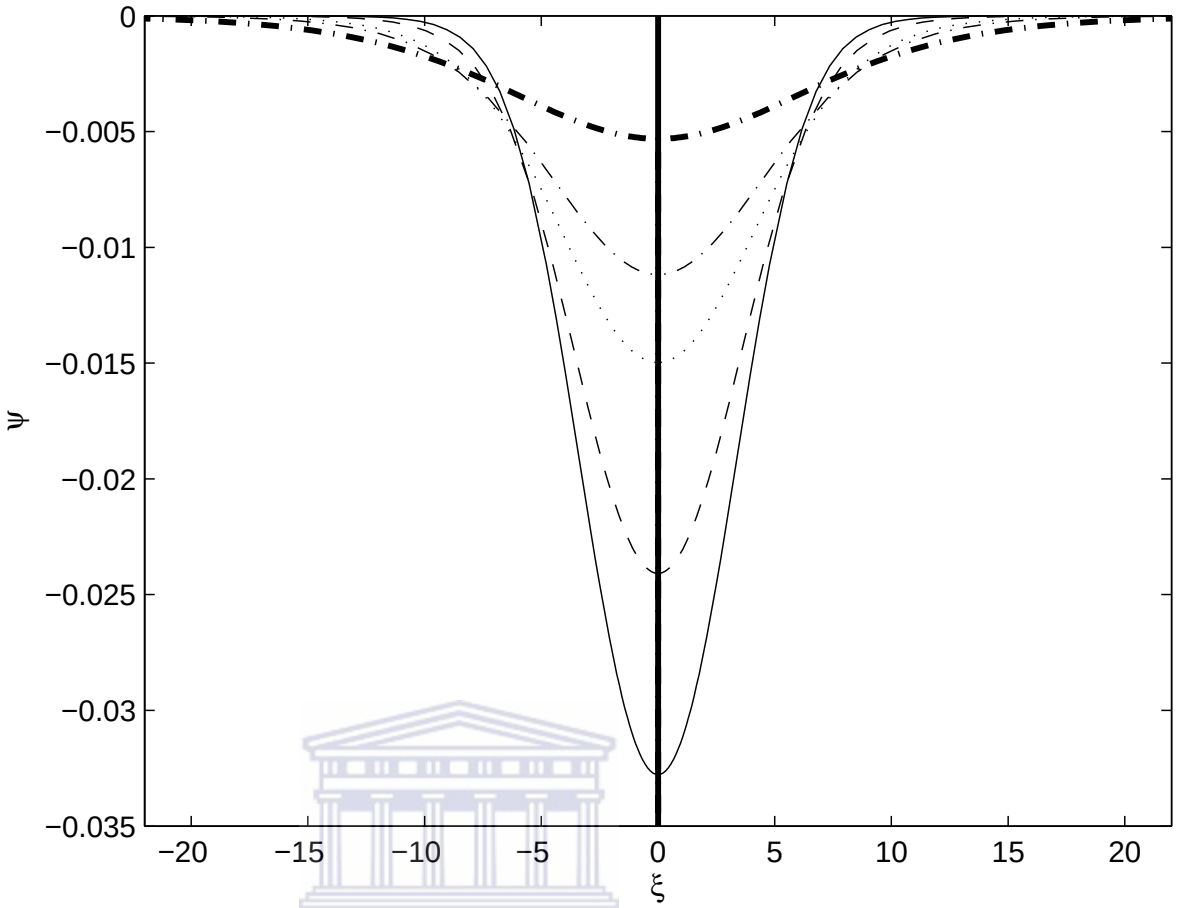

Figure 3.17: Electrostatic potential ψ vs ξ for the fixed parameters of Figure 3.16 with σ=0.0 (—), σ=0.005 (- - -), σ=0.01 (...), σ=0.012 (- . -) and σ=0.015 (−.−).

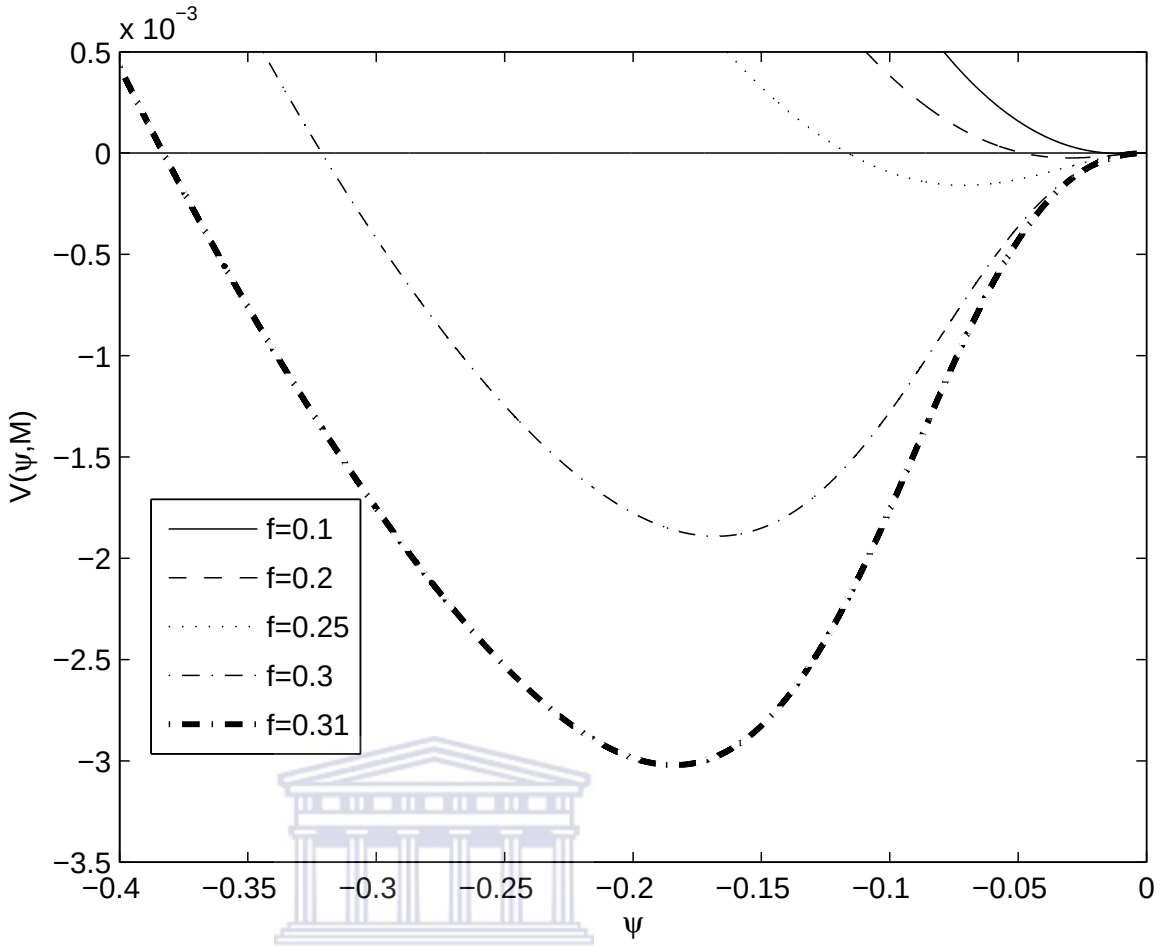

Figure 3.18: Sagdeev potential, $V(\psi, M)$ versus normalized potential ψ. The fixed parameters are τ= 0.04, σ=0.01, θ=15^o, M = 0.98 and f=0.1, 0.2, 0.25, 0.3 and 0.31.

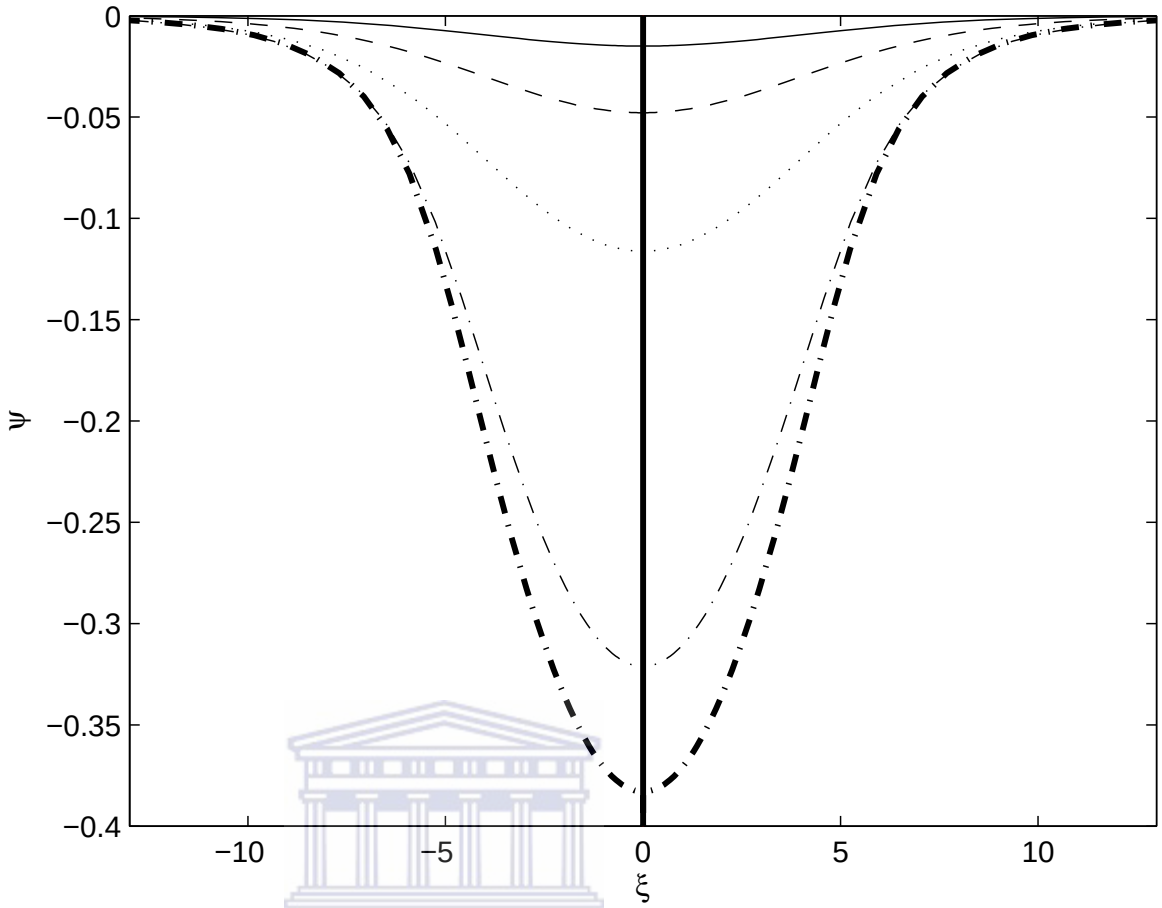

Figure 3.19: Electrostatic potential ψ vs ξ for the parameters of Figure 3.18 with f=0.1 (—), f=0.2 (- - -), f=0.25 (...), f=0.3 (- . -) and f=0.31 (—.—).

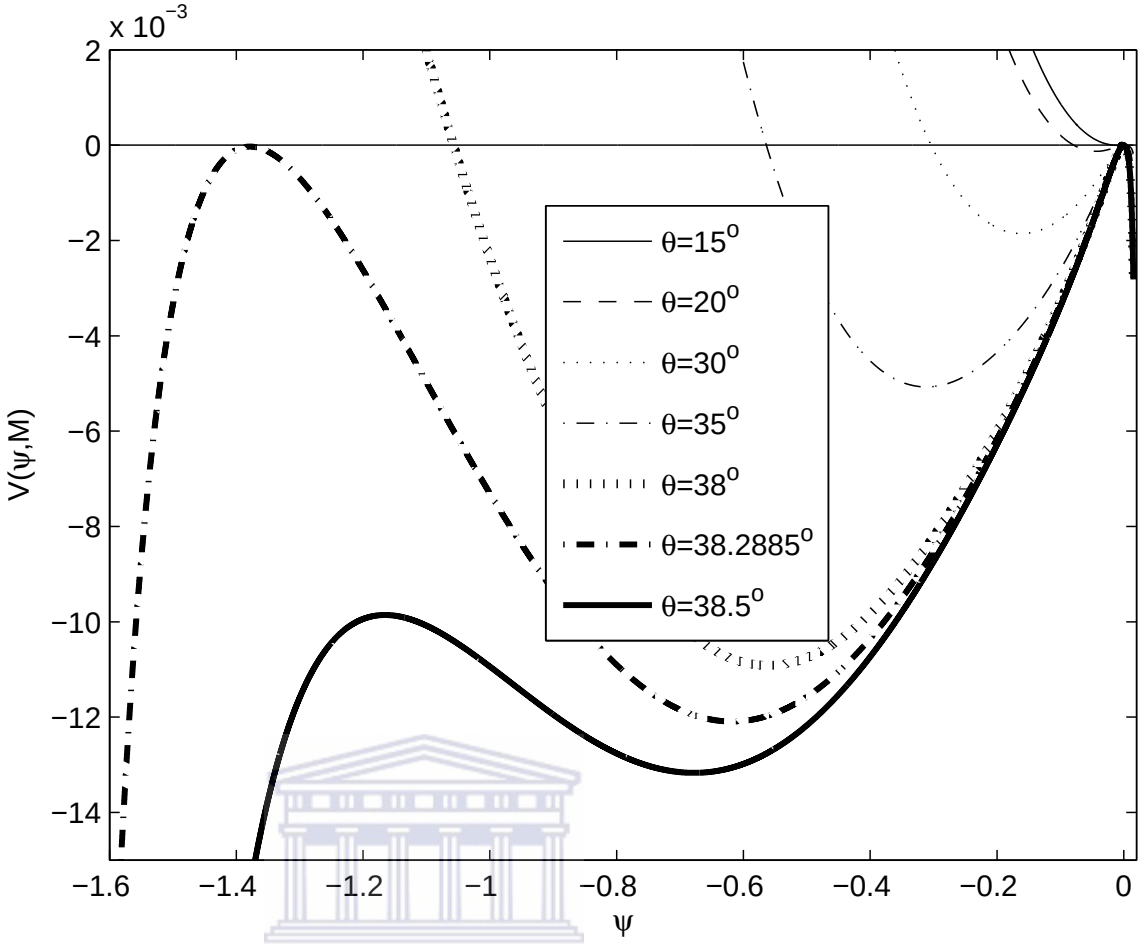

Figure 3.20: Sagdeev potential, $V(\psi, M)$ vs normalized potential ψ. The fixed parameters are τ= 0.04, σ=0.01, f=0.1, M = 0.98 and θ=15^o, 20^o, 30^o, 35^o, 38^o, 38.2885^o-double layer, 38.5^o- no solution.

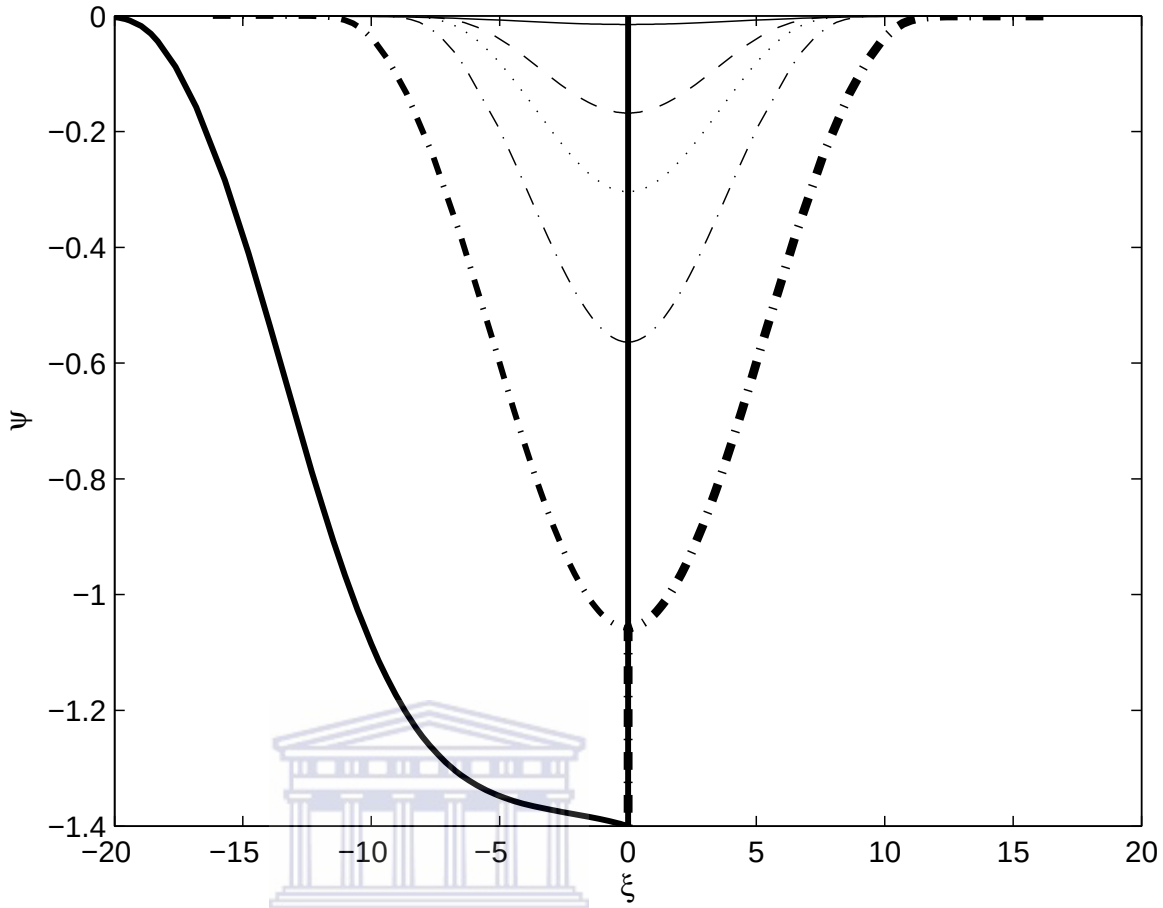

Figure 3.21: Electrostatic potential ψ vs ξ for the fixed parameters of Figure 3.20 with θ=15^o (—), θ=20^o (- - -), θ=30^o (...), θ=35^o (- . -) and θ=38^o (—.—), θ=38.2885^o(—) for a double layer.

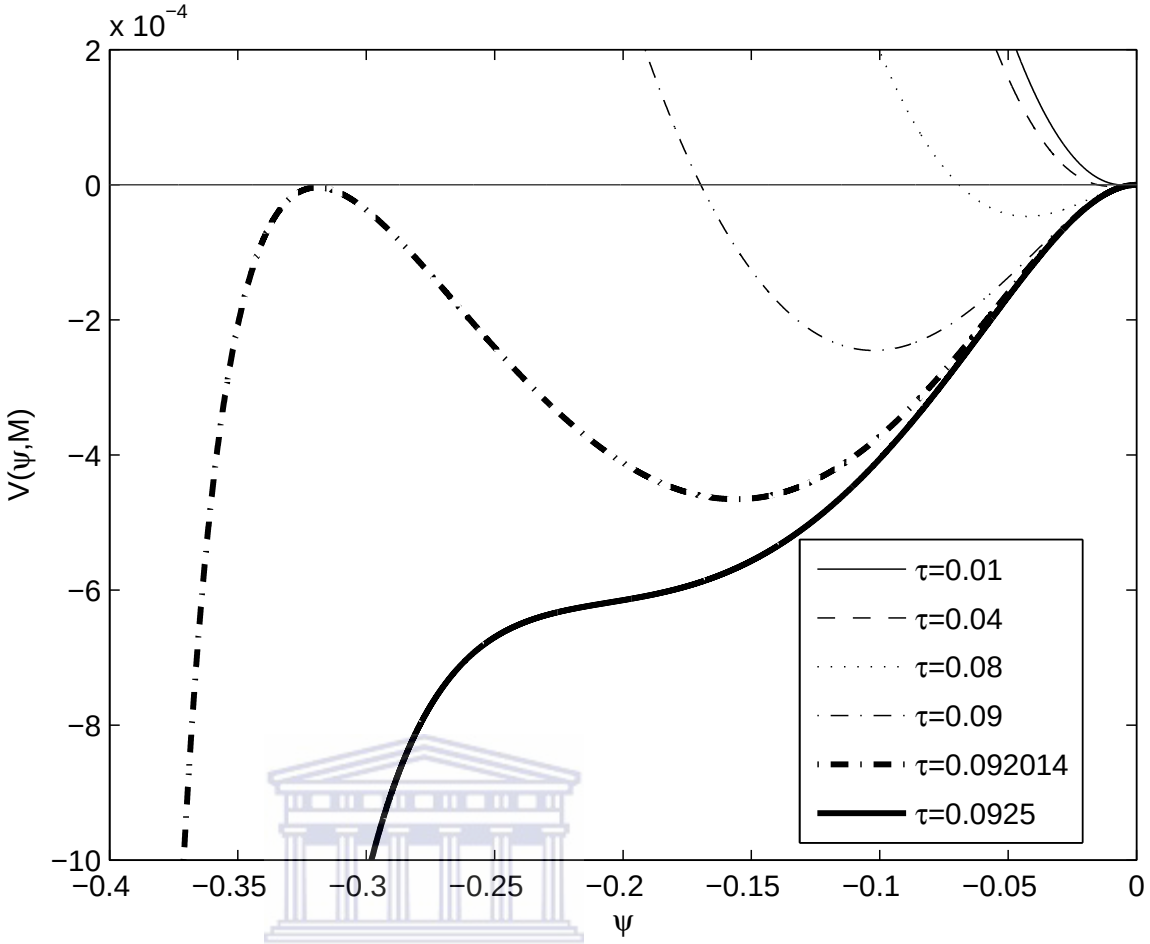

Figure 3.22: Sagdeev potential, $V(\psi, M)$ vs normalized potential ψ. The fixed parameters are θ= 15^o, σ=0.01, f=0.1, M = 0.98 and τ=0.01, 0.04, 0.08, 0.09, 0.092014- double layer, 0.0925- no solution.

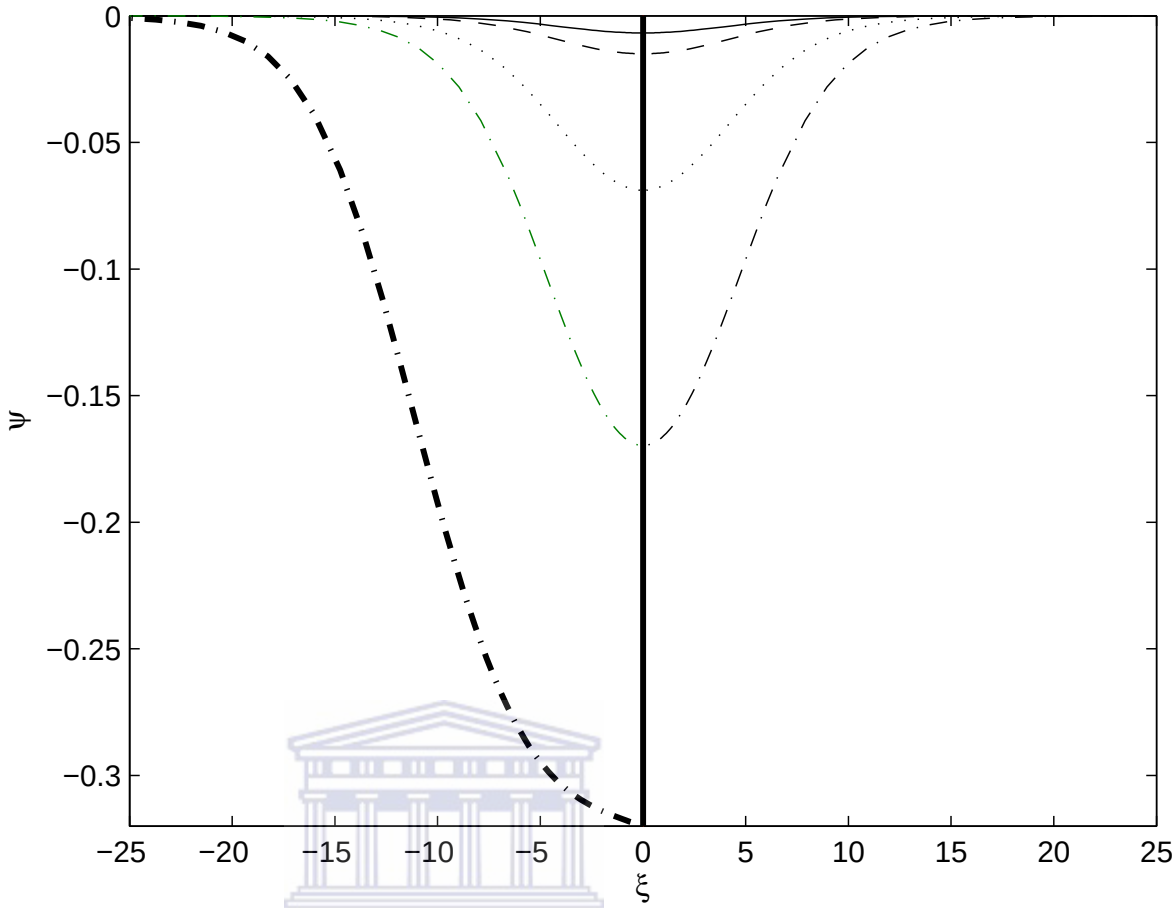

Figure 3.23: Electrostatic potential ψ vs ξ for the fixed parameters of Figure 3.22 with τ=0.01 (—), τ=0.04 (- - -), τ=0.08 (...), τ=0.09 (- . -) and τ=0.092014(—.—) for a double layer.

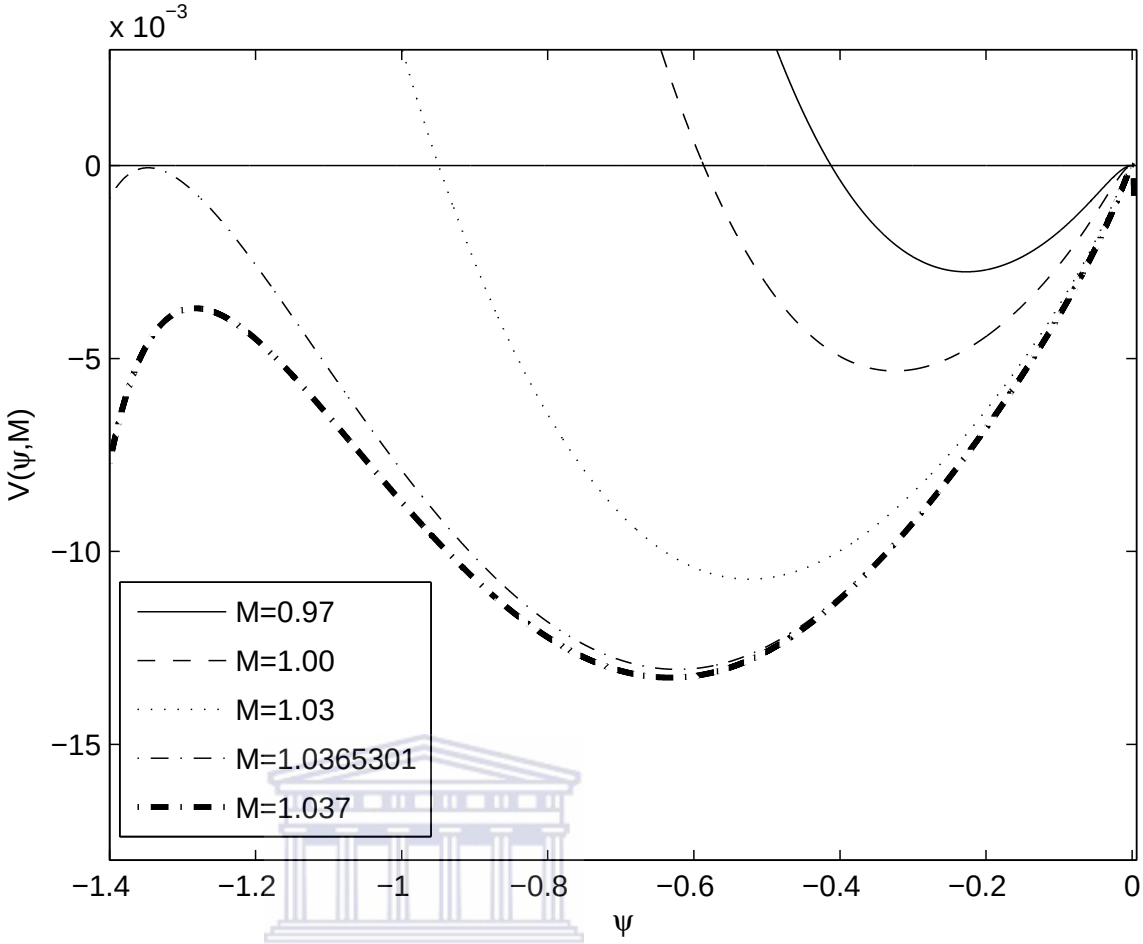

Figure 3.24: Sagdeev potential, $V(\psi, M)$ vs normalized potential ψ. The fixed parameters are σ=0.05, f=0.1, τ=0.04, θ=35^o and M=0.97, 1.00, 1.03, 1.0365301- double layer, 1.037- no solution.

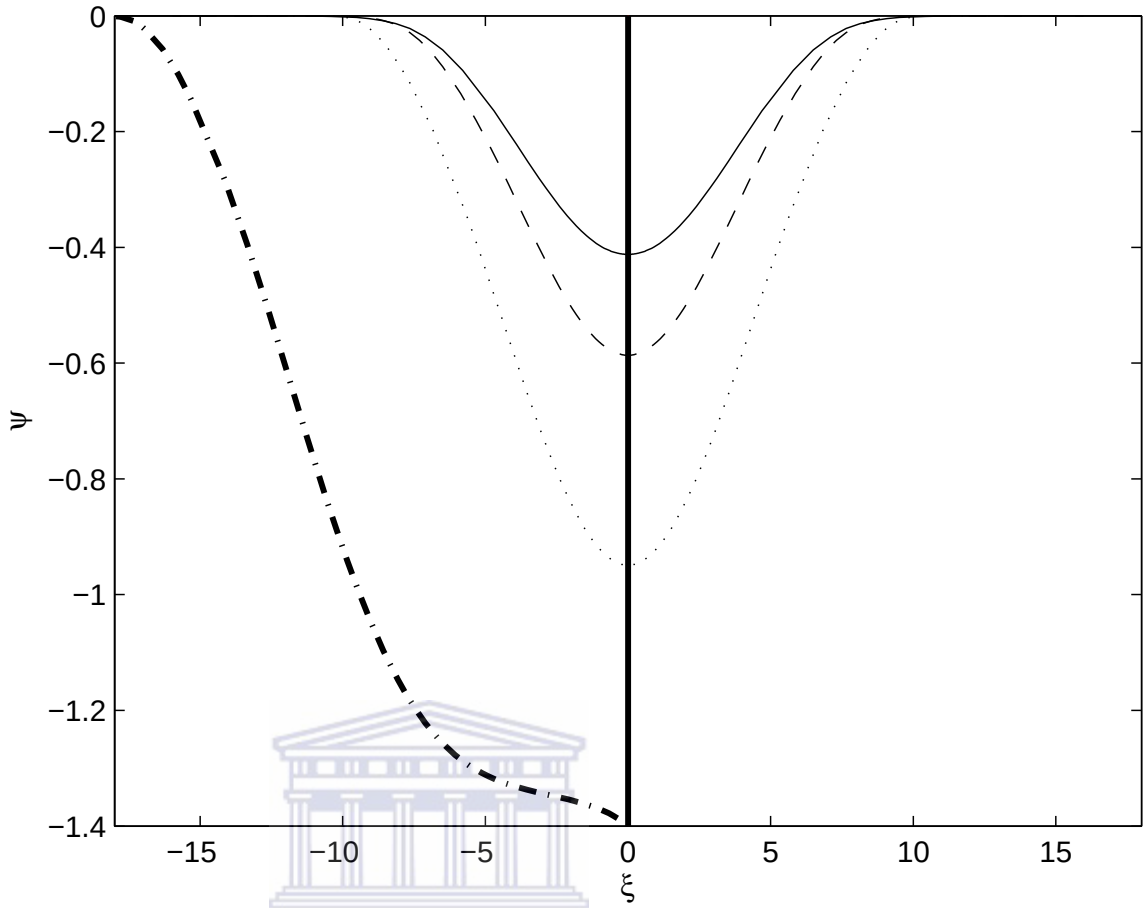

Figure 3.25: Electrostatic potential ψ vs ξ for the fixed parameters of Figure 3.24 with M=0.97(—), M=1.00 (- - -), M = 1.03 (...), and M=1.0365301(−.−) for a double layer.

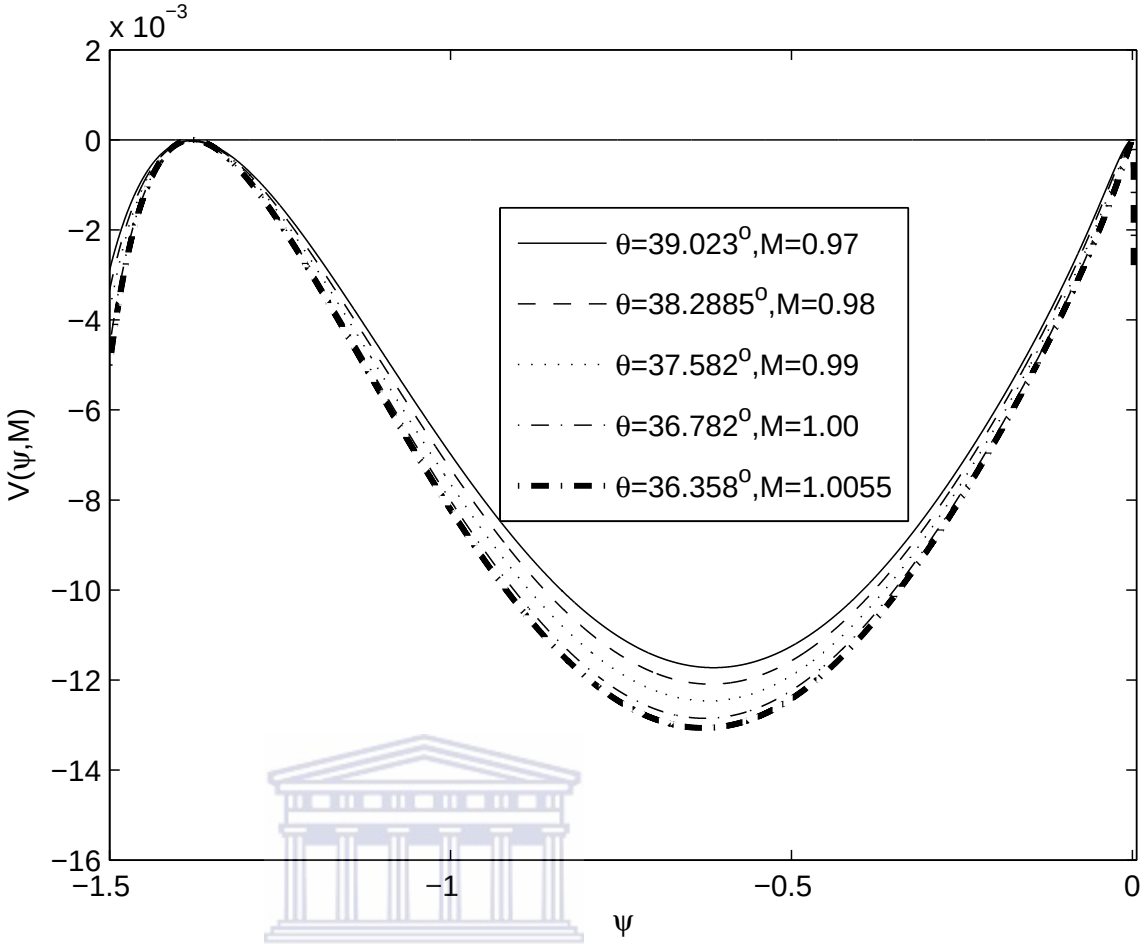

Figure 3.26: Sagdeev potential, $V(\psi, M)$ vs the normalized potential ψ. The fixed parameters are σ=0.01, f=0.1, τ=0.04 for M=0.97 and θ=39.023^o, M=0.98 and θ=38.28856^o, M=0.99 and θ=37.582^o, M=1.00 and θ=36.782^o, M=1.0055 and θ=36.358^o.

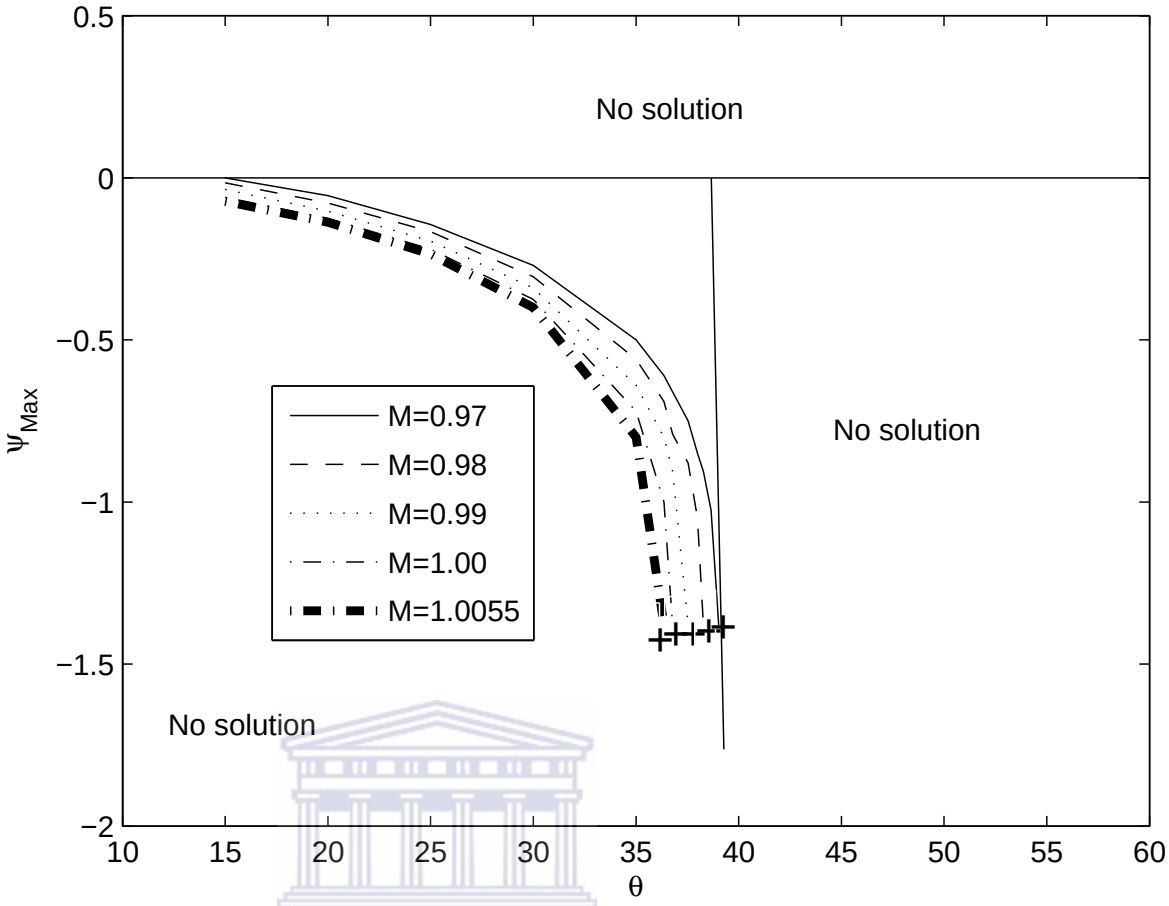

Figure 3.27: The existence domain of soliton for the fixed parameters of Figure 3.26. The upper bound for soliton with increasing θ is a double layer, shown as an "+".

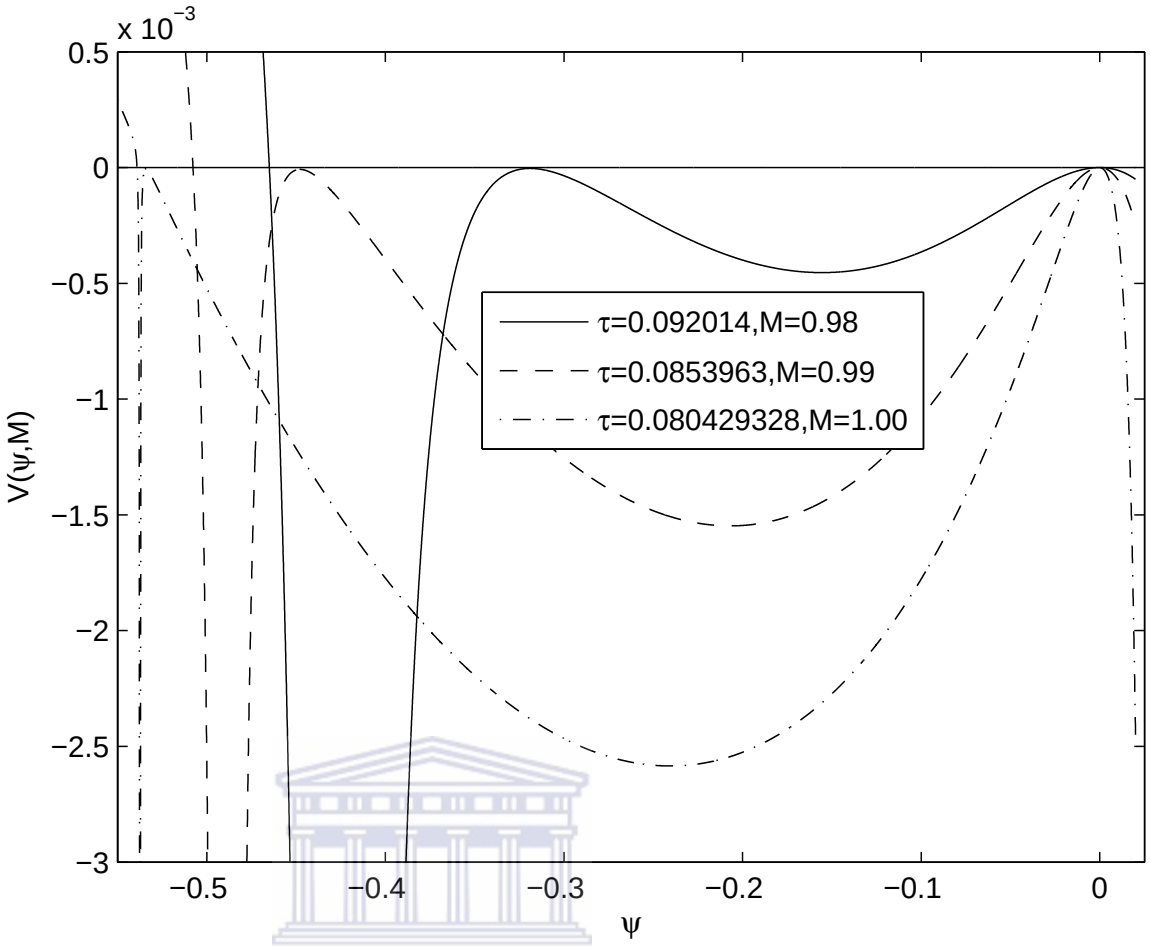

Figure 3.28: Sagdeev potential, $V(\psi, M)$ vs the normalized potential ψ. The fixed parameters are σ=0.01, f=0.1, θ=15^o and M=0.98 and τ=0.092014, M=0.99 and τ=0.0853963, M=1.00 and τ=0.080429328.

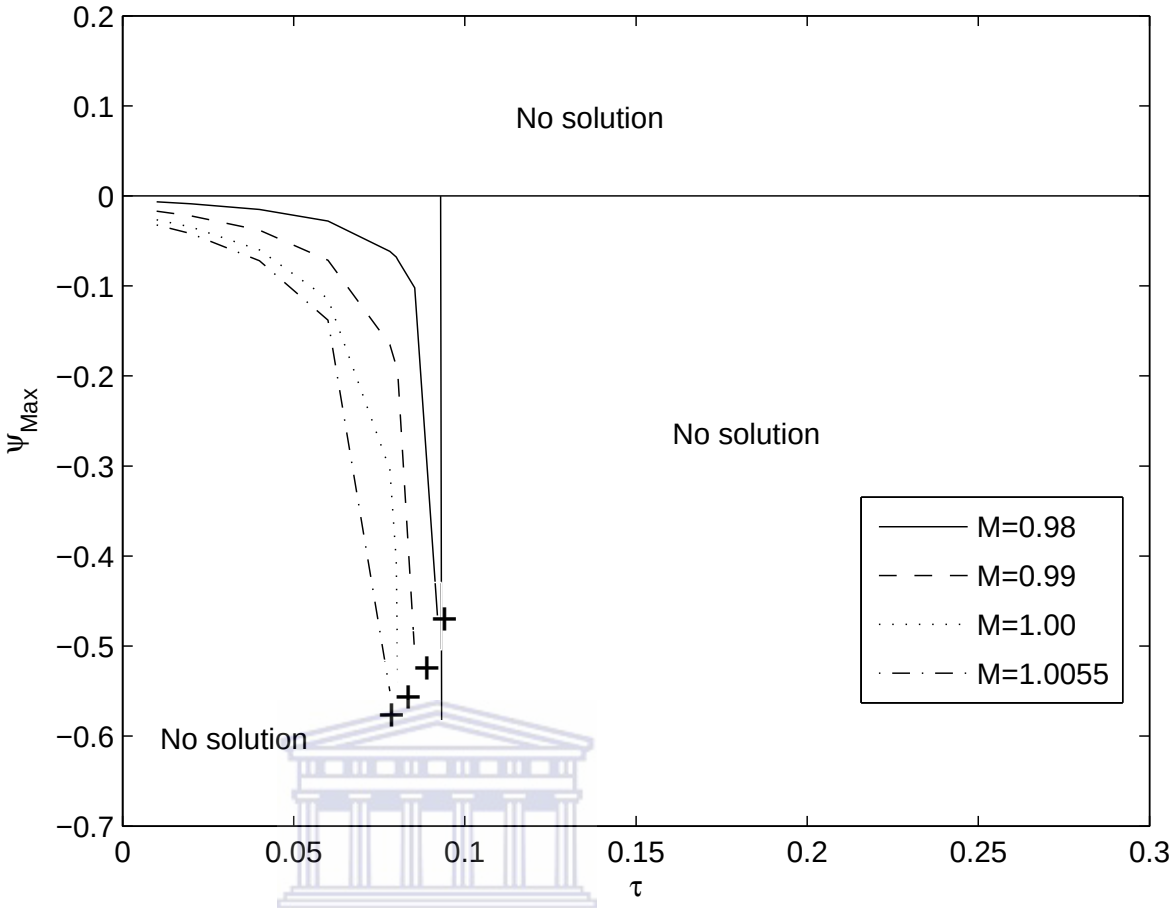

Figure 3.29: The maximum electrostatic potential ψ_{Max} against τ. The fixed parameters of Figure 3.28 and M=0.98, 0.99, 1.00, 1.0055.

This Section have been published in Communications in Nonlinear Science and Numerical Simulation.

O. R. Rufai, R. Bharuthram, S. V. Singh, and G. S. Lakhina
Effect of hot ion temperature on obliquely propagating ion-acoustic solitons and double layers in an auroral plasma, Comm. Nonlin. Sci. Numer. Simulat., ***19****, 1338-1346, 2014. http://dx.doi.org/10.1016/j.cnsns.2013.09.024.*

3.3 Model 3: Magnetized plasma with a cold ions, cool electrons and hot energetic electron species

In Model 1 and 2, we assumed the Boltzmann distribution function for both cool and hot electron densities arising from Maxwellian velocity distributions. As mentioned in Chapter 2, Section 2.2.2, satellite observations also reveal the presence of nonthermal species, in particular, for hot components (Cairns et al. 1995). This results in a modification to the hot electron density in equation (3.2), as shown below.

3.3.1 Basic equations

We consider the propagation of ion acoustic waves in a three-component collisionless plasma in the presence of an external magnetic field $\mathbf{B}_0\hat{z}$, along the z-direction. The dynamics of the cold ions are governed by fluid equations (3.3 - 3.4) and the cool electron density is given by equation (3.1). The hot electrons are allowed to deviate from Maxwellian behavior, as a result of high electrons temperature attributed to the solar radiation for space plasmas. Thus, we adopt for our population of energetic electrons the nonthermal distribution function given by Cairns et al. (1995):

$$f_e(v) = \frac{N_{h0}}{(3\alpha+1)\sqrt{2\pi v_e^2}}\left(1+\frac{\alpha v^4}{v_e^4}\right)\exp\left(-\frac{v^2}{2v_e^2}\right) \tag{3.49}$$

where N_{h0} is the density and v_e is the thermal speed of the hot electrons, and α is the nonthermal parameter. Thus, upon integrating over velocity space gives the following expression for the electron density (Cairns et al. 1995).

$$N_h = N_{ho}(1-\beta\phi+\beta\phi^2)\exp\left(\frac{e\phi}{T_h}\right) \tag{3.50}$$

where $\beta = \frac{4\alpha}{1+3\alpha}$. It is noted that $\alpha = 0$ corresponds to the Boltzmann density distribution of hot electron contribution, arising from the Maxwellian velocity distributions in (3.47).

To investigate the existence of arbitrary amplitude nonlinear waves in such a plasma, we normalize the variables: densities n_c, n_h with total ion equilibrium density $N_{io} = N_{co} + N_{ho}$, velocities V by the acoustic speed $C_s = (T_{eff}/m_i)^{1/2}$, distance x by effective ion Larmor radius, $\rho_i = c_s/\Omega$, time t by inverse of ion gyro-frequency Ω^{-1},

where $\Omega = eB_0/m_i c$ and potential ϕ by T_{eff}/e. Here the temperature ratio $\tau = T_c/T_h$, cool density ratio $f = N_{co}/N_o$, where $N_{jo} = (j = c, h, i)$ are the equilibrium densities, and effective temperature $T_{eff} = T_c/(f + (1-f)\tau)$, $\alpha_c = T_{eff}/T_c$, $\alpha_h = T_{eff}/T_h$, (for $\alpha_h \neq 0$ and $\tau \neq 0$) and $\psi = e\phi/T_{eff}$.

Hence, the normalized set of equations (3.11) - (3.14) can be written in the stationary frame $\xi = (\varphi x + \gamma z - Mt)/M$, as

$$\frac{d}{d\xi}(L_v n_i) = 0. \tag{3.51}$$

$$L_v \frac{dv_x}{d\xi} = -\varphi \frac{d\psi}{d\xi} + M v_y. \tag{3.52}$$

$$L_v \frac{dv_y}{d\xi} = -M v_x. \tag{3.53}$$

$$L_v \frac{dv_z}{d\xi} = -\gamma \frac{d\psi}{d\xi}. \tag{3.54}$$

with the quasi-neutrality condition

$$n_i = f \exp(\alpha_c \psi) + (1-f)(1 - \beta\psi + \beta\psi^2) \exp(\alpha_h \psi) \tag{3.55}$$

where $L_v = -M + \alpha V_x + \gamma V_z$, M is the Mach number (wave speed), $\varphi = \sin\theta$, $\gamma = \cos\theta$, (where $\varphi^2 + \gamma^2 = 1$ and θ is the angle of propagation).

Now, using the quasi-neutrality condition (3.55), and solving equations (3.51) - (3.54) with the boundary conditions (namely, $n_i \to 1$, $\psi \to 0$, and $d\psi/d\xi \to 0$ at $\xi \to \pm\infty$), and eliminating v_x, v_y, and v_z, we have,

$$\begin{aligned}
\frac{d}{d\xi}\left[\frac{d}{d\xi}\left(\psi + \frac{M^2}{2n_i^2}\right)\right] &= M^2(n_i - 1) - n_i\gamma^2 \left[\frac{f}{\alpha_c}(\exp(\alpha_c\psi - 1)\right. \\
&+(1-f)\left(\frac{1}{\alpha_h}(\exp(\alpha_h\psi) - 1) + \beta\psi(\psi - 1)\frac{\exp(\alpha_h\psi)}{\alpha_h}\right. \\
&-\frac{\beta}{\alpha_h^2}(1 - \exp(\alpha_h\psi) + 2\psi\exp(\alpha_h\psi) \\
&\left.\left.+\frac{2\beta}{\alpha_h^3}(\exp(\alpha_h\psi) - 1)\right)\right].
\end{aligned} \tag{3.56}$$

Let

$$\chi(\psi) = \left(\psi + \frac{M^2}{2n_i^2}\right), \tag{3.57}$$

we have

$$\frac{d\chi(\psi)}{d\xi} = \frac{d\psi}{d\xi} - \frac{M^2}{n_i^3}\frac{dn_i}{d\xi} \tag{3.58}$$

then differentiate n_i (given in equation (3.55)) w.r.t ψ, we obtain

$$\begin{aligned}\frac{dn_i}{d\xi} = &[f\alpha_c \exp(\alpha_c\psi) + (1-f)\,(\alpha_h \exp(\alpha_h\psi) \\ &-\beta(1+\alpha_h\psi)\exp(\alpha_h\psi) + \beta\psi(2+\alpha_h\psi)\exp(\alpha_h\psi))]\,\frac{d\psi}{d\xi}.\end{aligned} \tag{3.59}$$

Then, multiplying both sides of equation (3.56) by $2\frac{d\chi}{d\xi}$ and integrate with the boundary conditions $n_i \to 1$, $\psi \to 0$, and $d\psi/d\xi \to 0$ at $\xi \to \pm\infty$, (see Appendix C for the details) we obtain,

$$\frac{1}{2}\left(\frac{d\psi}{d\xi}\right)^2 + V(\psi, M) = 0, \tag{3.60}$$

where use has been made of (3.57) - (3.59).

As discussed in Section 2.3, equation (3.60) is regarded as an "Energy Integral" of an oscillating pseudo-particle of unit mass, with the velocity $d\psi/d\xi$ at time ξ and the position ψ in a potential $V(\psi, M)$.

The Sagdeev pseudo-potential (cf. Section 2.3) corresponds to

$$\begin{aligned}V(\psi, M) = &-\frac{1}{\left(1 - \frac{M^2(f\alpha_c\exp(\alpha_c\psi)+(1-f)(\alpha_h\exp(\alpha_h\psi)-\beta(1+\alpha_h\psi)\exp(\alpha_h\psi)+\beta\psi(2+\alpha_h\psi)\exp(\alpha_h\psi)))}{(f\exp(\alpha_c\psi)+(1-f)(1-\beta\psi+\beta\psi^2)\exp(\alpha_h\psi))^3}\right)^2}\times \\ &-\frac{M^4}{2n_i^2}(1-n_i)^2 - M^2(1-\gamma^2)\psi + M^2P(\psi) - \frac{\gamma^2P^2(\psi)}{2} - \frac{\gamma^2M^2P(\psi)}{n_i}\end{aligned} \tag{3.61}$$

where

$$P(\psi) = \frac{f}{\alpha_c}(\exp(\alpha_c\psi) - 1) + \frac{(1-f)}{\alpha_h}\left((\exp(\alpha_h\psi) - 1)\right.$$
$$+\beta\psi(\psi-1)\exp(\alpha_h\psi) - \frac{\beta}{\alpha_h}(1 - \exp(\alpha_h\psi) + 2\psi\exp(\alpha_h\psi))$$
$$\left.+\frac{2\beta}{\alpha_h^2}(\exp(\alpha_h\psi) - 1)\right). \tag{3.62}$$

3.3.2 Numerical results

In the isothermal limit for the hot electrons, $\alpha = \beta = 0$, the Sagdeev potential $V(\psi, M)$ given by (3.61) must satisfy the soliton conditions (cf. Section 2.3.2): $V(\psi, M) = 0$, $d\psi/d\xi = 0$, $V(\psi, M) = 0$ and $dV(\psi, M)/d(\psi) = 0$ at $\psi = 0$. $d^2V(\psi, M)/d(\psi)^2 < 0$ at $\psi = 0$; $V(\psi, M) = 0$ at $\psi = \psi_m$, $dV(\psi, M)/d(\psi) < (>)$ 0 at $\psi_m < (>)$ 0. Then, for the formation of a double layer, one more additional condition must be satisfied, i.e, $\frac{dV(\psi,M)}{d\psi}|_{\psi=\psi_m} = 0$. It can be seen from (3.61) that $V(\psi, M) = dV(\psi, M)/d\psi = 0$ at $\psi = 0$. Finding the second derivate of the Sagdeev potential in (3.61) at the equilibrium, reveals the region of velocity values where the soliton solutions may exist.

Therefore, for soliton solutions

$$\frac{d^2V(\psi, M)}{d\psi^2}|_{\psi=0} = \frac{M^2 - M_o^2}{M^2 - M_1^2} < 0 \tag{3.63}$$

where

$$M_o^2 = \frac{\gamma^2}{f\alpha_c + (1-f)\alpha_h - (1-f)\beta} \tag{3.64}$$

and the upper limit is

$$M_1^2 = \frac{1}{f\alpha_c + (1-f)\alpha_h - (1-f)\beta}. \tag{3.65}$$

For $\gamma, \beta \neq 0 : \gamma^2 = \cos^2\theta < 1$, which implies $M_o < M_1$, then if $M > M_1 \Rightarrow M > M_0$ from which $M^2 - M_o^2 > 0$ and $M^2 - M_1^2 > 0$, consequently (3.63) is not satisfied.

Similarly, if $M < M_0 \Rightarrow M < M_1$ from which $M^2 - M_o^2 < 0$ and $M^2 - M_1^2 < 0$, once again (3.63) is not satisfied.

Therefore, (3.63) is satisfied only if

$$M_o < |M| < M_1. \tag{3.66}$$

Therefore, from equation (3.66), noting that $f\alpha_c + \alpha_h(1-f) = 1$, then we have

$$\frac{\gamma}{\sqrt{1-(1-f)\beta}} < |M| < \frac{1}{\sqrt{1-(1-f)\beta}}, \tag{3.67}$$

which in the limit of isothermal hot electrons ($\alpha = \beta = 0$), reduces to equation (3.26) in Model 1 (section 3.1). We recall that for Model 1 (equation (3.24)), only subsonic solitons ($M < 1$) were possible. The presence of nonthermal hot electrons ($\beta \neq 0$) also allows for $M > 1$, i.e supersonic solitons, as discussed in detail below.

The nonlinear ion acoustic solitary waves propagating along the external magnetic field are investigated numerically for a plasma in which the dominant species are the energetic hot electrons. The typical parameters considered for the numerical evaluation are: density ratio, f, temperature ratio $\tau = T_c/T_h$, Mach number M, nonthermal contributions α and wave obliqueness $\gamma = \cos\theta$, where θ is the propagation angle.

Table 3.2: Properties of ion-acoustic solitons, such as Soliton Velocity (V), Mach number range ($M_o < |M| < M_1$), Electric Field (E), Soliton Width (W) and Pulse Duration (τ^*), for various values of the nonthermal parameter α, with $\theta = 35^o$, cool electron density $f = 0.1$, electron temperature ratio $\tau = 0.04$

α	β	$M_o < \|M\| < M_1$	$V(kms^{-1})$	$E(mVm^{-1})$	$W(m)$	$\tau^*(ms)$
0.0	0.0	0.820 - 0.999	21.24 - 25.87	0.012 - 23.52	1433.64 - 226.2	67.50 - 8.74
0.01	0.039	0.835 - 1.0185	21.63 - 26.38	0.016 - 18.67	1250 - 182.0	57.82 - 6.9
0.05	0.174	0.895 - 1.0865	23.18 - 28.14	0.043 - 11.72	790.4 - 150.28	34.1 - 5.34
0.1	0.308	0.969 - 1.1704	25.10 - 30.31	0.068 - 8.40	608.4 - 134.99	24.24 - 4.45
0.15	0.414	1.042 - 1.249	26.99 - 32.35	0.078 - 6.74	534.56 - 126.57	19.81 - 3.91
0.2	0.5	1.116 - 1.348	28.90 - 34.91	0.097 - 6.16	462.8 - 115.96	16.01 - 3.32

Table 3.2 shows the unnormalized values of the soliton velocity (V), electric field (E), soliton width (W), and pulse duration (τ^*) for various values of α and the Mach number range M, respectively. It can be seen from Table 3.2 that for the minimum Mach number M_o, the soliton velocity and electric field amplitude tend to increase with Mach number M_o and α, but the width and pulse duration seems to decrease. Also, at the maximum Mach number range M_1, only the soliton velocity tends to

increase with Mach number M_1 and α, but the maximum electric field, width and pulse duration decrease. Table 3.2 illustrates that as α (*beta*) increases the soliton structures shift from the subsonic domain ($M < 1$) to purely supersonic ($M > 1$) for $\alpha \geq 0.15$.

We have plotted the Sagdeev potential $V(\psi, M)$ with normalized potential ψ (i.e, amplitude and depth) for the above mentioned parameters for various values of plasma parameters.

Figure 3.30 shows the Mach number ranges (minimum Mach number M_o and maximum Mach number M_1) supported by the model for the existence of finite amplitude ion-acoustic solitons as a function of the electrons density f. The fixed parameters are $\gamma = \cos 15^o$, $\tau = 0.04$ and $\beta \approx 0.02$.

The curves in Figure 3.31 show the variation of the Sagdeev potential $V(\psi, M)$ against normalized electrostatic potential ψ for different values of the Mach number M. Other fixed parameters are f=0.1, α=0.005, τ=0.04 and θ=15^o. The maximum Mach number value is 1.007 for the nonthermal parameter $\alpha = 0.005$. The negative potential ion-acoustic solitons can exist within subsonic and supersonic Mach number regimes due to the nonthermal hot electron contribution, unlike in the plasma model consisting of two Maxwellian electron temperatures where only the subsonic Mach number regime is possible (Model 1). The soliton amplitude increases with an increase in the Mach number. Similar negative potential structures have been reported by Ali-Fedela et al. (2010), for an unmagnetized plasma consisting of positively charged ions, cool electrons and nonthermal hot electrons. On the other hand, several authors have reported both positive and negative potential structures (Cairns et al. 1995; Mamun, 1997; Verheest and Hellberg, 2010) for the ion-acoustic solitary waves in nonthermal plasmas. Figure 3.32 shows the real potential ψ vs ξ which has been usually obtained numerically by integrating the energy integral (see equation 2.1) for the parameters used in Figure 3.31. It clearly shows that as the Mach number increases, the ion-acoustic soliton amplitude increases and the width decreases.

The variation of the Sagdeev potential $V(\psi, M)$ vs normalized electrostatic potential ψ is shown in Figure 3.33 for different values of the nonthermal parameter α for other fixed parameters, namely, cool electron number density, $f = 0.1$, cool to hot electron temperature ratio, $\tau = 0.04$, angle of propagation, $\theta = 15^o$ and Mach number, $M = 0.98$. It is seen that as α increases, the ion-acoustic soliton amplitude decreases, which behavior is consistent with many earlier theoretical studies (Cairns et al. 1995;

Mamun, 1997; Singh and Lakhina, 2004; Bahamida et al. 2007; Ali-Fedela et al. 2010; Verheest and Hellberg, 2010; Pakzad, 2011; Singh et al. 2011). The curves also show that the soliton structures can only exist within the range $0.0 \leq \alpha \leq 0.007$ for Mach number value $M = 0.98$. For $\alpha > 0.007$, no soliton solution is possible. Figure 3.34 shows the electrostatic potential ψ against ξ, for the parameters used in Figure 3.33. It shows that the negative potential ion-acoustic soliton amplitude decreases with increase in width as the nonthermal contribution α increases.

Figure 3.35 shows the variation of the Sagdeev potential vs normalized electrostatic potential ψ for different values of the cool electron number density f. The other fixed parameters are $M = 0.98$, $\alpha = 0.005$, $\theta = 15^o$ and cool to hot electron temperature $\tau = 0.04$. It is seen that the negative potential ion-acoustic soliton amplitude ψ increases with an increase in f. When there is only one electron species (i.e.$f = 0$), no soliton solution is possible, as pointed out by Buti (1980) and Ali-Fedela et al. (2010). Our calculations show that soliton solutions are possible for f values in the range $0.1 \leq f \leq 0.37$. Unlike the case of an unmagnetized nonthermal plasma reported by Ail-Fedela et al. 2010, where a negative potential double layer was found to exist as a boundary to the soliton solutions. Figure 3.36 shows the real potential ψ against ξ, for the same parameters used in Figure 3.35. It shows that as the cool electron density f increases, the ion-acoustic solitons amplitude increases and the width also increases.

The curves in Figure 3.37 show the variation of the Sagdeev potential $V(\psi, M)$ against the real potential ψ for different values of the cool to hot electron temperature ratio τ. The chosen parameters are $f = 0.1$ and the other fixed parameters as in Figure 3.35. The soliton structures exist for the cool to hot electron temperature ratio $\tau = T_c/T_h$ of 0.04, 0.08, and 0.099, at a certain point where τ value is equal to 0.1006, a double layer appears (see Section 2.3), beyond that there are no soliton or double layer solutions, whereas in our previous study (Model 1), the double layer solution appears at $\tau = 0.0877117$ (see Figure 3.7). As the cool to hot electron temperature ratio increases the soliton amplitude also increases, as found by earlier studies (Baboolal et al. 1990; Baluku et al. 2010). Figure 3.38 shows the electrostatic potential ψ against ξ, for the parameters used in Figure 3.37. It is seen that as the cool to hot electron temperature increases, the amplitude as well as the width of the ion-acoustic soliton increases. The double layer bounding is also shown.

In Figure 3.39, the curves show the variation of the Sagdeev potential with real

potential ψ for different values of the propagation angle θ, (where $\cos\theta = \gamma$ the waves obliqueness). The fixed parameters are α=0.005, f=0.1, τ=0.04 and M=0.98. It is interesting to note that at $\theta = 42.9105^o$ a double layer structure appears. For $\theta > 42.9105^o$ there are no soliton or double layer solutions. The curves show that as the angle of propagation θ increases (obliquity increases), the soliton amplitude increases. Due to the waves obliqueness, it has been observed that the solutions for a magnetized plasma are more restricted compared to an unmagnetized plasma (Ghosh and Lakhina, 2004). Figure 3.40 shows the electrostatic potential ψ against ξ, for the same parameters used in Figure 3.39. It is seen from the curves that as we increase the propagation angle θ, the amplitude as well as width of the soliton increases until the double layer boundary is reached.

The variation of the Sagdeev potential $V(\psi, M)$ with normalized electrostatic potential ψ is shown in Figure 3.41 for different combinations of θ and M to produce a double a double layer. The fixed parameters are f=0.1, α=0.005, τ=0.04. As in Model 1 and 2, the curves show all combinations of (θ, M) yield exactly the same value for the double layer amplitude. This corresponds to a "point" solution as shown in Figure 4 of Djebli and Marif (2009). As a follow up, we show in Figure 3.41. Figure 3.42 shows the existence domain of solitons and double layers by plotting the amplitude ψ_{Max} against angle of propagation θ for different M values. For a given M, ψ_{Max} increases with θ until a double layer appears. We observe in Figure 3.41 that as M increases, the θ-value for a double layer solution decreases.

The variation of the Sagdeev potential $V(\psi, M)$ against the normalized potential ψ is shown in Figure 3.43 for different values of the cool to hot electron temperature ratio τ and the Mach number M for the fixed parameters f=0.1, α=0.005 and θ=15^o. It is interesting to point out that the supersoliton solution (Dubinov and Kolotkov, 2012; Verheest et al. 2013; Maharaj et al. 2013) has been found to exist only at τ=0.10006, with corresponding Mach number value M=0.98. It is noted that pseudo-potential well for the soliton that immediately follows the double layers is extremely deep. Above this particular point only soliton solutions are possible. Figure 3.44 shows the existence domain of solitons and supersolitons for the same parameters in Figure 3.45. The curves were plotted for the variation of the maximum electrostatic potential ψ_{Max} against τ for different values of the Mach number M. The maximum Mach number for negative potential solitions is bounded by those of the soliton and supersoliton solutions corresponding to a given cool and electron temperature ratio τ. The supersoliton potential is limited by the minimum Mach number value at higher

number of the cool to hot electron temperature ratio τ= 0.10006. Other existence domains were bounded by soliton solutions.

3.3.3 Discussion

In this Section we have studied the oblique propagation of nonlinear ion acoustic waves in magnetized plasma consisting of a cold ion fluid, Boltzmann distributions of the cool electrons and nonthermal distributions of the hot electron species using the Sagdeev pseudo-potential approach. In Model 1, we investigated the characteristics of a plasma model composed of a cold and hot Maxwellian electron species and a cold ion fluid. Here, we adopted Cairn's proposed nonthermal distribution model (Cairn et al. 1995) for the hot electron species due to the observed presence of fast energetic particles in auroral region while the cool electrons remain Maxwellian. It was found that the inclusion of nonthermal hot electrons extends the Mach number domain for solitons to exist to the supersonic region. The model supports the existence of negative potential ion-acoustic (low frequency) solitons and double layers. These are found to have much higher amplitudes than the two Boltzmann electrons temperature. The nonthermal distribution model of the fast energetic electrons are a common feature of magnetosphere and ionospheric plasmas. Therefore, the present study is applied to examine nonlinear ion-acoustic solitary waves of the mid-altitude region of the Earth's magnetosphere. The following parameters are taken from the Viking observations (Berthomier et al., 1998), namely, $n_c = 0.2cm^3$, $n_h = 1.8cm^3$, $T_c = 1eV$, $T_h = 26eV$, which gave $T_{eff} \approx 7eV$. The maximum electric field generated for $M = 0.98$, $\theta = 35^o$, $\alpha = 0.1$ is about $0.325mV/m$ and soliton width, pulse duration and speed comes out to be $\approx 364m$, $14.34ms$ and $25.4km/s$ respectively, which is within the predicted range of values. These results are in agreement with satellite observations (Dovner et al., 1994; Berthomier et al., 1998).

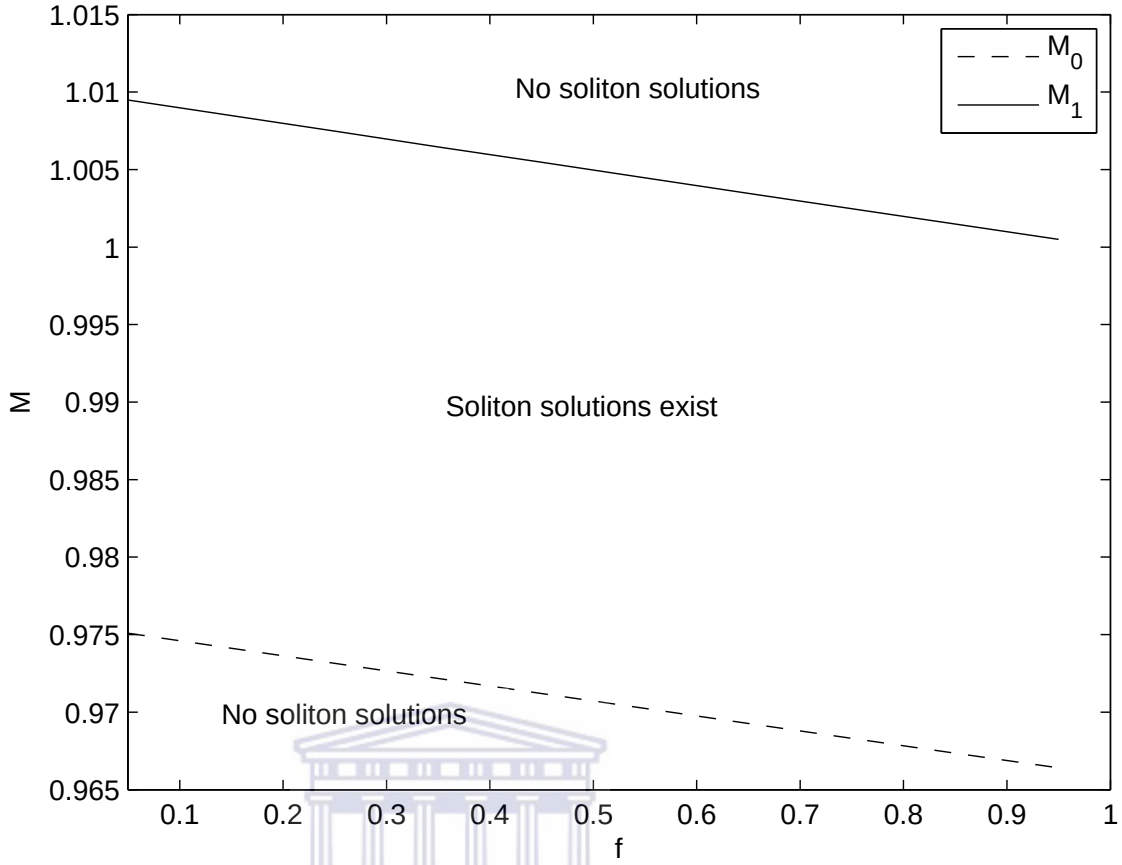

Figure 3.30: Existence domains of ion-acoustic solitons shown as a function of the normalized cool electron number density f, for fixed τ= 0.04, α=0.005, θ=15^o.

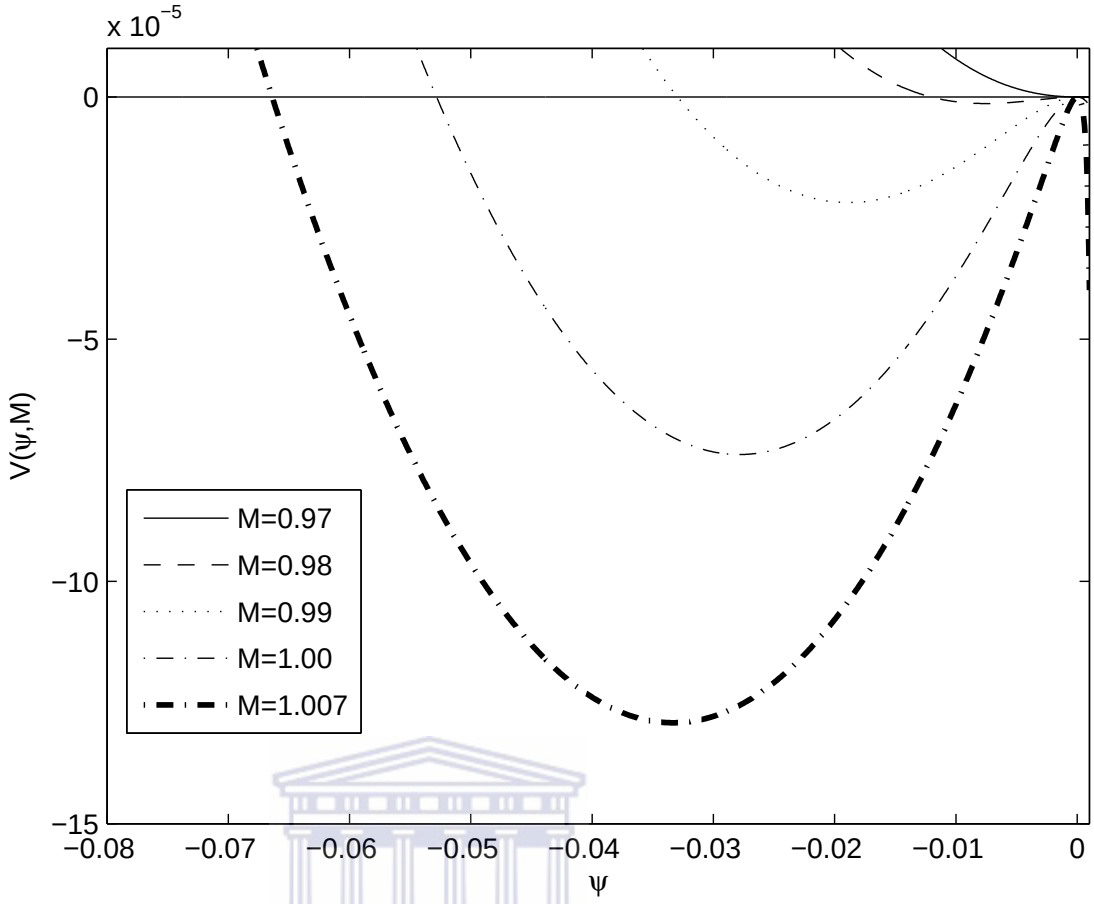

Figure 3.31: Sagdeev potential, $V(\psi, M)$ vs normalized electrostatic potential ψ. The fixed parameters are τ= 0.04, f=0.1, α=0.005, θ=15^o and M=0.97, 0.98, 0.99, 1.00, 1.007.

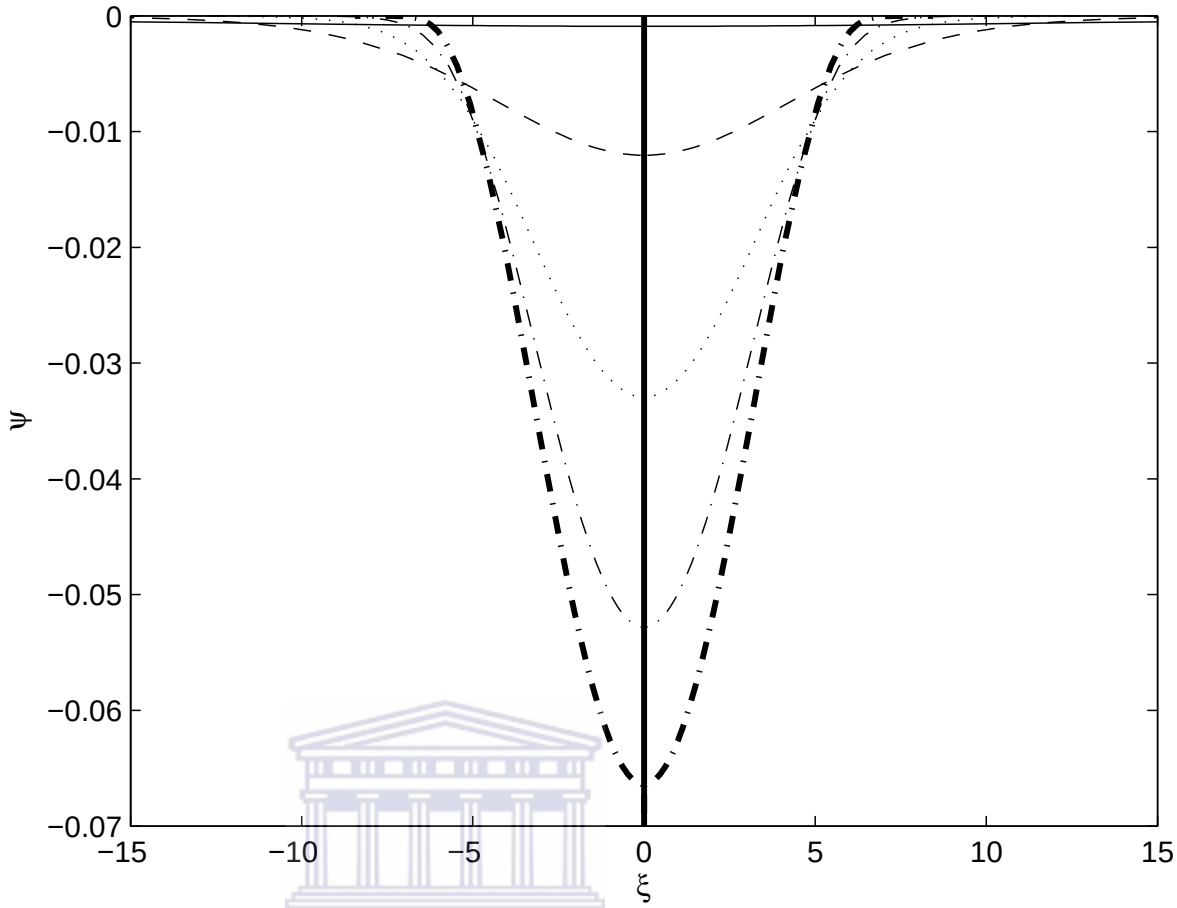

Figure 3.32: Electrostatic potential ψ vs ξ for the parameters of Figure 3.31, with M=0.975(—), M=0.98 (- - -), $M = 0.99$ (...), M=1.00 (- . -) and M=1.007(— — —).

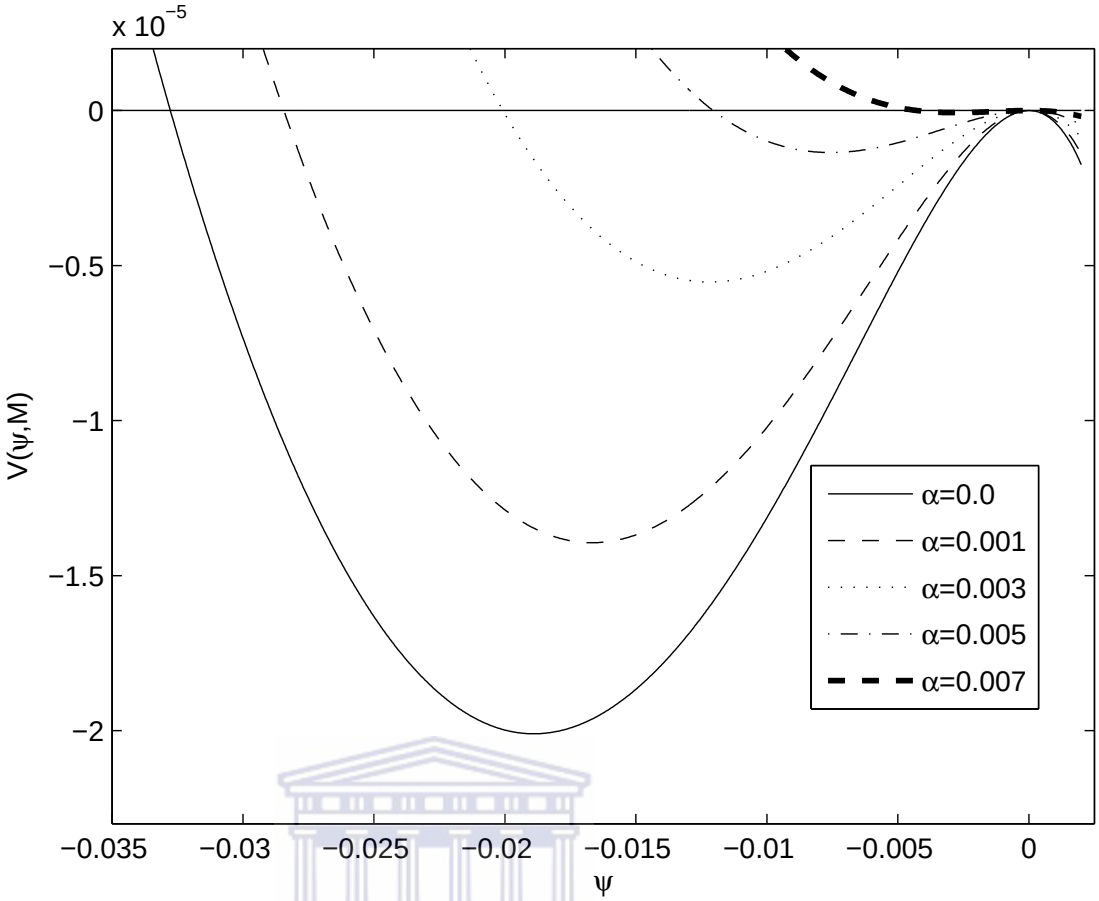

Figure 3.33: Sagdeev potential, $V(\psi, M)$ vs normalized electrostatic potential ψ. The fixed parameters are τ= 0.04, f=0.1, θ=15^o and M=0.98 with α=0.0, 0.001, 0.003, 0.005, 0.007.

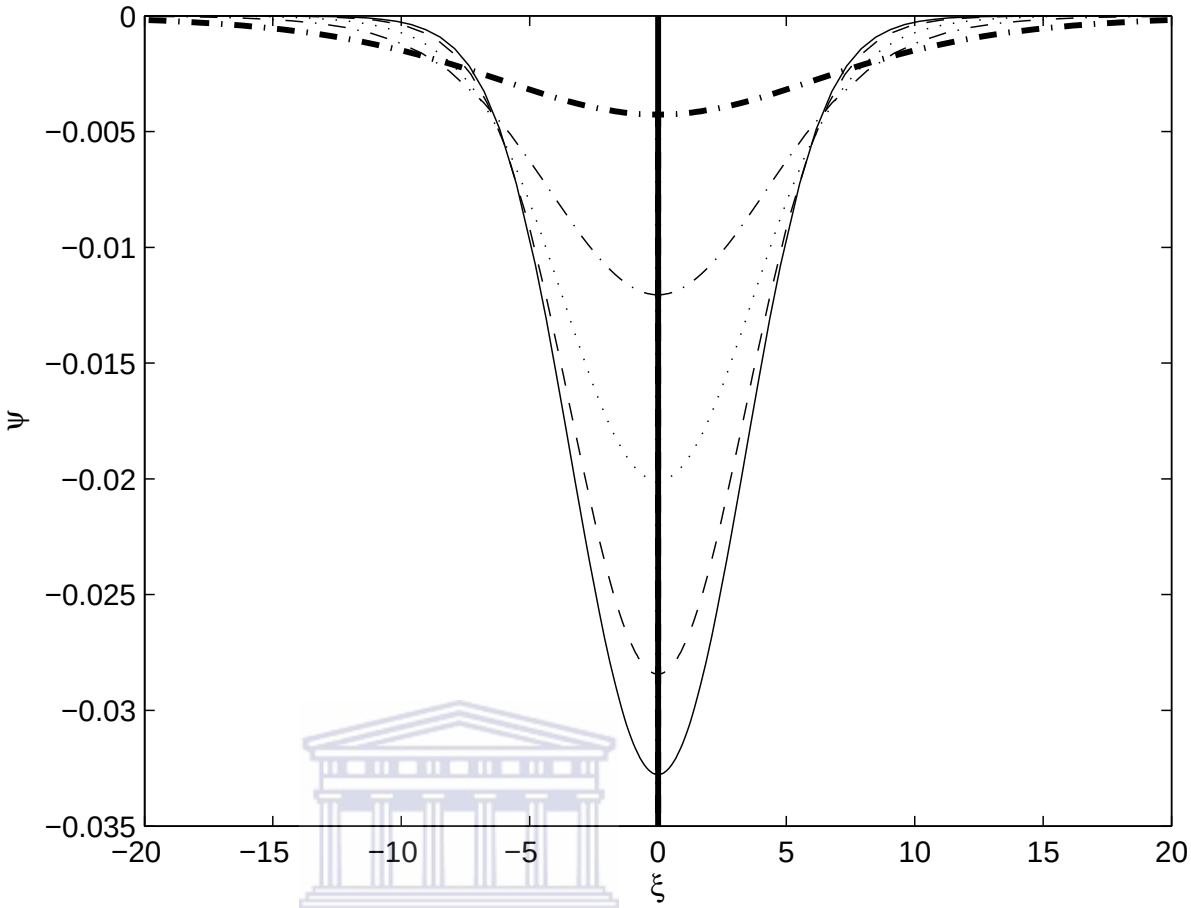

Figure 3.34: Normalized electrostatic potential ψ vs ξ for the parameters of Figure 3.33, with α=0.0 (—), α=0.001 (- - -), α=0.003 (. . .), α= 0.001 (- . -) and α=0.0 (−.−).

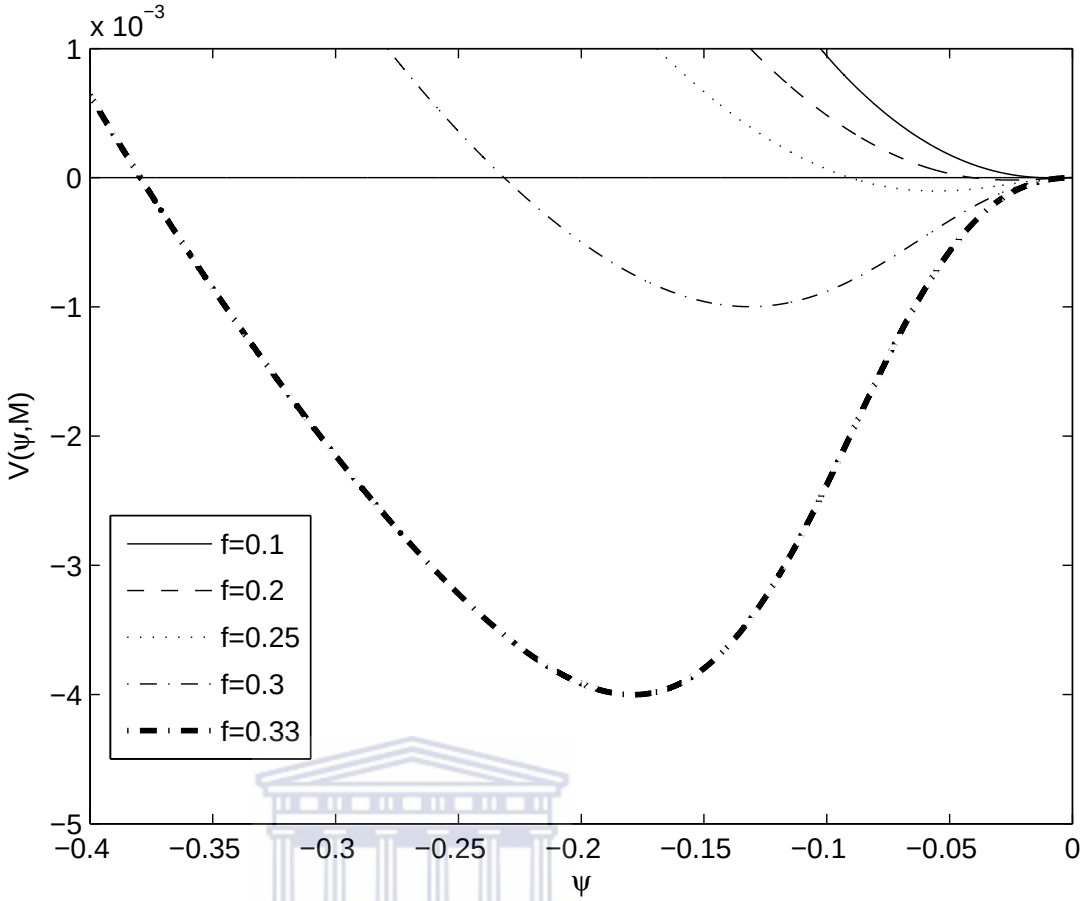

Figure 3.35: Sagdeev potential, $V(\psi, M)$ vs normalized electrostatic potential ψ. The fixed parameters are $\tau = 0.04$, α=0.005, θ=15^o and M=0.98, with f=0.1, 0.2, 0.25, 0.3, 0.33.

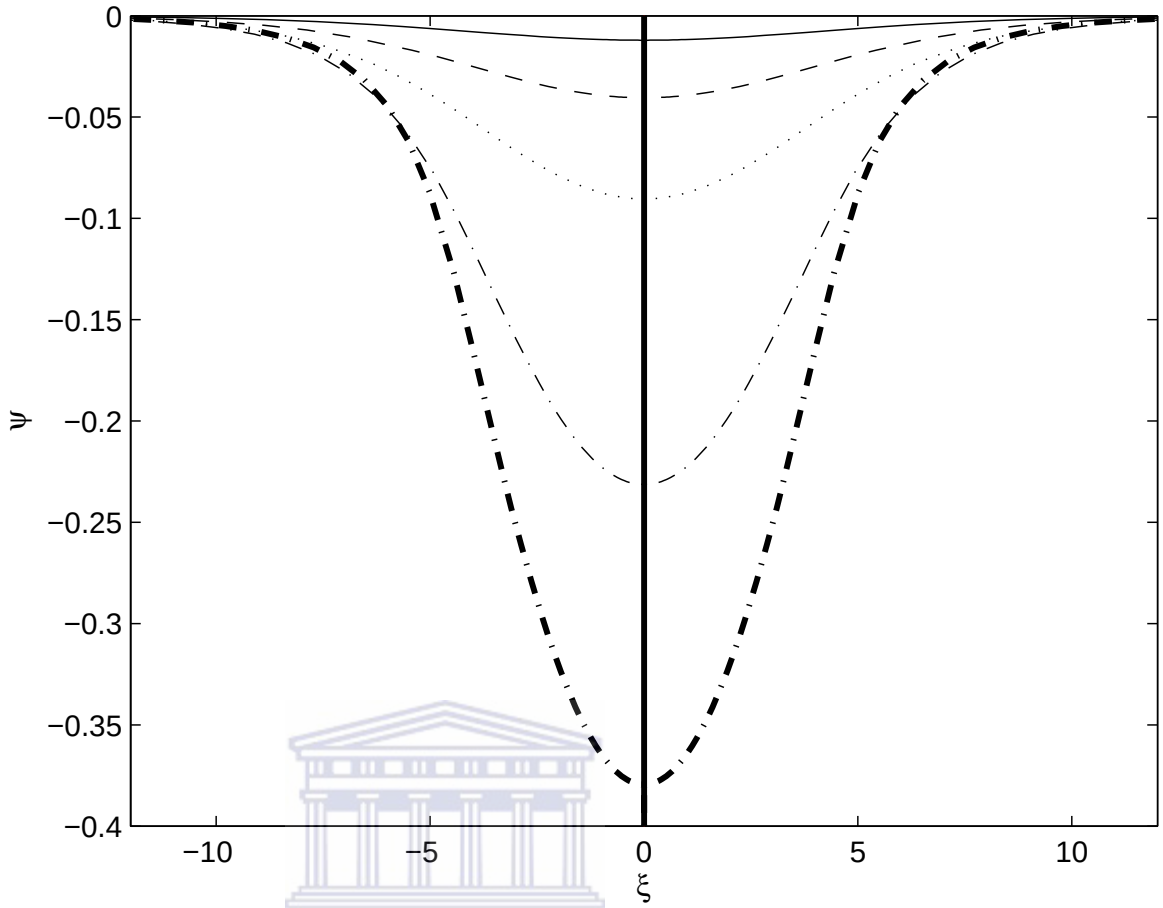

Figure 3.36: Normalized electrostatic potential ψ vs ξ for the parameters of Figure 3.35, with f=0.1(—), f=0.2 (- - -), f=0.25 (...), f=0.3 (- . -) and f=0.33(—.—).

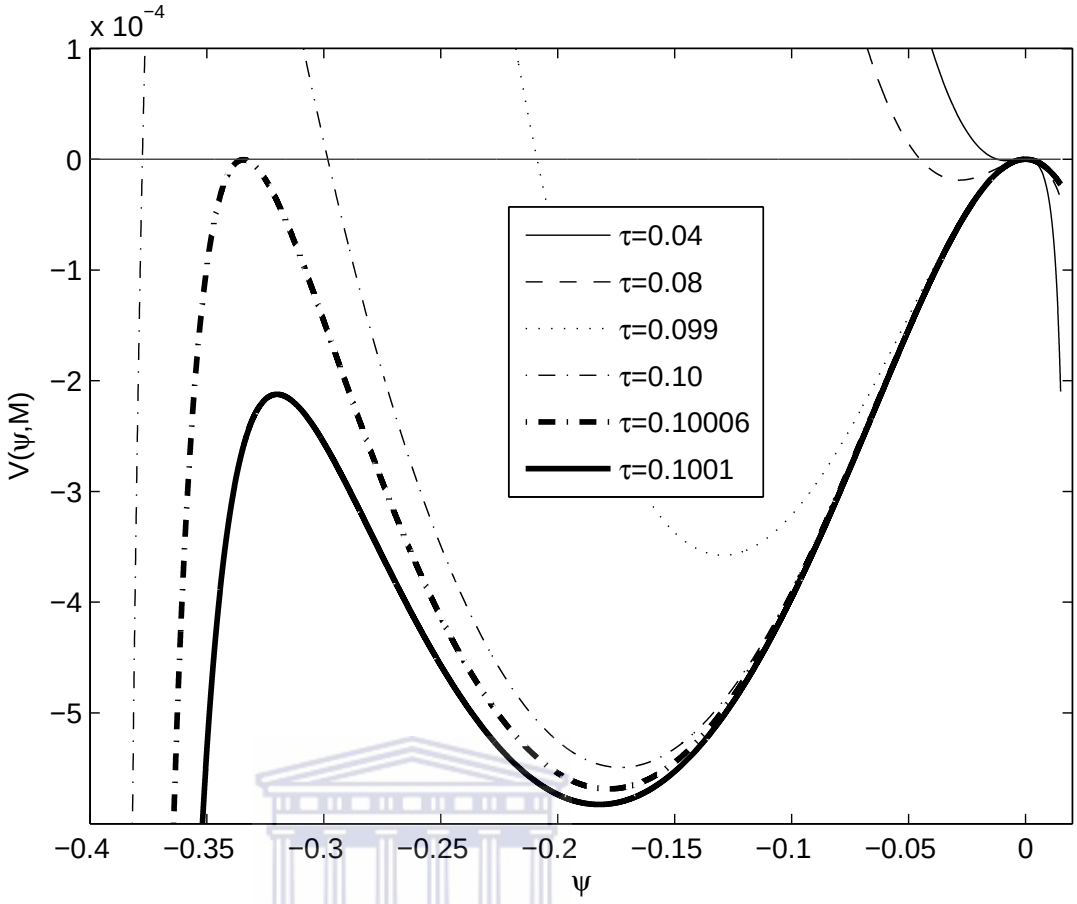

Figure 3.37: Sagdeev potential, $V(\psi, M)$ vs normalized electrostatic potential ψ. The fixed parameters are f=0.1, α=0.005, θ=15^o and M=0.98, with τ=0.04, 0.08, 0.099, 0.10, 0.10006 and 0.1001-no solution.

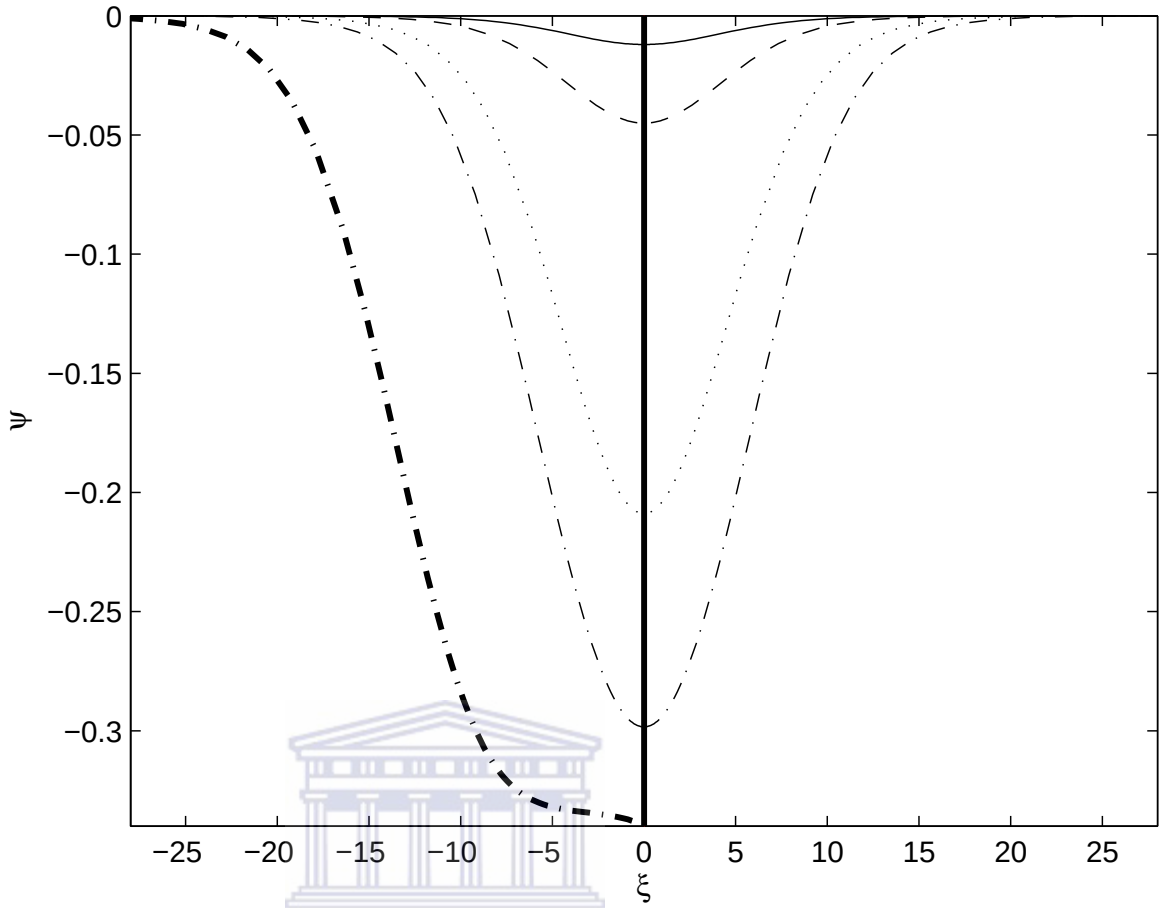

Figure 3.38: Normalized electrostatic potential ψ vs ξf for the parameters of Figure 3.37, with τ=0.04(—), τ=0.08 (- - -), τ=0.099 (...), τ=0.10 (- . -) and τ=0.10006(—.—)- (a double layer).

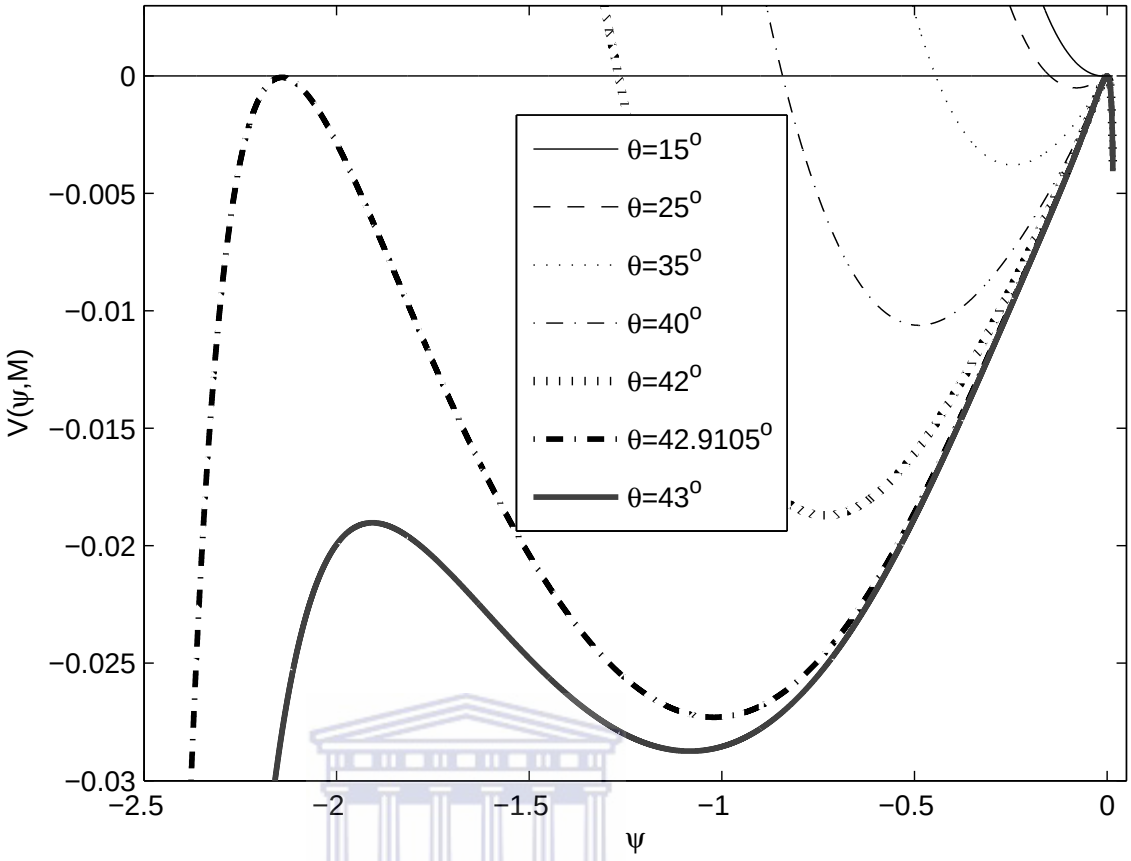

Figure 3.39: Sagdeev potential, $V(\psi, M)$ vs normalized electrostatic potential ψ. The fixed parameters are f=0.1, α=0.005, τ=0.04 and M=0.98, with θ=15^o, 25^o, 35^o, 40^o, 42^o, 42.9105^o and 43^o-(no solution).

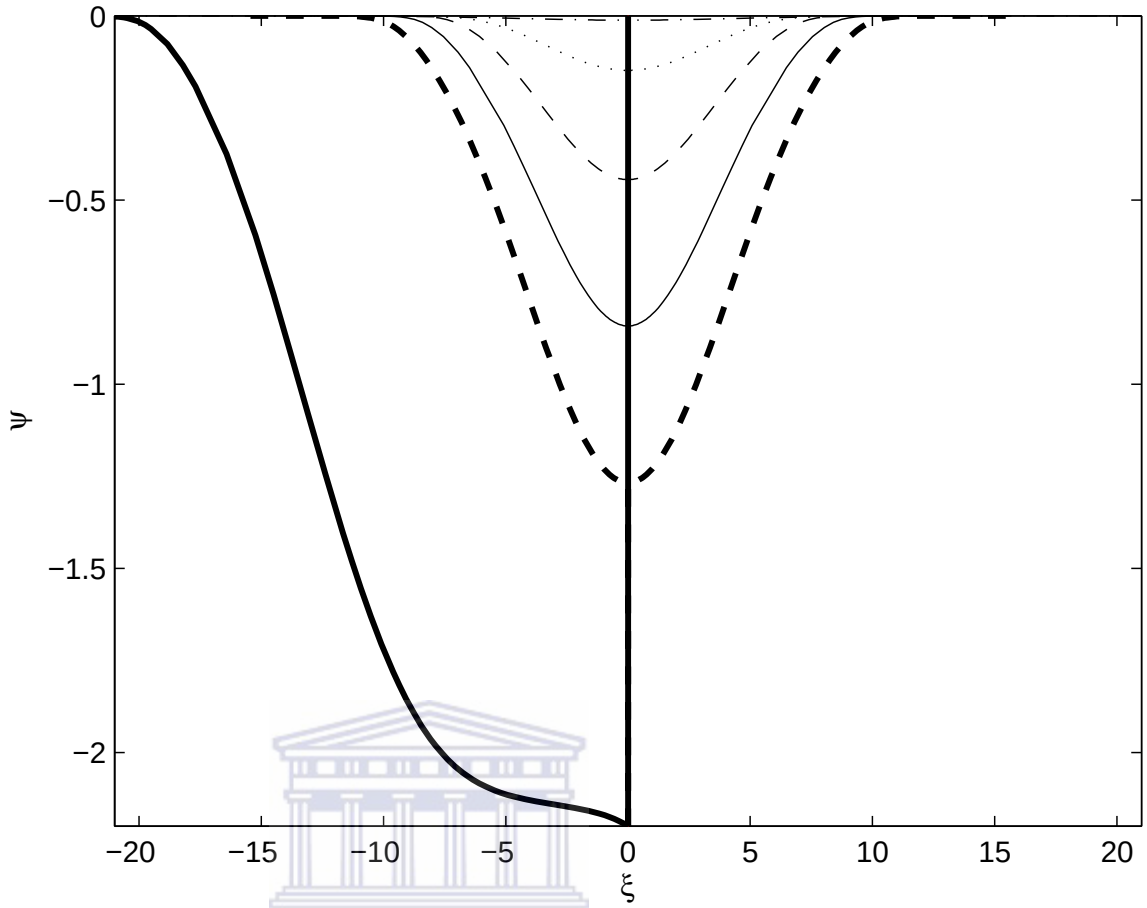

Figure 3.40: Normalized electrostatic potential ψ vs ξ for the parameters of Figure 3.39, with θ= 15^o (- . -), θ=25^o (. . .), θ=35^o (- - -), θ=40^o (—), θ=42^o (— — —), θ=42.9105 (—) (double layer).

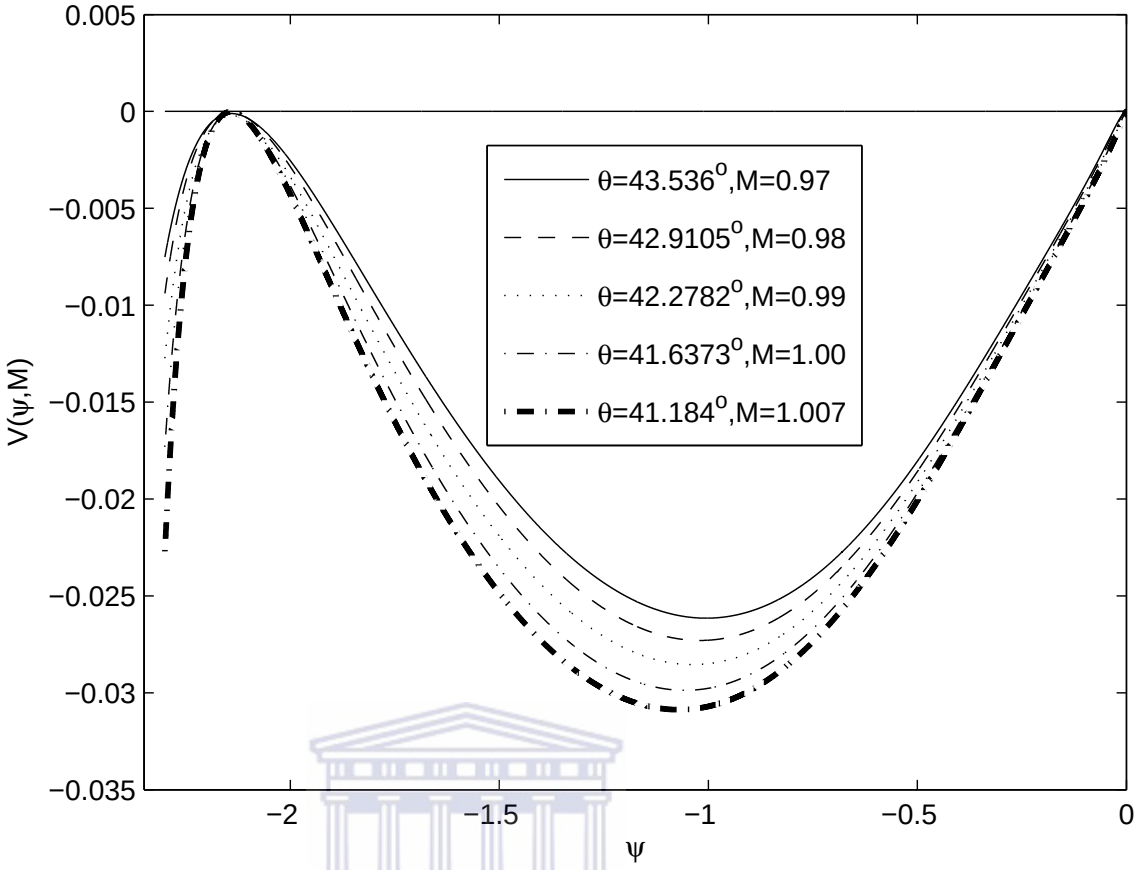

Figure 3.41: Sagdeev potential, $V(\psi, M)$ vs normalized electrostatic potential ψ. The fixed parameters are τ= 0.04, f=0.1 and α=0.005, for θ=43.536^o and M=0.97, θ=42.9105^o and M=0.98, 42.2782^o,M=0.99, θ=41.6373^o,M=1.00, θ=41.184^o and M=1.007.

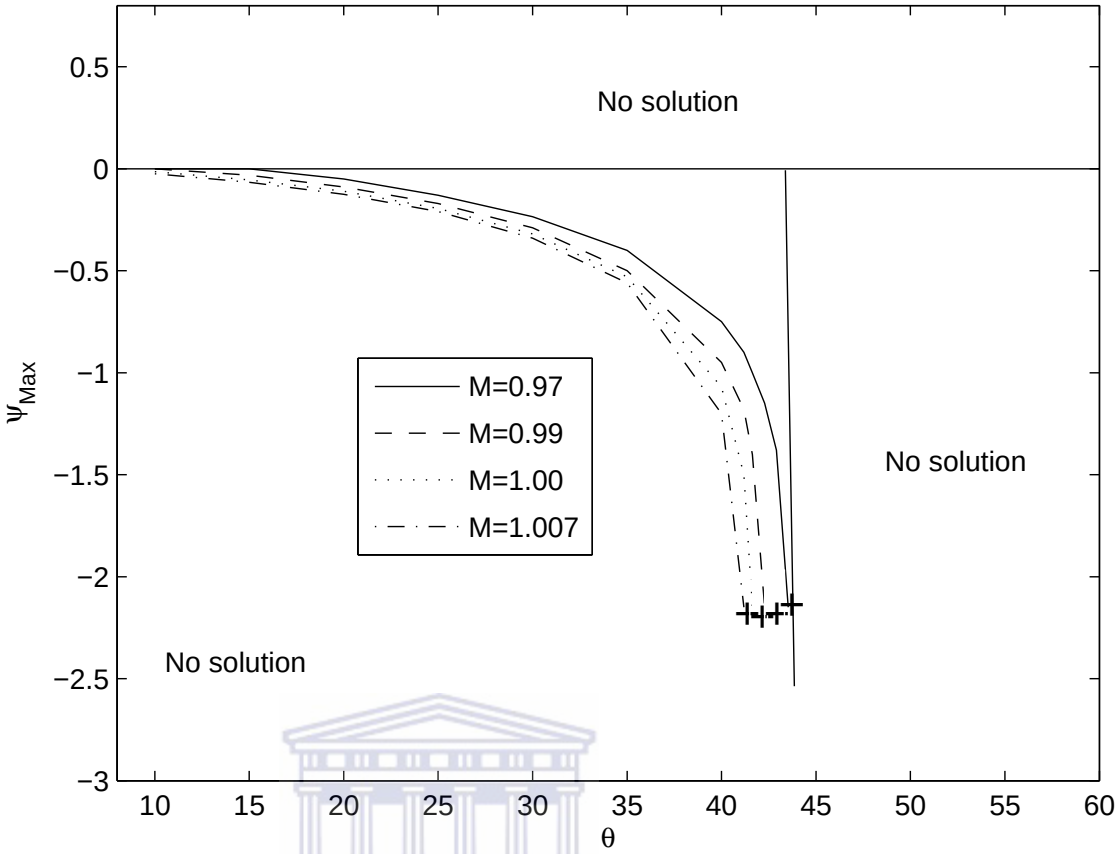

Figure 3.42: Maximum electrostatic potential, ψ_{Max} vs propagating angle θ for the parameters of Figure 3.41, with M=0.97, 0.99, 1.00, 1.007. The "+" indicates a double layer solution.

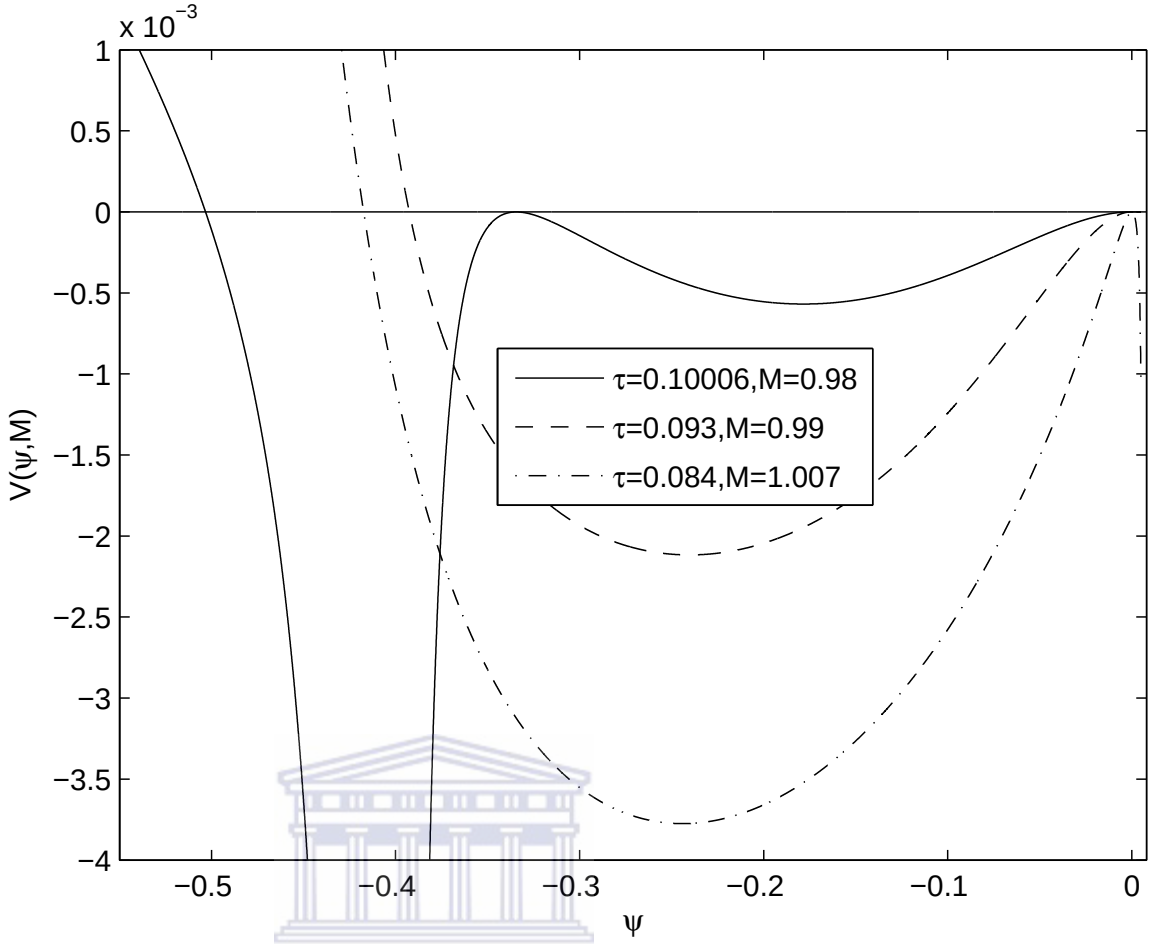

Figure 3.43: Sagdeev potential, $V(\psi, M)$ vs normalized electrostatic potential ψ. The parameters are σ=0.01, f=0.1, θ=15^o for τ=0.10006 and M=0.98, τ=0.093 and M=0.99, τ=0.084, M=1.007. The curve corresponding to $\tau = 0.10006$ and $M = 0.98$ represents a solution that follows immediately after a double layer and called a supersoliton.

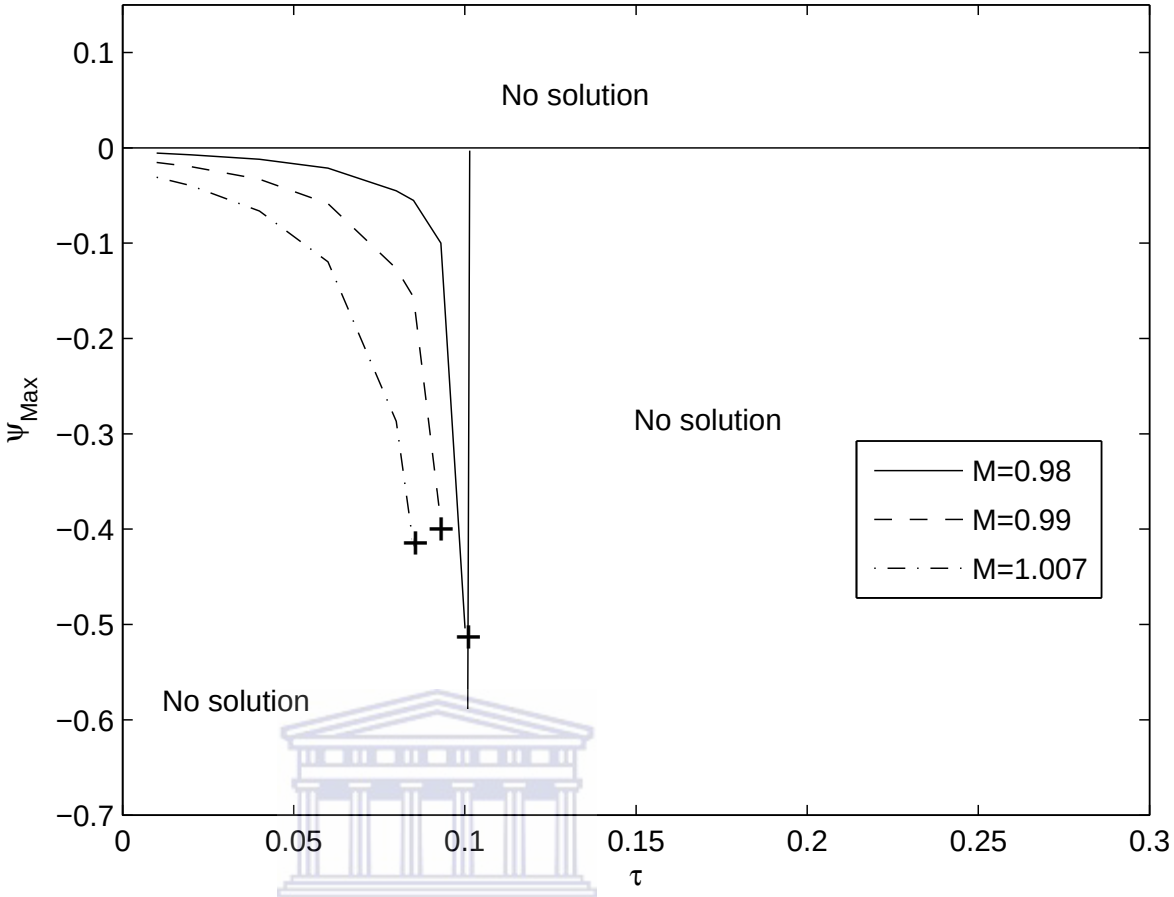

Figure 3.44: Maximum electrostatic potential, ψ_{Max} vs τ. The parameters of Figure 3.43 and τ=0.10006 and M=0.98, τ=0.093 and M=0.99, τ=0.084, M=1.007.

Chapter 4

Low frequency non-linear fluctuations in multi-ion plasmas

In this Chapter we use the techniques developed in the previous Chapter to study low frequency non-linear electrostatic fluctuations in multi-component plasma, with two-ion species. In the first model (Section 4.1), we consider a three component plasma model consisting of cold oxygen ions (temperature T_i=0) governed by fluid equations, and Boltzmann distributions of hot proton and cool electron species. Subsequently, we extent the model to include ion beams (Model 2 of Section 4.2) by considering a cold oxygen ion beam. We extend Model 1 (Section 4.1) to a four component plasma by including a hot electron species (Model 3, Section 4.3).

4.1 Model 1: Magnetized plasma with cold oxygen ions and Boltzmann distribution of hot protons and cool electrons

In this model, low frequency arbitrary amplitude electrostatic solitary waves are studied in a three component magnetized plasma consisting of a cold oxygen ion fluid and Boltzmann distribution of hot proton and electron species, using the Sagdeev pseudopotential technique (cf. Section 2.3.2).

4.1.1 Basic equations

We consider the propagation of ion-acoustic waves in a three-component collisionless plasma in the presence of an external magnetic field $\mathbf{B_0} = B_o\hat{\mathbf{z}}$, along the z-direction. The density and temperature of the Boltzmann distributed cool electrons (N_e, T_e) and hot protons (N_p, T_p) is given by,

$$N_e = N_{eo} \exp\left(\frac{e\phi}{T_e}\right). \tag{4.1}$$

$$N_p = N_{po} \exp\left(\frac{-e\phi}{T_p}\right). \tag{4.2}$$

where ϕ is the potential of the waves and $N_{eo,po}$ are the ambient densities of the electrons and protons, respectively, which satisfies charge neutrality condition at equilibrium, i.e. $n_{eo} = n_{io} + n_{po}$. The cold oxygen ion species are described by the set of fluid equations (i.e continuity and momentum equations) as presented by Mahmood et al. (2005).

$$\frac{\partial N_i}{\partial t} + \frac{\partial (N_i V_{ix})}{\partial x} + \frac{\partial (N_i V_{iz})}{\partial z} = 0. \tag{4.3}$$

$$\frac{\partial V_{ix}}{\partial t} + \left(V_{ix}\frac{\partial}{\partial x} + V_{iz}\frac{\partial}{\partial z}\right) V_{ix} = -\frac{e}{m_i}\frac{\partial \phi}{\partial x} + \Omega_i V_{iy}, \tag{4.4}$$

$$\frac{\partial V_{iy}}{\partial t} + \left(V_{ix}\frac{\partial}{\partial x} + V_{iz}\frac{\partial}{\partial z}\right) V_{iy} = -\Omega_i V_{ix}, \tag{4.5}$$

$$\frac{\partial V_{iz}}{\partial t} + \left(V_{ix}\frac{\partial}{\partial x} + V_{iz}\frac{\partial}{\partial z}\right) V_{iz} = -\frac{e}{m_i}\frac{\partial \phi}{\partial z}, \tag{4.6}$$

where N_i is the oxygen ion beam density, V_{ix}, V_{iy} and V_{iz} are the components of the oxygen ion velocity along x, y, and z directions, respectively, and $\Omega_i (= eB_0/m_i)$ is the oxygen ion gyrofrequency and m_i is the oxygen ion mass.

The oxygen ion acoustic wave linear mode can be derive from the fluid equation (i.e continuity and momentum equations). For harmonic oscillations varying as $e^{i(kz-\omega t)}$, i.e. propagating along the magnetic field $\mathbf{B}_o$, then $\frac{\partial}{\partial t} \rightarrow -i\omega$, $\nabla \rightarrow ik\hat{z}$. From the continuity equation (4.3), we have

$$-i\omega N_i + ikN_{io}V_{iz} = 0,$$

$$V_{iz} = \frac{\omega N_i}{N_{io} k}.$$

At equilibrium, we have

$$N_{io} + N_{po} = N_{eo},$$

from which

$$\frac{N_{io}}{N_{eo}} = 1 - \frac{N_{po}}{N_{eo}} = 1 - g,$$

where $g = \frac{N_{po}}{N_{eo}}$.

Then

$$n_e = \frac{N_e}{N_{eo}} = \exp\left(\frac{e\phi}{T_e}\right),$$

$$n_p = \frac{N_{po}}{N_{eo}} = g \exp\left(-\alpha_T \frac{e\phi}{T_e}\right),$$

where $\alpha_T = \frac{T_e}{T_p}$ is the electron to proton temperature ratio.

Using the quasi-neutrality condition, we have

$$N_i = N_e - N_p,$$

$$(1-g) + n_{i1} = \left[\exp\left(\frac{e\phi}{T_e}\right) - g \exp\left(-\alpha_T \frac{e\phi}{T_e}\right)\right]$$

then, we can expand the exponential in a Taylor series for $|e\phi/T_c| \ll 1$,

$$\exp\left(\frac{e\phi}{T_e}\right) = \left[1 + \frac{e\phi}{T_e} + \frac{1}{2}\left(\frac{e\phi}{T_e}\right)^2 + ...\right] \simeq \left(1 + \frac{e\phi}{T_e}\right).$$

Therefore, neglecting the higher order terms in the expansion, we have

$$n_i = \left(1 + \frac{e\phi}{T_e}\right) - g\left(1 - \alpha_T \frac{e\phi}{T_e}\right) = \frac{N_{io}}{N_{eo}} + n_{i1},$$

from which

$$n_{i1} = \left(\frac{e\phi}{T_e}\right)(1 + g\alpha_T), \tag{4.7}$$

From the momentum equation (4.6), we have

$$-i\omega V_{iz} = -\frac{eik\phi}{m_i},$$

$$\omega\left(\frac{\omega n_{i1}}{N_{io}k}\right) = \frac{k}{m_i}(e\phi).$$

Therefore,

$$\frac{\omega^2 n_{i1}}{1-g} = \frac{k^2}{m_i}e\phi \tag{4.8}$$

where $n_{i1} = \frac{N_{i1}}{N_{eo}}$.

From (4.7) and (4.8)

$$\frac{\omega^2}{k^2}\frac{e\phi}{T_e}(1+g\alpha_T) = \frac{T_e}{m_i}\frac{e\phi}{T_e}(1-g),$$

$$\frac{\omega^2}{k^2} = \left(\frac{1-g}{1+g\alpha_T}\right)\frac{T_e}{m_i},$$

$$\frac{\omega}{k} = \left[\left(\frac{1-g}{1+g\alpha_T}\right)\left(\frac{T_e}{m_i}\right)\right]^{1/2} \equiv c_s$$

is the ion acoustic phase speed, where T_e is the electron temperature.

Introducing dimensionless variables, $\iota = \Omega_i t$, $(\eta, \zeta) = (x, z)/\rho_i$, $v_k = V_{ik}/c_s$ (where $k = x, y, z$) the velocity, $\rho_i = c_s/\Omega_i$ is the ion gyro-radius, $M = V/c_s$ is the Mach number in terms of the ion acoustic speed, the potential $\psi = e\phi/T_e$, density $N_j = N_{jo}/N_{eo}$ (where $j = e, i, p$) and $c_s = ((1-g)T_e/(1+g\alpha_T)m_i)^{1/2}$ is the oxygen ion acoustic speed. Then, we define the nonlinear localized stationary solution in the moving frame $\xi = (\alpha\eta + \gamma\zeta - M\iota)/M$, where $\alpha = \sin\theta$, $\gamma = \cos\theta$ and θ is the angle between the direction of waves propagation and the magnetic field.

Now, assuming all the dependent variables are functions of ξ, equations (4.1) - (4.6) can be written as,

$$n_e = \exp(\psi). \tag{4.9}$$

$$n_p = g\exp(-\alpha_T\psi). \tag{4.10}$$

$$\alpha v_x + \gamma v_z = M\left(1 - \frac{1}{n_i}\right). \tag{4.11}$$

$$\frac{M}{n_i}\frac{dv_x}{d\xi} = \alpha\frac{d\psi}{d\xi} - Mv_y. \tag{4.12}$$

$$\frac{M}{n_i}\frac{dv_y}{d\xi} = Mv_x. \tag{4.13}$$

$$\frac{M}{n_i}\frac{dv_z}{d\xi} = \gamma\frac{d\psi}{d\xi}. \tag{4.14}$$

Then, the system of equation is closed with quasi-neutrality condition for low frequency phenomena

$$n_i = n_e - n_p = \frac{\exp(\psi) - g\exp(-\alpha_T\psi)}{1-g} \tag{4.15}$$

where $\alpha_T = \frac{T_e}{T_p}$, $g = \frac{N_{po}}{N_{eo}}$ (< 1), then $\frac{N_{io}}{N_{eo}} = 1 - g$. Combining equations (4.11) - (4.15) and eliminating v_x, v_y, v_z, then integrating with the boundary conditions for solitary wave structures (namely, $n_i \to 1$, $\psi \to 0$, and $d\psi/d\xi \to 0$ at $\xi \to \pm\infty$), we obtain the nonlinear differential equation,

$$\frac{d}{d\xi}\left(\frac{d\chi}{d\xi}\right) = M^2(n_i - 1) - \gamma^2 n_i\left[\frac{1}{1-g}\left[(\exp(\psi) + \frac{g}{\alpha_T}(\exp(-\alpha_T\psi) - 1)\right]\right] \tag{4.16}$$

where

$$\chi = \left(\psi + \frac{M^2}{2n_i^2}\right). \tag{4.17}$$

Now, multiplying both sides of equation (4.16) by $2d\chi/d\xi$, and after integrating once with appropriate boundary conditions, we obtain the "energy-balance equation" (see Appendix D for $\delta v_o = 0$)

$$\frac{1}{2}\left(\frac{d\psi}{d\xi}\right)^2 + V(\psi, M) = 0, \tag{4.18}$$

where we have used the expression for $n_i(\psi)$ given in (4.15) to arrive at the Sagdeev pseudo-potential $V(\psi, M)$ (cf. Section 2.3) given by

$$\begin{aligned} V(\psi, M) = &-\frac{1}{\left(1 - \frac{M^2}{n_i^3}\left(\frac{1}{1-g}(\exp(\psi) + \alpha_T g\exp(-\alpha_T\psi)\right)\right)^2} \times \left(-\frac{M^4}{2n_i^2}(1-n_i)^2\right. \\ &-M^2(1-\gamma^2)\psi + M^2\left(\frac{1}{1-g}\left((\exp(\psi) - 1) + \frac{g}{\alpha_T}(\exp(-\alpha_T\psi) - 1)\right)\right) \\ &-\frac{\gamma^2}{2}\left(\frac{1}{1-g}\left((\exp(\psi) - 1) + \frac{g}{\alpha_T}(\exp(-\alpha_T\psi) - 1)\right)\right)^2 \\ &\left.-\frac{M^2\gamma^2}{n_i}\left(\frac{1}{1-g}\left((\exp(\psi) - 1) + \frac{g}{\alpha_T}(\exp(-\alpha_T\psi) - 1)\right)\right)\right). \end{aligned} \tag{4.19}$$

For the soliton solutions, the Sagdeev pseudo-potential $V(\psi, M)$ given by (4.19) must satisfy the soliton conditions (cf. Section 2.3.2). (i.e. $V(\psi, M) = 0$, $d\psi/d\xi =$

0, $V(\psi, M) = 0$ and $dV(\psi, M)/d(\psi) = 0$ at $\psi = 0$. $d^2V(\psi, M)/d(\psi)^2 < 0$ at $\psi = 0$; $V(\psi, M) = 0$ at $\psi = \psi_m$, $dV(\psi, M)/d(\psi) < (>)\ 0$ at $\psi_m < (>)\ 0$). At the origin, the Sagdeev potential $V(\psi, M)$ and its first derivative with respect to ψ vanished, and from the condition $\frac{d^2V(\psi,M)}{d\psi^2} < 0$ at $\psi = 0$, we have

$$\frac{d^2V(\psi, M)}{d\psi^2}|_{\psi=0} = \frac{M^2 - M_o^2}{M^2 - M_1^2} < 0, \tag{4.20}$$

where the critical Mach number, which is the lower limit for soliton solutions to exist, is given by

$$M_o^2 = \frac{\gamma^2(1-g)}{1+g\alpha_T} < 1 \quad since \quad \gamma, g < 1 \tag{4.21}$$

and for the upper limit M_1, which is the maximum Mach number for soliton solution to exist, we have

$$M_1^2 = \frac{1-g}{1+g\alpha_T} < 1 \quad since \quad g < 1. \tag{4.22}$$

For $\gamma \neq 0 : \gamma^2 = \cos^2\theta < 1$; which implies $M_o < M_1$, then if $M > M_1 \Rightarrow M > M_0$ from which $M^2 - M_o^2 > 0$ and $M^2 - M_1^2 > 0$, consequently (4.20) is not satisfied.

Similarly, if $M < M_o \Rightarrow M < M_1$ from which $M^2 - M_o^2 < 0$ and $M^2 - M_1^2 < 0$, once again (4.20) is not satisfied.

Therefore, (4.20) is satisfied only if

$$M_o < |M| < M_1, \tag{4.23}$$

i.e.

$$\gamma\sqrt{\frac{1-g}{1+g\alpha_T}} < |M| < \sqrt{\frac{1-g}{1+g\alpha_T}} < 1 \tag{4.24}$$

which is the range values of Mach number M for a given value of wave obliqueness ($\gamma = \cos\theta$), where θ is the angle of propagation. It is interesting to mention that in the magnetized plasma consisting of cold oxygen ions and Boltzmann electron and hot proton species, nonlinear ion-acoustic wave solutions can exist only in the subsonic Mach number region (i.e $M < 1$, see equation 4.24). This Mach number regime is similar to the case of a magnetized plasma consisting of single cold ions and Boltzmann electron species studied by Choi et al. (2006), i.e. the nonlinear ion-acoustic waves solutions were also found to exist only in the subsonic Mach number region.

4.1.2 Numerical results

Now, we numerically examine the existence of arbitrary amplitude solitons. The energy integral and Sagdeev potential $V(\psi, M)$ in (4.18) and (4.19) are computed for different parameter values (e.g. Mach number M, proton density g, temperature ratio $\alpha_T = T_e/T_p$ and obliqueness angle θ).

Table 4.1: Properties of ion-acoustic solitons, such as Soliton Velocity (V), Mach number range ($M_o < |M| < M_1$), Electric Field (E), Soliton Width (W) and Pulse Duration (τ^*), for various values of hot proton density (g) with $\theta = 35^o$, temperature ratio $\alpha_T = 0.1$.

g	$M_o < \|M\| < M_1$	$V(kms^{-1})$	$E(mVm^{-1})$	$W(m)$	$\tau^*(ms)$
0.0	0.8192 - 0.999	21.22 - 25.87	0.0002 - 31.04	6058 - 119.6	285.49 - 4.62
0.01	0.8147 - 0.994	21.10 - 25.74	0.0003 - 30.53	5252 - 120.12	248.91 - 4.67
0.05	0.7965 - 0.972	20.63 - 25.17	0.0004 - 28.68	4680 - 120.9	226.85 - 4.80
0.1	0.7735 - 0.943	20.03 - 24.42	0.0021 - 26.25	2626 - 122.2	131.10 - 5.00
0.15	0.7499 - 0.915	19.42 - 23.70	0.0025 - 24.22	2381.6 - 123.14	122.64 - 5.20
0.2	0.7259 - 0.885	18.80 - 22.92	0.0049 - 22.09	1861.6 - 124.28	99.02 - 5.42

Table 4.1 describes the behavior of the nonlinear low frequency electrostatic structures for different values of the proton density, and other fixed parameters are $\theta = 35^o$ and $\alpha_T = 0.1$ respectively. In table 4.1, there is subsequently a decrease in the Mach number region as the hot proton density g increases. At the minimum Mach number region the soliton velocity, width and pulse duration tend to decrease with g but only the electric field seems to increase. On the other hand (i.e the maximum Mach number region), the soliton velocity and electric field tend to decrease with a further increase in g value, while the width and pulse duration increase.

The curves in Figure 4.1 show the variation of the Sagdeev potential $V(\psi, M)$ against normalized electrostatic potential ψ for different Mach number M. The fixed parameters are proton density ratio $g = 0.1$, temperature ratio $\alpha_T = 0.1$, and angle of propagation $\theta = 15^o$. The soliton solutions exist within the Mach number range $0.915 \leq M \leq 0.94$, which is consistent with the equation (4.24). It is seen clearly from the curves that the positive potential ion-acoustic solitons' amplitude is increasing as the Mach number increases. However, these positive potential structures have been a common feature of low frequency waves in a plasma consisting of a single electron species as shown by many authors (Temerin et al. 1982; Cairns et al. 1995; Nakamura, 1999; Mahmood et al. 2003; Choi et al. 2006; Mahmood and Akhtar, 2008; Barman and Talukdar, 2010; Das, 2012). Figure 4.2 shows the normalized

electrostatic potential ψ against ξ, for the same parameters used in Figure 4.1. It is obvious from the curves that as the Mach number increases, the positive amplitude of the ion-acoustic soliton increases and the width decreases.

The variation of the Sagdeev potential $V(\psi, M)$ versus normalized electrostatic potential ψ is shown in Figure 4.3 for different proton density ratio g. The fixed parameters are Mach number $M = 0.93$, $\alpha_T = 0.1$, and $\theta = 15^o$. Above $g > 0.11$, no soliton solutions are possible. The soliton amplitude increases as the proton density ratio increases. The effects of the protons' density on the nonlinear evolution of low frequency electrostatic waves have been investigated by a number of authors (e.g. Reddy et al. 2006; Moolla et al. 2010). Figure 4.4 shows the normalized electrostatic potential ψ against ξ, for the same parameters in Figure 4.3. It shows clearly that as the proton density ratio p increases, the ion-acoustic solitons potential amplitude increases and the width decreases.

Figure 4.5 shows the variation of the Sagdeev potential $V(\psi, M)$ against normalized electrostatic potential ψ for different temperature ratio $\alpha_T = T_e/T_p$. The fixed parameters are $M = 0.93$, $g = 0.1$, and $\theta = 15^o$. It is observed that as the temperature ratio increases, the soliton amplitude increases and numerical computation shows that the positive potential soliton solutions are not possible beyond $\alpha_T > 0.35$. In the case of the nonlinear electrostatic fluctuations arising from a coupling of ion cyclotron and ion acoustic waves, Moolla et al. (2010) showed the range of the electron-proton temperature ratio $T_e/T_p <> 1.0$ for the existence of the nonlinear structures. Figure 4.6 shows the normalized electrostatic potential ψ against ξ, for the same parameters used in Figure 4.5. It is very obvious from the curves that as we increase the temperature ratio α_T, the ion-acoustic soliton amplitude increases and the width decreases.

In Figure 4.7, The curves show the variation of the Sagdeev potential $V(\psi, M)$ versus normalized electrostatic potential ψ for different values of the wave's obliqueness (angle of propagation) θ. The fixed parameters are Mach number $M = 0.93$, proton density ratio $g = 0.1$ and temperature ratio $\alpha_T = 0.1$. The soliton structures exist only within the range value $15^o \leq \theta \leq 62^o$. In the case of a magnetized plasma consisting of cold ions and electron species study by Choi et al. 2006, it has been shown that the soliton solutions can only be found at the critical Mach number value equal to the wave's obliqueness value (i.e. $M_o = \gamma$), also in dusty plasma (Farid et al. 2001). It shows clearly that the higher the propagating angle θ, the greater the solitary wave's amplitude. Figure 4.8 shows the normalized electrostatic potential ψ

against ξ, for the same parameters used in Figure 4.7. It is seen that the positive potential amplitude as well as width of the soliton increases with the increase in angle of propagation.

Figure 4.9 shows the existence domain of solitons. The fixed parameters are α_T=0.1 and θ=15^o. The curves were plotted for the variation of the maximum electrostatic potential ψ_{Max} against p for different values of the Mach number M. The maximum Mach number for positive potential solitions is bounded by those of the soliton solutions corresponding to a given proton density ratio g. Only positive potential solutions can be found to exist, whereas Baboolal et al. (1990) showed the cut off conditions and existence domains for both positive and negative potential soliton and double layers for plasma consisting of positive and negative charged ions and two electron temperature.

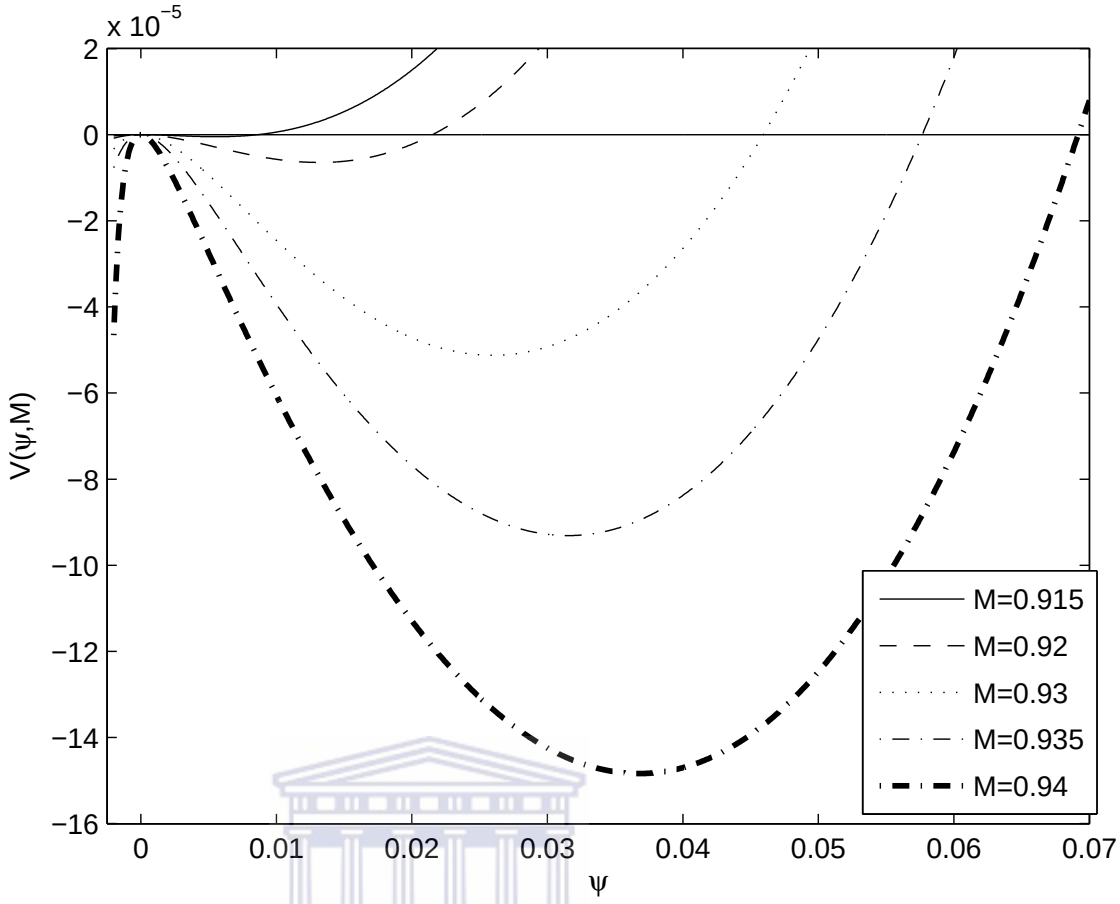

Figure 4.1: Sagdeev potential, $V(\psi, M)$ vs normalized electrostatic potential ψ. The fixed parameters are g= 0.1, α_T=0.1, θ=15^o and M=0.915, 0.92, 0.93, 0.935, 0.94.

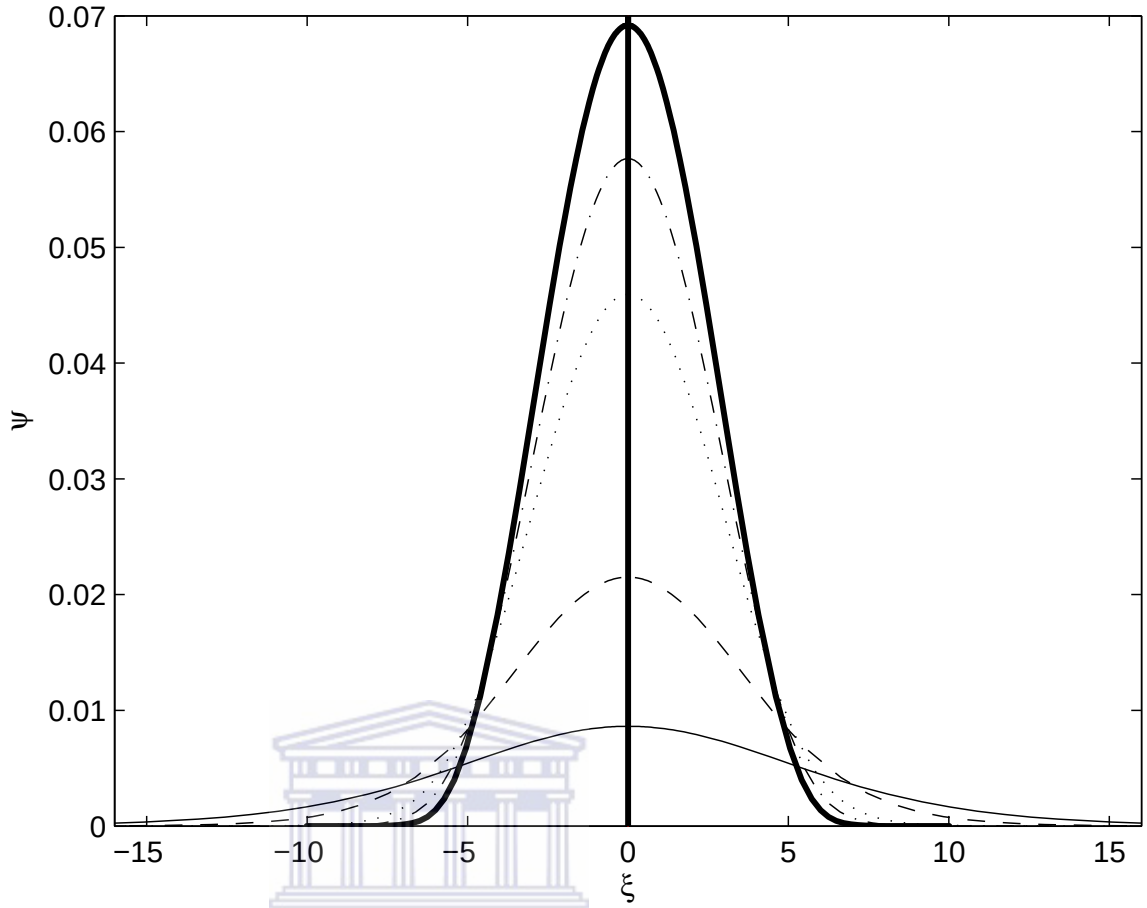

Figure 4.2: Normalized electrostatic potential ψ vs ξ for the parameters of Figure 4.1 with M= 0.915 (—), M=0.92 (- - -), M=0.93 (. . .), M=0.935 (- . -), M=0.94 (−).

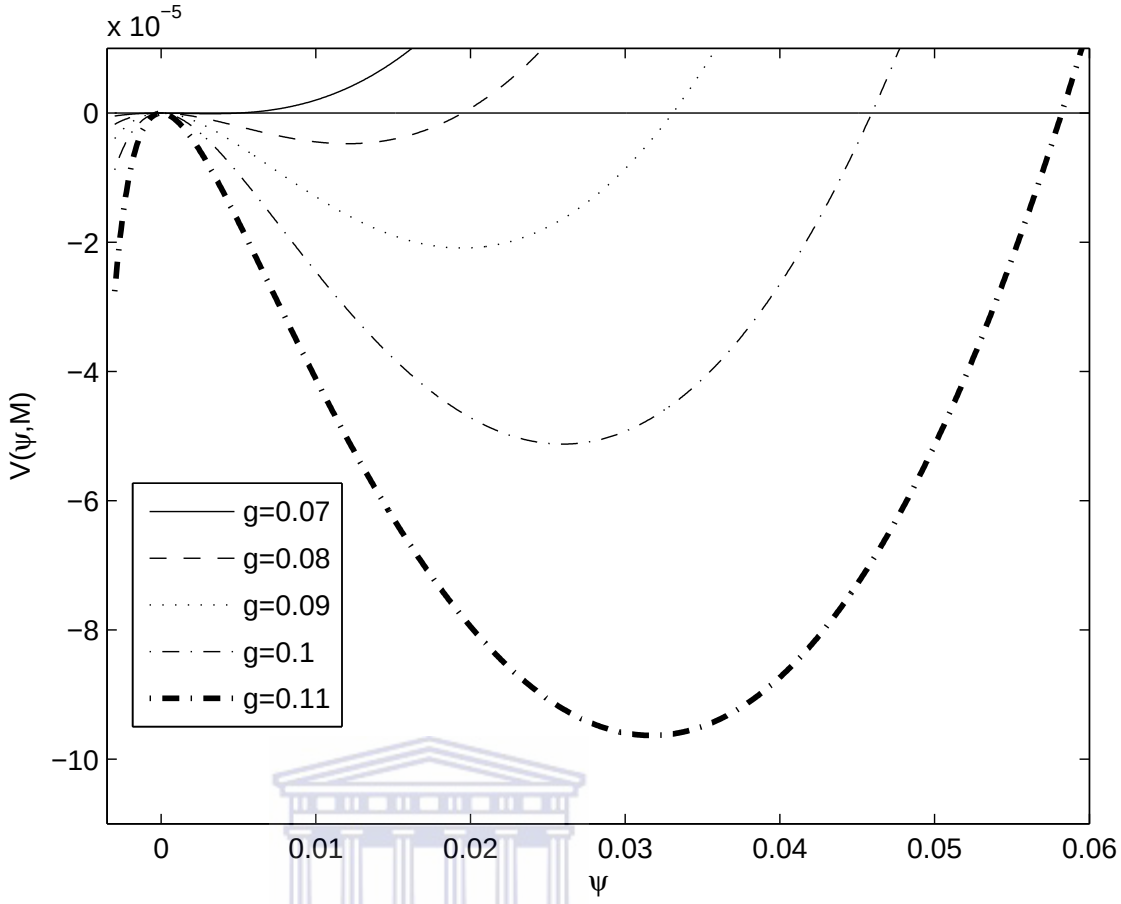

Figure 4.3: Sagdeev potential, $V(\psi, M)$ vs normalized electrostatic potential ψ. The fixed parameters are M=0.93, α_T=0.1, θ=15^o and g=0.07, 0.08, 0.09, 0.1, 0.11

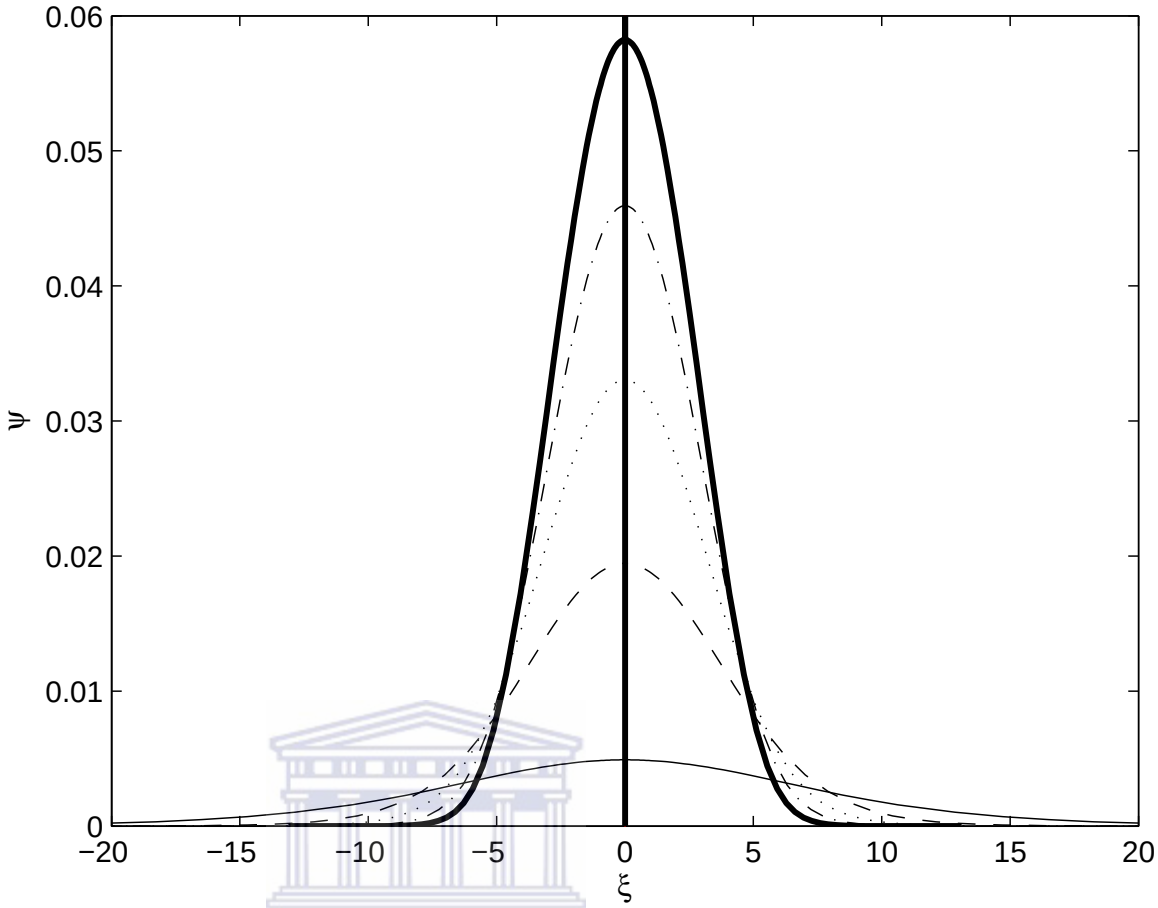

Figure 4.4: Normalized electrostatic potential ψ vs ξ for the parameters of Figure 4.3 with g= 0.07 (—), g=0.08 (- - -), g=0.09 (. . .), g=0.1 (- . -), g=0.11 (—)

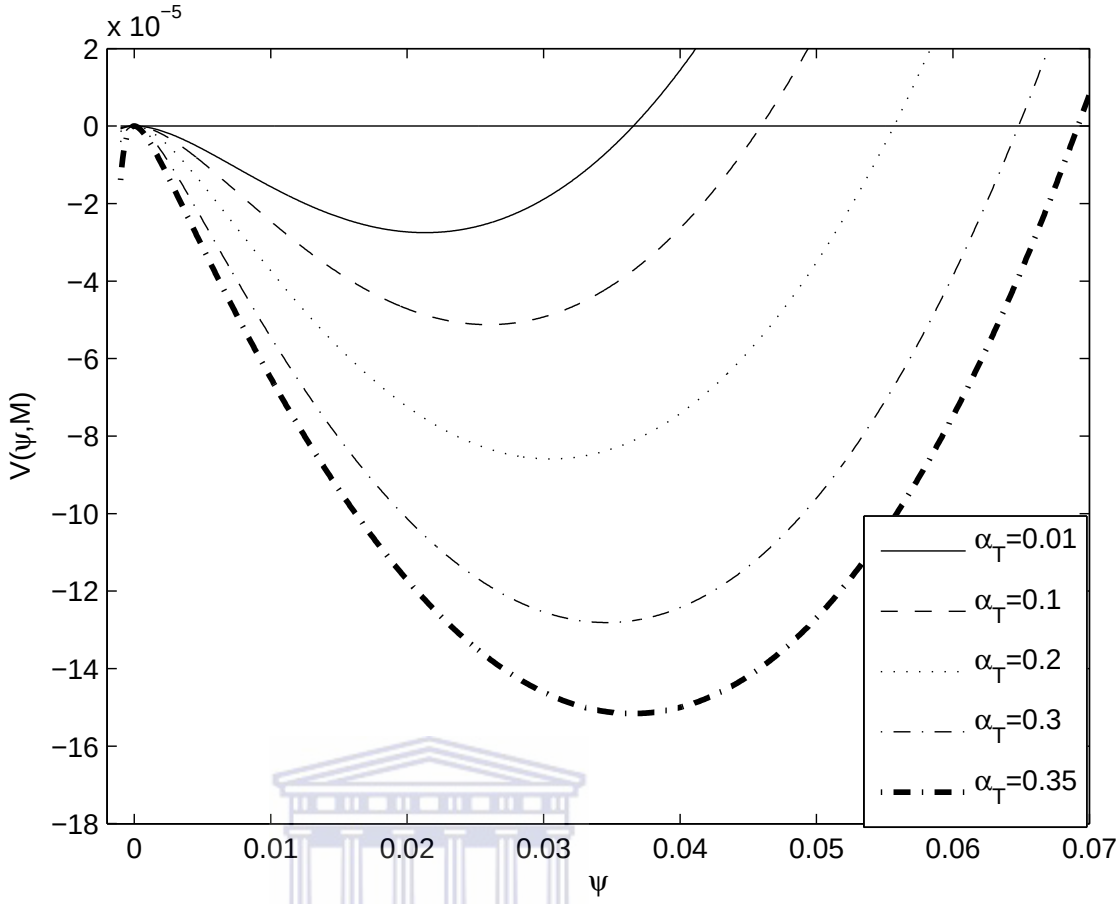

Figure 4.5: Sagdeev potential, $V(\psi, M)$ vs normalized electrostatic potential ψ. The fixed parameters are M=0.93, g=0.1, θ=15^o and α_T=0.01, 0.1, 0.2, 0.3, 0.35.

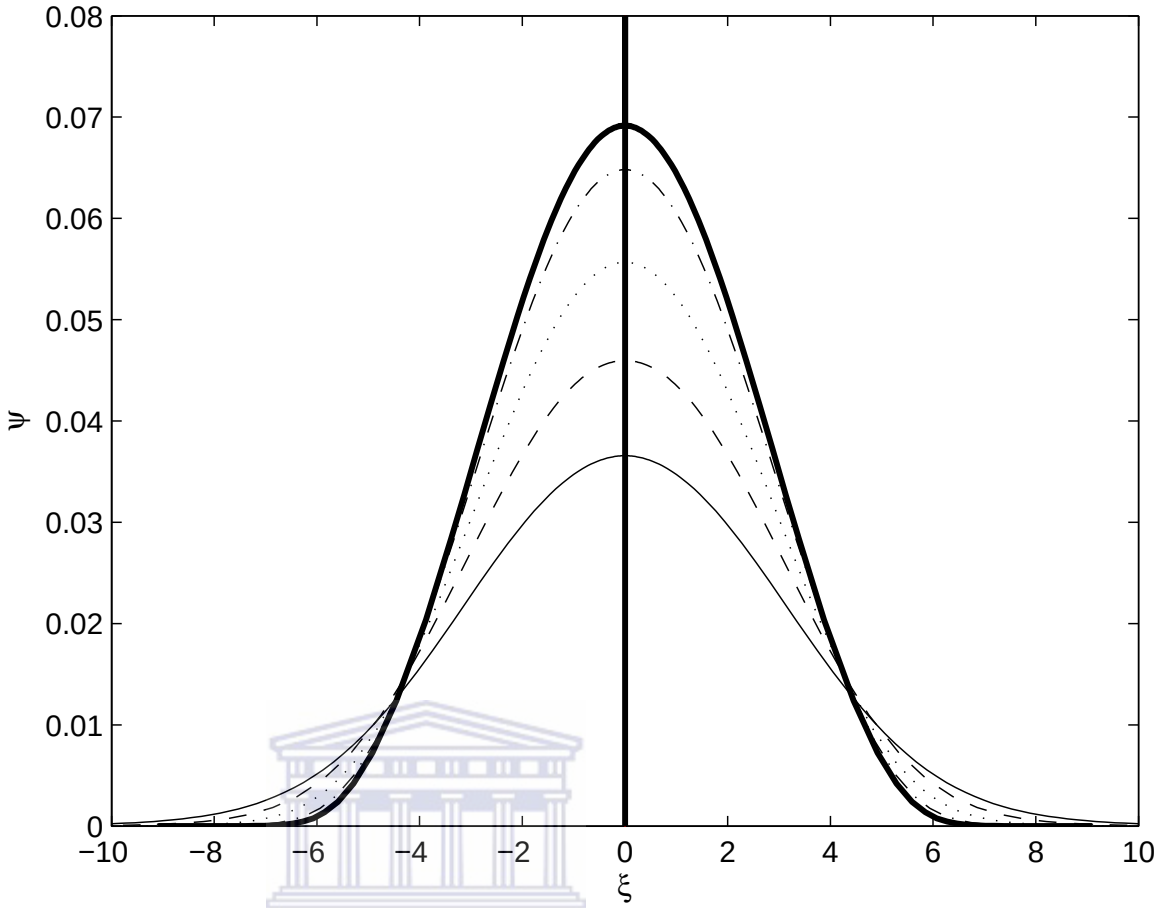

Figure 4.6: Normalized electrostatic potential ψ vs ξ for the parameters of Figure 4.5 with α_T= 0.01 (—), α_T=0.1 (- - -), α_T=0.2 (. . .), α_T=0.3 (- . -), α_T=0.35 (—).

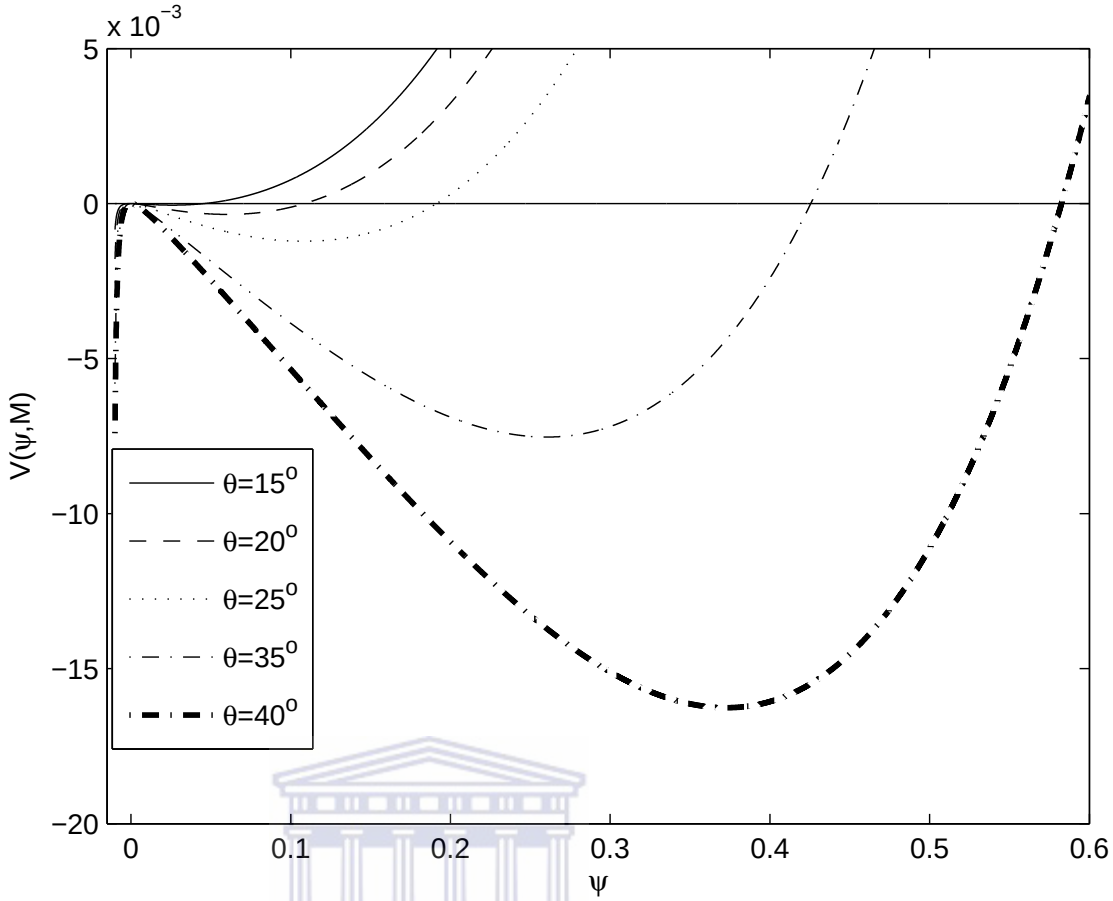

Figure 4.7: Sagdeev potential, $V(\psi, M)$ vs normalized electrostatic potential ψ. The fixed parameters are g= 0.1, M=0.93, α_T=0.1 and θ=15^o, 20^o, 25^o, 35^o, 40^o.

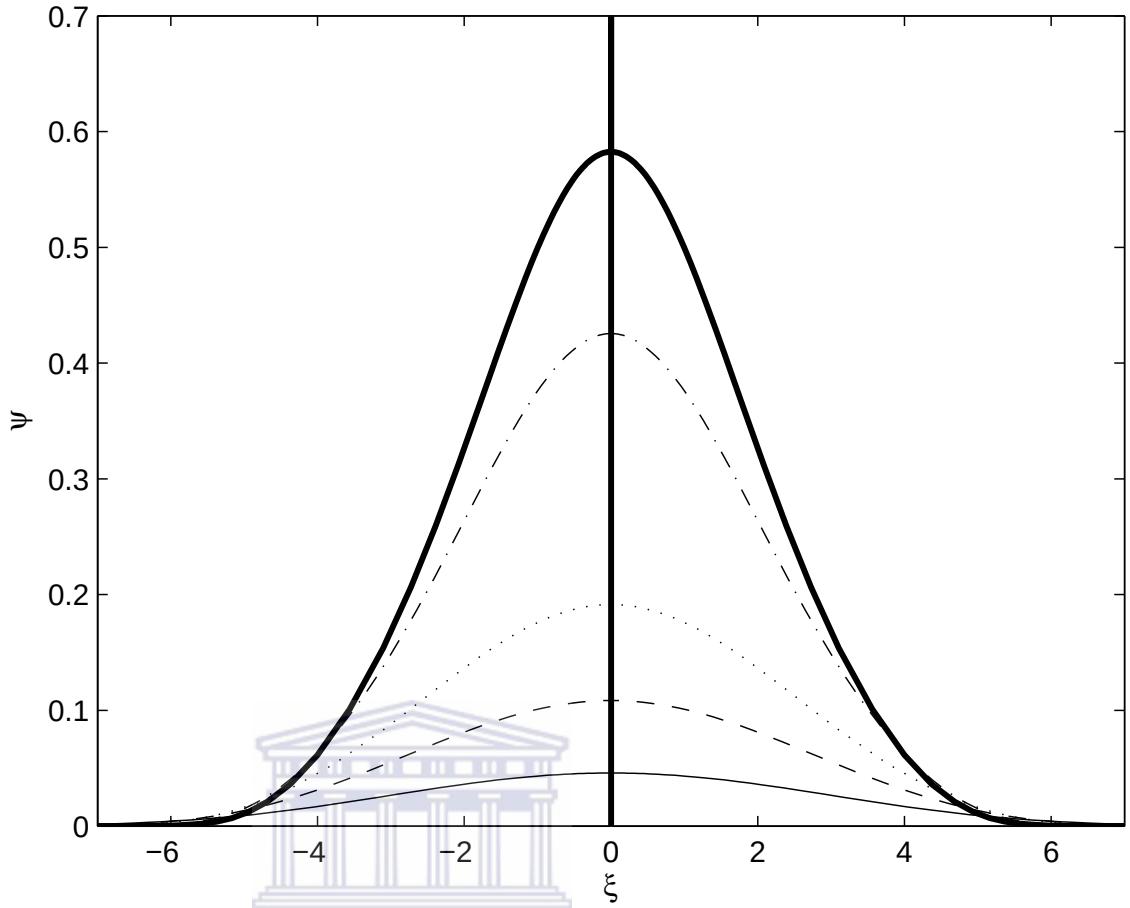

Figure 4.8: Normalized electrostatic potential ψ vs ξ for the parameters of Figure 4.7 with θ= 15^o (—), θ=20^o (- - -), θ=25^o (. . .), θ=35^o (- . -), θ=40^o (−).

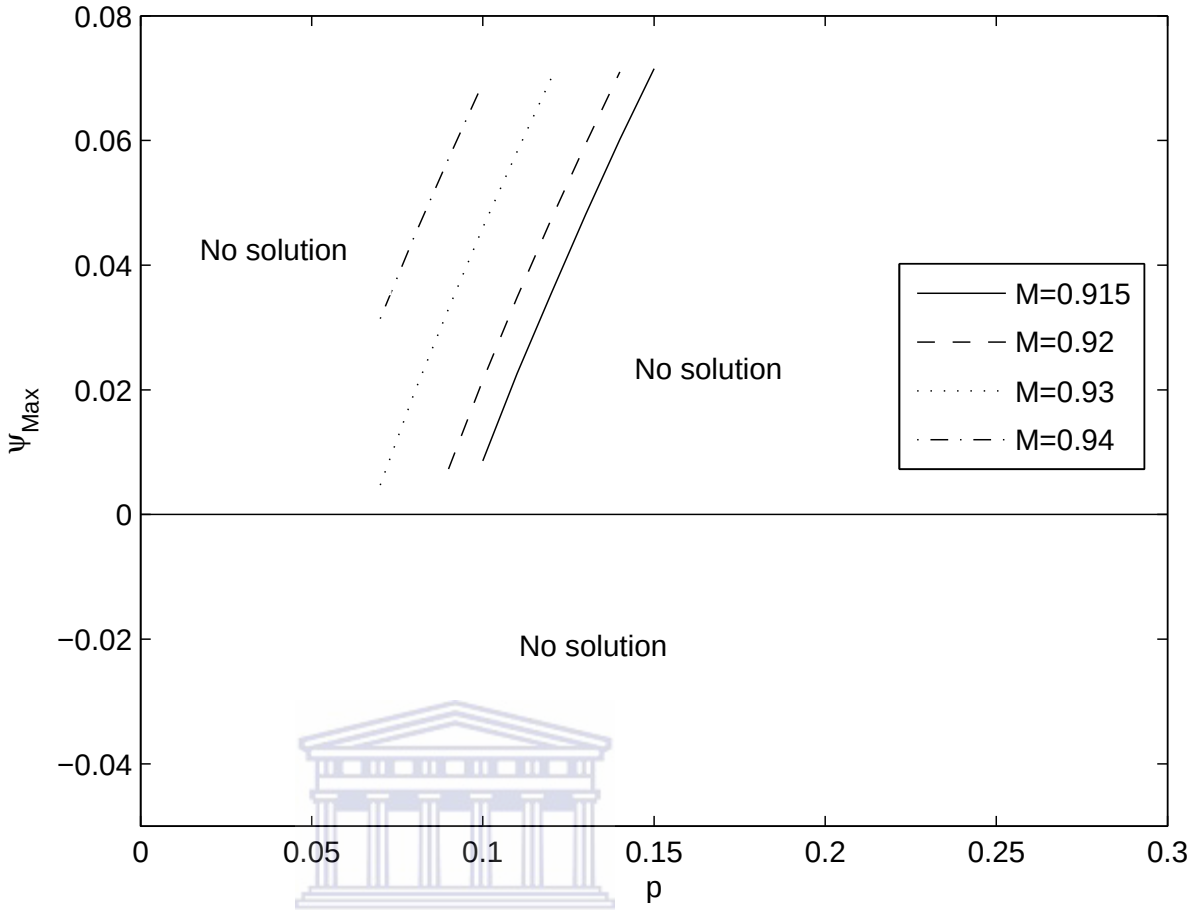

Figure 4.9: Maximum electrostatic potential, ψ_{Max} vs p. The parameters are α_T=0.1, θ=15^o and M=0.915, M=0.92, M=0.93, M=0.94.

4.2 Model 2: Magnetized plasma with cold oxygen ion beam and Boltzmann distribution of hot protons and cool electrons

In the previous model (Section 4.1), we assumed that the ion's beam velocity is zero ($v_o = 0$). In order to investigate the effect of a beam velocity propagating in (x,z) direction, we extend Model 1 to include the ion beam velocity, i.e. $\vec{v}_o = v_o\hat{z}$.

4.2.1 Basic equations

Our basic set of equations is the same as the set of equations (4.1)-(4.6) in Model 1 with $v_{iz} = v_o + v_{i1}$. Also, using the same dimensionless variables, we obtain the following set of normalized equations in the localized frame $\xi = (\alpha\eta + \gamma\zeta - M\iota)/M$, where $\alpha = \sin\theta$, $\gamma = \cos\theta$ and θ is the angle between the direction of waves propagation and the magnetic field.

$$\alpha v_x + \gamma v_z = M - \left(\frac{M-\delta}{n_i}\right), \tag{4.25}$$

$$\left(\frac{M-\delta}{n_i}\right)\frac{dv_x}{d\xi} = \alpha\frac{d\psi}{d\xi} - Mv_y, \tag{4.26}$$

$$\left(\frac{M-\delta}{n_i}\right)\frac{dv_y}{d\xi} = Mv_x, \tag{4.27}$$

$$\left(\frac{M-\delta}{n_i}\right)\frac{dv_z}{d\xi} = \gamma\frac{d\psi}{d\xi}, \tag{4.28}$$

where $\delta = \gamma v_o$ is the beam velocity. Eliminating v_x, v_y, v_z and combining equations (4.25) - (4.28) with the quasi-neutrality condition in equation (4.15), then integrating with the boundary conditions for solitary wave structures (i.e. $n_i \to 1$, $\psi \to 0$, and $d\psi/d\xi \to 0$ at $\xi \to \pm\infty$), we obtain the nonlinear differential equation,

$$\frac{d}{d\xi}\left(\frac{d\chi}{d\xi}\right) = M^2(n_i - 1) - \frac{\gamma^2 M^2 n_i}{(M-\delta)^2}\left[\frac{1}{1-g}\left[(\exp(\psi) + \frac{g}{\alpha_T}(\exp(-\alpha_T\psi) - 1)\right]\right] \tag{4.29}$$

where

$$\chi = \left(\psi + \frac{(M-\delta)^2}{2n_i^2}\right). \tag{4.30}$$

Now, multiplying both sides of equation (4.29) by $2d\chi/d\xi$ and after integrating once with appropriate boundary conditions, we obtain the "energy-balance equation" (see Appendix D for the details)

$$\frac{1}{2}\left(\frac{d\psi}{d\xi}\right)^2 + V(\psi, M) = 0, \tag{4.31}$$

where $V(\psi, M)$ is the Sagdeev pseudo-potential (cf. Section 2.3) and is given as

$$\begin{aligned}
V(\psi,M) = &-\frac{1}{\left(1-\frac{(M-\delta)^2}{n_i^3}\left(\frac{1}{1-g}(\exp(\psi)+g\alpha_T\exp(-\alpha_T\psi)\right)\right)^2}\times\left(-\frac{M^2(M-\delta)^2}{2n_i^2}(1-n_i)^2\right.\\
&-M^2(1-\gamma^2)\psi+M^2\left(\frac{1}{1-g}\left((\exp(\psi)-1)+\frac{g}{\alpha_T}(\exp(-\alpha_T\psi)-1)\right)\right)\\
&-\frac{\gamma^2}{2(M-\delta)^2}\left(\frac{1}{1-g}\left((\exp(\psi)-1)+\frac{g}{\alpha_T}(\exp(-\alpha_T\psi)-1)\right)\right)^2\\
&\left.-\frac{M^2\gamma^2}{n_i}\left(\frac{1}{1-g}\left((\exp(\psi)-1)+\frac{g}{\alpha_T}(\exp(-\alpha_T\psi)-1)\right)\right)\right).
\end{aligned} \tag{4.32}$$

In order to obtain soliton solutions of equation (4.32), the Sagdeev potential $V(\psi, M)$ given by (4.32) must satisfy the soliton conditions (cf. Section 2.3.2). (i.e. $V(\psi, M) = 0$, $d\psi/d\xi = 0$, $V(\psi, M) = 0$ and $dV(\psi, M)/d(\psi) = 0$ at $\psi = 0$. $d^2V(\psi, M)/d(\psi)^2 < 0$ at $\psi = 0$; $V(\psi, M) = 0$ at $\psi = \psi_m$, $dV(\psi, M)/d(\psi) < (>)$ 0 at $\psi_m < (>)$ 0).

Then, the soliton condition $\mathrm{d}^2V(\psi, M)/\mathrm{d}\psi^2 < 0$ at $\psi = 0$ can be written as

$$\frac{d^2V(\psi,M)}{d\psi^2}|_{\psi=0} = \frac{M^2\left((M-\delta)^2 - M_o^2\right)}{(M-\delta)^2\left((M-\delta)^2 - M_1^2\right)} < 0 \tag{4.33}$$

where

$$M_o^2 = \frac{\gamma^2(1-g)}{1+g\alpha_T} \quad and \quad M_1^2 = \frac{1-g}{1+g\alpha_T}$$

Then, from the numerator $M^2 < or > 0$ and $(M-\delta)^2 - M_o^2 < or > 0$, also in the denominator, $(M-\delta)^2 < or > 0$ and $(M-\delta)^2 - M_1^2 < or > 0$.

For $\gamma, \delta \neq 0$: $M_o + \delta < 1 = M_1 + \delta \Rightarrow M_o < M_1$, then if $M - \delta > M_1 \Rightarrow M - \delta > M_o$ from which $(M-\delta)^2 - M_o^2 > 0$, $(M-\delta)^2 - M_1^2 > 0$ consequently (4.33) is not satisfied.

Similarly, If $(M-\delta) < M_o \Rightarrow (M-\delta) < M_1$ from which $(M-\delta)^2 - M_o^2 < 0$ and

$(M-\delta)^2 - M_1^2 < 0$, once again (4.33) is not satisfied.

From equation (4.33), the lowest limit for a soliton solution to exist (the critical value) is given by

$$M_o + \delta = \frac{\gamma\sqrt{(1-g)(1+g\alpha_T)}}{1+g\alpha_T} + \delta > 0 \tag{4.34}$$

and the upper limit is

$$M_1 + \delta = \frac{\sqrt{(1-g)(1+g\alpha_T)}}{1+g\alpha_T} + \delta > 0 \tag{4.35}$$

for γ, δ and $g > 0$.

Therefore, (4.33) is satisfied only if

$$M_o + \delta < |M| < M_1 + \delta. \tag{4.36}$$

From equation (4.34 - 4.36), we obtain

$$\gamma\sqrt{\frac{1-g}{1+g\alpha_T}} + \delta < |M| < \sqrt{\frac{1-g}{1+g\alpha_T}} + \delta \tag{4.37}$$

for $\theta \neq 0$, equation (4.37) gives the Mach number range for fixed values of plasma parameters g, α_T and δ. At beam velocity $\delta = 0$, the conditions in equations (4.33 - 4.37) above will reduce to those in Model 1 (Section 4.1). It is interesting to point out that the inclusion of the beam velocity allows supersonic solutions ($M > 1$) for the upper limit of the Mach number $|M|$.

4.2.2 Numerical results

Now, we numerically examine the existence of arbitrary amplitude solitons. The energy integral and the Sagdeev potential $V(\psi, M)$ given by (4.31) and (4.32) are computed for different parameter values (e.g. Mach number M, proton density $g = N_{po}/N_{eo}$, temperature ratio $\alpha_T = T_e/T_p$, beam velocity $\delta = \gamma v_o$ and obliqueness angle θ).

Table 4.2 shows that the characteristics of the arbitrary amplitude nonlinear electrostatic structures in auroral plasmas for different values of the ion beam velocity δ and other fixed plasma parameters are, hot proton density $g = 0.1$, temperature

Table 4.2: Properties of ion-acoustic solitons, such as Soliton Velocity (V), Mach number range ($M_o < |M| < M_1$), Electric Field (E), Soliton Width (W) and Pulse Duration (τ^*), for various values of ion beam velocity (δ) with $\theta = 35^o$, hot proton density $g = 0.1$, temperature ratio $\alpha_T = 0.1$.

δ	$M_o < \|M\| < M_1$	$V(kms^{-1})$	$E(mVm^{-1})$	$W(m)$	$\tau^*(ms)$
0.0	0.7735 - 0.943	20.03 - 24.42	0.002 - 26.25	2626 - 122.2	131.1 - 5.00
0.01	0.7818 - 0.953	20.25 - 24.68	0.0037 - 26.71	2138.24 - 120.64	105.59 - 4.89
0.05	0.8148 - 0.984	21.10 - 25.49	0.0084 - 27.24	1588.6 - 117.0	75.29 - 4.59
0.1	0.8558 - 1.025	22.17 - 26.55	0.0098 - 28.56	1460.16 - 112.32	65.86 - 4.23
0.15	0.8969 - 1.066	23.23 - 27.61	0.014 - 29.66	1268.8 - 108.16	54.62 - 3.92
0.2	0.938 - 1.105	24.29 - 28.62	0.017 - 30.98	1107.6 - 104.0	45.60 - 3.63

ratio $\alpha_T = 0.1$ and angle of propagation $\theta = 35^o$ respectively. In Table 4.2, it clearly shows that both the minimum and maximum electric field amplitudes of the soliton increase with increases in the ion beam velocity. This may be attributed to the fact that as the ion beam δ increases, the minimum and maximum Mach numbers for which soliton solutions are obtained and soliton velocity also increase, leading to an increase in electric field amplitude. But the soliton width as well as pulse duration decreases with the increase in ion beam velocity.

The variation of the Sagdeev potential $V(\psi, M)$ versus the normalized potential (ψ) is shown in Figure 4.10 for various values of Mach number as shown in the graph. The fixed parameters are, proton density ratio, $g = 0.1$, beam velocity, $\delta = 0.1$, temperature ratio $T_e/T_p = 0.1$ and propagation angle, $\theta = 15^o$. It is seen that the positive potential ion-acoustic soliton amplitude, ψ increases with the increasing Mach number M. Further numerical computation reveals that soliton solutions are not found for $M > 0.953$. Unlike the case of small-amplitude ion acoustic solitons in magnetized plasmas reported by Das, (2012) both positive and negative potential solitons were found for plasma consisting of warm ions, cold ion-beams and electron species for $M < 1$. Figure 4.11 shows the normalized electrostatic potential ψ against ξ, for the same parameters used in Figure 4.10. It is obvious from the curves that as the Mach number increases, the positive potential amplitude ion-acoustic soliton increases and the width decreases.

The curves in Figure 4.12 show the variation of the Sagdeev potential $V(\psi, M)$ against the electrostatic potential ψ for different values of proton density ratio g. Other fixed parameters are M=0.93, α_T=0.1, δ=0.01 and θ=15^o. The positive poten-

tial soliton amplitude increases with an increase in proton density g, beyond $g > 0.138$, soliton solutions are not possible. Otherwise, if the proton density is assumed to be zero (i.e. $g = 0$), then the problem will automatically reduce to the case investigated by Choi et al. 2006. Figure 4.13 shows the normalized electrostatic potential ψ against ξ, for the same parameters in Figure 4.12. It shows clearly that as the proton density ratio g increases, the ion-acoustic soliton's potential amplitude increases and the width decreases.

In Figure 4.14, the graphs show the variation of the Sagdeev potential $V(\psi, M)$ versus the normalized potential (ψ) for different values of the angle of propagation θ. The chosen parameters are proton density ratio, $g = 0.1$, and other fixed parameters of Figure 4.12. It is observed that as the angle of propagation θ increases, the soliton amplitude increases. Also, the wave's obliqueness γ reduced the solitons amplitude, as mentioned by many authors (Farid et al. 2001; Choi et al. 2006; Barman and Talukdar, 2010). For $\theta > 70^o$ there are no soliton solutions. Figure 4.15 shows the normalized electrostatic potential ψ against ξ, for the same parameters used in Figure 4.14. It is seen that the positive potential amplitude as well as the width of the soliton increases with the increase in angle of propagation.

The variation of the Sagdeev potential $V(\psi, M)$ against the normalized electrostatic potential ψ is shown in Figure 4.16 for different values of the temperature ratio α_T. The other fixed parameters are, M=0.93, θ=15^o, g=0.1 and δ=0.01. It is seen that the positive potential soliton amplitude, ψ increases with the increasing temperature ratio α_T. Similar observations were recorded for the study of the parallel and perpendicular electric field structures that exhibit a spiky appearance (Reddy et al. 2006; Moolla et al. 2012). On the other hand, Das, (2012) revealed that it is the inclusion of ion temperature in the plasma consisting of warm ions, electrons and cold ion-beams, that is responsible for the existence of both compressive and rarefactive soliton structures. Figure 4.17 shows the normalized electrostatic potential ψ against ξ, for the same parameters used in Figure 4.16. It is very obvious from the curves that as the temperature ratio α_T increases, the ion-acoustic soliton amplitude increases and the width decreases.

Figure 4.18 shows the variation of the Sagdeev potential $V(\psi, M)$ against the electrostatic potential (ψ) for different values of beam velocity δ and other fixed plasma parameters namely proton $g = 0.1$, temperature ratio, $\alpha_T = 0.1$, angle of propagation, $\theta = 15^o$ and Mach number $M = 0.93$. The soliton amplitude decreases

as the beam velocity δ increases. Similar effect of beam velocity has been mentioned by many authors (e.g. Nakamura, 1999; Reddy et al. 2006; Lakhina et al. 2008; Moolla et al. 2010). Figure 4.19 shows the normalized electrostatic potential ψ against ξ, for the same parameters used in Figure 4.18. It clearly shows that as the beam velocity δ increases, the ion-acoustic soliton amplitude decreases and the width increases.

In Figure 4.20, the curves show the existence domain of solitons. The fixed parameters are α_T=0.1, δ=0.01, and θ=15^o. The curves were plotted for the variation of the maximum electrostatic potential ψ_{Max} against p for different values of the Mach number M. The maximum Mach number for positive potential solitions is bounded by those of the soliton solutions corresponding to a given proton density ratio g

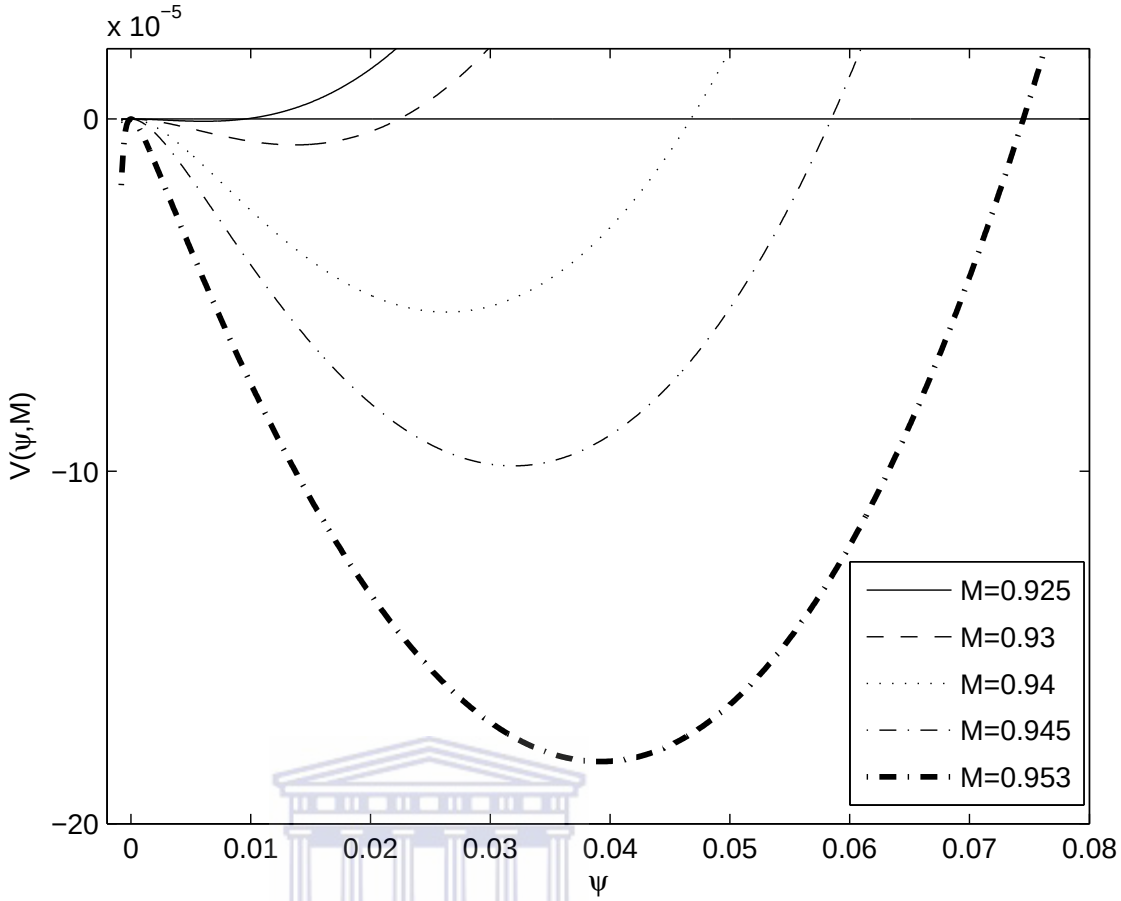

Figure 4.10: Sagdeev potential, $V(\psi, M)$ vs normalized electrostatic potential ψ. The parameters are g= 0.1, δ=0.01, α_T=0.1, θ=15^o and M=0.925, 0.93, 0.94, 0.945, 0.953.

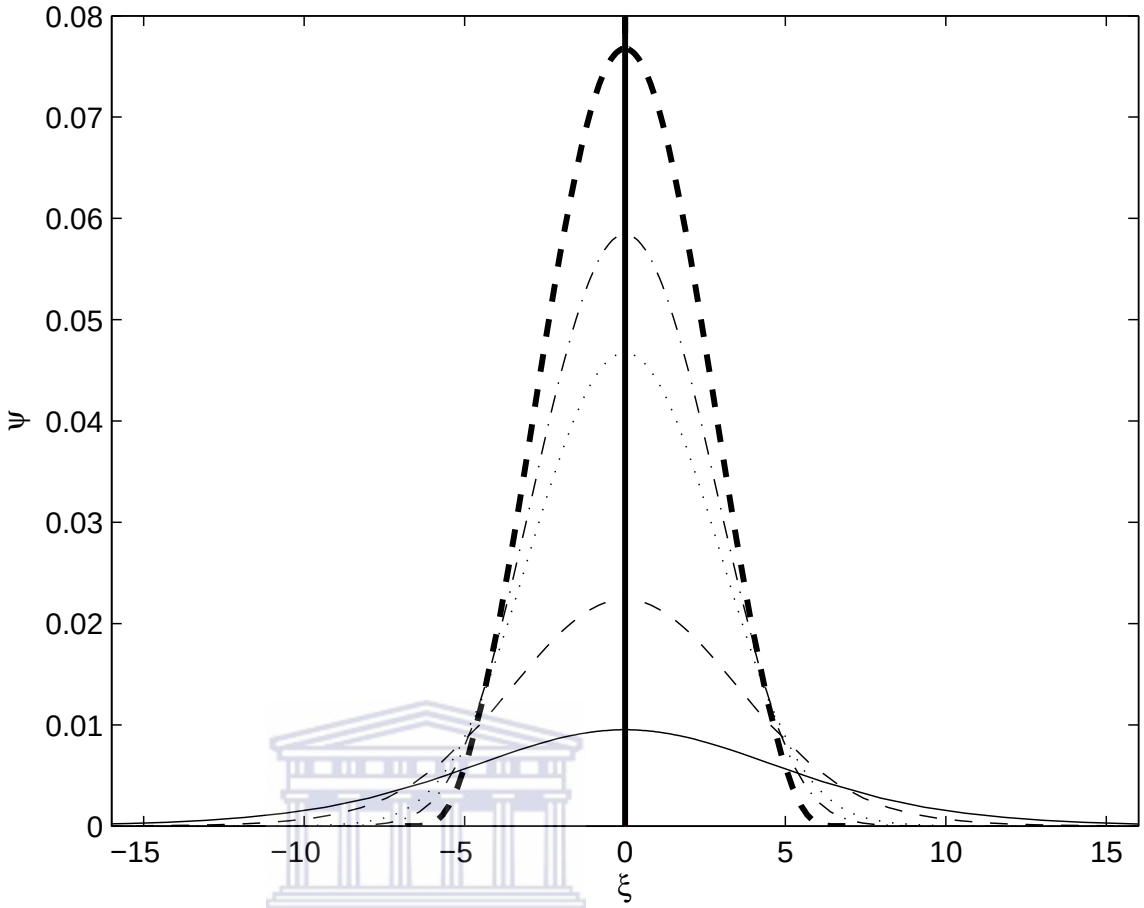

Figure 4.11: Normalized electrostatic potential ψ vs ξ for the parameters of Figure 4.10 with M= 0.925 (—), M=0.93 (- - -), M=0.94 (. . .), M=0.945 (- . -), M=0.953 (— — —).

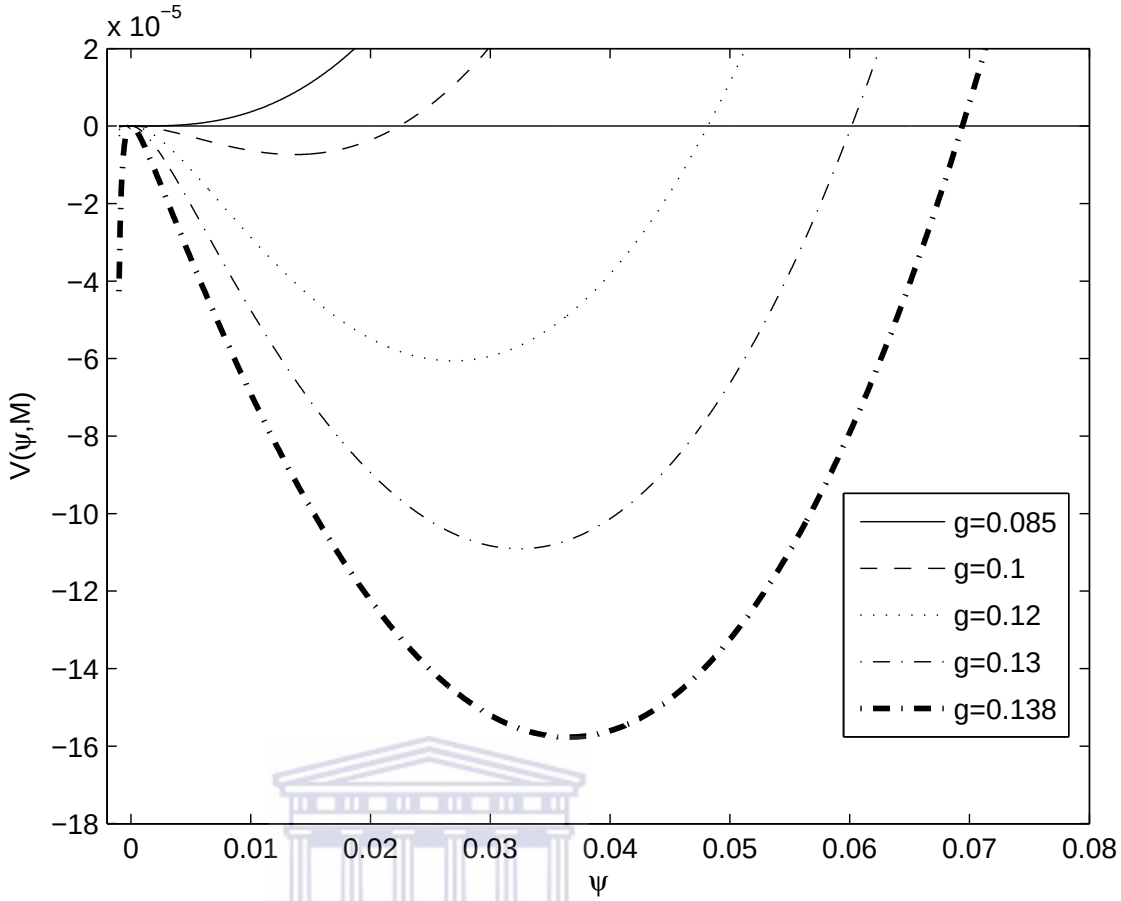

Figure 4.12: Sagdeev potential, $V(\psi, M)$ vs normalized electrostatic potential ψ. The paramters of δ= 0.01, M=0.93, α_T=0.1, θ=15^o and g=0.085, 0.1, 0.12, 0.13, 0.138.

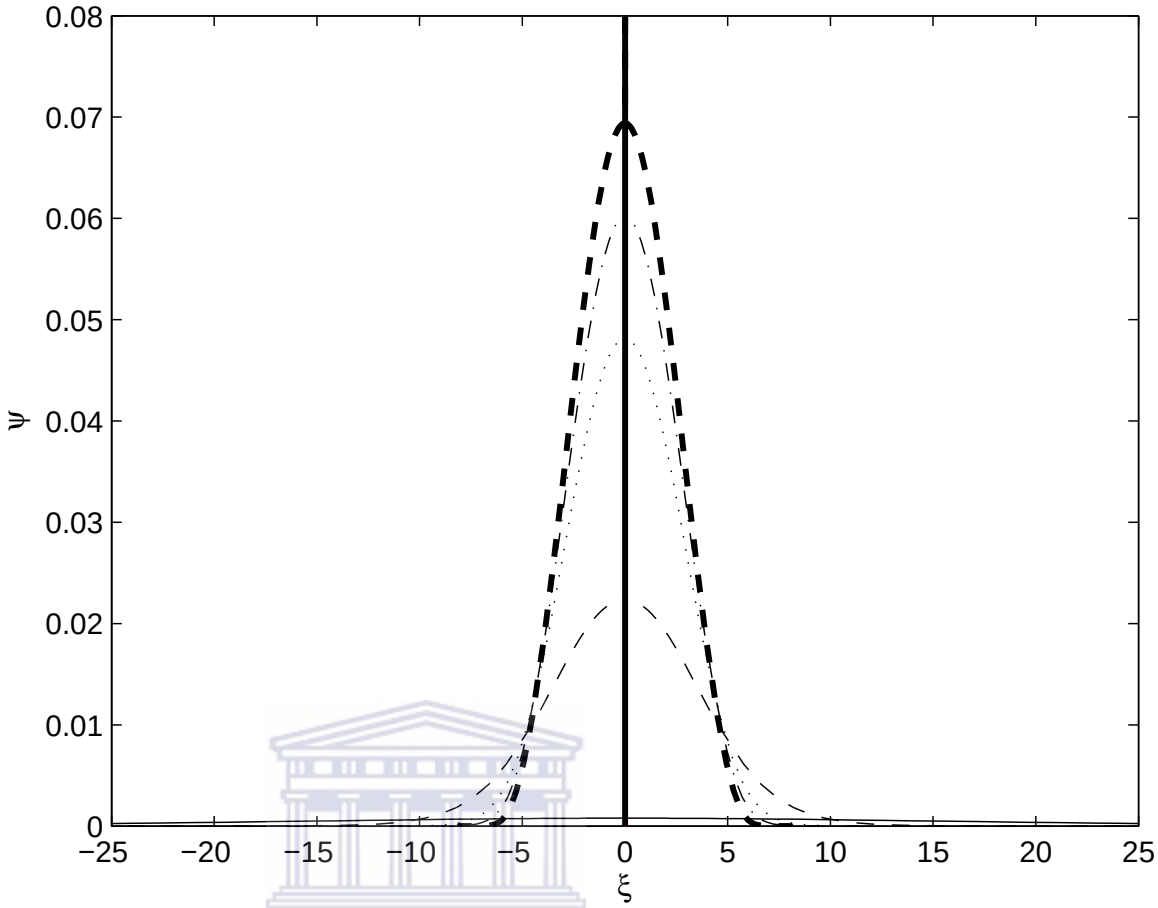

Figure 4.13: Normalized electrostatic potential ψ vs ξ for the parameters of Figure 4.13 with g= 0.085 (—), g=0.1 (- - -), g=0.12 (. . .), g=0.13 (- . -), g=0.138 (— — —).

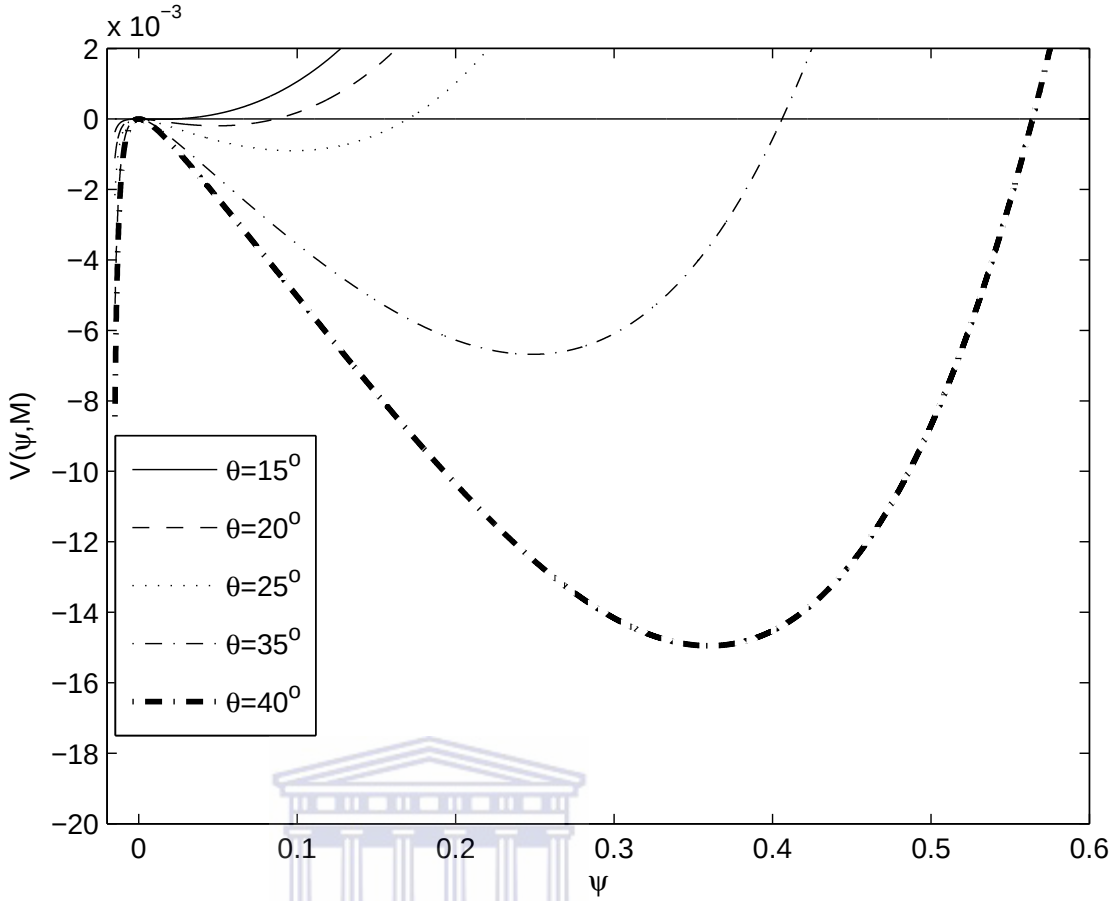

Figure 4.14: Sagdeev potential, $V(\psi, M)$ vs normalized electrostatic potential ψ. The parameters are δ= 0.01, M=0.93, α_T=0.1, g=0.1 and θ=15^o, 20^o, 25^o, 35^o, 40^o.

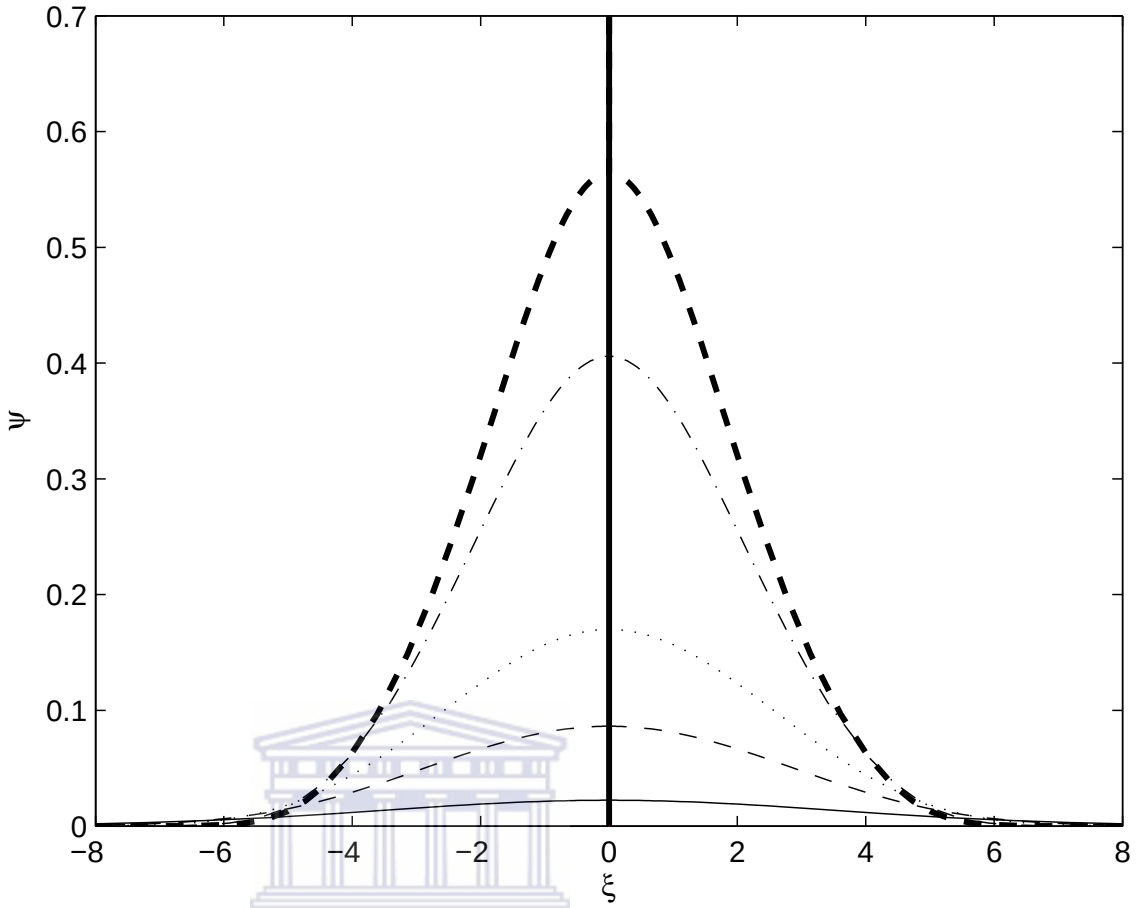

Figure 4.15: Normalized electrostatic potential ψ vs ξ for the parameters of Figure 4.15 with θ= 15^o (—), θ=20^o (- - -), θ=25^o (. . .), θ=35^o (- . -), θ=40^o (— — —).

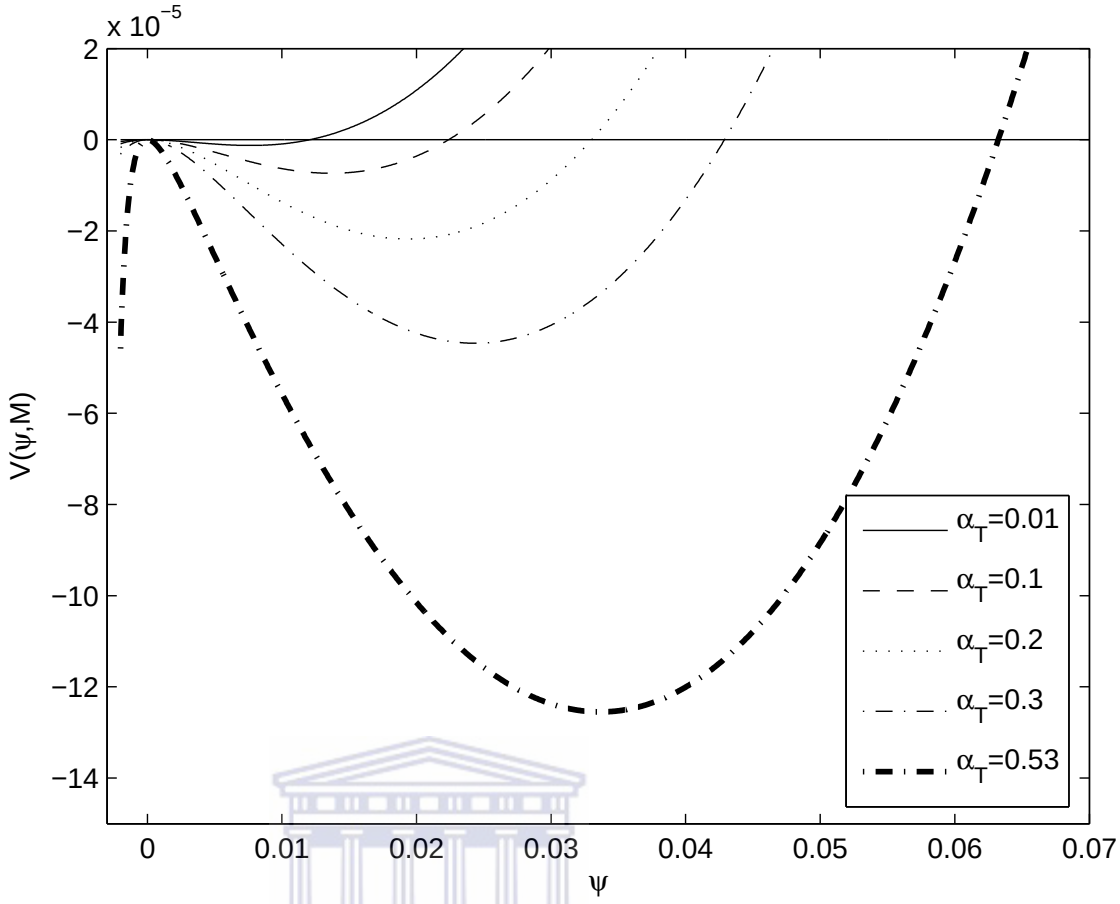

Figure 4.16: Sagdeev potential, $V(\psi, M)$ vs normalized electrostatic potential ψ. The parameters are δ= 0.01, M=0.93, g=0.1, θ=15^o and α_T=0.01, 0.1, 0.2, 0.3, 0.53.

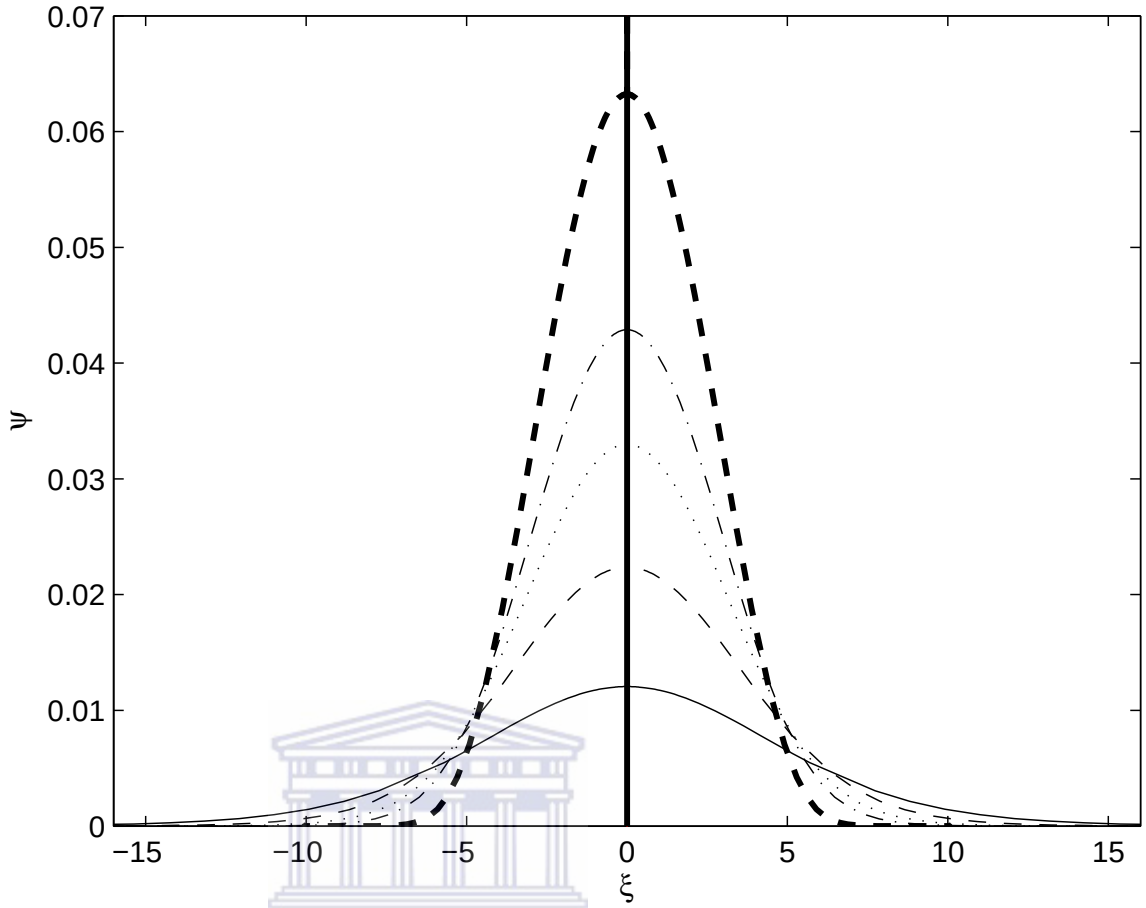

Figure 4.17: Normalized electrostatic potential ψ vs ξ for the parameters of Figure 4.17 with α_T= 0.01 (—), α_T=0.1 (- - -), α_T=0.2 (. . .), α_T=0.3 (- . -), α_T=0.53 (— — —).

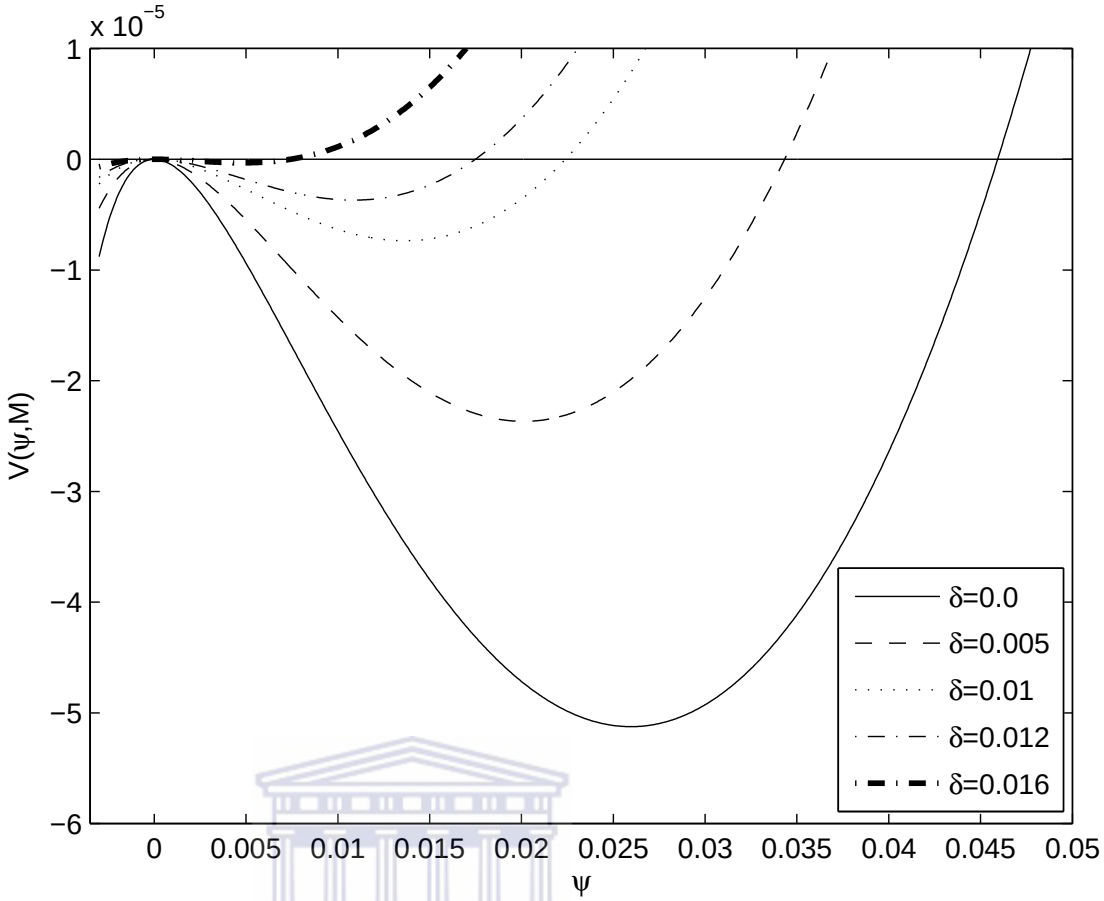

Figure 4.18: Sagdeev potential, $V(\psi, M)$ vs normalized electrostatic potential ψ. The parameters are g= 0.1, M=0.93, α_T=0.1, θ=15^o and δ=0.0, 0.005, 0.01, 0.012, 0.016.

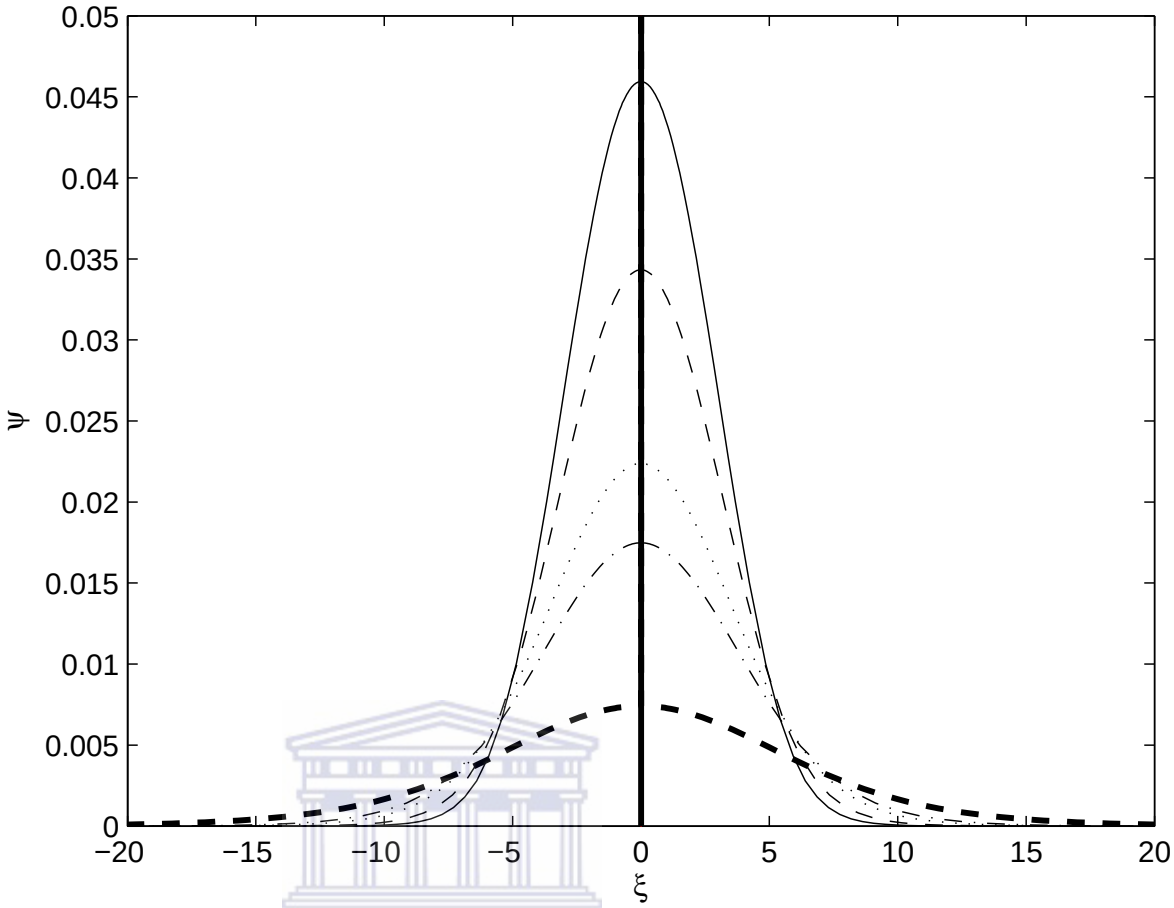

Figure 4.19: Normalized electrostatic potential ψ vs ξ for the parameters of Figure 4.19 with δ= 0.0 (—), δ=0.005 (- - -), δ=0.01 (. . .), δ=0.012 (- . -), δ=0.016 (— — —).

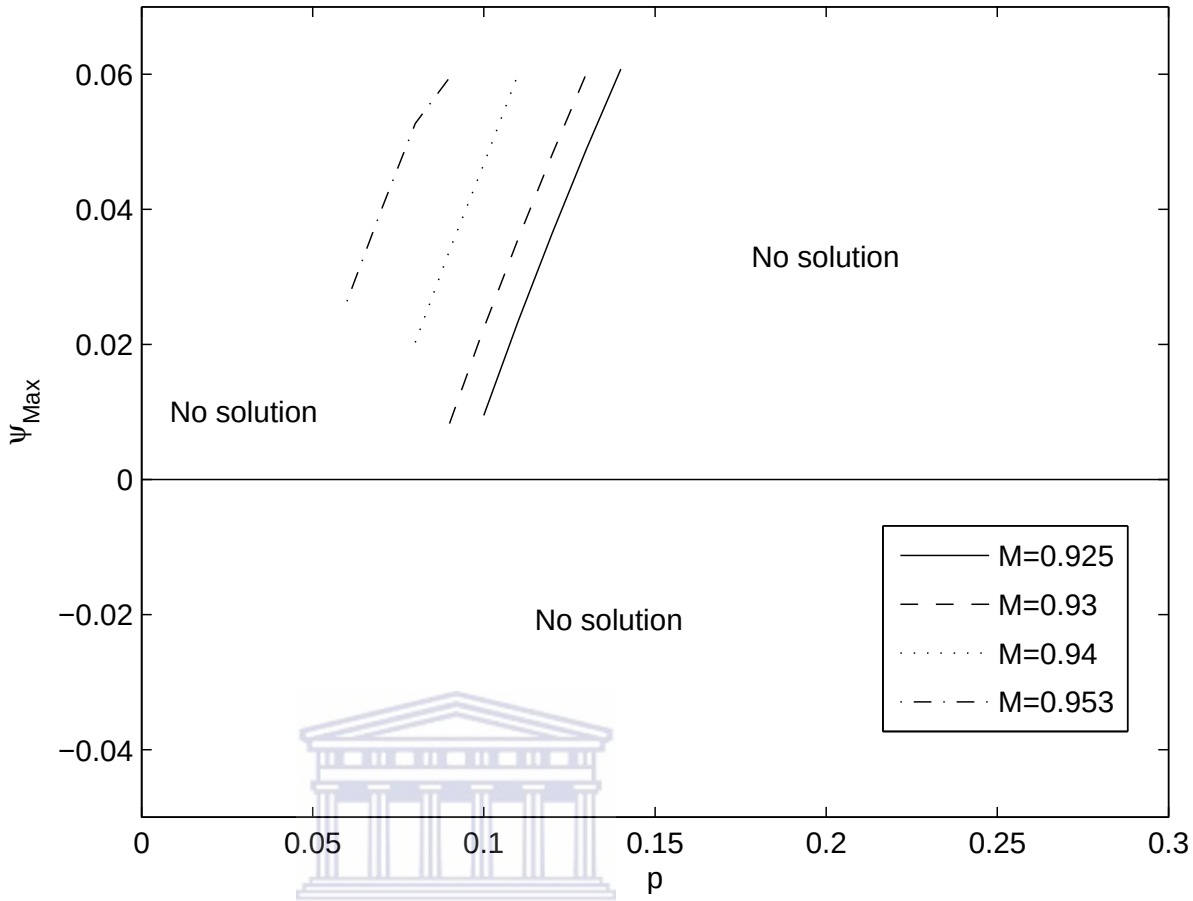

Figure 4.20: Maximum electrostatic potential, ψ_{Max} vs g. The parameters are α_T=0.1, θ=15^o and M=0.925, M=0.93, M=0.94, M=0.953.

4.2.3 Discussion

We have examined finite amplitude ion-acoustic solitary waves in a magnetized three components space plasma with cold oxygen-ions beams and Boltzmann distributions of proton and electron species. Motivated by FAST satellite observations of waves near the cyclotron frequencies of H^+, O^+ and He^+ in the auroral region reported by Cattell et al., (1998), we investigated in detail the evolution of solitons in the auroral region of the Earth's magnetosphere, and the existence of the Mach number domain for solitary wave solutions to exist. The numerical computation of plasma parameters (i.e. Mach number, temperature ratio, proton concentration, beam velocity and obliqueness) variational effect on the properties of the ion-acoustic solitons was obtained with positive potential structures. The model supports only positive potential ion-acoustic solitons. The model allowed the solitons to exist only in the subsonic Mach number regime, whereas the inclusion of an ion beams allowed the nonlinear structures to exist at both subsonic and supersonic Mach number regime (see Table 4.1). For the plasma parameters, Mach number $M = 0.93$, beam velocity δ=0.01 and propagating angle θ=35^o, the electric field amplitude, width, pulse duration and speed of the soliton structures comes out to be $22mV/m$, $130m$, $5ms$ and $24km/s$, respectively.

4.3 Model 3: Magnetized plasma with cold oxygen ions, Maxwellian ions and two-Boltzmann electrons

In this Section, we extend Model 1 (Section 4.1), to a four component plasma, by including a Boltzmann distribution of hot electron species. This Model is also a modification of Model 1 (Section 3.1) with additional Maxwellian ion species. We shall investigate the effect of the additional component in the plasma model. This results in the set of equations below.

4.3.1 Basic equations

We consider a four-component, homogeneous, collisionless, and magnetized plasma comprising of Boltzmann distributions of cool ions (N_{ci}, T_{ci}), cool electrons (N_{ce}, T_{ce}) and hot electrons (N_{he}, T_{he}) and background cold oxygen-ions fluid (N_i, T_i, V_i). The finite amplitude ion-acoustic waves are propagating in the z direction at angle θ to the external magnetic field $\mathbf{B_o}$, which is assumed to be in the (x, z)-plane. The Boltzmann distribution is assumed for the densities of the cool (N_{ce}) and hot (N_{he}) electrons and cool (N_{ci}) ion species, and are given as follows:

$$N_{ce} = N_{ceo} \exp\left(\frac{e\phi}{T_{ce}}\right), \tag{4.38}$$

$$N_{he} = N_{heo} \exp\left(\frac{e\phi}{T_{he}}\right), \tag{4.39}$$

$$N_{ci} = N_{cio} \exp\left(\frac{e\phi}{T_{ci}}\right), \tag{4.40}$$

where ϕ is the electrostatic potential and N_{ceo} (T_{ce}), N_{heo} (T_{he}) and N_{cio} (T_{ci}) are the equilibrium densities (temperature) of the cool, hot electrons and cool ions respectively. The assumption of the Boltzmann distribution means that the electrons and cool ions are in thermal equilibrium, which is a valid assumption for low frequency phenomena, well below the electron plasma frequency. The dynamics of the cold oxygen ions is described by the fluid equations, namely, the continuity and the momentum equations:

$$\frac{\partial N_i}{\partial t} + \nabla(N_i V_i) = 0 \tag{4.41}$$

and

$$\left(\frac{\partial}{\partial t} + \mathbf{V_i}.\nabla\right)\mathbf{V_i} = -\frac{e\nabla\phi}{m_i} + e\frac{\mathbf{V}_i \times \mathbf{B}_o}{m_i c}, \tag{4.42}$$

where N_i, m_i and V_i are the number density, mass and the fluid velocity of the oxygen ions, respectively, e is the magnitude of the electron charge, c is the speed of light in a vacuum.

We begin with a linear analysis, using the continuity and momentum equation in (4.41 - 4.42) with the Boltzmann distribution of cool ions, cool and hot electron densities. For harmonic oscillations varying as $e^{i(kz-\omega t)}$, i.e propagating along the magnetic field $\mathbf{B}_o$, then $\frac{\partial}{\partial t} \to -i\omega$, $\nabla \to ik\hat{z}$. From the continuity equation, we have

$$-i\omega N_i + ikN_o V_i = 0,$$

$$V_i = \frac{\omega N_i}{N_o k}.$$

At equilibrium, we have

$$N_{io} = N_{ceo} + N_{heo} - N_{cio} = N_o,$$

from which

$$\frac{N_{heo}}{N_o} = 1 - \frac{N_{ceo}}{N_o} = 1 - f$$

and

$$\frac{N_{io}}{N_o} = 1 - \frac{N_{cio}}{N_o} = 1 - g$$

where $f = \frac{N_{ceo}}{N_o}$ and $g = \frac{N_{cio}}{N_o}$.

Then

$$n_{ce} = \frac{N_{ce}}{N_o} = f\exp\left(\frac{e\phi}{T_{ce}}\right),$$

$$n_{he} = \frac{N_{he}}{N_o} = (1-f)\exp\left(\frac{e\phi}{T_{he}}.\frac{T_{ce}}{T_{ce}}\right),$$

$$n_{he} = (1-f)\exp\left(\frac{e\phi}{T_{ce}}.\tau\right),$$

$$n_{cio} = \frac{N_{cio}}{N_o} = g\exp\left(-\alpha_{ci}\frac{e\phi}{T_{ce}}\right),$$

where $\tau = \frac{T_{ce}}{T_{he}}$ and where $\alpha_{ci} = \frac{T_{ce}}{T_{ci}}$.

Using the quasi-neutrality condition, we have

$$(1-g) + n_{i1} = \frac{N_i}{N_o} = \left[f \exp\left(\frac{e\phi}{T_{ce}}\right) + (1-f)\exp\left(\frac{e\phi}{T_{ce}}.\tau\right) - g\exp\left(-\alpha_{ci}\frac{e\phi}{T_{ce}}\right)\right]$$

then, we can expand the exponential in a Taylor series for $|e\phi/T_c| \ll 1$,

$$\exp\left(\frac{e\phi}{T_{ce}}\right) = \left[1 + \frac{e\phi}{T_{ce}} + \frac{1}{2}\left(\frac{e\phi}{T_{ce}}\right)^2 + ...\right] \simeq 1 + \frac{e\phi}{T_{ce}}.$$

Therefore, neglecting the higher order terms in the expansion, we have

$$n_i = f\left(1 + \frac{e\phi}{T_{ce}}\right) + (1-f)\left(1 + \frac{e\phi}{T_{ce}}.\tau\right) - g\left(1 - \alpha_{ci}\frac{e\phi}{T_{ce}}\right) = 1 - g + n_{i1},$$

from which

$$n_{i1} = (f + (1-f)\tau + g\alpha_{ci})\left(\frac{e\phi}{T_{ce}}\right), \tag{4.43}$$

From the momentum equation (4.42), we have

$$-i\omega V_i = -\frac{eik\phi}{m_i},$$

$$\omega\left(\frac{\omega n_{i1}}{N_o k}\right) = \frac{k}{m_i}(e\phi),$$

$$\frac{\omega^2 n_{i1}}{1-g} = \frac{k^2}{m_i}(e\phi), \tag{4.44}$$

where $n_{i1} = \frac{N_{i1}}{N_o}$.

From (4.43) and (4.44)

$$\left(\frac{\omega^2}{k^2}\right)\frac{e\phi}{T_{ce}}(f + (1-f)\tau + g\alpha_{ci}) = \frac{T_{ce}}{m_i}\left(\frac{e\phi}{T_{ce}}(1-g)\right),$$

for which

$$\frac{\omega}{k} = \left[\left(\frac{(1-g)}{(f + (1-f)\tau + g\alpha_{ci})}\right)\left(\frac{T_{ce}}{m_i}\right)\right]^{1/2} \equiv c_s$$

is the ion acoustic phase speed.

Then the normalized set of the governing equations are

$$n_{ce} = f\exp(\alpha_{ce}\psi), \tag{4.45}$$

$$n_{he} = (1-f)\exp(\alpha_{he}\psi), \tag{4.46}$$

$$n_{ci} = g\exp(-\alpha_{ci}\psi), \tag{4.47}$$

$$\frac{\partial n_i}{\partial \iota} + \frac{\partial (n_i v_{ix})}{\partial \eta} + \frac{\partial (n_i v_{iz})}{\partial \zeta} = 0, \tag{4.48}$$

$$\frac{\partial v_{ix}}{\partial \iota} + \left(v_{ix}\frac{\partial}{\partial \eta} + v_{iz}\frac{\partial}{\partial \zeta} \right) v_{ix} = -\frac{\partial \psi}{\partial \eta} + v_{iy}, \tag{4.49}$$

$$\frac{\partial v_{iy}}{\partial \iota} + \left(v_{ix}\frac{\partial}{\partial \eta} + v_{iz}\frac{\partial}{\partial \zeta} \right) v_{iy} = -v_{ix}, \tag{4.50}$$

$$\frac{\partial v_{iz}}{\partial \iota} + \left(v_{ix}\frac{\partial}{\partial \eta} + v_{iz}\frac{\partial}{\partial \zeta} \right) v_{iz} = -\frac{\partial \psi}{\partial \zeta}. \tag{4.51}$$

and our system of the equation is closed with the quasi-neutrality condition (cf. Section 2.3)

$$n_i = n_{ce} + n_{he} - n_{ci} = \frac{f e^{\alpha_{ce}\psi} + (1-f)e^{\alpha_{he}\psi} - g e^{-\alpha_{ci}\psi}}{1-g}. \tag{4.52}$$

The normalisations used are oxygen-ion gyro-frequency $\Omega(= eB_0/m_i c)$, $\iota = \Omega_i t$, $(\eta, \zeta) = (x, z)/\rho_i$, $V_k = v_{ik}/c_s$ (where $k = x, y, z$) is the velocity, effective ion-acoustic speed $c_s = ((1-g)T_{ce}/m_i(f+(1-f)\tau+g\alpha_{ci}))^{1/2}$, $\rho_i = c_s/\Omega_i$ is the ion gyro-radius, the total ion equilibrium density $N_{io} = N_{ceo} + N_{heo} - N_{cio} = N_o$, $\tau = T_{ce}/T_{he}$ is the cool to hot electron temperature ratio, $f = N_{ceo}/N_o$ is cool to hot electron density ratio, the ion density ratio, $g = N_{cio}/N_o$, $T_{eff} = T_{ce}/(f + (1-f)\tau)$ is an effective electron temperature, then $\alpha_{ce} = T_{eff}/T_{ce}$, $\alpha_{he} = T_{eff}/T_{he}$, $\alpha_{ci} = T_{eff}/T_{ci}$ and electrostatic potential $\psi = e\phi/T_{eff}$.

In order to derive the Sagdeev potential (cf. Section 2.3), we transformed all the dependent variables in equation (4.48) - (4.51) to a single independent variable $\xi = (\alpha\eta + \gamma\zeta - M\iota)/M$, where $M = V/c_s$ is the Mach number, $\alpha = \sin\theta$, $\gamma = \cos\theta$; θ is the angle between the direction of wave propagation and the magnetic field. Then, integrating with appropriate boundary conditions for solitary wave structure (namely, $n_i \to 1$, $\psi \to 0$, and $d\psi/d\xi \to 0$ at $\xi \to \pm\infty$), we obtain a single dimensionless

nonlinear differential equation in terms of oxygen-ion density n_i and electrostatic potential ψ as,

$$\frac{d}{d\xi}\left(\frac{d\chi(\psi)}{d\xi}\right) = M^2(n_i - 1)$$
$$-\gamma^2 n_i\left(\frac{1}{1-g}\left(\frac{f}{\alpha_{ce}}(e^{\alpha_{ce}\psi}-1)+\frac{1-f}{\alpha_{he}}(e^{\alpha_{he}\psi}-1)+\frac{g}{\alpha_{ci}}(e^{-\alpha_{ci}\psi}-1)\right)\right) \quad (4.53)$$

where

$$\chi(\psi) = \left(\psi + \frac{M^2}{2n_i^2}\right) \quad (4.54)$$

with n_i given by equation (4.52).

Multiplying both sides of equation (4.53) by $2d\chi(\psi)/d\xi$ and integrating once with appropriate boundary conditions (see Appendix E for the details), we obtain

$$\frac{1}{2}\left(\frac{d\chi(\psi)}{d\xi}\right)^2 + V(\psi, M) = 0, \quad (4.55)$$

which can be expressed as

$$\frac{1}{2}\left(\frac{d\psi}{d\xi}\right)^2 + V(\psi, M) = 0, \quad (4.56)$$

where the Sagdeev pseudo-potential $V(\psi, M)$ is given by

$$V(\psi, M) = -\frac{1}{\left(1-\frac{M^2}{n_i^3}\left(\frac{1}{1-g}(f\alpha_{ce}e^{\alpha_{ce}\psi}+(1-f)\alpha_{he}e^{\alpha_{he}\psi}+g\alpha_{ci}e^{-\alpha_{ci}\psi}\right)\right)^2}\times$$
$$\left(-\frac{M^4}{2n_i^2}(1-n_i)^2 - M^2(1-\gamma^2)\psi\right.$$
$$+M^2\left(\frac{1}{1-g}\left(\frac{f}{\alpha_{ce}}(e^{\alpha_{ce}\psi}-1)+\frac{1-f}{\alpha_{he}}(e^{\alpha_{he}\psi}-1)+\frac{g}{\alpha_{ci}}(e^{-\alpha_{ci}\psi}-1)\right)\right)$$
$$-\frac{\gamma^2}{2}\left(\frac{1}{1-g}\left(\frac{f}{\alpha_{ce}}(e^{\alpha_{ce}\psi}-1)+\frac{1-f}{\alpha_{he}}(e^{\alpha_{he}\psi}-1)+\frac{g}{\alpha_{ci}}(e^{-\alpha_{ci}\psi}-1)\right)\right)^2$$
$$\left.-\frac{M^2\gamma^2}{n_i}\left(\frac{1}{1-g}\left(\frac{f}{\alpha_{ce}}(e^{\alpha_{ce}\psi}-1)+\frac{1-f}{\alpha_{he}}(e^{\alpha_{he}\psi}-1)+\frac{g}{\alpha_{ci}}(e^{-\alpha_{ci}\psi}-1)\right)\right)\right). \quad (4.57)$$

Equation (4.56) is the "energy balance equation" for a unit mass in a conserva-

tive force field, with velocity $d\psi/d\xi$ at position ψ, and time ξ in a pseudo-potential $V(\psi, M)$.

4.3.2 Soliton and double layer solutions

We examined the Sagdeev pseudo-potential $V(\psi, M)$ given by (4.57) to determine the conditions and the behavior of localized solutions necessary for the ion-acoustic solitons and double layer structures to exist. In doing this, the soliton and double layer conditions (cf. Section 2.3.2) (i.e. $V(\psi, M) = 0$, $d\psi/d\xi = 0$, $V(\psi, M) = 0$ and $dV(\psi, M)/d(\psi) = 0$ at $\psi = 0$. $d^2V(\psi, M)/d(\psi)^2 < 0$ at $\psi = 0$; $V(\psi, M) = 0$ at $\psi = \psi_m$, $dV(\psi, M)/d(\psi) < (>)\ 0$ at $\psi_m < (>)\ 0$. Then, for the formation of a double layers, one more additional condition must be satisfied, i.e, $\frac{dV(\psi,M)}{d\psi}|_{\psi=\psi_m} = 0$).

Moreover, the soliton condition $\mathrm{d}^2V(\psi, M)/\mathrm{d}\psi^2 < 0$ at $\psi = 0$ can be written as

$$\frac{d^2V(\psi, M)}{d\psi^2}|_{\psi=0} = \frac{M^2 - M_0^2}{M^2 - M_1^2} < 0 \tag{4.58}$$

where

$$M_0^2 = \frac{\gamma^2(1-g)}{f\alpha_{ce} + (1-f)\alpha_{he} + g\alpha_{ci}} \tag{4.59}$$

is the critical Mach number and

$$M_1^2 = \frac{1-g}{f\alpha_{ce} + (1-f)\alpha_{he} + g\alpha_{ci}} \tag{4.60}$$

the upper limit of the Mach number.

Since $f\alpha_{ce} + (1-f)\alpha_{he} = 1$ and $g < 1$, equation (4.59) and (4.60) can be written as

$$|M_0| = \frac{\gamma\sqrt{(1-g)(1+g\alpha_{ci})}}{1+g\alpha_{ci}} < 1 \tag{4.61}$$

and

$$|M_1| = \frac{\sqrt{(1-g)(1+g\alpha_{ci})}}{1+g\alpha_{ci}} < 1. \tag{4.62}$$

For $\gamma \neq 0 : \gamma^2 = \cos^2\theta < 1$; which implies $M_o < M_1$, then if $M > M_1 \Rightarrow M > M_0$ from which $M^2 - M_o^2 > 0$ and $M^2 - M_1^2 > 0$, consequently (4.58) is not satisfied.

Similarly, if $M < M_0 \Rightarrow M < M_1$ from which $M^2 - M_o^2 < 0$ and $M^2 - M_1^2 < 0$, once again (4.58) is not satisfied.

Therefore, (4.58) is satisfied only if

$$M_0 < |M| < M_1. \tag{4.63}$$

From equation (4.63), we obtain a condition

$$\gamma\sqrt{\frac{1-g}{1+g\alpha_{ci}}} < |M| < \sqrt{\frac{1-g}{1+g\alpha_{ci}}} < 1 \tag{4.64}$$

which determines the existing domain of the corresponding nonlinear wave solutions. It is very important to mention that the soliton characteristic allows the same Mach number M range values in subsonic Mach number regime with the plasma model in Section 4.1 (Model 1). If the second ions (Maxwellian) species equal to zero (i.e. g = 0) then, the system will automatically reduce to Model 1 (Section 3.1).

4.3.3 Numerical results

We now apply our results to the Viking satellite observations in the auroral region of the Earth's magnetosphere as reported by Berthomier et al. (1998). The parameters are as follows: the cool electron density and temperature $n_{ce} = 0.2cm^{-3}$ and $T_{ce} = 1eV$, hot electron density and temperature $n_{he} = 1.8cm^{-3}$ and $T_{he} = 26eV$, which gives the effective temperature $T_{eff} \approx 7eV$ with an electric field amplitude less than $100mV/m$. We further present the numerical computations of the energy integral in equation (4.56) and Sagdeev potential $V(\psi, M)$ given by (4.57) for different plasma parameters such as Mach number $M = 0.93$, electron density ratio $f = 0.1$, electron temperature ratio $\tau = 0.04$, propagating angle $\theta = 15^o$, ion density ratio $g = 0.1$, where $\alpha_{ci} = T_{eff}/T_{ci}$ is taken as 0.1.

Table 4.3 describe the behavior of the nonlinear low frequency electrostatic structures for different values of cool ion density g, for other fixed parameters $f = 0.1$, $\tau = 0.04$ and $\theta = 35^o$ respectively. In Table 4.3, it is clearly shown that the Mach number region (both the minimum M_o and maximum M_1) and soliton velocity are subsequently decreased with an increase in cool ion density g. Also at the M_o region, both the width and pulse duration tend to decrease with g but only the electric field seems to increase. On the other hand (i.e the maximum Mach number region M_1), the width and pulse duration tend to increase with an increase in g value. Meanwhile, the electric field slightly tends to increase as cool ion density increases, but it is very

Table 4.3: Properties of ion-acoustic solitons, such as Soliton Velocity (V), Mach number range ($M_o < |M| < M_1$), Electric Field (E), Soliton Width (W) and Pulse Duration (τ^*), for various values of cool ion density (g) with $\theta = 35^o$, cool electron density $f = 0.1$, electron temperature $\tau = 0.04$ and ion temperature $\alpha_{ci} = 0.1$.

g	$M_o < \|M\| < M_1$	$V(kms^{-1})$	$E(mVm^{-1})$	$W(m)$	$\tau^*(ms)$
0.0	0.8192 - 0.999	21.22 - 25.87	0.00016 - 23.54	6058 - 226.2	285.49 - 8.74
0.01	0.8147 - 0.994	21.10 - 25.74	0.00025 - 24.43	5252 - 232.96	248.91 - 9.05
0.05	0.7965 - 0.965406(DL)	20.63 - 25.00	0.00039 - 21.41	4659.2 - 392.6	225.85 - 15.70
0.1	0.7735 - 0.913235(DL)	20.03 - 23.65	0.0024 - 16.80	2626 - 446.16	131.10 - 18.87
0.15	0.7499 - 0.8625081(DL)	19.42 - 22.34	0.0036 - 14.44	2397.2 - 456.04	123.44 - 20.41
0.2	0.7259 - 0.8130593(DL)	18.80 - 21.06	0.009 - 12.09	1862.12 - 477.36	99.05 - 22.67

interesting to notice that at g=0.05 the double layer solution starts to appear and the electric field gradually reduces.

The variation of the Sagdeev potential $V(\psi, M)$ against the normalized potential ψ is shown in Figure 4.21 for different values of Mach number M. The fixed parameters are cool electron number density, $f = 0.1$, cool ion density, $g = 0.1$, cool to hot electron temperature ratio, $\tau = 0.04$ and angle of propagation, $\theta = 15^o$. The curves show that the soliton's amplitude increases with an increase in the Mach number. No soliton solutions are found for $M > 0.942$. This result is consistent with Ghosh and Lakhina, 2004. Further numerical computation shows that the nonlinear solutions can exist only in the subsonic Mach number region. In this case, the Mach number regime is dependent upon the cool ion density ratio, this confirmed very well in Table 4.3 that the upper Mach number limit is $M < 1$ at $g = 0$ (see Section 3.1). Unlike the case of an unmagnetized plasma consisting of two ion species and double Maxwellian electrons, the nonlinear solutions were found to exist only in the supersonic Mach number regime (i.e. $M > 1$) (Baboolal et al. 1990; Jain et al. 1990). Figure 4.22 shows the normalized electrostatic potential ψ against ξ which has been obtained numerically by integrating equation (4.56) for the same parameters used in Figure 4.21. It is seen clearly that as the Mach number increases, the solitons' potential amplitude increases and the width decreases.

Figure 4.23 shows the variation of the Sagdeev potential $V(\psi, M)$ versus the real electrostatic potential ψ for different cool electron number density f. The chosen parameters are Mach number $M = 0.93$ and the other parameters are the same as in Figure 4.21. As the cool electron density increases, the solitons amplitude increases

and numerical computations show that the soliton solutions are not possible beyond $f > 0.30$. Jain et al. (1990) have shown the existence of double layer solutions for the electron density ratio of 0.1 and 0.3. Also, Ghosh and Lakhina, (2004) showed the existence of rarefactive ion acoustic solitary waves for two different initial cold electron concentrations (0.15 and 0.35) for propagating angle $\theta = 30^o$. Figure 4.24 shows the potential ψ against ξ, for the same parameters used in Figure 4.23. It shows that as the cool electron density f increases, the ion-acoustic solitons potential amplitude increases and the width also increases.

In Figure 4.25, the curves show the variation of the Sagdeev potential $V(\psi, M)$ versus the real electrostatic potential ψ for different cool ion number density g. Other fixed parameters are $\tau = 0.04$, $f = 0.1$, $\theta = 15^o$ and $M = 0.93$. It is seen that the ion-acoustic solitons' amplitude increases with increasing ion density ratio g. Beyond $g > 0.12$ no soliton solution is possible. It is very important to mention that the Mach number existence domain is deeply dependent on cool ion density. The inclusion of the second ion species has been investigated by many authors (e.g. Baboolal et al. 1990; Jain et al. 1990; Bychekov et al. 1995; Ghosh and Lakhina 2004). Figure 4.26 shows the normalized electrostatic potential ψ against ξ for the same parameters used in Figure 4.25. It clearly shows that as the Mach number increases, the solitons' potential amplitude increases and the width decreases.

The curves plotted in Figure 4.27 show the variation of the Sagdeev potential $V(\psi, M)$ versus the normalized electrostatic potential ψ for different values of the oblique propagation angle θ. The fixed parameters are cool ion density ratio g=0.1 and other parameters of Figure 4.25. It is observed that a unique nonlinear structure (double layer) appears at θ=33.46808^o. The curves clearly shows that as the angle of propagation *theta* increases, the solitons' potential amplitude increases. There is no soliton or double layer solution above $\theta > 33.46808^o$. Whereas, in Figure 2 of Ghosh and Lakhina, (2004) they showed the existence of only positive and negative potential solitons for a magnetized plasma consisting of two ion species and two electrons temperature, for $\theta = 0^o$ to 60^o. Figure 4.28 shows the normalized potential ψ against ξ, for the same parameters used in Figure 4.27. It is very obvious from the curves that as we increase the propagation angle θ, the amplitude as well as width of the soliton and double layer increases.

Figure 4.29 shows the variation of the Sagdeev potential $V(\psi, M)$ against the real electrostatic potential ψ for different values of the cool to hot electron temperature

ratio τ=T_{ce}/T_{he}. The fixed parameters are θ=15^o, g=0.1, f=0.1 and M=0.93. It is interesting to note that at τ=0.0724351 a double layer structure appears. Above $\tau > 0.724351$ there is no soliton or double layer solution possible. The curves clearly shown that the negative potential ion-acoustic solitons amplitude increases with the increase in cool to hot electron temperature ratio. Likewise, the effect of the cool to hot electron temperature ratio has been mentioned by many authors (Nishihara and Tajiri, 1981; Baboolal et al. 1990; Baluku et al. 2010). Figure 4.30 shows the potential ψ against ξ, for the same parameters used in Figure 4.29. It clearly shows that as the cool to hot electron temperature increases, the amplitude as well as width of the soliton and double layer increases.

The curves in Figure 4.31 show the variation of the Sagdeev potential $V(\psi, M)$ against the normalized electrostatic potential ψ for different values of Mach number M. The fixed parameters are cool electron density, f=0.1, cool to hot electron temperature, τ=0.04, cool ion density, g=0.05 and propagating angle, θ=35^o. It is very interesting to note that at M=0.965406, a double layer solution appears. Also, the negative potential ion-acoustic soliton amplitude, ψ increases with increasing M. It has been mentioned by Ghosh and Lakhina, (2004) that for a large θ the rarefactive solitary wave solutions may turn out to be a weak double layer. Figure 4.32 shows the normalized electrostatic potential ψ against ξ for the same parameters used in Figure 4.31. It is seen clearly that as the Mach number increases, the solitons potential amplitude increases and the width decreases.

In Figure 4.33, the curves show the variation of the Sagdeev potential with real potential corresponds to the double layer solutions for different values of θ and M. Other fixed parameters are cool electron density $f = 0.1$, cool to hot electron temperature ratio $\tau = 0.04$ and cool ion density $g = 0.1$. The curves show all combinations of (θ, M) yield exactly the same value for the double layer amplitude, as shown in Model 1, 2 and 3 of Chapter 1. This corresponds to a "point" solution as found in a study by Djebli and Marif (2009). Figure 4.34 shows the existence domain of solitons and double layers for the fixed parameters in Figure 4.33. The curves show that a double layer solution is the upper bound as we increase the angle of propagation θ, for different M values. The maximum Mach number for negative potential solitons are bounded by those of the double layer solutions corresponding to a given θ value.

The variation of the Sagdeev potential $V(\psi, M)$ against the normalized potential ψ is shown in Figure 4.35 for different values of the cool to hot electron temperature

ratio τ and the Mach number M for the fixed parameters $f = 0.1$, $g = 0.1$ and $\theta = 15^o$. It is interesting to point out that the supersoliton (Dubinov and Kolotkov, 2012; Verheest et al. 2013; Maharaj et al. 2013) solution has been found to exist for $\tau = 0.080898$ and $M = 0.916$, $\tau = 0.077948$ and $M = 0.92$, $\tau = 0.0724351$ and $M = 0.93$. Similar results have been shown in Model 1, 2 and 3 of Chapter 1. Figure 4.36 shows the existence domain of solitons, double layers and supersolitons for the same parameters in Figure 4.35. The curves were plotted for the variation of the maximum electrostatic potential ψ_{Max} against τ for different values of the Mach number M. In an unmagnetized plasma consisting of positive and negative ions and two electron temperature, Baboolal et al. (1990) showed the existence domain for compressive and rarefaction solitons bounded by negative potential double layer solutions. The reason for smaller amplitudes for larger τ=$\frac{T_c}{T_h}$ can be seen from the expression for the effective temperature $T_{eff} = T_c/(f + (1 - f)\tau)$ which shows that for fixed f the normalization factor T_{eff} decreases with increasing τ so that the corresponding normalized potential ψ would linearly increase in magnitude. Similar behavior has been reported by Baboolal, (1988).

4.3.4 Discussion

We have studied four component ion-acoustic solitons in a magnetized multi-ions space plasma consisting of cold oxygen-ion fluid, Maxwellian ions and two distinct groups of Boltzmann distributions electron (cool and hot). It was found that the inclusion of second ion species (Maxwellian) in the model enhanced the amplitude of the ion-acoustic solitary waves and allowed the nonlinear structures to exist at subsonic Mach number regime. Regarding the auroral region parameters, the Viking satellite observations (Berthomier et al. 1998) reported the cool electron density and temperature $n_{ce} = 0.2cm^{-3}$ and $T_{ce} = 1eV$, hot electron density and temperature $n_{he} = 1.8cm^{-3}$ and $T_{he} = 26eV$, which gives the effective temperature $T_{eff} \approx 7eV$ with total electric field amplitude of less than $100mV/m$, width of about $100m$, about $20ms$ of pulse duration and $\approx 10 - 50km/s$ soliton velocities range respectively. For M=0.93, θ=15^o the maximum electric field comes out to be $2mV/m$ and corresponding soliton width, pulse duration and speed comes out to be $\approx$ $189m$, $8ms$ and $24km/s$, respectively.

The inclusion of a second ion species allowed the nonlinear structures to exist at subsoinc Mach number regime of the same region with the plasma model consisting of

magnetized cold oxygen-ion fluid and Boltzmann distributions of proton and electron species described in Section 4.1. To our surprise, the numerical results showed the existence of negative potential solitons and double layers in the same Mach numbers regime. Our findings may be useful for improving our understanding of the nonlinear fluctuations in the auroral region of the Earth's magnetosphere.

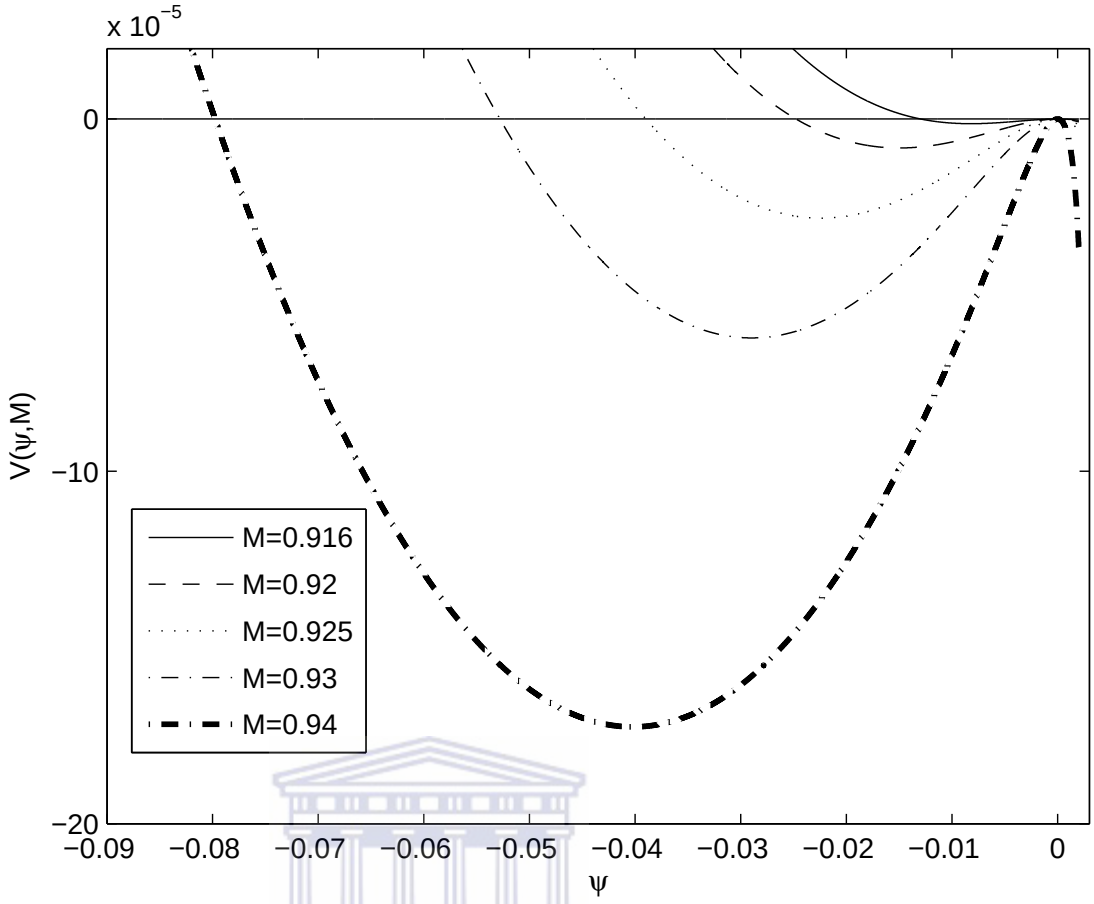

Figure 4.21: Sagdeev potential, $V(\psi, M)$ vs normalized electrostatic potential ψ. The parameters are τ= 0.04, f=0.1, g=0.1, θ=15^o and M = 0.916, 0.92, 0.925, 0.93, 0.94.

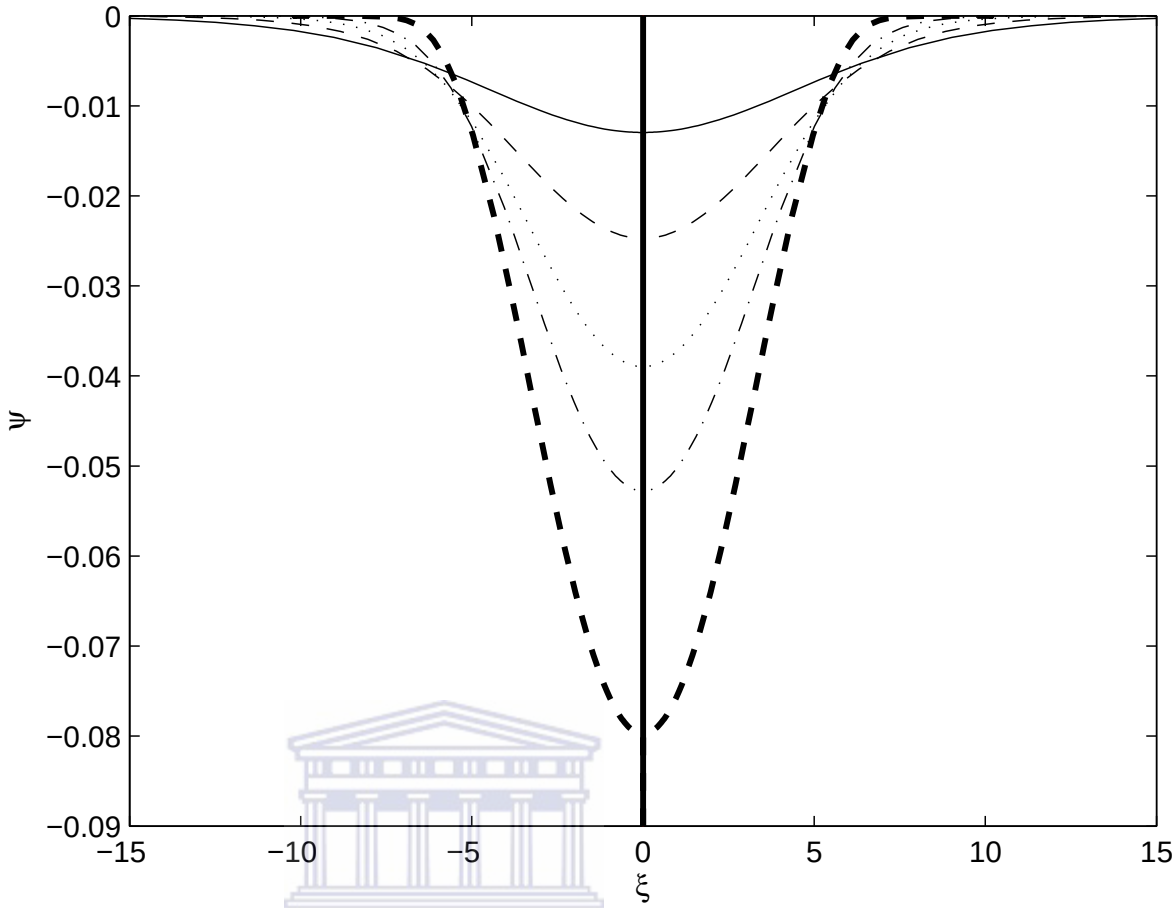

Figure 4.22: Electrostatic potential ψ vs ξ. The parameters of Figure 4.21 and M=0.916 (—), 0.92 (- - -), 0.925 (...), 0.93 (- . -) and 0.94 (— — —).

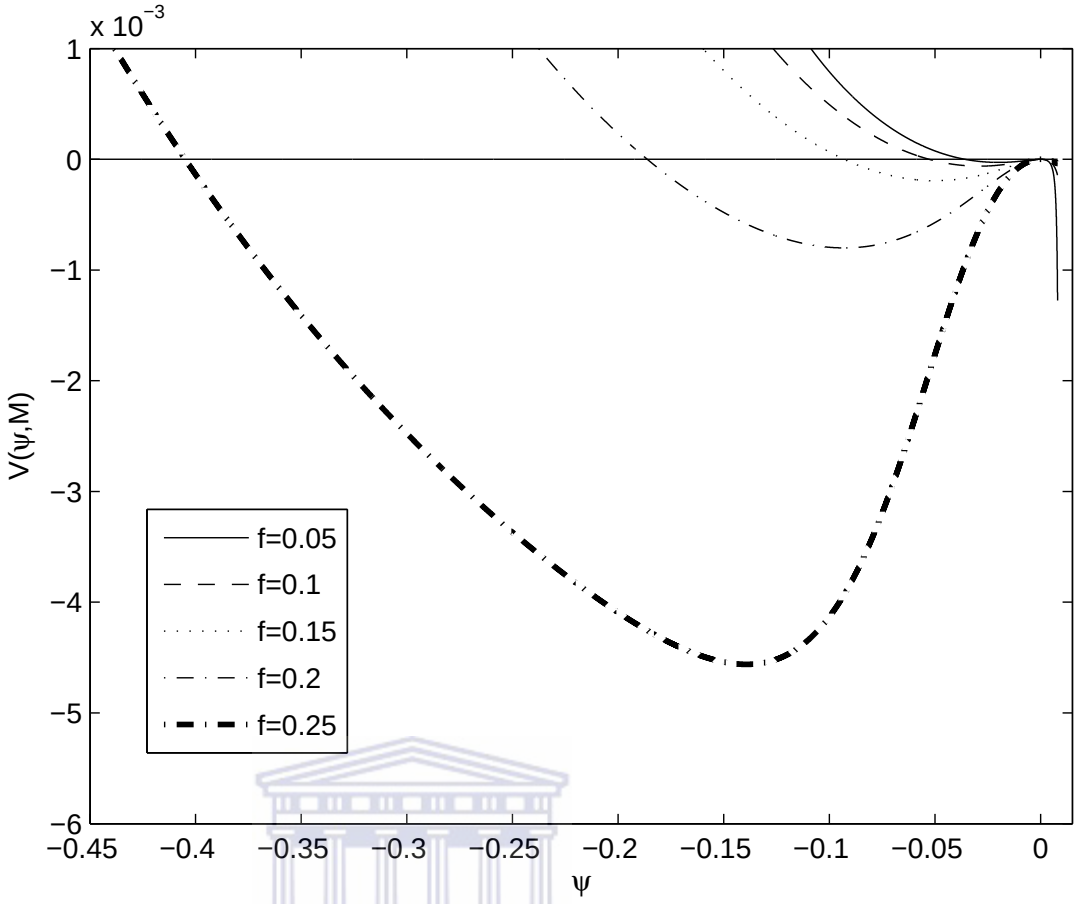

Figure 4.23: Sagdeev potential, $V(\psi, M)$ vs normalized electrostatic potential ψ. The parameters are τ= 0.04, g=0.1, θ=15^o, M=0.93 and f=0.05, 0.1, 0.15, 0.2, 0.25.

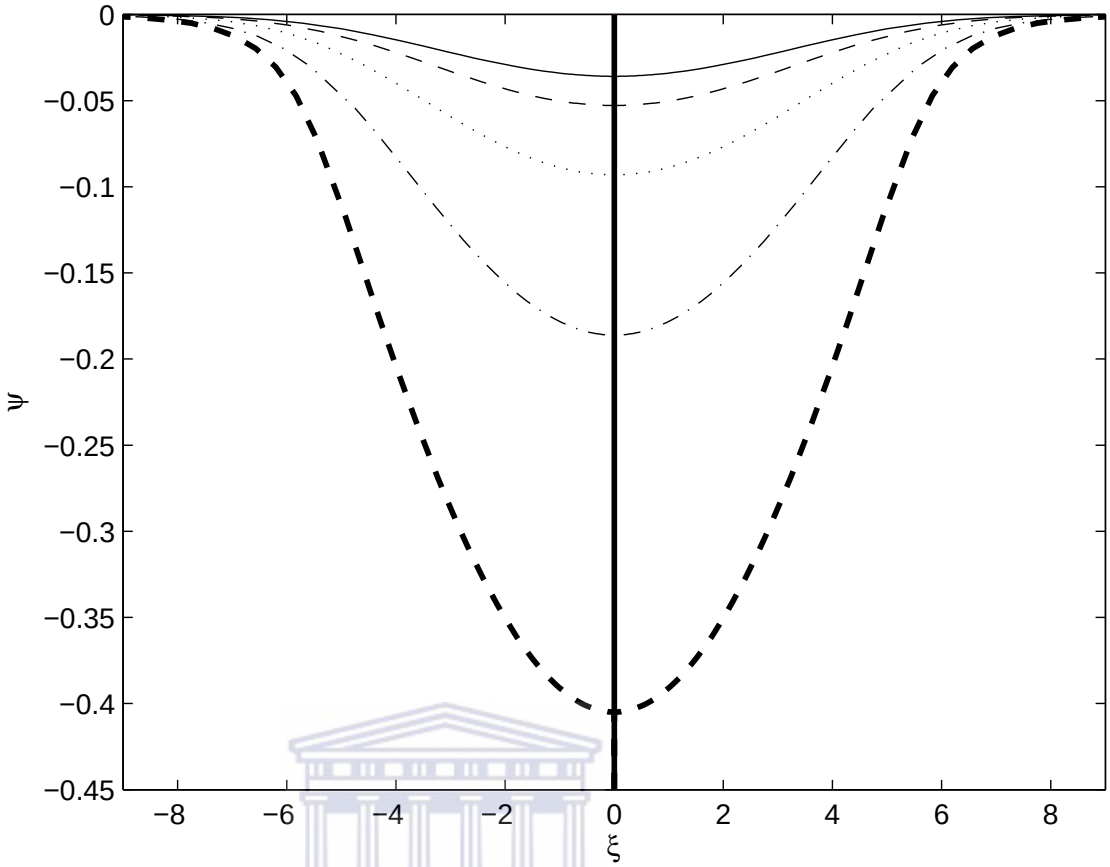

Figure 4.24: Electrostatic potential ψ vs ξ. The parameters of Figure 4.23 and f=0.05 (—), 0.1 (- - -), 0.15 (...), 0.2 (- . -) and 0.25 (— — —).

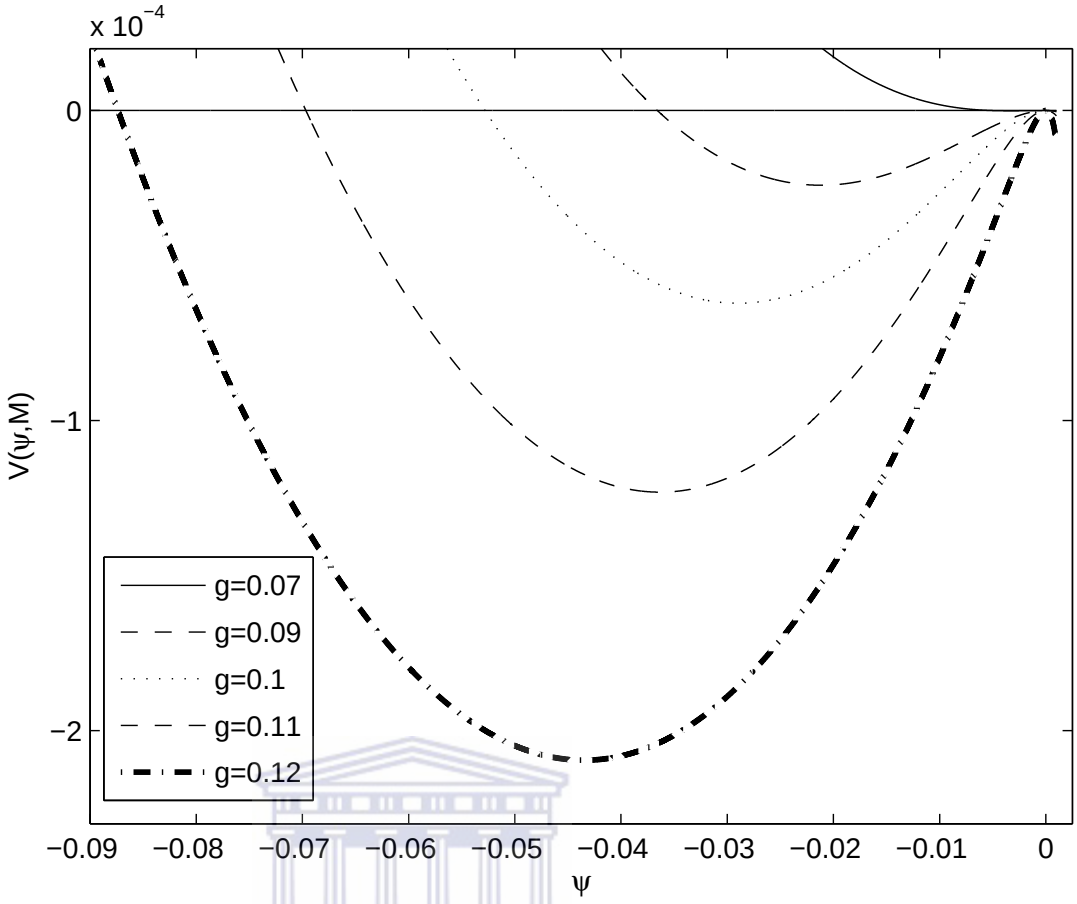

Figure 4.25: Sagdeev potential, $V(\psi, M)$ vs normalized electrostatic potential ψ. The parameters are τ= 0.04, f=0.1, θ=15^o, M=0.93 and g=0.07, 0.09, 0.1, 0.11, 0.12.

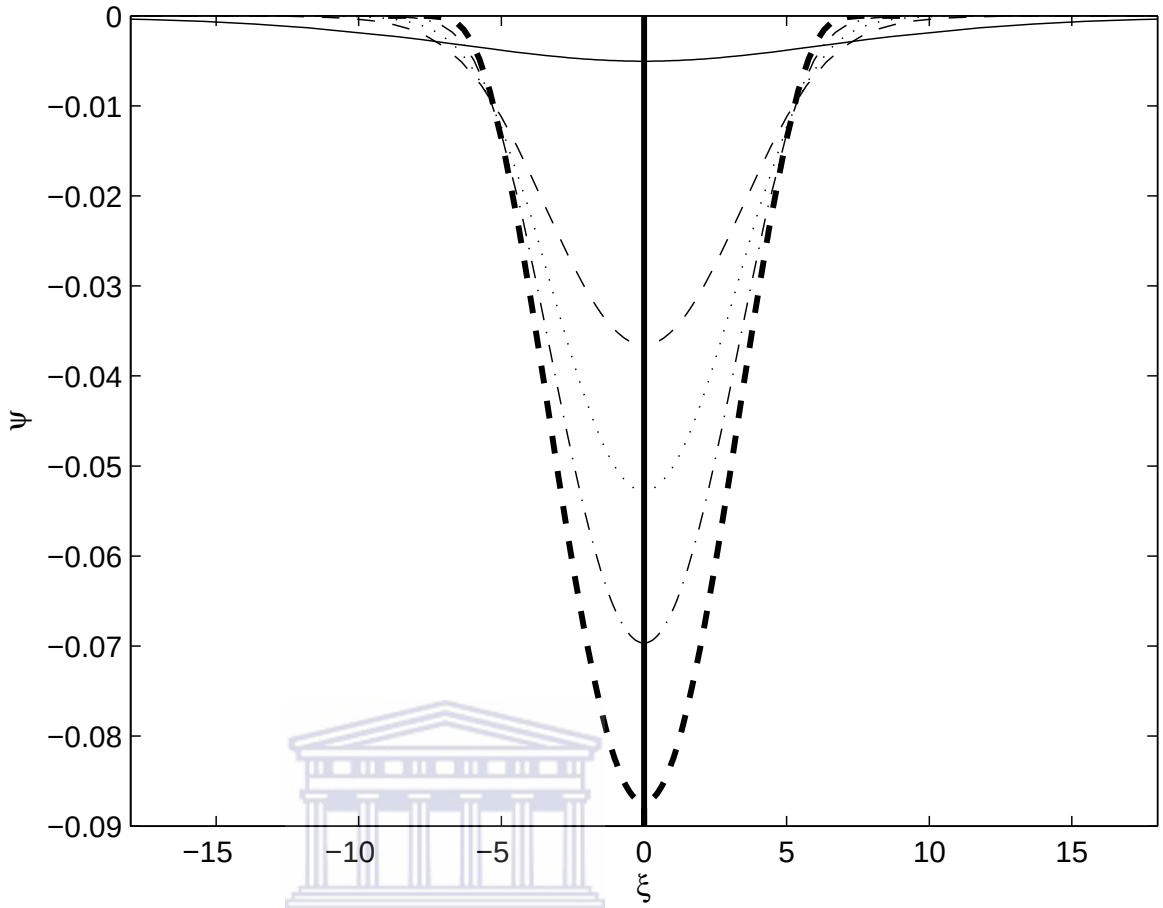

Figure 4.26: Electrostatic potential ψ vs ξ. The parameters of Figure 4.25 and g=0.07 (—), 0.09 (- - -), 0.1 (...), 0.11 (- . -) and 0.12 (— — —).

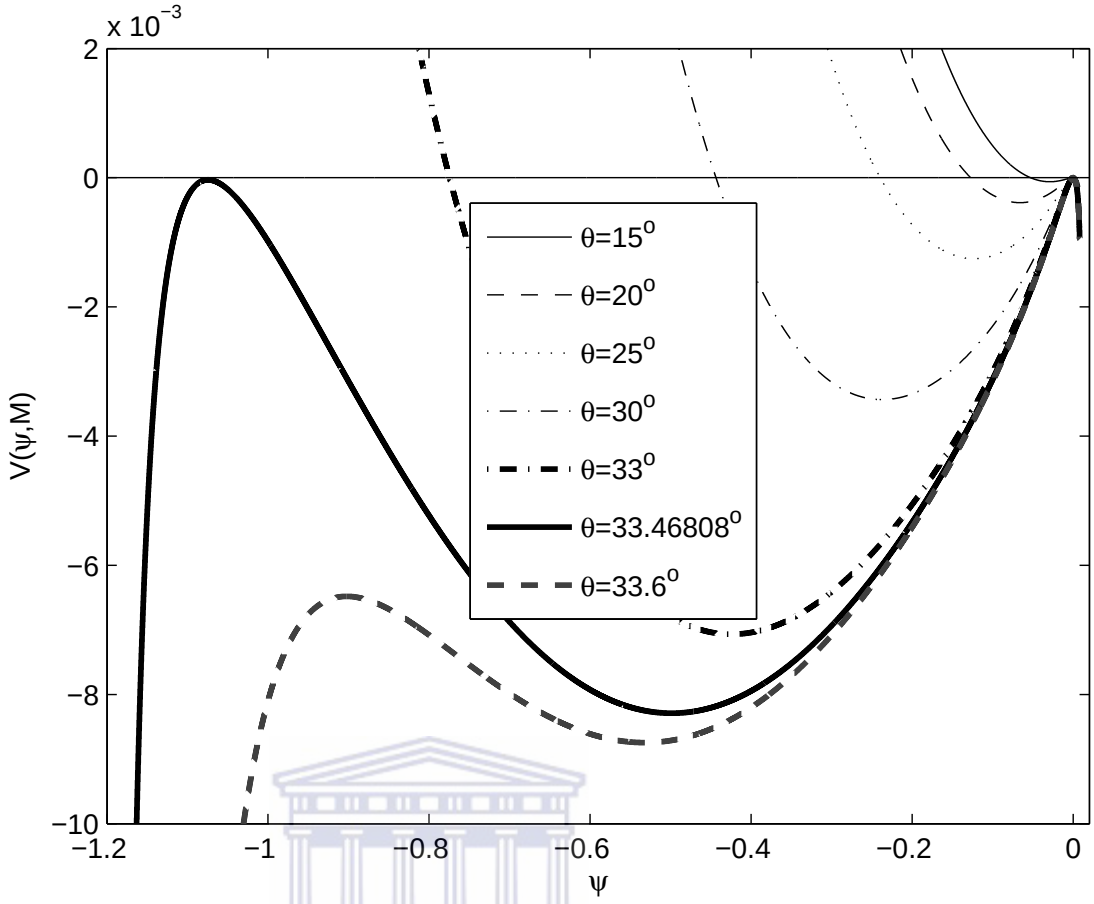

Figure 4.27: Sagdeev potential, $V(\psi, M)$ vs normalized electrostatic potential ψ. The parameters are τ= 0.04, f=0.1, g=0.1, M=0.93 and θ=15^o, 20^o, 25^o, 30^o, 33^o, 33.46808^o, 33.6.

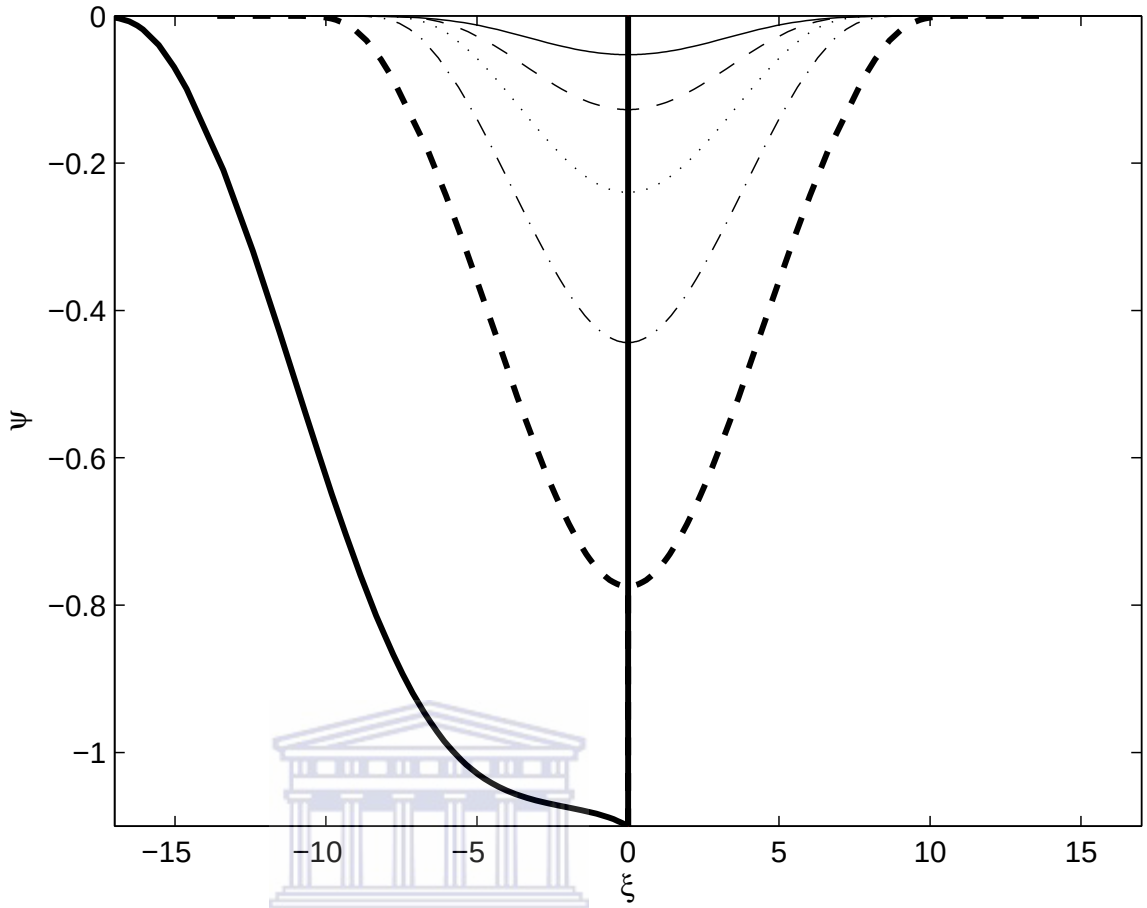

Figure 4.28: Electrostatic potential ψ vs ξ. The parameters of Figure 4.27 and θ=15^o (—), 20^o (- - -), 25^o (...), 30^o (- . -), 33^o (— — —), 33.46808^o(—) for double layer.

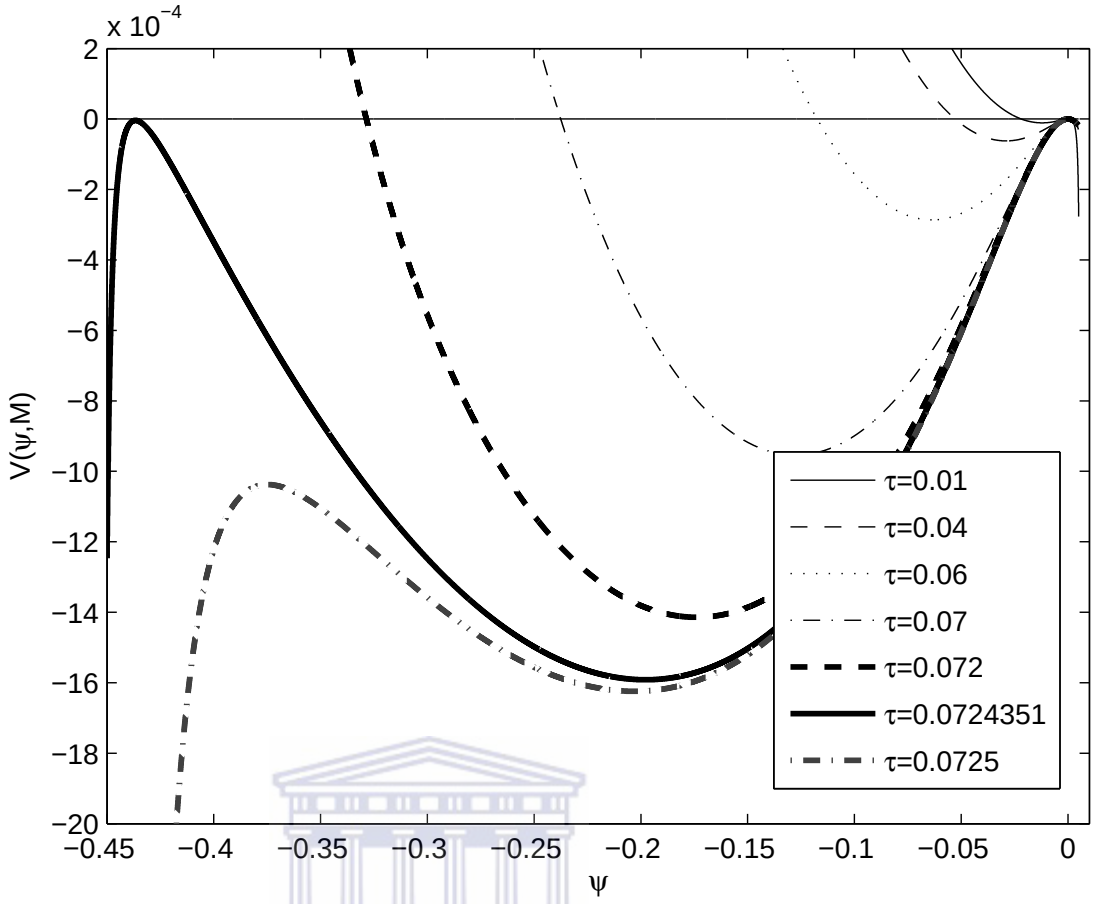

Figure 4.29: Sagdeev potential, $V(\psi, M)$ vs normalized electrostatic potential ψ. The parameters are f=0.1, g=0.1, θ=15^o, M=0.93 and τ=0.01, 0.04, 0.06, 0.07, 0.072, 0.0724351, 0.0725.

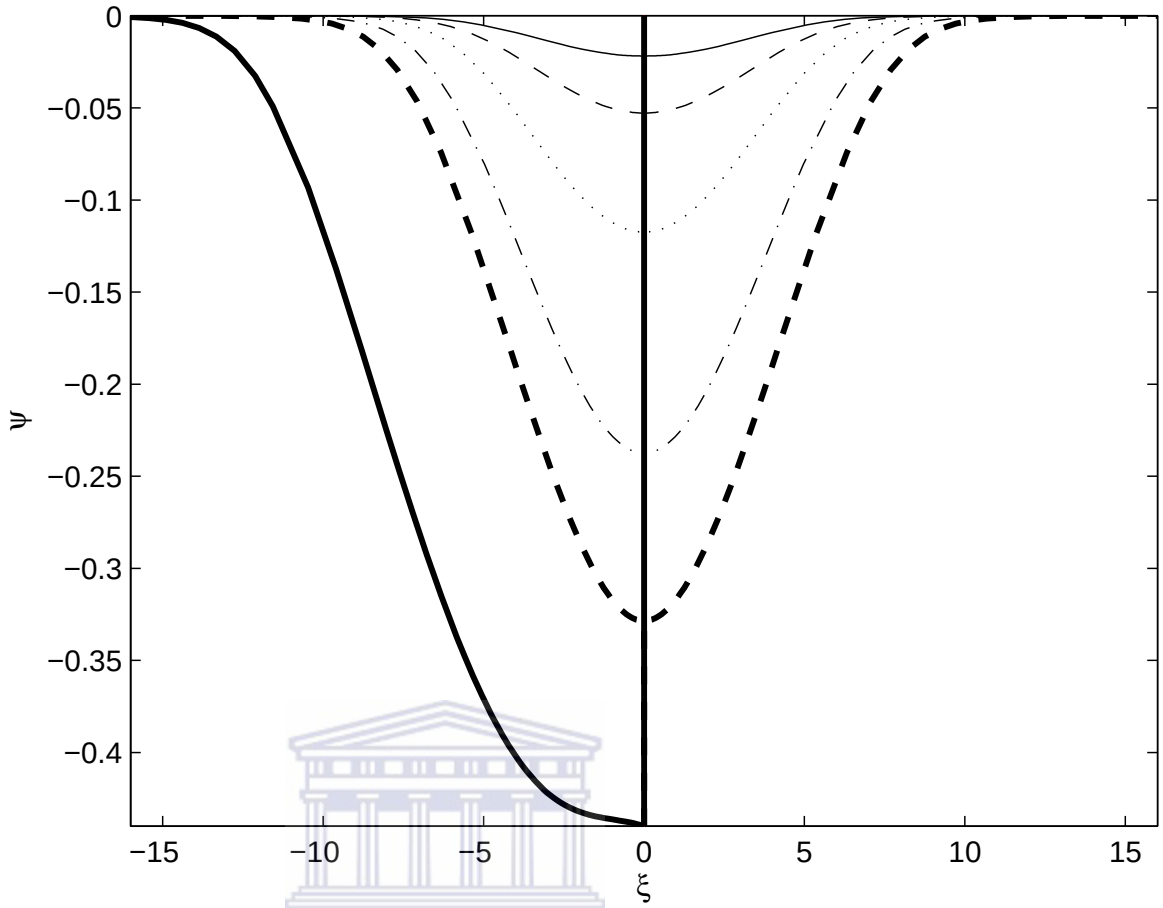

Figure 4.30: Electrostatic potential ψ vs ξ. The parameters of Figure 4.29 and τ=0.01 (—), 0.04 (- - -), 0.06 (...), 0.07 (- . -), 0.072 (— — —), 0.0724351 (—) for double layer.

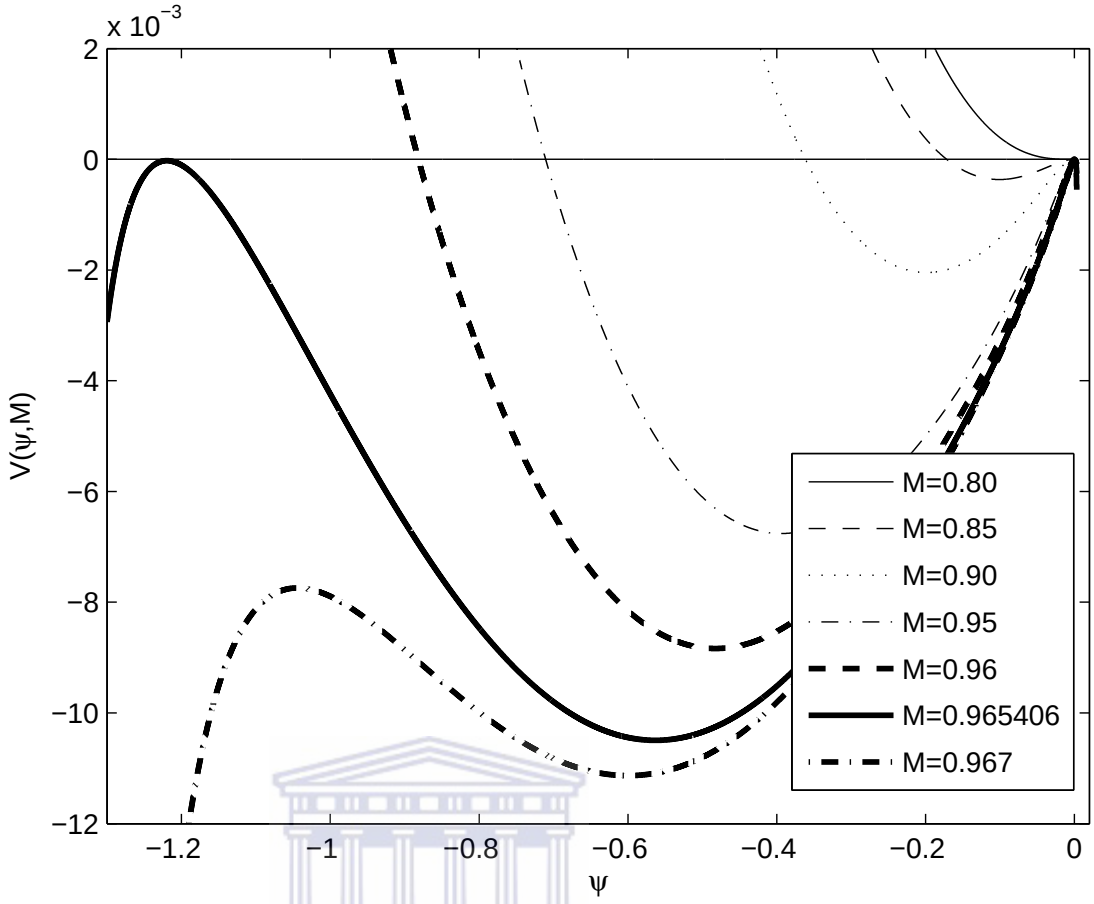

Figure 4.31: Sagdeev potential, $V(\psi, M)$ vs normalized electrostatic potential ψ. The parameters are f=0.1, g=0.05, θ=35^o, τ=0.04 and M=0.80, 0.85, 0.90, 0.95, 0.96, 0.965406, 0.967.

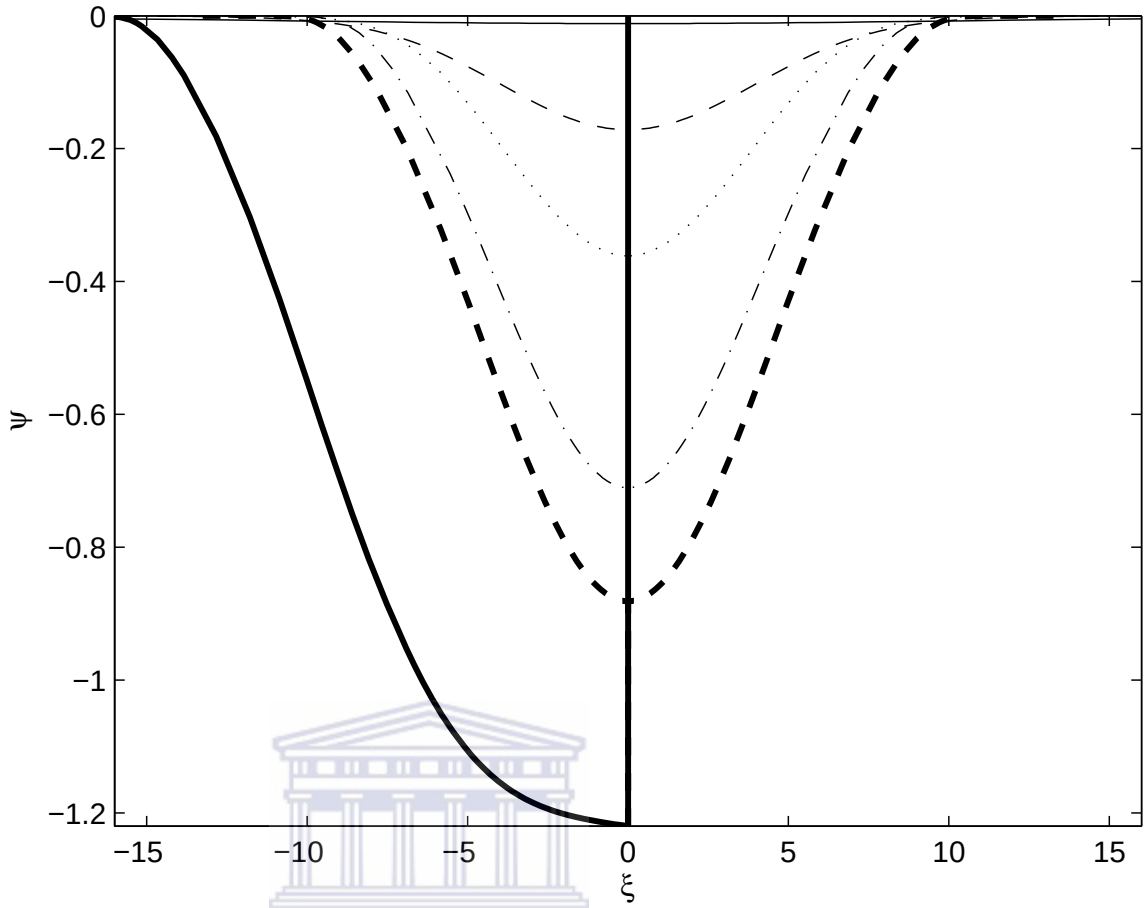

Figure 4.32: Electrostatic potential ψ vs ξ. The parameters of Figure 4.31 and M=0.80 (—), 0.85 (- - -), 0.90 (...), 0.95 (- . -) 0.96 (— — —) and 0.965406 (—).

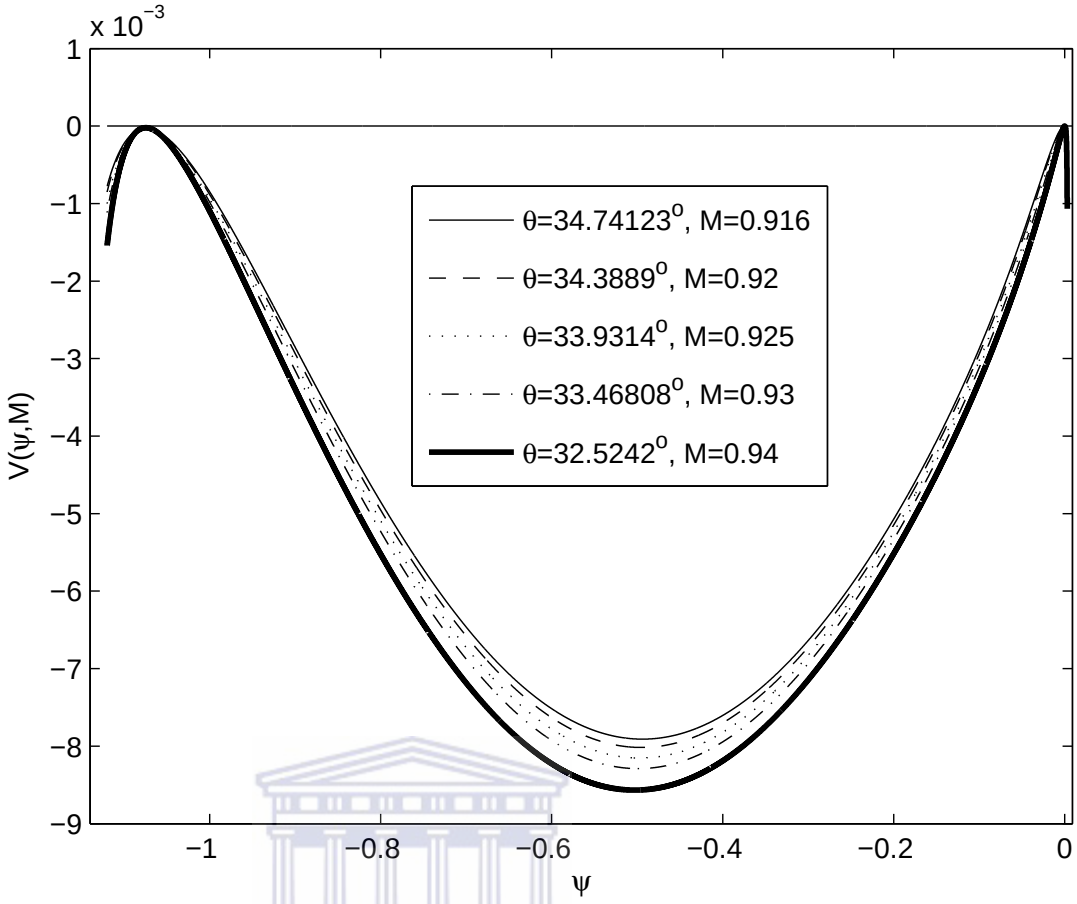

Figure 4.33: Sagdeev potential, $V(\psi, M)$ vs normalized electrostatic potential ψ. The parameters are f=0.1, g=0.1 for θ=34.74123^o and M=0.916, θ=34.3889^o and M=0.92, θ=33.9314^o and M=0.925, θ=33.46808^o and M=0.93, θ=32.5242^o and M=0.94.

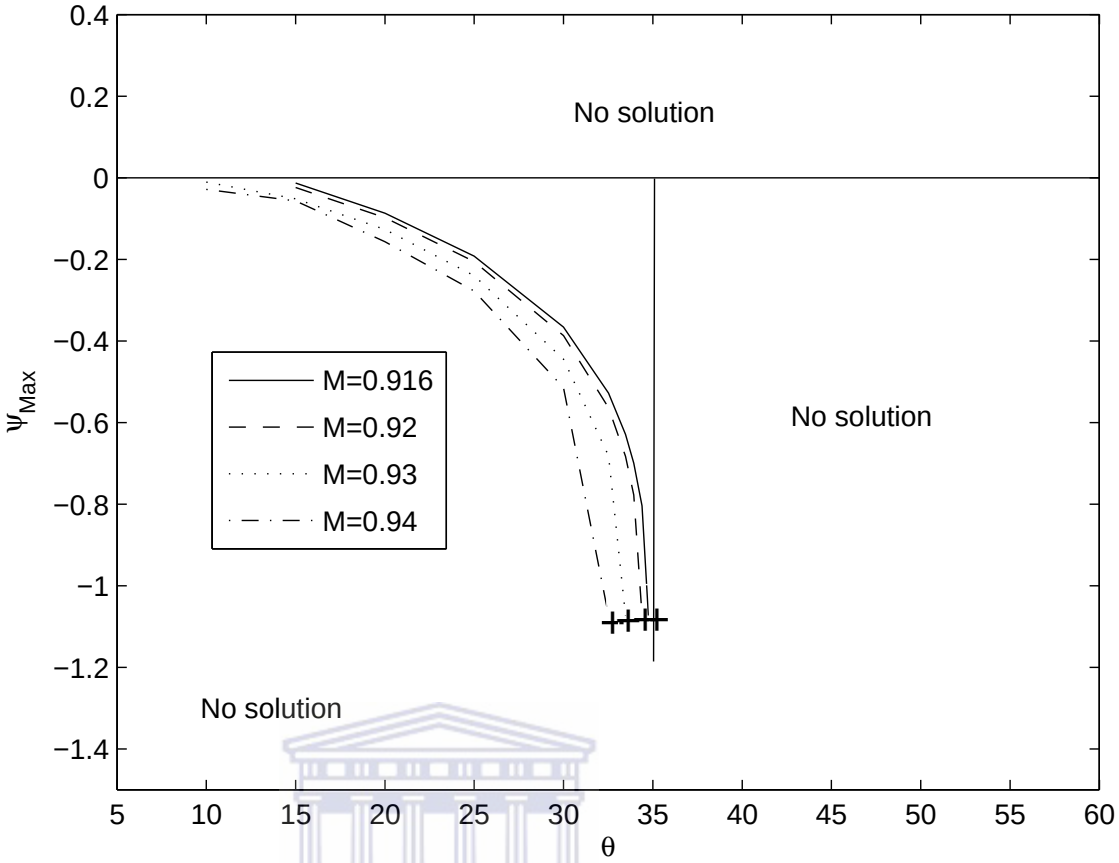

Figure 4.34: The maximum electrostatic potential ψ_{Max} vs θ. The parameters of Figure 4.33 and M=0.916, 0.92, 0.925, 0.93, 0.94.

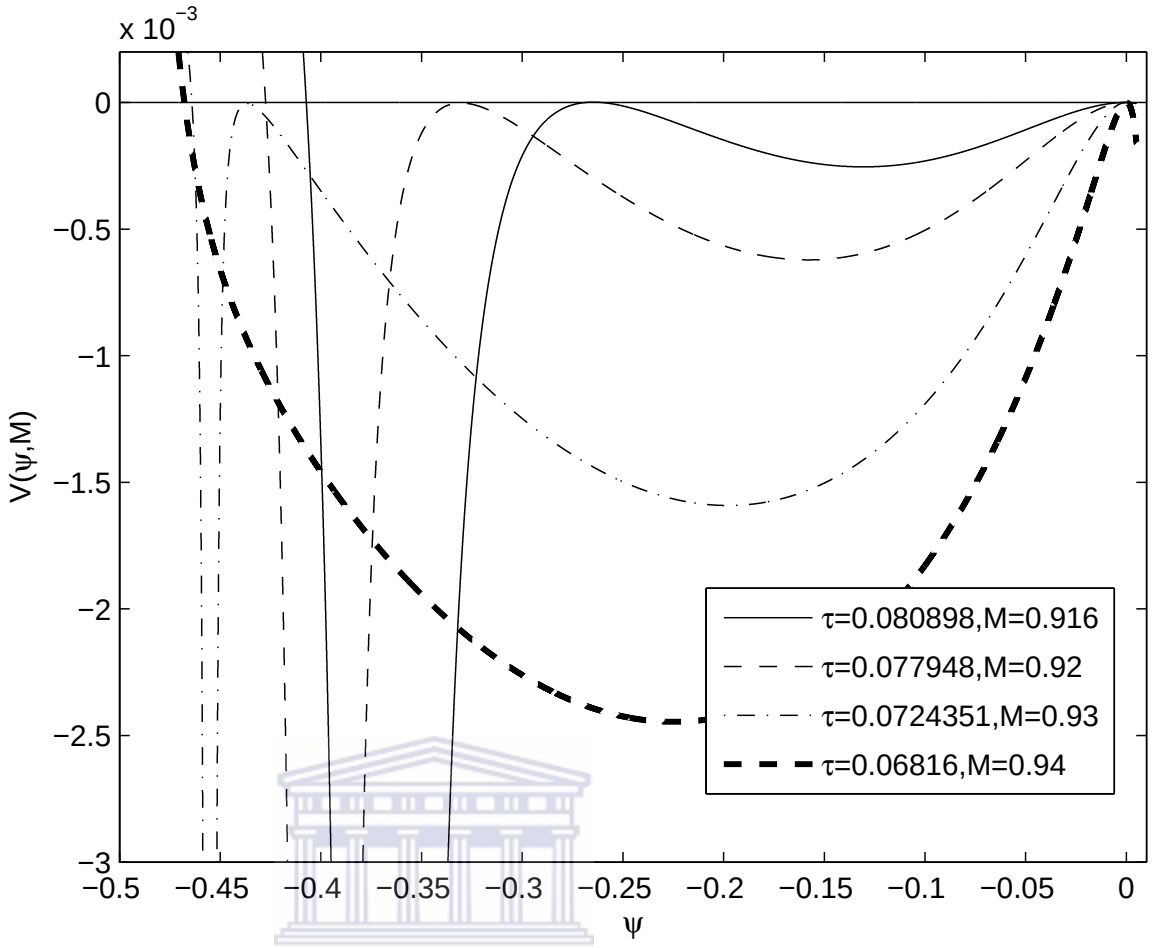

Figure 4.35: Sagdeev potential, $V(\psi, M)$ vs the normalized potential ψ. The parameters are g=0.1, f=0.1, θ=15^o and M=0.916 and τ=0.080898, M=0.92 and τ=0.077948, M=0.93 and τ=0.0724351, M=0.94 and τ=0.06816- soliton solution only.

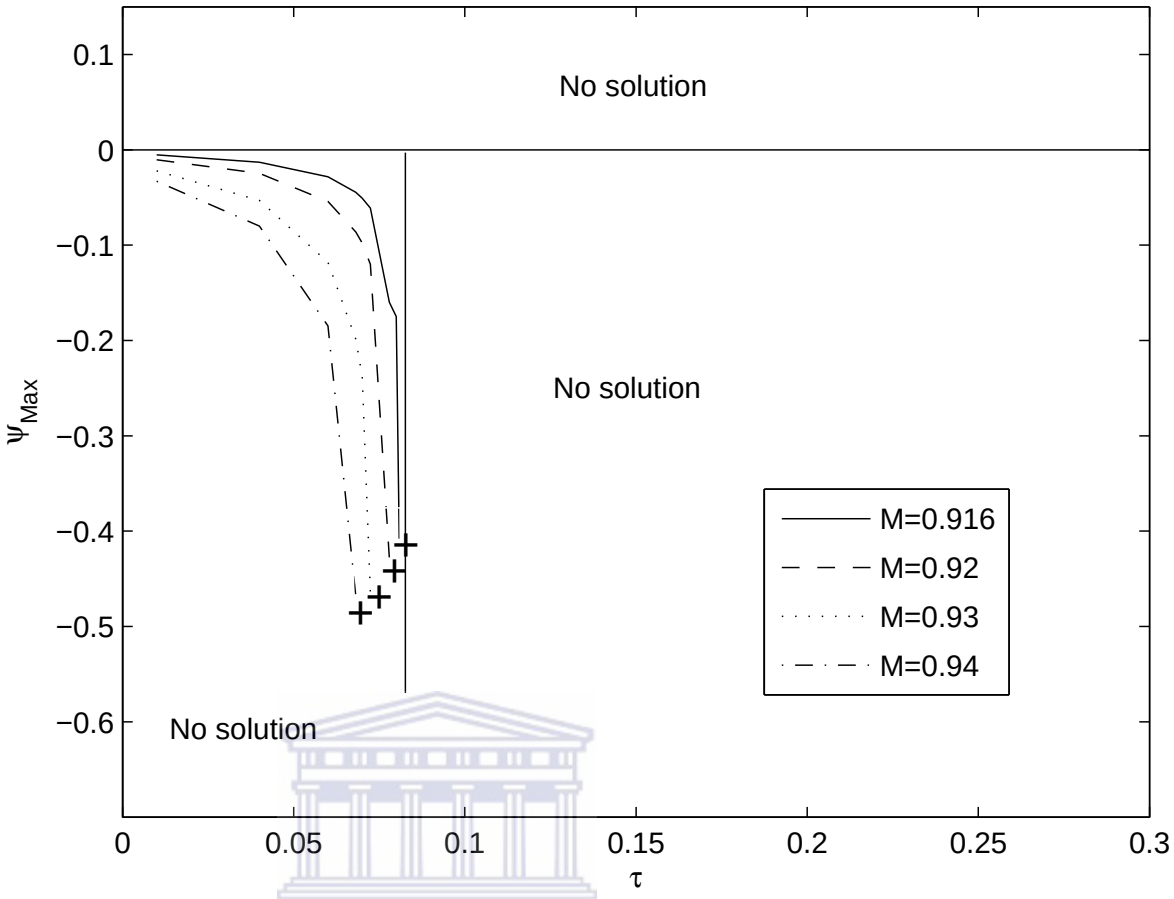

Figure 4.36: The maximum electrostatic potential ψ_{Max} vs τ. The parameters of Figure 4.35 and M=0.916, 0.92, 0.93, 0.94- soliton solution only.

Chapter 5

Summary and conclusion

In this chapter, the summary and conclusion of our investigations on nonlinear low frequency wave phenomena in space plasmas are presented. This study investigated in detail the nonlinear electrostatic structures in a magnetized plasma propagating along the auroral magnetic field lines of the Earth's magnetosphere, as reported by several spacecraft missions (i.e. S3-3, FREJA, POLAR, FAST, CLUSTER and WIND). Nonlinear low frequency (ion-acoustic) electrostatic modes have been detected in several regions of the Earth's magnetosphere (Temerin et al. 1982, Bostrom et al. 1988). These waves were categorized as low frequency due to the presence of stationary ion species (which are almost 10^3 times heavier than an electron). Several theoretical studies have been undertaken to study the nonlinear structures in multicomponent plasmas.

Chapter 3 presents a plasma model that can describe the evolution of solitons and double layers in the auroral zone of the Earth's magnetosphere, with two Boltzmann electrons distribution and cold ions fluid. The present study is an extension of the earlier work carried out by Berthomier et al. (1998), and Baluku et al. (2010), by including the magnetized effect, using the Sagdeev potential techniques. Analytical investigations of plasma consisting of Boltzmann distribution of two electron species and cold ions governed by fluid dynamic equations, were performed. Consequently, a numerical investigation of the Sagdeev potential amplitude on different plasma parameters such as Mach number, cool to hot electron density ratio, propagation angle and cool to hot electron temperature ratio, were done.

This model supports the negative potential ion-acoustic solitons and double layers,

and which were found to exist only in the subsonic Mach numbers regime. In contrast as shown (Berthomier et al. 1998; Baluku et al. 2010), for the case of unmagnetized plasma, these negative potential nonlinear structures can exist only in the supersonic Mach number regime. The amplitude of the ion-acoustic solitons increases with Mach number, increased angle of propagation, cool electron density, and cool to hot electron temperature ratio.

The study was extended to investigate the finite ions' temperature effects on plasma consisting of two distinct groups of Boltzmann distributions of electrons and ions fluid. Assuming quasi-neutrality condition, the Sagdeev pseudo-potential technique was used to obtain the nonlinear localized solution and further investigation of the soliton characteristics was done to obtain critical Mach numbers for the existence of the soliton solutions. The inclusion of adiabatic ion temperature allows the nonlinear structure to exist for both subsonic and supersonic Mach number regimes. The double layers exist at a lower angle of propagation as hot ion temperature is increased. The amplitude of ion-acoustic solitary waves increases with Mach number, cool electron density, propagating angle and decreases with ions temperature. The present results concur with the Viking satellite observations in the auroral region.

This study was motivated by Cairn's nonthermal velocity distribution model for the energetic hot electron species in the study of soliton structures with density depletions observed by FREJA and Viking satellites in auroral regions of the Earth's Magnetosphere (Cairns et al. 1995). The theoretical investigation of solitary waves and double layers in auroral plasmas with two temperature electron population was also conducted. The effect of energetic hot electron species on the magnetized plasma model consisting of cold ions fluid, Boltzmann distribution of cool electrons and nonthermal distribution of hot energetic electron species was investigated. A detailed description of where the limitations in parameter space originate from, in terms of the two sonic points (lower and upper limit) and the occurrence of double layers was provided.

Chapter 4 described the finite amplitude, ion-acoustic solitary waves in magnetized three-components plasma consisting of cold oxygen ion beams, hot protons and cool electrons. The electrons and protons were considered as point particles and their density distribution taken as Boltzmann, while the heavy ions component was considered as a fluid. Using the Sagdeev potential technique and assuming charge neutrality condition, the investigation showed the evolution of only positive potential solitons.

The speed of obliquely propagating soliton was found only at subsonic Mach number region without a beam. Then the inclusion of beam velocity to the plasma model extended the solitons existence domain to both subsonic and supersonic Mach number regimes. Subsequently, numerical investigations of the Sagdeev potential and electrostatic potential variations were done on the following plasma parameters: Mach number, propagation angle and hot proton density.

Furthermore, the occurrence of nonlinear low frequency waves in a multi components plasma made up of a magnetized cold oxygen-ions fluid, Maxwellian cool ion species and Boltzmann distributions of cool and hot electron population were studied, using the Sagdeev pseudo-potential technique. This model is a modification of Model 1 (Section 3.1) by including second ion species (Boltzmann distributed), likewise it is also a modification of three-component plasma model in Section 4.1 by including additional Boltzmann electron distribution. The inclusion of additional species in this plasma model was studied and the conditions under which the soliton and double layer solutions can exist were found both analytically and numerically. The theoretical analysis showed that the Mach number regime was found to exist only in the subsonic domain. This model also supports the negative potential ion-acoustic solitons and double layers, which were found to exist only in the subsonic Mach numbers regime.

The Sagdeev potential variations were plotted on Mach numbers, electron density, propagation angle, cool to hot temperature ratio and cool ions contributions, and also showed the electrostatic potential profile. This investigation has shown that the additional species has a lot of influence on the nonlinear structures.

The theoretical results were compared to the actual satellite measurements. The findings provide good agreement.

Appendices

Appendix A

Algebraic expression for the Sagdeev potential in a magnetized plasma with cold ions and two temperature electrons

The Boltzmann distribution is assumed for the densities and temperature of the cool (N_c, T_c) and hot (N_h, T_h) electron species and are given as follows:

cool electrons

$$N_c = N_{c0} \exp(\frac{e\phi}{T_c}). \tag{A.1}$$

hot electrons

$$N_h = N_{h0} \exp(\frac{e\phi}{T_h}). \tag{A.2}$$

Cold ions (described by the fluid equations)

continuity equation

$$\frac{\partial N_i}{\partial t} + \nabla(N_i V_i) = 0. \tag{A.3}$$

momentum equation

$$\left(\frac{\partial}{\partial t} + \mathbf{V_i}.\nabla\right)\mathbf{V_i} = -\frac{e\nabla\phi}{m_i} + e\frac{\mathbf{V}_i \times \mathbf{B}_o}{m_i c}, \tag{A.4}$$

eqations (A.1)-(A.4) are unnormalized.

Normalized set of equations

$$n_c = \frac{n_{c0}}{n_{i0}} \exp\left(\frac{e\phi}{T_{eff}}.\frac{T_{eff}}{T_c}\right)$$

$$n_c = f \exp(\alpha_c \psi) \tag{A.5}$$

$$n_h = \frac{n_{h0}}{n_{i0}} \exp\left(\frac{e\phi}{T_{eff}}.\frac{T_{eff}}{T_h}\right)$$

$$n_h = (1-f) \exp(\alpha_h \psi) \tag{A.6}$$

$$\frac{\partial n_i}{\partial t} + \nabla.(n_i v_i) \tag{A.7}$$

$$\frac{\partial v_i}{\partial t} + v_i \nabla v_i = -\nabla\psi + v_i \times z \tag{A.8}$$

use transformation

$$\xi = (\alpha x + \gamma z - Mt)/M \tag{A.9}$$

The quasi-neutrality condition is

$$n_c + n_h = n_i \tag{A.10}$$

from equations (A.7)-(A.8)

$$\frac{\partial n_i}{\partial t} + \frac{\partial (n_i v_x)}{\partial x} + \frac{\partial (n_i v_z)}{\partial z} = 0 \tag{A.11}$$

$$\frac{\partial v_x}{\partial t} + (v_x \frac{\partial}{\partial x} + v_z \frac{\partial}{\partial z}) v_x = -\frac{\partial \psi}{\partial x} + v_y \tag{A.12}$$

$$\frac{\partial v_y}{\partial t} + (v_x \frac{\partial}{\partial x} + v_z \frac{\partial}{\partial z}) v_y = -v_x \tag{A.13}$$

$$\frac{\partial v_z}{\partial t} + (v_x \frac{\partial}{\partial x} + v_z \frac{\partial}{\partial z}) v_z = -\frac{\partial \psi}{\partial z} \tag{A.14}$$

from equation (A.9)

$$\frac{\partial \xi}{\partial x} = \alpha/M, \frac{\partial \xi}{\partial z} = \gamma/M, \frac{\partial \xi}{\partial t} = -1, \frac{\partial}{\partial t} = -\frac{\partial}{\partial \xi}, \frac{\partial}{\partial x} = \alpha/M \frac{\partial}{\partial \xi}, \frac{\partial}{\partial z} = \gamma/M \frac{\partial}{\partial \xi}, \tag{A.15}$$

equation (A.15) into (A.11)

$$-\frac{dn_i}{d\xi} + \frac{\alpha}{M} \frac{d(n_i v_x)}{d\xi} + \frac{\gamma}{M} \frac{d(n_i v_z)}{d\xi} = 0 \tag{A.16}$$

$$-M \frac{dn_i}{d\xi} + \alpha \frac{d(n_i v_x)}{d\xi} + \gamma \frac{d(n_i v_z)}{d\xi} = 0 \tag{A.17}$$

$$\frac{dn_i}{d\xi}(-M + \alpha v_x + \gamma v_z) = 0 \tag{A.18}$$

$$\frac{d}{d\xi}(L_v n_i) = 0 \tag{A.19}$$

where

$$L_v = -M + \alpha v_x + \gamma v_z$$

equation (A.15) into (A.12)

$$-\frac{dv_x}{d\xi} + \left(\frac{\alpha}{M} v_x \frac{d}{d\xi} + \frac{\gamma}{M} v_z \frac{d}{d\xi} \right) v_x = -\frac{\alpha}{M} \frac{d\psi}{d\xi} + v_y. \tag{A.20}$$

$$-M \frac{dv_x}{d\xi} + \alpha v_x \frac{dv_x}{d\xi} + \gamma v_z \frac{dv_x}{d\xi} = -\alpha \frac{d\psi}{d\xi} + M v_y \tag{A.21}$$

$$(-M + \alpha v_x + \gamma v_z) \frac{dv_x}{d\xi} = -\alpha \frac{d\psi}{d\xi} + M v_y \tag{A.22}$$

$$L_v \frac{dv_x}{d\xi} = -\alpha \frac{d\psi}{d\xi} + M v_y \tag{A.23}$$

equation (A.15) into (A.13)

$$-\frac{dv_y}{d\xi} + \left(\frac{\alpha}{M}v_x\frac{d}{d\xi} + \frac{\gamma}{M}v_z\frac{d}{d\xi}\right)v_y = -v_x. \tag{A.24}$$

$$-M\frac{dv_y}{d\xi} + \alpha v_x\frac{dv_y}{d\xi} + \gamma v_z\frac{dv_y}{d\xi} = -Mv_x \tag{A.25}$$

$$(-M + \alpha v_x + \gamma v_z)\frac{dv_y}{d\xi} = -Mv_x \tag{A.26}$$

$$L_v\frac{dv_y}{d\xi} = -Mv_x \tag{A.27}$$

equation(A.15) into (A.14)

$$-\frac{dv_z}{d\xi} + (\frac{\alpha}{M}v_x\frac{d}{d\xi} + \frac{\gamma}{M}v_z\frac{d}{d\xi})v_z = -\frac{\gamma}{M}\frac{d\psi}{d\xi}. \tag{A.28}$$

$$-M\frac{dv_z}{d\xi} + \alpha v_x\frac{dv_z}{d\xi} + \gamma v_z\frac{dv_z}{d\xi} = -\gamma\frac{d\psi}{d\xi}. \tag{A.29}$$

$$(-M + \alpha v_x + \gamma v_z)\frac{dv_z}{d\xi} = -\gamma\frac{d\psi}{d\xi} \tag{A.30}$$

$$L_v\frac{dv_z}{d\xi} = -\gamma\frac{d\psi}{d\xi}. \tag{A.31}$$

from equation (A.18)

$$\frac{dn_i}{d\xi}(-M + \alpha v_x + \gamma v_z) = 0 \tag{A.32}$$

$\xi = \infty$, $n_i = 1$, $v_z = 0$,$v_x = 0$

$$n_i(-M + \alpha v_x + \gamma v_z) = C \tag{A.33}$$

$$C = -M$$

$$n_i(-M + \alpha v_x + \gamma v_z) = -M$$

$$-M + \alpha v_x + \gamma v_z = -\frac{M}{n_i} \tag{A.34}$$

$$L_v = -\frac{M}{n_i} \tag{A.35}$$

from equation(A.30) we have

$$-\frac{M}{n_i}\frac{dv_z}{d\xi} = -\gamma\frac{d\psi}{d\xi} \tag{A.36}$$

$$\frac{dv_i}{d\xi} = \frac{\gamma n_i}{M}\frac{d\psi}{d\xi} \tag{A.37}$$

from (A.35) we have

$$-M + \alpha v_x + \gamma v_z = -\frac{M}{n_i}$$

differentiate w.r.t $d\xi$ we have

$$0 + \alpha\frac{dv_x}{d\xi} + \gamma\frac{dv_z}{d\xi} = \frac{M}{n_i^2}\frac{dn_i}{d\xi} \tag{A.38}$$

$$\frac{dv_x}{d\xi} = -\frac{\gamma^2 n_i}{\alpha M}\frac{d\psi}{d\xi} + \frac{M}{\alpha n_i^2}\frac{dn_i}{d\xi} \tag{A.39}$$

from equation (A.10)

$$n_i = n_c + n_h$$

$$f\exp(\alpha_c\psi) + (1-f)\exp(\alpha_h\psi)$$

integrate equation (A.40)

$$\int\frac{dv_x}{d\xi}d\xi + \frac{\gamma^2}{M}\int(f\exp(\alpha_c\psi) + (1-f)\exp(\alpha_h\psi))\frac{d\psi}{d\xi}d\xi = \int\frac{M}{n_i^2}\frac{dn_i}{d\xi}d\xi. \tag{A.40}$$

$$\alpha v_x + \frac{\gamma^2}{M}(\frac{f}{\alpha_c}\exp(\alpha_c\psi) + \frac{(1-f)}{\alpha_h}\exp(\alpha_h\psi)) = -\frac{m}{n_i} + C \tag{A.41}$$

$v_x = 0$, $n_i = 1$, $\psi = 0$

$$\frac{\gamma^2 f}{\alpha_c M} + \frac{\gamma^2(1-f)}{\alpha_h M} + M = C$$

$$\alpha v_x = M - \frac{M}{n_i} - \frac{\gamma^2}{M}(\frac{f}{\alpha_c}(\exp(\alpha_c\psi) - 1) + \frac{(1-f)}{\alpha_h}(\exp(\alpha_h\psi) - 1))$$

$$v_x = \frac{1}{\alpha}[M - \frac{M}{n_i} - \frac{\gamma^2}{M}[\frac{f}{\alpha_c}(\exp(\alpha_c\psi) - 1) + \frac{(1-f)}{\alpha_h}(\exp(\alpha_h\psi) - 1)]] \qquad \text{(A.42)}$$

from equation (A.22)

$$\begin{aligned}
(-M + \alpha v_x + \gamma v_z)\frac{dv_x}{d\xi} &= -\alpha\frac{d\psi}{d\xi} + Mv_y \\
-\frac{M}{n_i}\frac{dv_x}{d\xi} &= -\alpha\frac{d\psi}{d\xi} + Mv_y \\
-\frac{M}{n_i}\left[-\frac{\gamma^2 n_i}{\alpha M}\frac{d\psi}{d\xi} + \frac{M}{\alpha n_i^2}\frac{dn_i}{d\xi}\right] &= -\alpha\frac{d\psi}{d\xi} + Mv_y \\
\frac{\gamma^2}{\alpha}\frac{d\psi}{d\xi} - \frac{M^2}{\alpha n_i^3}\frac{dn_i}{d\xi} + \alpha\frac{d\psi}{d\xi} &= Mv_y \\
(\frac{\alpha^2+\gamma^2}{\alpha M})\frac{d\psi}{d\xi} - \frac{M^2}{\alpha n_i^3}\frac{dn_i}{d\xi} &= v_y \qquad \text{(A.43)}
\end{aligned}$$

$$\alpha^2 + \gamma^2 = \sin^2\theta + \cos^2\theta = 1$$

from equation (A.26)

$$\begin{aligned}
(-M + \alpha v_x + \gamma v_z)\frac{dv_y}{d\xi} &= -Mv_x \\
-\frac{M}{n_i}\frac{dv_y}{d\xi} &= -Mv_x \\
\frac{dv_y}{d\xi} &= n_i v_x. \qquad \text{(A.44)}
\end{aligned}$$

equation (A.43) into (A.44)

$$\frac{d}{d\xi}\left[\frac{1}{\alpha M}\frac{d\psi}{d\xi}-\frac{m}{\alpha n_i^3}\frac{dn_i}{d\xi}\right] = n_i v_x.$$

$$\frac{d}{d\xi}\left[(\frac{1}{\alpha M})\frac{d\psi}{d\xi}-\frac{m^2}{n_i^3}\frac{dn_i}{d\xi}\right] = n_i\left[\frac{1}{\alpha}\left(M-\frac{M}{n_i}-\frac{\gamma^2}{M}[\frac{f}{\alpha_c}(\exp(\alpha_c\psi)-1)+\frac{(1-f)}{\alpha_h}(\exp(\alpha_h\psi)-1)\right.\right.$$

$$\frac{d}{d\xi}\left[\frac{d}{d\xi}(\psi+\frac{M^2}{2n_i^2})\right] = M^2(n_i-1)+n_i\gamma^2\left[\frac{f}{\alpha_c}(\exp(\alpha_c\psi)-1)+\frac{(1-f)}{\alpha_h}(\exp(\alpha_h\psi)-1)\right] \quad \text{(A.45)}$$

let

$$t = \psi + \frac{M^2}{2n_i^2}.$$

$$\frac{dt}{d\xi} = \frac{d\psi}{d\xi} - \frac{M^2}{n_i^3}\frac{dn_i}{d\xi}. \quad \text{(A.46)}$$

$$n_i = n_c + n_h.$$

$$n_i = f\exp(\alpha_c\psi)+(1-f)\exp(\alpha_h\psi).$$

$$\frac{dn_i}{d\xi} = \left[\alpha_c f\exp(\alpha_c\psi)+\alpha_h(1-f)\exp(\alpha_h\psi)\right]\frac{d\psi}{d\xi}.$$

$$\frac{dt}{d\xi} = \frac{d\psi}{d\xi} - \frac{M^2}{n_i^3}\alpha_c f\exp(\alpha_c\psi)+\alpha_h(1-f)\exp(\alpha_h\psi)\frac{d\psi}{d\xi}.$$

$$\frac{dt}{d\xi} = \left(1-M^2\frac{(\alpha_c f\exp(\alpha_c\psi)+\alpha_h(1-f)\exp(\alpha_h\psi))}{(f\exp(\alpha_c\psi)+(1-f)\exp(\alpha_h\psi))^3}\right)\frac{d\psi}{d\xi}. \quad \text{(A.47)}$$

multiply both side of equation (A.46) by $2\frac{dt}{d\xi}$ and integrate

$$\int 2\frac{dt}{d\xi}\frac{d}{d\xi}(\frac{dt}{d\xi})d\xi =$$
$$\int 2\left[M^2(n_i-1)+n_i\gamma^2\left(\frac{f}{\alpha_c}(\exp(\alpha_c\psi)-1)+\frac{(1-f)}{\alpha_h}(\exp(\alpha_h\psi)-1)\right)\right]\frac{dt}{d\xi}d\xi.$$

$$\left(\frac{dt}{d\xi}\right)^2 =$$
$$2\left[\int M^2(n_i-1)\frac{dt}{d\xi}d\xi + \gamma^2\int n_i\left(\frac{f}{\alpha_c}(\exp(\alpha_c\psi)-1)+\frac{(1-f)}{\alpha_h}(\exp(\alpha_h\psi)-1)\right)\right]\frac{dt}{d\xi}.d\xi.$$

$$\frac{1}{2}\left[1-M^2\left(\frac{\alpha_c f\exp(\alpha_c\psi)+\alpha_h(1-f)\exp(\alpha_h\psi)}{(f\exp(\alpha_c\psi)+(1-f)\exp(\alpha_h\psi))^3}\right)\right]^2\left(\frac{d\psi}{d\xi}\right)^2$$
$$= M^2\left[\frac{f}{\alpha_c}(\exp(\alpha_c\psi)-1)+\frac{(1-f)}{\alpha_h\psi}(\exp(\alpha_h\psi)-1)\right]-M^2\psi-M^4\left[-\frac{1}{n_i}+\frac{1}{2n_i^2}+\frac{1}{2}\right]$$
$$-\gamma^2\int f\exp(\alpha_c\psi)+(1-f)\exp(\alpha_h\psi)\left[\frac{f}{\alpha_c}(\exp(\alpha_c\psi)-1)+\frac{(1-f)}{\alpha_h}(\exp(\alpha_h\psi)-1)\right]d\psi$$
$$+M^2\gamma^2\int\left[\frac{f}{\alpha_c}(\exp(\alpha_c\psi)-1)+\frac{(1-f)}{\alpha_h}(\exp(\alpha_h\psi)-1)\right]$$
$$\left(\frac{\alpha_c f\exp(\alpha_c\psi)+\alpha_h(1-f)\exp(\alpha_h\psi)}{(f\exp(\alpha_c\psi)+(1-f)\exp(\alpha_h\psi))^2}\right)d\psi.$$

let

$$\frac{f}{\alpha_c}(\exp(\alpha_c\psi)-1)+\frac{(1-f)}{\alpha_h}(\exp(\alpha_h\psi)-1)=p$$
$$f\exp(\alpha_c\psi)+(1-f)\exp(\alpha_h\psi)=\frac{dp}{d\psi}. \tag{A.48}$$

$$\frac{1}{2}\left[1-M^2\left(\frac{\alpha_c f\exp(\alpha_c\psi)+\alpha_h(1-f)\exp(\alpha_h\psi)}{(f\exp(\alpha_c\psi)+(1-f)\exp(\alpha_h\psi))^3}\right)\right]^2\left(\frac{d\psi}{d\xi}\right)^2$$
$$= -\frac{M^4}{2n_i^2}(1-n_i)^2-M^2\psi+M^2\left[\frac{f}{\alpha_c}(\exp(\alpha_c\psi)-1)+\frac{(1-f)}{\alpha_h\psi}(\exp(\alpha_h\psi)-1)\right]$$
$$-\gamma^2\int\frac{dp}{d\psi}.p.d\psi \quad +M^2\gamma^2\int\left[\frac{f}{\alpha_c}(\exp(\alpha_c\psi)-1)+\frac{(1-f)}{\alpha_h}(\exp(\alpha_h\psi)-1)\right]$$
$$\left(\frac{\alpha_c f\exp(\alpha_c\psi)+\alpha_h(1-f)\exp(\alpha_h\psi)}{(f\exp(\alpha_c\psi)+(1-f)\exp(\alpha_h\psi))^2}\right)d\psi.$$

now, let

$$g=f\exp(\alpha_c\psi)+(1-f)\exp(\alpha_h\psi).$$
$$\alpha_c f\exp(\alpha_c\psi)+\alpha_h(1-f)\exp(\alpha_h\psi)d\psi=dg. \tag{A.49}$$

$$\frac{1}{2}\left[1-M^2\left(\frac{\alpha_c f\exp(\alpha_c\psi)+\alpha_h(1-f)\exp(\alpha_h\psi)}{(f\exp(\alpha_c\psi)+(1-f)\exp(\alpha_h\psi))^3}\right)\right]^2\left(\frac{d\psi}{d\xi}\right)^2$$
$$=-\frac{M^4}{2n_i^2}(1-n_i)^2-M^2\psi+M^2\left[\frac{f}{\alpha_c}(\exp(\alpha_c\psi)-1)+\frac{(1-f)}{\alpha_h\psi}(\exp(\alpha_h\psi)-1)\right]-\gamma^2\left[\frac{p^2}{2}\right]$$
$$+M^2\gamma^2\int\left[\frac{f}{\alpha_c}(\exp(\alpha_c\psi)-1)+\frac{(1-f)}{\alpha_h}(\exp(\alpha_h\psi)-1)\right]\frac{dg}{g^2}.$$

Also,let

$$dv=\frac{dg}{g^2}. \tag{A.50}$$

$$v=-\frac{1}{g}. \tag{A.51}$$

$$\int pdv=pv-\int vdp. \tag{A.52}$$

we have

$$\frac{1}{2}\left[1-M^2\left(\frac{\alpha_c f\exp(\alpha_c\psi)+\alpha_h(1-f)\exp(\alpha_h\psi)}{(f\exp(\alpha_c\psi)+(1-f)\exp(\alpha_h\psi))^3}\right)\right]^2\left(\frac{d\psi}{d\xi}\right)^2$$
$$=-\frac{M^4}{2n_i^2}(1-n_i)^2-M^2\psi+M^2\left[\frac{f}{\alpha_c}(\exp(\alpha_c\psi)-1)+\frac{(1-f)}{\alpha_h\psi}(\exp(\alpha_h\psi)-1)\right]$$
$$-\frac{\gamma^2}{2}\left[\frac{f}{\alpha_c}(\exp(\alpha_c\psi)-1)+\frac{(1-f)}{\alpha_h}(\exp(\alpha_h\psi)-1)\right]^2$$
$$+M^2\gamma^2\left[\frac{\frac{f}{\alpha_c}(\exp(\alpha_c\psi)-1)+\frac{(1-f)}{\alpha_h}(\exp(\alpha_h\psi)-1)}{f\exp(\alpha_c\psi)+(1-f)\exp(\alpha_h\psi)}\right]+M^2\gamma^2\psi.$$

$$\frac{1}{2}\left(\frac{d\psi}{d\xi}\right)^2+V(\psi)=0 \tag{A.53}$$

$$V(\psi)=-\frac{1}{\left(1-M^2\left(\frac{\alpha_c f\exp(\alpha_c\psi)+\alpha_h(1-f)\exp(\alpha_h\psi)}{(f\exp(\alpha_c\psi)+(1-f)\exp(\alpha_h\psi))^3}\right)\right)^2}\times$$
$$\left\{\begin{array}{l}-\frac{M^4}{2n_i^2}(1-n_i)^2-M^2(1-\gamma^2)\psi\\+M^2\left(\frac{f}{\alpha_c}(\exp(\alpha_c\psi)-1)+\frac{(1-f)}{\alpha_h}(\exp(\alpha_h\psi)-1)\right)\\-\frac{\gamma^2}{2}\left[\frac{f}{\alpha_c}(\exp(\alpha_c\psi)-1)+\frac{(1-f)}{\alpha_h}(\exp(\alpha_h\psi)-1)\right]^2\\+M^2\gamma^2\left[\frac{\frac{f}{\alpha_c}(\exp(\alpha_c\psi)-1)+\frac{(1-f)}{\alpha_h}(\exp(\alpha_h\psi)-1)}{f\exp(\alpha_c\psi)+(1-f)\exp(\alpha_h\psi)}\right].\end{array}\right\}$$

Appendix B

Algebraic expression for the Sagdeev potential in a magnetized plasma with adiabatic ion and two temperature electrons

The Boltzmann distribution is assumed for the densities and temperature of the cool(n_c, T_c) and hot (n_h, T_h) electron species and are given in normalized form as follows:

cool electrons

$$n_c = \frac{n_{c0}}{n_{i0}} \exp\left(\frac{e\phi}{T_{eff}} . \frac{T_{eff}}{T_c}\right)$$

$$n_c = f \exp(\alpha_c \psi) \tag{B.1}$$

hot electrons

$$n_h = \frac{n_{h0}}{n_{i0}} \exp\left(\frac{e\phi}{T_{eff}} . \frac{T_{eff}}{T_h}\right)$$

$$n_h = (1 - f) \exp(\alpha_h \psi) \tag{B.2}$$

The hot adiabatic ions is described by the fluid equations.

Continuity equation:

$$\frac{\partial n_i}{\partial t} + \nabla(n_i V_i) = 0.$$

Momentum equation:

$$\left(\frac{\partial}{\partial t} + \mathbf{V_i}.\nabla\right)\mathbf{V_i} = -\frac{e\nabla\phi}{m_i} + e\frac{\mathbf{V}_i \times \mathbf{B}_o}{m_i c} - \frac{1}{n_i m_i}\nabla\tilde{p}_i.$$

equation of state

$$\frac{\partial p_i}{\partial t} + V_i\nabla.p_i + \delta p_i.\nabla V_i = 0$$

from the equation of state

$$V_i.\nabla p_i = 0$$

then

$$\frac{1}{p}\frac{dp_i}{dt} = -\frac{\delta}{n}\frac{dn_i}{dt},$$

where

$$\delta\nabla.V_i = \frac{1}{n}\frac{dn_i}{dt}$$

then, integrate

$$p_i = p_{i0}\left(\frac{n_o}{n_{i0}}\right)^{\delta}$$

if N is the number of degrees of freedom, δ is given by

$$\delta = \frac{N+2}{N}$$

from continuty and momentum equations (normalized)

$$\frac{\partial n_i}{\partial t} + \frac{\partial(n_i v_x)}{\partial x} + \frac{\partial(n_i v_z)}{\partial z} = 0 \tag{B.3}$$

$$\frac{\partial v_x}{\partial t} + \left(v_x\frac{\partial}{\partial x} + v_z\frac{\partial}{\partial z}\right)v_x = -\frac{\partial\psi}{\partial x} + v_y - \frac{\sigma}{n_i}\frac{\partial}{\partial x}.(n_i)^{5/3} \tag{B.4}$$

$$\frac{\partial v_y}{\partial t} + \left(v_x\frac{\partial}{\partial x} + v_z\frac{\partial}{\partial z}\right)v_y = -\frac{\partial\psi}{\partial y} - v_x \tag{B.5}$$

$$\frac{\partial v_z}{\partial t} + \left(v_x\frac{\partial}{\partial x} + v_z\frac{\partial}{\partial z}\right)v_z = -\frac{\partial\psi}{\partial z} - \frac{\sigma}{n_i}\frac{\partial}{\partial z}.(n_i)^{5/3} \tag{B.6}$$

then, the set of equations are closed with the quasi-neutrality condition

$$n_i = n_c + n_h = f\exp(\alpha_c\psi) + (1-f)\exp(\alpha_h\psi) \tag{B.7}$$

stationary frame

$$\xi = (\alpha x + \gamma z - Mt)/M \tag{B.8}$$

$$\frac{\partial \xi}{\partial x} = \frac{\alpha}{M}, \frac{\partial \xi}{\partial z} = \frac{\gamma}{M}, \frac{\partial \xi}{\partial t} = -1$$

from equation (3)

$$-\frac{dn_i}{d\xi} + \frac{\alpha}{M}\frac{dn_i v_x}{d\xi} + \frac{\gamma}{M}\frac{dn_i v_x}{d\xi} = 0$$

$$M\frac{dn_i}{d\xi} = \frac{dn_i}{d\xi}(\alpha v_x + \gamma v_z)$$

integrate with the boundary condition

$$\xi \to 0, n_i \to 1, \psi = 0, v_x = v_z = 0$$

$$M = -C$$

$$Mn_i - M = n_i(\alpha v_x + \gamma v_z)$$

$$\alpha v_x + \gamma v_z = M\left(1 - \frac{1}{n_i}\right) \tag{B.9}$$

from equation (B.4)

$$-\frac{dv_x}{d\xi} + \left(\frac{\alpha}{M}v_x\frac{d}{d\xi} + \frac{\gamma}{M}v_z\frac{d}{d\xi}\right)v_x = -\frac{\alpha}{M}\frac{d\psi}{d\xi} + v_y - \frac{5\sigma\alpha}{3n_i^{1/3}M}\frac{dn_i}{d\xi}$$

$$-M\frac{dv_x}{d\xi} + (\alpha v_x + \gamma v_z)\frac{dv_x}{d\xi} = -\alpha\frac{d\psi}{d\xi} + Mv_y - \frac{5\sigma\alpha}{3n_i^{1/3}}\frac{dn_i}{d\xi}$$

$$\left(-M + M - \frac{M}{n_i}\right)\frac{dv_x}{d\xi} = -\alpha\frac{d\psi}{d\xi} + Mv_y - \frac{5\sigma\alpha}{3n_i^{1/3}}\frac{dn_i}{d\xi}$$

$$-\frac{M}{n_i}\frac{dv_x}{d\xi} = -\alpha\frac{d\psi}{d\xi} - \frac{5\sigma\alpha}{3n_i^{1/3}}\frac{dn_i}{d\xi} + Mv_y \tag{B.10}$$

from equation (B.5)

$$-\frac{dv_y}{d\xi} + \left(\frac{\alpha}{M}v_x\frac{d}{d\xi} + \frac{\gamma}{M}v_z\frac{d}{d\xi}\right)v_y = -v_x$$

$$-M\frac{dv_y}{d\xi} + (\alpha v_x + \gamma v_z)\frac{dv_y}{d\xi} = -Mv_x$$

$$\left(-M + M - \frac{M}{n_i}\right)\frac{dv_y}{d\xi} = -Mv_x$$

$$\frac{1}{n_i}\frac{dv_y}{d\xi} = v_x \tag{B.11}$$

from equation (B.6)

$$-\frac{dv_z}{d\xi}+\left(\frac{\alpha}{M}v_x\frac{d}{d\xi}+\frac{\gamma}{M}v_z\frac{d}{d\xi}\right)v_z=-\frac{\gamma}{M}\frac{d\psi}{d\xi}-\frac{5\sigma\alpha}{3n_i^{1/3}M}\frac{dn_i}{d\xi}$$

$$-M\frac{dv_z}{d\xi}+(\alpha v_x+\gamma v_z)\frac{dv_z}{d\xi}=-\gamma\frac{d\psi}{d\xi}+\frac{5\sigma\alpha}{3n_i^{1/3}}\frac{dn_i}{d\xi}$$

$$\left(-M+M-\frac{M}{n_i}\right)\frac{dv_z}{d\xi}=-\gamma\left(\frac{d\psi}{d\xi}+\frac{5\sigma\alpha}{3n_i^{1/3}}\frac{dn_i}{d\xi}\right)$$

$$\frac{M}{n_i}\frac{dv_z}{d\xi}=\gamma\left(\frac{d\psi}{d\xi}+\frac{5\sigma\alpha}{3n_i^{1/3}}\frac{dn_i}{d\xi}\right) \tag{B.12}$$

differentiate equation (B.9) w.r.t . ∂_ξ, we have

$$\alpha\frac{dv_x}{d\xi}+\gamma\frac{dv_z}{d\xi}=\frac{M}{n_i^2}\frac{dn_i}{d\xi} \tag{B.13}$$

then, substitute equation (B.12) into (B.13)

$$\alpha\frac{dv_x}{d\xi}+\gamma\left(\frac{\gamma n_i}{M}\left(\frac{d\psi}{d\xi}+\frac{5\sigma}{3n_i^{1/3}}\frac{dn_i}{d\xi}\right)\right)=\frac{M}{n_i^2}\frac{dn_i}{d\xi}$$

$$\frac{dv_x}{d\xi}=\frac{M}{\alpha n_i^2}\frac{dn_i}{d\xi}-\frac{5\gamma^2\sigma n_i^{2/3}}{3\alpha M}\frac{dn_i}{d\xi}-\frac{\gamma^2 n_i}{\alpha M}\frac{d\psi}{d\xi} \tag{B.14}$$

integrate equation (B.14)

$$\alpha\int\frac{dv_x}{d\xi}d\xi+\frac{\gamma^2}{M}\int n_i\frac{d\psi}{d\xi}d\xi=M\int\frac{1}{n_i^2}\frac{dn_i}{d\xi}d\xi-\frac{5\gamma^3\sigma}{3M}\int n_i^{2/3}\frac{dn_i}{d\xi}d\xi$$

$$\alpha v_x+\frac{\gamma^2}{M}\left(\frac{f}{\alpha_c}\exp(\alpha_c\psi)+\frac{(1-f)}{\alpha_h}\exp(\alpha_h\psi)\right)=-\frac{M}{n_i}-\frac{\gamma^2\sigma}{M}n_i^{5/3}+C$$

at

$$v_x=0,n_i=1,\psi=0$$

$$\frac{\gamma^2}{M}\left(\frac{f}{\alpha_c}+\frac{1-f}{\alpha_h}\right)+M+\frac{\gamma^2\sigma}{M}=C$$

therefore,

$$\alpha v_x = M\left(1-\frac{1}{n_i}\right)+\frac{\gamma^2\sigma}{M}(1-n_i^{5/3})-\frac{\gamma^2}{M}\left(\frac{f}{\alpha_c}(\exp(\alpha_c\psi)-1)+\frac{1-f}{\alpha_h}(\exp(\alpha_c\psi)-1)\right) \tag{B.15}$$

equation (B.14) into (B.10)

$$-\frac{\gamma^2}{\alpha}\frac{d\psi}{d\xi}-\frac{M^2}{\alpha n_i^3}\frac{dn_i}{d\xi}+\frac{5\gamma^2\sigma n_i^{-1/3}}{3\alpha}\frac{dn_i}{d\xi}=-\alpha\frac{d\psi}{d\xi}-\frac{5\alpha\sigma}{3n_i^{1/3}}\frac{dn_i}{d\xi}+Mv_y$$

$$\left(\frac{\gamma^2+\alpha^2}{\alpha}\right)\frac{d\psi}{d\xi}-\frac{M^2}{\alpha n_i^3}\frac{dn_i}{d\xi}+\frac{5\sigma n_i^{-1/3}}{3}\left(\frac{\gamma^2+\alpha^2}{\alpha}\right)\frac{dn_i}{d\xi}=Mv_y$$

then

$$\gamma^2+\alpha^2=1,$$

since

$$\cos^2\theta+\sin^2\theta=1$$

we have,

$$\frac{1}{\alpha M}\left(\frac{d\psi}{d\xi}-\frac{M^2}{n_i^3}\frac{dn_i}{d\xi}+\frac{5\sigma n_i^{-1/3}}{3}\frac{dn_i}{d\xi}\right)=v_y \tag{B.16}$$

now, substitute equation (B.11) into (B.16)

$$\frac{d}{d\xi}\left(\frac{d\psi}{d\xi}-\frac{M^2}{n_i^3}\frac{dn_i}{d\xi}+\frac{5\sigma n_i^{-1/3}}{3}\frac{dn_i}{d\xi}\right)=M\alpha n_i v_x \tag{B.17}$$

$$\begin{aligned}&\frac{d}{d\xi}\left(\frac{d}{d\xi}\left(\psi+\frac{M^2}{2n_i^2}+\frac{5}{2}\sigma n_i^{2/3}\right)\right)\\&=M^2(n_i-1)+\gamma^2\sigma n_i(1-n_i^{5/3})-\gamma^2 n_i\left(\frac{f}{\alpha_c}(\exp(\alpha_c\psi)-1)+\frac{1-f}{\alpha_h}(\exp(\alpha_c\psi)-1)\right)\end{aligned} \tag{B.18}$$

let

$$t=\psi+\frac{M^2}{2n_i^2}+\frac{5}{2}\sigma n_i^{2/3},$$

then

$$\frac{dt}{d\xi}=\frac{d\psi}{d\xi}-\frac{M^2}{n_i^3}\frac{dn_i}{d\xi}+\frac{5}{3}\sigma n_i^{-1/3}\frac{dn_i}{d\xi}$$

$$n_i=f\exp(\alpha_c\psi)+(1-f)\exp(\alpha_h\psi)$$

$$\frac{dn_i}{d\xi} = (\alpha_c f \exp(\alpha_c \psi) + \alpha_h (1-f)\exp(\alpha_h \psi)\frac{d\psi}{d\xi}$$

$$\frac{dt}{d\xi} = \left(1 - \frac{M^2}{n_i^3}(\alpha_c f \exp(\alpha_c \psi) + \alpha_h (1-f)\exp(\alpha_h \psi) + \frac{5\sigma n_i^{-1/3}}{3}(\alpha_c f \exp(\alpha_c \psi) + \alpha_h (1-f)\exp(\alpha_h \psi)\right)\frac{d\psi}{d\xi}$$

Mutiply both sides of equation (B.18) by $2\frac{dt}{d\xi}$ and integrate

$$2\int \frac{dt}{d\xi}.\frac{d}{d\xi}\left(\frac{dt}{d\xi}\right)d\xi = 2\left[\int M^2(n_i - 1) + \gamma^2\sigma n_i(1 - n_i^{5/3}) - \gamma^2 n_i\left(\frac{f}{\alpha_c}(\exp(\alpha_c\psi) - 1) + \frac{1-f}{\alpha_h}(\exp(\alpha_h\psi) - 1)\right)\right]\frac{dt}{d\xi}$$

$$\frac{1}{2}\left(\frac{dt}{d\xi}\right)^2 = -\frac{M^4}{2n_i^2}(1-n_i)^2 - M^2(1-\gamma^2)\psi + M^2\left(\frac{f}{\alpha_c}(\exp(\alpha_c\psi) - 1) + \frac{1-f}{\alpha_h}(\exp(\alpha_h\psi) - 1)\right)$$
$$+ \sigma M^2\left(n_i^{5/3} - \frac{5n_i^{2/3}}{2} + \frac{3}{2}\right) + \gamma^2\sigma\left(\frac{f}{\alpha_c}(\exp(\alpha_c\psi) - 1) + \frac{1-f}{\alpha_h}(\exp(\alpha_h\psi) - 1)\right)$$
$$- \gamma^2 M^2\sigma\left(-\frac{1}{n_i} - \frac{3n_i^{2/3}}{2} + \frac{5}{2}\right) + \gamma^2\sigma^2\left(n_i^{5/3} - \frac{n_i^{10/3}}{2} - \frac{1}{2}\right)$$
$$- \frac{\gamma^2}{2}\left(\frac{f}{\alpha_c}(\exp(\alpha_c\psi) - 1) + \frac{1-f}{\alpha_h}(\exp(\alpha_h\psi) - 1)\right)^2$$
$$- \frac{\gamma^2 M^2}{n_i}\left(\frac{f}{\alpha_c}(\exp(\alpha_c\psi) - 1) + \frac{1-f}{\alpha_h}(\exp(\alpha_h\psi) - 1)\right)$$
$$- \gamma^2\sigma n_i^{5/3}\left(\frac{f}{\alpha_c}(\exp(\alpha_c\psi) - 1) + \frac{1-f}{\alpha_h}(\exp(\alpha_h\psi) - 1)\right)$$

then, we obtain

$$\frac{1}{2}\left(\frac{d\psi}{d\xi}\right)^2 = \frac{1}{\left(1-\frac{M^2}{n_i^3}\left(\alpha_c f(e^{\alpha_c\psi}+\alpha_h(1-f)e^{\alpha_h\psi}\right)+\frac{5\sigma}{3n_i^{1/3}}\left(\alpha_c f(e^{\alpha_c\psi}+\alpha_h(1-f)e^{\alpha_h\psi}\right)\right)^2}\times$$
$$-\frac{M^4}{2n_i^2}(1-n_i)^2 - M^2(1-\gamma^2)\psi + M^2\left(\frac{f}{\alpha_c}(\exp(\alpha_c\psi)-1)+\frac{1-f}{\alpha_h}(\exp(\alpha_h\psi)-1)\right)$$
$$+\sigma M^2\left(n_i^{5/3}-\frac{5n_i^{2/3}}{2}+\frac{3}{2}\right)+\gamma^2\sigma\left(\frac{f}{\alpha_c}(\exp(\alpha_c\psi)-1)+\frac{1-f}{\alpha_h}(\exp(\alpha_h\psi)-1)\right)$$
$$-\gamma^2M^2\sigma\left(-\frac{1}{n_i}-\frac{3n_i^{2/3}}{2}+\frac{5}{2}\right)+\gamma^2\sigma^2\left(n_i^{5/3}-\frac{n_i^{10/3}}{2}-\frac{1}{2}\right)$$
$$-\frac{\gamma^2}{2}\left(\frac{f}{\alpha_c}(\exp(\alpha_c\psi)-1)+\frac{1-f}{\alpha_h}(\exp(\alpha_h\psi)-1)\right)^2$$
$$-\frac{\gamma^2M^2}{n_i}\left(\frac{f}{\alpha_c}(\exp(\alpha_c\psi)-1)+\frac{1-f}{\alpha_h}(\exp(\alpha_h\psi)-1)\right)$$
$$-\gamma^2\sigma n_i^{5/3}\left(\frac{f}{\alpha_c}(\exp(\alpha_c\psi)-1)+\frac{1-f}{\alpha_h}(\exp(\alpha_h\psi)-1)\right) \tag{B.19}$$

Appendix C

Algebraic expression for the Sagdeev potential in a magnetized plasma with cold ion, cool electron and nonthermal hot electron

The density and temperature of the Boltzmann distributed cool electrons (n_c, T_c) and nonthermal distributed hot electrons (n_h, T_h) in normalized form are:

cool electrons

$$n_c = \frac{n_{c0}}{n_{i0}} \exp\left(\frac{e\phi}{T_{eff}}.\frac{T_{eff}}{T_c}\right)$$

$$n_c = f \exp(\alpha_c \psi) \tag{C.1}$$

hot electrons (nonthermal)

$$n_h = \frac{n_{h0}}{n_{i0}}(1 - \beta\phi + \beta\phi^2) \exp\left(\frac{e\phi}{T_{eff}}.\frac{T_{eff}}{T_h}\right)$$

$$n_h = (1 - f)(1 - \beta\phi + \beta\phi^2) \exp(\alpha_h \psi) \tag{C.2}$$

where

$$\beta = \frac{4\alpha}{1 + 3\alpha}$$

magnetized cold ions (described by the fluid equations) (normalized)

$$\frac{\partial n_i}{\partial t} + \frac{\partial (n_i v_x)}{\partial x} + \frac{\partial (n_i v_z)}{\partial z} = 0 \tag{C.3}$$

$$\frac{\partial v_x}{\partial t} + (v_x \frac{\partial}{\partial x} + v_z \frac{\partial}{\partial z}) v_x = -\frac{\partial \psi}{\partial x} + v_y \tag{C.4}$$

$$\frac{\partial v_y}{\partial t} + (v_x \frac{\partial}{\partial x} + v_z \frac{\partial}{\partial z}) v_y = -v_x \tag{C.5}$$

$$\frac{\partial v_z}{\partial t} + (v_x \frac{\partial}{\partial x} + v_z \frac{\partial}{\partial z}) v_z = -\frac{\partial \psi}{\partial z} \tag{C.6}$$

the quasi-neutrality condition

$$n_i = n_{c0} + n_{h0} = f \exp(\alpha_c \psi) + (1-f)(1 - \beta\psi + \beta\psi^2) \exp(\alpha_h \psi) \tag{C.7}$$

localized frame

$$\xi = (\alpha x + \gamma z - Mt)/M \tag{C.8}$$

$$\frac{\partial \xi}{\partial x} = \frac{\alpha}{M}, \frac{\partial \xi}{\partial z} = \frac{\gamma}{M}, \frac{\partial \xi}{\partial \xi} \partial t = -1,$$

$$\partial_t = -\partial_\xi, \partial_x = \frac{\alpha}{M} \partial_\xi, \partial_z = \frac{\gamma}{M} \partial_\xi$$

from equation (C.3)

$$-\frac{dn_i}{d\xi} + \frac{\alpha}{M} \frac{dn_i v_x}{d\xi} + \frac{\gamma}{M} \frac{dn_i v_z}{d\xi} = 0$$

$$-M \frac{dn_i}{d\xi} + \alpha \frac{dn_i v_x}{d\xi} + \gamma \frac{dn_i v_z}{d\xi} = 0$$

$$\frac{dn_i}{d\xi} (-M + \alpha v_x + \gamma v_z) = 0$$

$$\frac{d}{d\xi} (L_v n_i) = 0 \tag{C.9}$$

where

$$L_v = -M + \alpha v_x + \gamma v_z$$

from equation (C.4)

$$-\frac{dv_x}{d\xi} = \left(\frac{\alpha v_x}{M} \frac{d}{d\xi} + \frac{\gamma v_z}{M} \frac{d}{d\xi} \right) v_x = -\frac{\alpha}{M} \frac{d\psi}{d\xi} + v_y$$

$$-M \frac{dv_x}{d\xi} + \alpha v_x \frac{dv_x}{d\xi} + \gamma v_z \frac{dv_x}{d\xi} = -\alpha \frac{d\psi}{d\xi} + M v_y$$

$$(-M + \alpha v_x + \gamma v_z)\frac{dv_x}{d\xi} = -\alpha\frac{d\psi}{d\xi} + Mv_y$$

$$L_v\frac{dv_x}{d\xi} = -\alpha\frac{d\psi}{d\xi} + Mv_y \tag{C.10}$$

from equation (C.5)

$$-\frac{dv_y}{d\xi} = \left(\frac{\alpha v_x}{M}\frac{d}{d\xi} + \frac{\gamma v_z}{M}\frac{d}{d\xi}\right)v_y = -v_x$$

$$-M\frac{dv_y}{d\xi} + \alpha v_x\frac{dv_y}{d\xi} + \gamma v_z\frac{dv_y}{d\xi} = -Mv_x$$

$$(-M + \alpha v_x + \gamma v_z)\frac{dv_y}{d\xi} = -Mv_x$$

$$L_v\frac{dv_y}{d\xi} = -Mv_x \tag{C.11}$$

from equation (C.6)

$$-\frac{dv_z}{d\xi} = \left(\frac{\alpha v_x}{M}\frac{d}{d\xi} + \frac{\gamma v_z}{M}\frac{d}{d\xi}\right)v_z = -\frac{\gamma}{M}\frac{d\psi}{d\xi}$$

$$-M\frac{dv_z}{d\xi} + \alpha v_x\frac{dv_z}{d\xi} + \gamma v_z\frac{dv_z}{d\xi} = -\gamma\frac{d\psi}{d\xi}$$

$$(-M + \alpha v_x + \gamma v_z)\frac{dv_z}{d\xi} = -\gamma\frac{d\psi}{d\xi}$$

$$L_v\frac{dv_z}{d\xi} = -\gamma\frac{d\psi}{d\xi} \tag{C.12}$$

now, integrate equation (C.9) with boundary conditions

$$\xi \to \infty, n_i = 1, v_x = v_z = 0$$

we have

$$n_i(-M + \alpha v_x + \gamma v_z) = C$$

$$C = M$$

then

$$-M + \alpha v_x - \gamma v_z = -\frac{M}{n_i}$$

$$L_v = -\frac{M}{n_i} \tag{C.13}$$

equation (C.13) into (C.12)

$$(-M + \alpha v_x + \gamma v_z)\frac{dv_z}{d\xi} = -\gamma\frac{d\psi}{d\xi}$$

$$\frac{M}{n_i}\frac{dv_z}{d\xi} = \gamma\frac{d\psi}{d\xi}$$

$$\frac{dv_z}{d\xi} = \frac{\gamma n_i}{M}\frac{d\psi}{d\xi} \tag{C.14}$$

differentiate equation (C.19) w.r.t ξ, we have

$$0 + \alpha\frac{dv_x}{d\xi} + \gamma\frac{dv_z}{d\xi} = \frac{M}{n_i}\frac{dn_i}{d\xi}$$

$$\alpha\frac{dv_x}{d\xi} + \frac{\gamma^2 n_i}{M} = \frac{M}{n_i}\frac{dn_i}{d\xi}$$

$$\frac{dv_x}{d\xi} = -\frac{\gamma^2 n_i}{\alpha M}\frac{d\psi}{d\xi} + \frac{M}{\alpha n_i}\frac{dn_i}{d\xi} \tag{C.15}$$

then integrate with boundary conditions

$$\xi \to 0, v_x = 0, n_i = 1, \psi = 0$$

we obtain

$$\alpha v_x + \frac{\gamma^2}{M}\left[\frac{f e^{\alpha_c\psi}}{\alpha_c} + (1-f)\left(\frac{e^{\alpha_h\psi}}{\alpha_h} - \beta\left(\psi - \frac{1}{\alpha_h}\right)\frac{e^{\alpha_h\psi}}{\alpha_h} + \beta\left(\psi^2 - \frac{2\psi}{\alpha_h} + \frac{2}{\alpha_h^2}\right)\frac{e^{\alpha_h\psi}}{\alpha_h}\right)\right] = -\frac{M}{n_i} +$$

then

$$\frac{\gamma^2}{M}\left[\frac{f}{\alpha_c} + (1-f)\left(\frac{1}{\alpha_h} + \frac{\beta}{\alpha_h^2} + \frac{2\beta}{\alpha_h^3}\right)\right] + M = C$$

we have

$$v_x = \frac{1}{\alpha}\left[M\left(1 - \frac{1}{n_i}\right) - \frac{\gamma^2}{M}\left(\frac{f}{\alpha_c}(e^{\alpha_c\psi} - 1) + (1-f)\left(\frac{1}{\alpha_h}(e^{\alpha_h\psi} - 1) + \beta\psi(\psi - 1)\frac{e^{\alpha_h\psi}}{\alpha_h}\right.\right.\right.$$
$$\left.\left.\left. - \frac{\beta}{\alpha_h^2}(1 - e^{\alpha_h\psi} + 2\psi e^{\alpha_h\psi} + \frac{2\beta}{\alpha_h^3}(e^{\alpha_h\psi} - 1)\right)\right)\right] \tag{C.16}$$

equation (C.15) into (C.10)

$$-\frac{M}{n_i}\left(-\frac{\gamma^2 n_i}{\alpha M}\frac{d\psi}{d\xi} + \frac{M}{\alpha n_i^2}\frac{dn_i}{d\xi}\right) = -\alpha\frac{d\psi}{d\xi} + M v_y$$

$$\left(\frac{\gamma^2+\alpha^2}{\alpha M}\right)\frac{d\psi}{d\xi}-\frac{M}{\alpha n_i^3}\frac{dn_i}{d\xi}=v_y$$

since

$$\gamma^2+\alpha^2=\cos^2\theta+\sin^2\theta=1$$

we have

$$\frac{1}{\alpha M}\left(\frac{d\psi}{d\xi}-\frac{M^2}{n_i^3}\frac{dn_i}{d\xi}\right)=v_y$$

$$\frac{1}{\alpha M}\left[\frac{d}{d\xi}\left(\psi+\frac{M^2}{2n_i^2}\right)\right]=v_y \tag{C.17}$$

from equation (C.11)

$$(-M+\alpha v_x+\gamma v_z)\frac{dv_y}{d\xi}=-Mv_x$$

$$-\frac{M}{n_i}\frac{dv_y}{d\xi}=-Mv_x$$

$$\frac{dv_y}{d\xi}=n_iv_x \tag{C.18}$$

equation (C.16), (C.17) and (C.18) together

$$\frac{d}{d\xi}\left[\frac{d}{d\xi}\left(\psi+\frac{M^2}{2n_i^2}\right)\right]=M^2(n_i-1)-n_i\gamma^2\left[\frac{f}{\alpha_c}(e^{\alpha_c\psi}-1)+(1-f)\right.$$
$$\left.\left(\frac{1}{\alpha_h}(e^{\alpha_h\psi}-1)+\beta\psi(\psi-1)\frac{e^{\alpha_h\psi}}{\alpha_h}-\frac{\beta}{\alpha_h^2}(1-e^{\alpha_h\psi}+2\psi e^{\alpha_h\psi})+\frac{2\beta}{\alpha_h^3}(e^{\alpha_h\psi}-1)\right)\right] \tag{C.19}$$

let

$$t=\psi+\frac{M^2}{2n_i^2}$$

then

$$\frac{dt}{d\xi}=\frac{d\psi}{d\xi}-\frac{M^2}{n_i^3}\frac{dn_i}{d\xi}$$

$$n_i=fe^{\alpha_c\psi}+(1-f)(1-\beta\psi+\beta\psi^2)e^{\alpha_h\psi}$$

$$\frac{dn_i}{d\xi}=\left[f\alpha_ce^{\alpha_c\psi}+(1-f)\left(\alpha_he^{\alpha_h\psi}-\beta(1+\alpha_h\psi)e^{\alpha_h\psi}+\beta\psi(2+\alpha_h\psi)e^{\alpha_h\psi}\right)\right]\frac{d\psi}{d\xi}$$

and

$$\frac{dt}{d\xi}=\frac{d\psi}{d\xi}-\frac{M^2}{n_i^3}\left[f\alpha_ce^{\alpha_c\psi}+(1-f)\left(\alpha_he^{\alpha_h\psi}-\beta(1+\alpha_h\psi)e^{\alpha_h\psi}+\beta\psi(2+\alpha_h\psi)e^{\alpha_h\psi}\right)\right]\frac{d\psi}{d\xi}$$

now, multiply both side of equation (C.19) with $2\frac{dt}{d\xi}$ and integrate, we obtain

$$\frac{1}{2}\left(\frac{dt}{d\xi}\right)^2 = -\frac{M^4}{2n_i^2}(1-n_i)^2 - M^2(1-\gamma^2)\psi + M^2P(\psi) - \frac{\gamma^2P(\psi)^2}{2} - \frac{\gamma^2M^2P(\psi)}{n_i}$$

then, we obtain

$$\frac{1}{2}\left(\frac{d\psi}{d\xi}\right)^2 + \frac{1}{\left(1 - \frac{M^2(f\alpha_c\exp(\alpha_c\psi)+(1-f)(\alpha_h\exp(\alpha_h\psi)-\beta(1+\alpha_h\psi)\exp(\alpha_h\psi)+\beta\psi(2+\alpha_h\psi)\exp(\alpha_h\psi)))}{(f\exp(\alpha_c\psi)+(1-f)(1-\beta\psi+\beta\psi^2)\exp(\alpha_h\psi))^3}\right)^2}\times$$
$$-\frac{M^4}{2n_i^2}(1-n_i)^2 - M^2(1-\gamma^2)\psi + M^2P(\psi) - \frac{\gamma^2P(\psi)^2}{2} - \frac{\gamma^2M^2P(\psi)}{n_i} = 0 \qquad \text{(C.20)}$$

where

$$\begin{aligned} P(\psi) = {} & \frac{f}{\alpha_c}(\exp(\alpha_c\psi)-1) + \frac{(1-f)}{\alpha_h}\left((\exp(\alpha_h\psi)-1)\right. \\ & +\beta\psi(\psi-1)\exp(\alpha_h\psi) - \frac{\beta}{\alpha_h}(1-\exp(\alpha_h\psi)+2\psi\exp(\alpha_h\psi)) \\ & \left.+\frac{2\beta}{\alpha_h^2}(\exp(\alpha_h\psi)-1)\right) \end{aligned} \qquad \text{(C.21)}$$

Appendix D

Algebraic expression for the Sagdeev potential in a magnetized plasma with two ion species and electrons

The density and temperature of the Boltzmann distributed cool electrons (n_e, T_e) and hot protons (n_p, T_p) in normalized form are given by

cool electron

$$n_e = n_{eo} \exp\left(\frac{e\phi}{T_e}\right) \tag{D.1}$$

hot proton

$$n_p = n_{po} \exp\left(\frac{-e\phi}{T_p}\right) \tag{D.2}$$

and

$$n_e = n_i + n_p \tag{D.3}$$

now, let $\psi = \frac{e\phi}{T_e}$, $\frac{n_{po}}{n_{eo}} = p$

$$n_e = \frac{n_{eo}}{n_{eo}} \exp(\psi) = \exp(\psi) \tag{D.4}$$

$$n_p = \frac{n_{po}}{n_{eo}} \exp\left(\frac{-e\phi}{T_p}\right)$$

$$= g \exp\left(\frac{-e\phi}{T_e}\frac{T_e}{T_p}\right)$$

$$n_p = g\exp(-\alpha_T\psi) \tag{D.5}$$

where $\alpha_T = \frac{T_e}{T_p}$

Therefore,

$$n_i = \frac{\exp(\psi) - g\exp(-\alpha_T\psi)}{1-g} \tag{D.6}$$

Magnetized cold oxygen ion beam (described by the fluid equations) (normalized)

$$\frac{\partial n_i}{\partial t} + \frac{\partial(n_i v_{ix})}{\partial x} + \frac{\partial(n_i v_{iz})}{\partial z} = 0 \tag{D.7}$$

$$\frac{\partial v_{ix}}{\partial t} + \left(v_{ix}\frac{\partial}{\partial x} + v_{iz}\frac{\partial}{\partial z}\right)v_{ix} = -\frac{e}{m_i}\frac{\partial\phi}{\partial x} + \Omega_i v_{iy} \tag{D.8}$$

$$\frac{\partial v_{iy}}{\partial t} + \left(v_{ix}\frac{\partial}{\partial x} + v_{iz}\frac{\partial}{\partial z}\right)v_{iy} = -\Omega_i v_{ix} \tag{D.9}$$

$$\frac{\partial v_{iz}}{\partial t} + \left(v_{ix}\frac{\partial}{\partial x} + v_{iz}\frac{\partial}{\partial z}\right)v_{iz} = -\frac{e}{m_i}\frac{\partial\phi}{\partial z} \tag{D.10}$$

dimensionless variables: $\iota = \Omega_i t$, $(\eta, \zeta) = (x, z)/\rho_s$, $V_k = v_{ik}/c_s$ (where $k = x, z$), $\Omega = c_s/\rho_s$. Then, equation (D.7)-(D.10) becomes

$$\frac{\partial n_i}{\partial \iota} + \frac{\partial(n_i v_x)}{\partial \eta} + \frac{\partial(n_i v_z)}{\partial \zeta} = 0 \tag{D.11}$$

$$\frac{\partial v_x}{\partial \iota} + \left(v_x\frac{\partial}{\partial \eta} + v_z\frac{\partial}{\partial \zeta}\right)v_x = -\frac{\partial\psi}{\partial\eta} + v_y \tag{D.12}$$

$$\frac{\partial v_y}{\partial \iota} + \left(v_x\frac{\partial}{\partial \eta} + v_z\frac{\partial}{\partial \zeta}\right)v_y = -v_x \tag{D.13}$$

$$\frac{\partial v_z}{\partial \iota} + \left(v_x\frac{\partial}{\partial \eta} + v_z\frac{\partial}{\partial \zeta}\right)v_z = -\frac{\partial\psi}{\partial\zeta} \tag{D.14}$$

define a localized stationary frame

$$\xi = (\alpha\eta + \gamma\zeta - M\iota)/M \tag{D.15}$$

where

$$\partial_\iota = -\partial_\xi, \partial_\eta = \frac{\alpha}{M}\partial_\xi, \partial_\zeta = \frac{\gamma}{M}\partial_\xi \tag{D.16}$$

from equation (D.11)

$$-\frac{dn_i}{d\xi} + \frac{\alpha}{M}\frac{dn_i v_x}{d\xi} + \frac{\gamma}{M}\frac{dn_i v_x}{d\xi} = 0$$

$$M\frac{dn_i}{d\xi} = \frac{dn_i}{d\xi}(\alpha v_x + \gamma v_z)$$

integrate with the boundary condition

$$\xi \to 0, n_i \to 1, \psi = 0, v_x = 0, v_z = v_o$$

we have

$$Mn_i + C = n_i(\alpha v_x + \gamma v_z)$$

$$M + C = \gamma v_o$$

$$C = \delta - M \tag{D.17}$$

where $\delta = \gamma v_o$

$$n_i(\alpha v_x + \gamma v_z) = Mn_i + \delta - M$$

$$\alpha v_x + \gamma v_z = M - \frac{M - \delta}{n_i} \tag{D.18}$$

from equation (D.12)

$$-\frac{dv_x}{d\xi} + \left(\frac{\alpha}{M}v_x\frac{d}{d\xi} + \frac{\gamma}{M}v_z\frac{d}{d\xi}\right)v_x = -\frac{\alpha}{M}\frac{d\psi}{d\xi} + v_y$$

$$-M\frac{dv_x}{d\xi} + (\alpha v_x + \gamma v_z)\frac{dv_x}{d\xi} = -\alpha\frac{d\psi}{d\xi} + Mv_y$$

$$(-M + \alpha v_x + \gamma v_z)\frac{dv_x}{d\xi} = -\alpha\frac{d\psi}{d\xi} + Mv_y$$

$$\left(-M + M - \frac{M - \delta}{n_i}\right)\frac{dv_x}{d\xi} = -\alpha\frac{d\psi}{d\xi} + Mv_y$$

$$-\left(\frac{M - \delta}{n_i}\right)\frac{dv_x}{d\xi} = -\alpha\frac{d\psi}{d\xi} + Mv_y \tag{D.19}$$

from equation (D.13)

$$-\frac{dv_y}{d\xi} + \left(\frac{\alpha}{M}v_x\frac{d}{d\xi} + \frac{\gamma}{M}v_z\frac{d}{d\xi}\right)v_y = -v_x$$

$$-M\frac{dv_y}{d\xi} + (\alpha v_x + \gamma v_z)\frac{dv_y}{d\xi} = -Mv_x$$

$$\left(-M + M - \frac{M - \delta}{n_i}\right)\frac{dv_y}{d\xi} = -Mv_x$$

$$\left(\frac{M-\delta}{n_i}\right)\frac{dv_y}{d\xi} = Mv_x \tag{D.20}$$

from equation (D.14)

$$-\frac{dv_z}{d\xi} + \left(\frac{\alpha}{M}v_x\frac{d}{d\xi} + \frac{\gamma}{M}v_z\frac{d}{d\xi}\right)v_z = -\frac{\gamma}{M}\frac{d\psi}{d\xi}$$

$$-M\frac{dv_z}{d\xi} + (\alpha v_x + \gamma v_z)\frac{dv_z}{d\xi} = -\gamma\frac{d\psi}{d\xi}$$

$$\left(-M + M - \frac{M-\delta}{n_i}\right)\frac{dv_z}{d\xi} = -\gamma\frac{d\psi}{d\xi}$$

$$\left(\frac{M-\delta}{n_i}\right)\frac{dv_z}{d\xi} = \gamma\frac{d\psi}{d\xi} \tag{D.21}$$

now, differentiate equation (D.18) w. r .t. $d\Omega$, we have

$$\alpha\frac{dv_x}{d\xi} + \gamma\frac{dv_z}{d\xi} = \left(\frac{M-\delta}{n_i^2}\right)\frac{dn_i}{d\xi} \tag{D.22}$$

substitute equation (D.21) in equation (D.22)

$$\frac{dv_x}{d\xi} = -\left(\frac{\gamma^2 n_i}{\alpha(M-\delta)}\right)\frac{d\psi}{d\xi} + \left(\frac{M-\delta}{\alpha n_i^2}\right)\frac{dn_i}{d\xi} \tag{D.23}$$

integrate equation (D.23), we have

$$\alpha v_x + \frac{\gamma^2}{M-\delta}\left[\frac{1}{1-g}\left(e^x + \frac{g}{\alpha_T}e^{-\alpha_T\psi}\right)\right] = -\frac{M-\delta}{n_i} + C \tag{D.24}$$

using boundary conditions

$$v_x = 0, n_i = 1, \psi = 0$$

we obtain

$$\frac{\gamma^2}{M-\delta}\left[\frac{1}{1-g}\left(1 + \frac{g}{\alpha_T}\right)\right] + (M-\delta) = C$$

$$\alpha v_x = (M-\delta)\left(1 - \frac{1}{n_i}\right) - \frac{\gamma^2}{M-\delta}\left[\frac{1}{1-g}\left((e^{\psi}-1) + \frac{g}{\alpha_T}(e^{-\alpha_T\psi}-1)\right)\right] \tag{D.25}$$

equation (D.23) into (D.19), we have

$$\frac{\gamma^2}{\alpha}\frac{d\psi}{d\xi} - \frac{(M-\delta)^2}{\alpha n_i^3}\frac{dn_i}{d\xi} = -\alpha\frac{d\psi}{d\xi} + Mv_y$$

$$\frac{1}{\alpha M}\left[\frac{d\psi}{d\xi}-\frac{(M-\delta)^2}{n_i^3}\frac{dn_i}{d\xi}\right]=v_y \tag{D.26}$$

since

$$\alpha^2+\gamma^2=1$$

equation (D.20) into (D.26), we have

$$\frac{1}{\alpha M}\left[\frac{d}{d\xi}\left(\frac{d\psi}{d\xi}-\frac{(M-\delta)^2}{n_i^3}\frac{dn_i}{d\xi}\right)\right]=\frac{n_i M v_x}{M-\delta}$$

$$\frac{d}{d\xi}\left[\frac{d}{d\xi}\left(\psi+\frac{(M-\delta)^2}{2n_i^2}\right)\right]=\frac{\alpha n_i M^2 v_x}{M-\delta}$$

$$\frac{d}{d\xi}\left[\frac{d}{d\xi}\left(\psi+\frac{(M-\delta)^2}{2n_i^2}\right)\right]=M^2(n_i-1)-\frac{\gamma^2 M^2 n_i}{(M-\delta)^2}\left[\frac{1}{1-g}\left((e^{\psi}-1)+\frac{g}{\alpha_T}(e^{-\alpha_T\psi}-1)\right)\right] \tag{D.27}$$

let

$$\chi=\psi+\frac{(M-\delta)^2}{2n_i^2}$$

$$\frac{d\chi}{d\xi}=\frac{d\psi}{d\xi}-\frac{(M-\delta)^2}{n_i^3}\frac{dn_i}{d\xi}$$

or

$$\frac{d\chi}{d\xi}=\left(1-\frac{(M-\delta)^2\left(\frac{1}{1-g}(e^{\psi}+\alpha_T g e^{-\alpha_T\psi}\right)}{n_i^3}\right)\frac{d\psi}{d\xi} \tag{D.28}$$

Multiply both sides of equation (D.27) by $2\frac{d\chi}{d\xi}$ and integrate

$$\begin{aligned}\frac{1}{2}\left(\frac{d\chi}{d\xi}\right)^2=\Bigg(&-\frac{M^2(M-\delta)^2}{2n_i^2}(1-n_i)^2\\&-M^2(1-\gamma^2)\psi+M^2\left(\frac{1}{1-g}\left((\exp(\psi)-1)+\frac{g}{\alpha_T}(\exp(-\alpha_T\psi)-1)\right)\right)\\&-\frac{\gamma^2}{2(M-\delta)^2}\left(\frac{1}{1-g}\left((\exp(\psi)-1)+\frac{g}{\alpha_T}(\exp(-\alpha_T\psi)-1)\right)\right)^2\\&-\frac{M^2\gamma^2}{n_i}\left(\frac{1}{1-g}\left((\exp(\psi)-1)+\frac{g}{\alpha_T}(\exp(-\alpha_T\psi)-1)\right)\right)\Bigg)\end{aligned} \tag{D.29}$$

equation (D.28) into (D.29), we have

$$\frac{1}{2}\left(\frac{d\psi}{d\xi}\right)^2 = \frac{1}{\left(1-\frac{(M-\delta)^2}{n_i^3}\left(\frac{1}{1-g}(\exp(\psi)+g\alpha_T\exp(-\alpha_T\psi)\right)\right)^2}\times\left(-\frac{M^2(M-\delta)^2}{2n_i^2}(1-n_i)^2\right.$$
$$-M^2(1-\gamma^2)\psi + M^2\left(\frac{1}{1-g}\left((\exp(\psi)-1)+\frac{g}{\alpha_T}(\exp(-\alpha_T\psi)-1)\right)\right)$$
$$-\frac{\gamma^2}{2(M-\delta)^2}\left(\frac{1}{1-g}\left((\exp(\psi)-1)+\frac{g}{\alpha_T}(\exp(-\alpha_T\psi)-1)\right)\right)^2$$
$$\left.-\frac{M^2\gamma^2}{n_i}\left(\frac{1}{1-g}\left((\exp(\psi)-1)+\frac{g}{\alpha_T}(\exp(-\alpha_T\psi)-1)\right)\right)\right) = 0 \tag{D.30}$$

which can be written as "Energy integral equation"

$$\frac{1}{2}\left(\frac{d\psi}{d\xi}\right)^2 + V(\psi, M) = 0 \tag{D.31}$$

where

$$V(\psi,M) = -\frac{1}{\left(1-\frac{(M-\delta)^2}{n_i^3}\left(\frac{1}{1-g}(\exp(\psi)+g\alpha_T\exp(-\alpha_T\psi)\right)\right)^2}\times\left(-\frac{M^2(M-\delta)^2}{2n_i^2}(1-n_i)^2\right.$$
$$-M^2(1-\gamma^2)\psi + M^2\left(\frac{1}{1-g}\left((\exp(\psi)-1)+\frac{g}{\alpha_T}(\exp(-\alpha_T\psi)-1)\right)\right)$$
$$-\frac{\gamma^2}{2(M-\delta)^2}\left(\frac{1}{1-g}\left((\exp(\psi)-1)+\frac{g}{\alpha_T}(\exp(-\alpha_T\psi)-1)\right)\right)^2$$
$$\left.-\frac{M^2\gamma^2}{n_i}\left(\frac{1}{1-g}\left((\exp(\psi)-1)+\frac{g}{\alpha_T}(\exp(-\alpha_T\psi)-1)\right)\right)\right) \tag{D.32}$$

at beam velocity = 0 (i.e., $\delta = \gamma v_o = 0$).

$$V(\psi,M) = -\frac{1}{\left(1-\frac{M^2}{n_i^3}\left(\frac{1}{1-g}(\exp(\psi)+g\alpha_T\exp(-\alpha_T\psi)\right)\right)^2}\times\left(-\frac{M^4}{2n_i^2}(1-n_i)^2\right.$$
$$-M^2(1-\gamma^2)\psi + M^2\left(\frac{1}{1-g}\left((\exp(\psi)-1)+\frac{g}{\alpha_T}(\exp(-\alpha_T\psi)-1)\right)\right)$$
$$-\frac{\gamma^2}{2}\left(\frac{1}{1-g}\left((\exp(\psi)-1)+\frac{g}{\alpha_T}(\exp(-\alpha_T\psi)-1)\right)\right)^2$$
$$\left.-\frac{M^2\gamma^2}{n_i}\left(\frac{1}{1-g}\left((\exp(\psi)-1)+\frac{g}{\alpha_T}(\exp(-\alpha_T\psi)-1)\right)\right)\right) \tag{D.33}$$

Appendix E

Algebraic expression for the Sagdeev potential in a magnetized plasma with cold oxygen ions, cool ions and two temperature electrons

The density and temperature of the Boltzmann distribution of the cool (n_{ce}, T_{ce}) and hot (n_{he}, T_{he}) electrons and cool (n_{ci}, T_{ci}) ion species and are given in normalized form as follows:

cool electrons:

$$n_{ce} = n_{ce0} \exp\left(\frac{e\phi}{T_{ce}}\right)$$

$$n_{ce} = \frac{n_{ce0}}{n_{i0}} \exp\left(\frac{e\phi}{T_{eff}} \frac{T_{eff}}{T_{ce}}\right)$$

$$n_{ce} = f \exp(\alpha_{ce}\psi) \tag{E.1}$$

hot electrons:

$$n_{he} = n_{he0} \exp\left(\frac{e\phi}{T_{he}}\right)$$

$$n_{he} = \frac{n_{he0}}{n_{i0}} \exp\left(\frac{e\phi}{T_{eff}} \frac{T_{eff}}{T_{he}}\right)$$

$$n_{he} = (1 - f) \exp(\alpha_{he}\psi) \tag{E.2}$$

Cool ions:

$$n_{ci} = n_{ci0} \exp\left(-\frac{e\phi}{T_{ci}}\right)$$

$$n_{ci} = \frac{n_{ci0}}{n_{i0}} \exp\left(-\frac{e\phi}{T_{eff}} \frac{T_{eff}}{T_{ci}}\right)$$

$$n_{ci} = g \exp(-\alpha_{ci}\psi) \tag{E.3}$$

Magnetized Cool Oxygen ions (normalized)(described by the fluid equations) :

$$\frac{\partial n_i}{\partial t} + \frac{\partial (n_i v_x)}{\partial x} + \frac{\partial (n_i v_z)}{\partial z} = 0 \tag{E.4}$$

$$\frac{\partial v_x}{\partial t} + \left(v_x \frac{\partial}{\partial x} + v_z \frac{\partial}{\partial z}\right) v_x = -\frac{\partial \psi}{\partial x} + v_y \tag{E.5}$$

$$\frac{\partial v_y}{\partial t} + \left(v_x \frac{\partial}{\partial x} + v_z \frac{\partial}{\partial z}\right) v_y = -v_x \tag{E.6}$$

$$\frac{\partial v_z}{\partial t} + \left(v_x \frac{\partial}{\partial x} + v_z \frac{\partial}{\partial z}\right) v_z = -\frac{\partial \psi}{\partial z} \tag{E.7}$$

The quasi-neutrality condition

$$n_i = n_{ce} + n_{he} - n_{ci} = \frac{f e^{\alpha_{ce}\psi} + (1-f) e^{\alpha_{he}\psi} - g e^{-\alpha_{ci}\psi}}{1-g} \tag{E.8}$$

stationary frame

$$\xi = (\alpha x + \gamma z - Mt)/M \tag{E.9}$$

$$\frac{\partial \xi}{\partial x} = \frac{\alpha}{M}, \frac{\partial \xi}{\partial z} = \frac{\gamma}{M}, \frac{\partial \xi}{\partial t} = -1$$

from equation (E.4)

$$-\frac{dn_i}{d\xi} + \frac{\alpha}{M} \frac{dn_i v_x}{d\xi} + \frac{\gamma}{M} \frac{dn_i v_x}{d\xi} = 0$$

$$M \frac{dn_i}{d\xi} = \frac{dn_i}{d\xi} (\alpha v_x + \gamma v_z)$$

integrate with the boundary condition

$$\xi \to 0, n_i \to 1, \psi = 0, v_x = v_z = 0$$

then

$$M = -C$$

$$Mn_i - M = n_i(\alpha v_x + \gamma v_z)$$
$$\alpha v_x + \gamma v_z = M\left(1 - \frac{1}{n_i}\right) \tag{E.10}$$

from equation (E.5)

$$-\frac{dv_x}{d\xi} + \left(\frac{\alpha}{M}v_x\frac{d}{d\xi} + \frac{\gamma}{M}v_z\frac{d}{d\xi}\right)v_x = -\frac{\alpha}{M}\frac{d\psi}{d\xi} + v_y$$
$$-M\frac{dv_x}{d\xi} + (\alpha v_x + \gamma v_z)\frac{dv_x}{d\xi} = -\alpha\frac{d\psi}{d\xi} + Mv_y$$
$$\left(-M + M - \frac{M}{n_i}\right)\frac{dv_x}{d\xi} = -\alpha\frac{d\psi}{d\xi} + Mv_y$$
$$-\frac{M}{n_i}\frac{dv_x}{d\xi} = -\alpha\frac{d\psi}{d\xi} + Mv_y \tag{E.11}$$

from equation (E.6)

$$-\frac{dv_y}{d\xi} + \left(\frac{\alpha}{M}v_x\frac{d}{d\xi} + \frac{\gamma}{M}v_z\frac{d}{d\xi}\right)v_y = -v_x$$
$$-M\frac{dv_y}{d\xi} + (\alpha v_x + \gamma v_z)\frac{dv_y}{d\xi} = -Mv_x$$
$$\left(-M + M - \frac{M}{n_i}\right)\frac{dv_y}{d\xi} = -Mv_x$$
$$\frac{1}{n_i}\frac{dv_y}{d\xi} = v_x \tag{E.12}$$

from equation (E.7)

$$-\frac{dv_z}{d\xi} + \left(\frac{\alpha}{M}v_x\frac{d}{d\xi} + \frac{\gamma}{M}v_z\frac{d}{d\xi}\right)v_z = -\frac{\gamma}{M}\frac{d\psi}{d\xi}$$
$$-M\frac{dv_z}{d\xi} + (\alpha v_x + \gamma v_z)\frac{dv_z}{d\xi} = -\gamma\frac{d\psi}{d\xi}$$
$$\left(-M + M - \frac{M}{n_i}\right)\frac{dv_z}{d\xi} = -\gamma\frac{d\psi}{d\xi}$$
$$\frac{M}{n_i}\frac{dv_z}{d\xi} = \gamma\frac{d\psi}{d\xi} \tag{E.13}$$

differentiate equation (E.10) w.r.t . ∂_ξ, we have

$$\alpha\frac{dv_x}{d\xi}+\gamma\frac{dv_z}{d\xi}=\frac{M}{n_i^2}\frac{dn_i}{d\xi} \tag{E.14}$$

equation (E.13) into (E.14)

$$\alpha\frac{dv_x}{d\xi}+\gamma^2\left(\frac{n_i}{M}\frac{d\psi}{d\xi}\right)=\frac{M}{n_i^2}\frac{dn_i}{d\xi}$$

i.e

$$\frac{dv_x}{d\xi}=-\frac{\gamma^2 n_i}{\alpha M}\frac{d\psi}{d\xi}+\frac{M}{\alpha n_i^2}\frac{dn_i}{d\xi} \tag{E.15}$$

integrate equation(E.15)

$$\alpha\int\frac{dv_x}{d\xi}d\xi+\frac{\gamma^2}{M}\int n_i\frac{d\psi}{d\xi}d\xi=M\int\frac{1}{n_i^2}\frac{dn_i}{d\xi}d\xi$$

$$\alpha v_x+\frac{\gamma^2}{M}\left(\frac{1}{1-g}\left(\frac{f}{\alpha_{ce}}e^{\alpha_{ce}\psi}+\frac{1-f}{\alpha_{he}}e^{\alpha_{he}\psi}+\frac{g}{\alpha_{ci}}e^{-\alpha_{ci}\psi}\right)\right)=-\frac{M}{n_i}+C$$

using boundary conditions:

$$v_x=0,n_i=1,\psi=0$$

we have

$$\frac{\gamma^2}{M}\left(\frac{1}{1-g}\left(\frac{f}{\alpha_{ce}}+\frac{1-f}{\alpha_{he}}+\frac{g}{\alpha_{ci}}\right)\right)+M=C$$

therefore,

$$\alpha v_x=M\left(1-\frac{1}{n_i}\right)-\frac{\gamma^2}{M}\left(\frac{1}{1-g}\left(\frac{f}{\alpha_{ce}}(e^{\alpha_{ce}\psi}-1)+\frac{1-f}{\alpha_{he}}(e^{\alpha_{he}\psi}-1)+\frac{g}{\alpha_{ci}}(e^{-\alpha_{ci}\psi}-1)\right)\right) \tag{E.16}$$

equation (E.15) into (E.11)

$$\frac{\gamma^2}{\alpha}\frac{d\psi}{d\xi}-\frac{M^2}{\alpha n_i^3}\frac{dn_i}{d\xi}=-\alpha\frac{d\psi}{d\xi}+Mv_y$$

$$\left(\frac{\gamma^2+\alpha^2}{\alpha}\right)\frac{d\psi}{d\xi}-\frac{M^2}{\alpha n_i^3}\frac{dn_i}{d\xi}=Mv_y$$

Since

$$\alpha^2+\gamma^2=1$$

$$\frac{1}{\alpha M}\left(\frac{d\psi}{d\xi}-\frac{M^2}{n_i^3}\frac{dn_i}{d\xi}\right)=v_y \tag{E.17}$$

equation (E.17) into (E.12)

$$\frac{d}{d\xi}\left(\frac{d\psi}{d\xi}-\frac{M^2}{n_i^3}\frac{dn_i}{d\xi}\right)=\alpha M n_i v_x \tag{E.18}$$

equation (E.18) becomes

$$\frac{d}{d\xi}\left(\frac{d}{d\xi}\left(\psi+\frac{M^2}{2n_i^2}\right)\right)=M^2(n_i-1)-\gamma^2 n_i\left(\frac{1}{1-g}\left(\frac{f}{\alpha_{ce}}(e^{\alpha_{ce}\psi}-1)\right.\right.$$
$$\left.\left.+\frac{1-f}{\alpha_{he}}(e^{\alpha_{he}\psi}-1)+\frac{g}{\alpha_{ci}}(e^{-\alpha_{ci}\psi}-1)\right)\right) \tag{E.19}$$

let

$$t=\psi+\frac{M^2}{2n_i^2}$$

$$\frac{dt}{d\xi}=\frac{d\psi}{d\xi}-\frac{M^2}{n_i^3}\frac{dn_i}{d\xi}$$

$$\frac{dn_i}{d\xi}=\frac{1}{1-g}\left(f\alpha_{ce}e^{\alpha_{ce}\psi}+(1-f)\alpha_{he}e^{\alpha_{he}\psi}+g\alpha_{ci}e^{-\alpha_{ci}\psi}\right)\frac{d\psi}{d\xi}$$

i.e

$$\frac{dt}{d\xi}=\left(1-\frac{M^2}{n_i^3}\left(\frac{1}{1-g}\left(f\alpha_{ce}e^{\alpha_{ce}\psi}+(1-f)\alpha_{he}e^{\alpha_{he}\psi}+g\alpha_{ci}e^{-\alpha_{ci}\psi}\right)\right)\right)\frac{d\psi}{d\xi}$$

Multiply both side of equation (E.19) by $2\frac{dt}{d\xi}$ and integate

$$\int 2\frac{dt}{d\xi}\frac{d}{d\xi}\left(\frac{dt}{d\xi}\right)d\xi=2\left[\int M^2(n_i-1)-\gamma^2 n_i\left(\frac{1}{1-g}\left(\frac{f}{\alpha_{ce}}(e^{\alpha_{ce}\psi}-1)\right.\right.\right.$$
$$\left.\left.\left.+\frac{1-f}{\alpha_{he}}(e^{\alpha_{he}\psi}-1)+\frac{g}{\alpha_{ci}}(e^{-\alpha_{ci}\psi}-1)\right)\right)\right]\frac{dt}{d\xi}$$

we obtain

$$\frac{1}{2}\left(\frac{dt}{d\xi}\right)^2 = \left(-\frac{M^4}{2n_i^2}(1-n_i)^2 - M^2(1-\gamma^2)\psi \right.$$
$$+M^2\left(\frac{1}{1-g}\left(\frac{f}{\alpha_{ce}}(e^{\alpha_{ce}\psi}-1)+\frac{1-f}{\alpha_{he}}(e^{\alpha_{he}\psi}-1)+\frac{g}{\alpha_{ci}}(e^{-\alpha_{ci}\psi}-1)\right)\right)$$
$$-\frac{\gamma^2}{2}\left(\frac{1}{1-g}\left(\frac{f}{\alpha_{ce}}(e^{\alpha_{ce}\psi}-1)+\frac{1-f}{\alpha_{he}}(e^{\alpha_{he}\psi}-1)+\frac{g}{\alpha_{ci}}(e^{-\alpha_{ci}\psi}-1)\right)\right)^2$$
$$\left.-\frac{M^2\gamma^2}{n_i}\left(\frac{1}{1-g}\left(\frac{f}{\alpha_{ce}}(e^{\alpha_{ce}\psi}-1)+\frac{1-f}{\alpha_{he}}(e^{\alpha_{he}\psi}-1)+\frac{g}{\alpha_{ci}}(e^{-\alpha_{ci}\psi}-1)\right)\right)\right)$$

then, substitute for t

$$\frac{1}{2}\left(\frac{d\psi}{d\xi}\right)^2 = \frac{1}{\left(1-\frac{M^2}{n_i^3}\left(\frac{1}{1-g}(f\alpha_{ce}e^{\alpha_{ce}\psi}+(1-f)\alpha_{he}e^{\alpha_{he}\psi}+g\alpha_{ci}e^{-\alpha_{ci}\psi}\right)\right)^2}\times$$
$$\left(-\frac{M^4}{2n_i^2}(1-n_i)^2 - M^2(1-\gamma^2)\psi \right.$$
$$+M^2\left(\frac{1}{1-g}\left(\frac{f}{\alpha_{ce}}(e^{\alpha_{ce}\psi}-1)+\frac{1-f}{\alpha_{he}}(e^{\alpha_{he}\psi}-1)+\frac{g}{\alpha_{ci}}(e^{-\alpha_{ci}\psi}-1)\right)\right)$$
$$-\frac{\gamma^2}{2}\left(\frac{1}{1-g}\left(\frac{f}{\alpha_{ce}}(e^{\alpha_{ce}\psi}-1)+\frac{1-f}{\alpha_{he}}(e^{\alpha_{he}\psi}-1)+\frac{g}{\alpha_{ci}}(e^{-\alpha_{ci}\psi}-1)\right)\right)^2$$
$$\left.-\frac{M^2\gamma^2}{n_i}\left(\frac{1}{1-g}\left(\frac{f}{\alpha_{ce}}(e^{\alpha_{ce}\psi}-1)+\frac{1-f}{\alpha_{he}}(e^{\alpha_{he}\psi}-1)+\frac{g}{\alpha_{ci}}(e^{-\alpha_{ci}\psi}-1)\right)\right)\right) \quad \text{(E.20)}$$

Bibliography

[1] Abrol, P. S., and Tagare, S. G., *Plasma Phys.* **22**, 831, 1980.

[2] Abrol, P. S., and Tagare, S. G., *Plasma Phys.* **23**, 656, 1981.

[3] Ali-Fedela, D., Marif, H. and Djebli, M., *Adv. in Space Res.* **45**, 785-789, 2010.

[4] Ameniya, H. and Nakamura, Y., *Plasma Phys. Contr. Fusion* **28**, 1613, 1986.

[5] Anderson, J. D., Fundamentals of Aerodynamics (3rd ed), *McGraw-Hill Science/Engineering/Math,* (January 2001) 1984. ISBN 0-07-237335-0.

[6] Antipov, S. V., Nezlin, M. V., Snezhkin, E. N. and Trubnikov, A. S., *Sov. Phys. JETP* **62**, 1097, 1985.

[7] Baboolal, S., *Phd Thesis,* University of Natal, Durban, 1988.

[8] Baboolal, S., *J. Phys. Soc. Jpn.* **57**, 750, 1988.

[9] Baboolal, S., Bharuthram, R. and Hellberg, M. A., *J. Plasma Phys.* **44**, 1, 1990.

[10] Bahamida, S., Annou, K. and Annou, R., *34th EPS Conf. on Plasma Phys. ECA,* **31F**, 4.139, 2007.

[11] Bale, S. D., Kellogg, P. J., Larson, D. E., Lin, R. P., Goetz, K., and Lepping, R. P., *J. Geophys. Res.* **25**, 2929-2932, 1998.

[12] Baluku, T. K., Hellberg, M. A., and Verheest, F., *EPL* **91**, 15001, 2010.

[13] Barman, S. N. and Talukdar, A., *Int. J. of Appl. Math and Mech.* **6**, 47-62, 2010.

[14] Bharuthram, R. and Shukla, P. k., *Physica Scripta.* **34**, 732, 1985 .

[15] Bharuthram, R. and Shukla, P. k., *Phys. Fluids.* **29**, 10, 1986.

[16] Bharuthram, R and Shukla, P. K., *Phys. Review A* **35**, 3, 1987.

[17] Bharuthram, R. and Shukla, P. K., *Planet. Space Sci.* **40**, 647, 1992.

[18] Bharuthram, R., Reddy, R. V., Lakhina, G. S. and Singh, N., *Physica Scripta.* **T98**, 137-140, 2002.

[19] Bergmann, R., Roth, I., and Hudson, M. K., *J. Geophys. Res.* **93**, 4005-4020, 1988.

[20] Berthomier, M., Pottelette, R., and Malingre, M., *J. Geophys. Res.* **103**, A3, 4261, 1998.

[21] Berthomier, M., Pottelette, R., Malingre, M., and Khotyaintsev, Y., *Phys. Plasmas* **7**, 2987-2994, 2000.

[22] Boehm, M. H., Carlson, C. W., McFadden, J. and Mozer, F. S., *Geophys. Res. Lett.* **11**, 511, 1984.

[23] Borovsky, J. E., *Proc. of the 2nd Symp. on Double layers and Related Topics*(ed. R. Schrittwieser and G. Eder), Innsbruck (Austria), p.33, 1984.

[24] Boström,R., Gustafsson,G., Holback,B., Holmgren, G., Koskinen, H.,and Kintner, P.,*Phys. Rev. Lett.* **61**, 82-85, 1988.

[25] Boström, R., *IEEE Trans. Plasma Sci.* **20**, 756-0763, 1992.

[26] Block, L. P., *Cosm. Electrodyn.* **3**,349, 1972.

[27] Block, L. P., *Astrophys. Space Sci.* **55**, 1978.

[28] Bounds et al., *J. Geophys. Res.* **104**, 709, 1999.

[29] Boström et al., *Phys. Rev. Lett.* **61**, 82-85, 1988.

[30] Buti, B., *Phys. Lett.* **76A**, 251, 1980.

[31] Bychenkov, V. Yu., Rozmus, W. and Tikhonchuk. V. T., *Phy. Rewiew E* **51**, 2, 1400-1407, 1995.

[32] Cairns, R. A., Mamum, A. A., Bingham, R., Boström, R., Dendy, R. O., Nairn, C. M. C. and Shukla, P. K., *Geophys. Res. Lett.* **22**, 2709, 1995.

[33] Cattell, C. A., et al., *Geophys. Res. Lett.* **25**, 2053-2056, 1998.

[34] Cattel, C. A., et al., *J. Geophys. Res.* **26**, 425-428, 1999.

[35] Cattel, C. A., Crumley, J., Dombeck, J., Lysak, R., Kletzing, C., Peterson, W. K., and Collin, C., *Adv. Space Res.* **28**, 1631, 2001.

[36] Chakrabarti, N., Fruchtman, A., Arad, R., and Maron, Y., *Phys. Letters A*, 2002.

[37] Chang, R. P . H., and Porkolab M., *Phys.Rev.Lett.* **25**, 1262-1268, 1970.

[38] Choi, C. R., Lee, D. Y., and Yonggi, K., *J. Astron. Space Sci.* **3**, 23, 209-216, 2006.

[39] Choi, C. -R., Min, K. -W., Woo, M. -H. and Ryu, C. -M., *Phys. of Plasmas* **17**, 092904, 2010.

[40] Coakley, P., Johnson, L. and Hershkowitz, N., *Phys. Lett.* **70A**, 425, 1979.

[41] Crymley, J. P., Cattel, C. A., Lysak, R. L., and Dombeck, J. P., *J. Geophys. Res.* **106**, 6007-6015, 2001.

[42] Das, G. C., Madhuri, T., and Sarma, J., *Conts. Plasma Phys.* **38**, 5-6, pp.55-618, 1998.

[43] Das, R., *Astrophys Space Sci.*, 2012. DOI:10.1007/s10509-012-1094-6.

[44] Danehkar, A., Saini, N. S. and Hellberg, M. A., *Phys. of Plasmas* **18**, 072902, 2011.

[45] David, G. S., *2008 Themis Science Nuggets.*

[46] Deng, X. H., Tang, R. X., Matsumoto, H., Pickett, J. S., Fazakerley, A. N., Kojima, H., Baumjohann, W., Coates, A., Nakamura, R., Gurnett, D. A. and Liu, Z. X., *Adv. Space Res.* **37**, 1373-1381, 2006.

[47] Djebli, M. and Marif, H., *Phys. of Plasmas* **16**, 063708, 2009.

[48] Dombeck et.al., *Geophys. Res.* **106**, 19013-19021, 2001.

[49] Dovner, P. O., Eriksson, A. I., Boström, R. and Holback, B., *Geophys. Res. Lett* **21**, 1827-1830, 1994.

[50] Drazin, P. G and Johnson, R. S., *Solitons: an international (2nd ed.). Cambridge University press.*, 1989. ISBN 978-0-19-857063-9.

[51] Dubinov, A. E. and Kolotkov, D. Yu., *IEEE Trans. Plasma Sci.* **40**, 1429, 2012.

[52] Dubouloz, N., Pottelette. R., Malingre, M., and Treumann, R. A., *Geophys. Res.Lett.* **18**, 155-158, 1991.

[53] Eliasson, B. and Shukla, P. K., *Physics Reports* **422**, 225-290, 2006.

[54] El-Labany, S. K., Sabry, R., El-Taibany, W. F. and Elghmaz, E. A., *Phys. of Plasmas* **17**, 042301, 2010.

[55] Ergun et al., *Geophys. Res. Lett.* **25**, 2041, 1998.

[56] Farid, T., Mamun, A. A., Shukla, P. K. and Mirza, A. M., *Phys. of Plasmas* **8**, 5, 1529-1532, 2001.

[57] Franz, J. R., Kintner, P. M., and Pickett, J. S., *J. Geophys. Res.* **25**, 1277-1280, 1998.

[58] Gardner, C. S. and Morikawa, G. K., *Comm. Pure Appl. Math. XVIII,* **35**, 1965.

[59] Gavin, E. J. O., Tegen, R. and Zimak, P., *Abstract I6, 32nd S.Afr. Inst. Phys. Conf., University of Natal (Durban),* 1987.

[60] Gell, Y., and Roth, I. *Plasma Phys.* **19**, 915, 1977.

[61] Ghosh, S. S., Ghosh, K. K. and Iyengar, A. N. S., *Phys. Plasmas* **3**, 3939, 1996.

[62] Ghosh, S. S., and Iyengar, A. N. S., *Phys. Plasmas* **5**, 3204, 1997.

[63] Ghosh, S. S., and Iyengar, A. N. S., *J. Plasma Phys.* **67**, 223-233, 2002.

[64] Ghosh, S. S., and Lakhina, G. S., *Non-lin. Proc. Geophys.* **11**, 219-228, 2004.

[65] Ghosh, S. S., and Lakhina, G. S., National Conf. on Nonlin. Systems and Dynamics, Uni. of Madras, Chennai, 6-8 Feb. 2006.

[66] Giacobbe, F. W., *Elect. J. of Theoretical Phys.* **2** (6), 30-38, 2005.

[67] Gill, T. S., Bala, P., Kaur, H., Saini, N. S., Bansal, S. and Kaur, J., *Eur. Phys. J.* D **13**, 91-100, 2004.

[68] Gurnett, D. A., Frank L. A., and Lepping R. P., *J. Geophys. Res.* **81**, 6059-6071, 1976.

[69] Hasegawa, A., *Adv. Phys.* **34**, 1, 1985.

[70] Heeger, A. J., Kivelson, S., Schrieffer, J. R., and Su, W. -P., *Rev. Mod. Phys.* **60**, 781, 1988.

[71] Hellberg, M. A., and Frank, V., *Phys. Plasmas* **15**, 062307, 2008.

[72] Hellberg, M. A., Mace, R. L., Baluku, T. K., Kourakis, I. and Saini, N. S., *Phys. of Plasmas* **16**, 094701, 2009.

[73] Hudson, M. K., Lotko, W., Roth, I. and Witt, E., *J. Geophys. Res.,* **88**, 916-926, 1983.

[74] Ikezi, H., Taylor, R. J. and Baker, D. R., *Phys. Rev. Lett.* **25**, 11, 1970.

[75] Ikezi, H., *Phys. Fluids* **16**, 1668, 1973.

[76] Jain, S. L., Tiwari, R. S., and Sharma, S. R., *Can. J. Phys.* **68**, 474, 1990.

[77] Jilani, K., Mirza, A. M., and Khan, T. A., *Astrophys Space Sci.* **344**, 135-143, 2013.

[78] Jones, W. D., Lee, A., Gleman, S. M. and Doucet, H. J., *Phys. Rev. Lett.* **35**, 1349, 1975.

[79] Jung, Y. -D. and Hong, W. -P., *Phys. of Plasmas* **18**, 024502, 2011.

[80] Kakad, A. P., Singh, S. V., Reddy, R. V., Lakhina, G. S., Tagare. S. G., and Verheest. F., *Phys. Plasmas* **14**, 052305, 2007.

[81] Kaladze, T. D. and Tsamalashvili, L. V., *Phys. Lett.* **A**, 232, 269, 1997.

[82] Kivelson, M. G. and Russell, C. T., *eds., Introduction to space physics,* Cambridge University Press, 1995

[83] Koskinen, H. E., Lundin, R., and Holback, B., *J. Geophys. Res.* **95**, 5921-5929, 1990.

[84] Kourakis, I. and Shukla, P. K., *J. Phys. A: Math. Gen.* **36**, 11901, 2003.

[85] Kuehl, H. H., and Imen, K., *IEEE Trans. Plasma Sci.* **PS-13**, 37, 1985.

[86] Lakhina, G. S., *J. Geophys. Res.* **92**, 12, 1987.

[87] Lakhina, G. S., Tsurutani, B. T., Singh, S, V., and Reddy, R. V., *Nonlin. Proc. in Geophys.* **10**, 65, 2003.

[88] Lakhina, G. S., Singh, S. V., Kakad, A. P., Verheest, F. and Bharuthram, R., *Nonlin. Proc. Geophys.* **15**, 903-913, 2008a.

[89] Lakhina, G. S., Kakad, A. P., Singh, S. V. and Verheest, F., *Phys. Plasmas* **15**, 062903, 2008b.

[90] Lakhina, G. S., Singh, S. V., Kakad, A. P., Goldstein, M. L., Vinas, A. F. and Pickett, J. S., *J. Geophys. Res.* **114**, A09212, 2009. doi:10.1029/2009JA014306.

[91] Lakhina, G. S., Singh, S. V. and Kakad, A. P., *Adv. Space Res.* **47**, 1558, 2011.

[92] Langmuir, I., *Phys. Rev.* **33**, 954; **34**, 876, 1929.

[93] Lee, L.C and Kan J.R., *Phys. Fluids* **24**, 430, 1981.

[94] Lotko, W., *Phys. Fluids* **26**, 1771-1779, 1983.

[95] Lotko, W., *J. Geophys. Res.* **91**, 191-203, 1986.

[96] Lotko, W., and Kennel, C. F., *J. Geophys. Res.* **88**, 381-394, 1983.

[97] Ludmirsky, A., Eliezer, S., Arad, B., Borowitz, A., Gazit, Y., Jackel, S., Krumbein, A. D., Saltzmann, D. and Szichman, H., *IEEE Trans. Plasma Sci.* **PS-13**, 132, 1985.

[98] Ma, J. Z. G., and Hirose, A., *Nonlin. Proc. Geophys.* **17**, 245-268, 2010.

[99] Mace, R. L., Baboolal, S., Bharuthram, R., and Hellberg, M. A., *J. Plasma Phys.* **45**, 323, 1991.

[100] Maharaj, S. K., Bharuthram, R., Singh, S. V. and Lakhina, G. S., *Phys. of Plasmas* **20**, 083705, 2013.

[101] Mahmood, S., Mushtaq, A. and Saleem, H., *New J. of Phys.* **5**, 1-28, 2003.

[102] Mahmood, Ansar. M., Mahmood, S., Mirza, A. M. and Saleem, H., *CHIN.PHYS.LETT.* **22**, 3, 632, 2005.

[103] Mahmood, S., *Phd Thesis,* COMSATS Institute of Information Technology, Islamabad, Pakistan, 2007.

[104] Mahmood, S. and Akhtar, N., *Eur. Phys. J. D* **49**, 217-222, 2008.

[105] Malka et.al., *Phys. Rev. Lett.* **79**, 2053, 1997.

[106] Mamun, A. A., *Phys. Review E* **55**, 2, 1997.

[107] Mann, G. *J. Plasma Phys.* **36**, 25, 1986.

[108] Mann, G., Hackenberg, P., and Marsch, E., *J. Plasma Phys.* **58**, 2, 205-221, 1997.

[109] Masood, W. and Rizvi, H., *Phys. of Plasmas* **18**, 062304, 2011.

[110] Mälkki, A., Koskinen, H., Boström, R. and Holback, B., *Physica Scripta* **39**, 787-793, 1989.

[111] Matsumoto. H., et al., *Geophys. Res. Lett.* **21**, 2915-2918, 1994.

[112] McFadden, J. P., Calson, C. W., Ergun, R. E., Mozer, F. S., Roth, I., and Mödius, E., *J. Geophys. Res.* **108**, A4, 8018, 2003.

[113] McFadden, J. P., Carlson, C. W., and Ergun, R., *J. Geophys. Res.* **104**, 14453-14480, 1999.

[114] Moolla, S., *Phd thesis,* University of KwaZulu Natal, Durban, 2004.

[115] Moolla, S., Bharuthram, R., Singh, S. V., Lakhina, G. S., and Reddy, R. V., *Phys. Plasmas* **17**, 022903, 2010.

[116] Mozer, F. S. and Temerin. M., *in High Latitude Space Plasma Phys.* (ed. B. Hultquist and T. Hagfors) Plenum (New York) p.453, 1983.

[117] Mozer. F. S., Boehm, M. H., Cattel, C. A., Temerin, M. and Wygant, J. R., *Space Sci. Reviews* **42**, 313, 1985.

[118] Mozer et al., *Phys. Rev. Lett.* **79**, 1281, 1997.

[119] Mishra, M. K., Chhabra, R. S., and Sharma, S. R., *J. Plasma Phys.* **52**, 409, 1994.

[120] Murphy, G. B., et al., *The Netherlands. Eur. Space Agency,* **ESA SP-198,** 73-78, 1983.

[121] Mushtaq, A., *J. Phys.A: Math. Theor.* **43**, 315501, 2010.

[122] Nakamura, Y., *Proc. XVIII Int. Conf. on Phenomena in Ionized Gases, Invited Papers,* (Swansea, UK) p.116, 1987.

[123] Nakamura, Y., *J. Plasma Phys.* **38**, 461, 1987.

[124] Nakamura, Y., *Plasma Phys. Control. Fusion* **41**, A469, 1999.

[125] NASA, *NASA Science* "Magnetosphere", 2010.

[126] Nishihara, K., and Tajiri, M., *J. Phys. Soc. Jpn.* **50**, 4047, 1981.

[127] Omura, Y., Kojima, H., and Matsumoto, H., *Geophys. Res. Lett.* **21**, 2923-2926, 1994.

[128] Omura, Y., Kojima, H., Miki, N., Mukai, T., Matsumoto, H., and Anderson, R., *J. Geophys. Res.* **104**, 14,627-14637, 1999.

[129] Olson, P. and Amit, H., *Naturwissenschsften,* doi.org/10.1007/s00114-006-0138-6, 2006.

[130] Pakzad, H. R., *World Academy of Science, Eng. and Tech.* **81**, 997-1001, 2011.

[131] Parks, G. K., *Physics of Space Plasmas - An Introduction,* Addison - Wesley Publishing Company, CA. 1991.

[132] Pecseli, H. L., *IEEE Trans. Plasma Sci.* **PS-13**, 53, 1985.

[133] Peratt, A. L., *Physics of the Plasma Universe*, Springer-Verlag New York, Inc. 1991.

[134] Pickett, J. S., Menietti, J. D., Gurnett, D. A., Tsurutani, B., Kintner, P. M., Klatt, E., and Balogh, A., *Nonlin. Processes Geophys.* **10**, 3-11, 2003.

[135] Pickett, J. S., et al., *Ann. Geophys.* **22**, 2515, 2004.

[136] Pickett, J. S., et al., *Nonlin. Processes Geophys.* **12**, 181-193, 2005.

[137] Pickett, J. S., Chen, L. -J., Mutel, R. L., Christopher, I, W., Santolik, O., Lakhina, G. S., Singh, S. V., Reddy, R. V., Gurnett, D. A., Tsurutani, B. T., Lucek, E. and Lavraud, B., *Adv. Space Res.* **41**, 1666-1676, 2008.

[138] Pottelette, R., Malingre, M., Dubouloz, N., Aparicio, B., Lundin, R., Holmgren, G., and Marklund, G., *J. Geophys. Res.* **95**, 5957-5971, 1990.

[139] Pottelette, R., Ergun, R. E., Treumann, R. A., Berthomier, M., Carlson, C. W., McFadden, J. P., and Roth, I., *Geophys. Res. Lett.* **26**, 2629-2632, 1999.

[140] Qian, S., Lotko, W., and Hudson, M. K., *Phys. Fluids* **31**, 1339-1346, 1988.

[141] Qian, S., Lotko, W., and Hudson, M. K., *J. Geophys. Res.* **94**, 1339-1346, 1989.

[142] Qureshi, M. N. S., Shi, J., Torkar, K. and Liu, Z., *Adv. Space Res.* **45**, 1219-1223, 2010.

[143] Raychaudhuri, S., Gabl, E. F., Das. K. P., and Sengupta, S. N., *Plasma Phys. and Contr. Fusion* **27**, 3, 299-306, 1985.

[144] Reddy, R. V., and Lakhina, G. S., *Planet Space Sci.* **39**, 10, 1343-1350 1991.

[145] Reddy, R. V., Lakhina, G. S., and Verheest, F., *Planet Space Sci.* **40**, 8, 1055-1062, 1992.

[146] Reddy, R. V., Singh, S. V., Lakhina, G. S., and Bharuthram, R., *Earth Planets Space* **58**, 1227-1232, 2006.

[147] Reza Pakzad, H., *World Acad. of Sci,Eng. and Tech.* **81**, 997-1001, 2011.

[148] Romagnani et al., *Phys. Rev. Lett.* **101**, 025004, 2008.

[149] Rufai, O. R., Bharuthram, R., Singh, S. V and Lakhina, G. S., *Phys. Plasmas* **19**, 122308, 2012.

[150] Rufai, O. R., Bharuthram, R., Singh, S. V and Lakhina, G. S., *Commun Nonlin. Sci. Numer. Simulat.* **19**, 1338-1346, 2014.

[151] Russel, J. S., *Report on Waves, Rep. 14th Meet. British Assoc. Adv. Sci.* (John Muray) **311**, 1844.

[152] Sabry, R., *Phys. Plasmas* **16**, 072307, 2009.

[153] Sagdeev, R. Z., *Reviews of Plasma Phys.* (consultants Bureau, New York), Vol.4, 1969.

[154] Sahu, B., *Phys. of Plasmas* **18**, 082302, 2011.

[155] Sarri et.al., *Phys. Plasmas* **17**, 010701, 2010.

[156] Sato, N., *Proc. of Symp. on Plasma Double layers* (ed. P. Michelsen and J. Juul Rasmussen), Report **RISO-R-472**, Riso National Lab. (Denmark) p.116, 1982.

[157] Sato, N. and Okuda, H., *Phys. Rev. Lett.* **44**, 740, 1980.

[158] Sato, N. and Okuda, H., *J. Geophys. Res.* **86A**, 3357, 1981.

[159] Sauer, K., Dubinin, E., and McKenzie, J. F., *Phy. Scripta* **T98**, 52-57, 2002.

[160] Sauer, K., Dudinin, E., and McKenzie, J. F., *Nonlin. Proc. Geophys.* **10**, 121-130, 2003.

[161] Sayal, V. K., Yadav, L. L. and Sharma, S. R., *Physica Scripta.* **47**, 576, 1993.

[162] Schamel, H. *Proceedings of Symposium on Plasma Double Layers* (ed. P. Michelsen and J. Juul Rasmussen), Report **RISO-R-472**, Riso National Lab. (Denmark) p.274, 1982a.

[163] Schamel, H. *Physica Scripta* **T2/1**, 238, 1982b.

[164] Schwartz, S. J., Owen, C. J. and Burgess, D., *Astrophysical Plasmas* (Astronomy Unit, Queen Mary), University of London, UK, 2004.

[165] Scott, A. C., Chu, F. Y. F. and McLaughlin, D. W., *Proc. IEEE* **61**, 1443, 1973.

[166] Shah, A., Mahmood, S., and Haque, Q., *Phys. Plasmas* **17**, 112320, 2010.

[167] Shin, K., Kojima, H., Matsumoto, H., and Mukai, T., *J. Geophys. Res.* **113**, A03101, 12, 2008.

[168] Shukla, P. K., *Nonlinear Waves* (ed. L.Debnath), Cambridge University Press (cambridge). p.197, 1983.

[169] Shukla, P. K. and Mamun, A. A., *Introduction to Dusty Plasma Physics*, Institute of Physics Publishing (Bristol and Philadelphia). p.221, 2002.

[170] Shukla, P. K. and Stenflo, L., *Phys. Plasmas*, **4**, 3445, 1997.

[171] Singh, S. V. and Lakhina, G. S., *Nonlin. Pro. in Geophys.* **11**, 275-279, 2004.

[172] Singh, S. V., Lakhina, G. S., Bharuthram, R. and Pillay, S. R., *Phys. of Plasmas* **18**, 122306, 2011.

[173] Singh, K., Kumar, V., and Malik, H. K., *Phys. Plasmas* **12**, 052103, 2005.

[174] Smith, R. A., *Physica Scripa* **T2/1**, 238, 1982.

[175] Sreenivasan. B. and Jones, C. A., *Geophys. Res. Lett.* **32**, 20, 2005.

[176] Strangeway, R. J., et al., *Geophys. Res. Lett.* **25**, 2065-2068, 1998.

[177] Sultana, S., Kourakis, I., Saini, N. S. and Hellberg, M. A., *Phys. of Plasmas* **17**, 032310, 2010.

[178] Tagare, S. G., *Plasma Phys.* **15**, 1247, 1973.

[179] Tagare, S. G., *Phys. Plasmas* **7**, 3, 2000.

[180] Temerin, M. Cerny, K. Lotko, W. and Mozer. F. S., *Phys. Rev. Lett.* **48**, 1175, 1982.

[181] Temerin, M. and Mozer, F. S., *Proc. 2nd Symp. on Plasma Double Layer and Related Topics* (ed. R. Schrittwieser and G. Eder) (Innsbruck, Austria) p.119, 1984.

[182] Ting, L., Viscous vortical flows. Lecture notes in physics. *Springer-Verlag*, ISBN 3-540-53713-9. 1991.

[183] Tran, M. Q., *Physica Scripta* **20**, 317. 1979.

[184] Tsurutani, B. T., Arballo, J. K., Lakhina, G. S., Ho, C. M., Buti, B., Pickett, J. S., and Gurnett, D. A., *Geophys. Res. Lett.* **25**, 4117-4120, 1998.

[185] Verheest, F., Cattaert, T., and Hellberg, M. A., *Space Sci. Rev.* **121**, 299-311, 2005.

[186] Verheest, F., Hellberg, M. A. and Lakhina, G. S., *Astrophys. Space Sci. Trans.* **3**, 15, 2007.

[187] Verheest, F. and Hellberg, M. A., *Phys. of Plasmas* **17**, 102312, 2010.

[188] Verheest, F., Hellberg, M. A., and Hereman, W. A., *Phys. of Plasmas* **19**, 092302, 2012; http://dx.doi.org/10.1063/1.4752217.

[189] Verheest, F., Hellberg, M. A. and Kourakis, L., *Phys. of Plasmas* **20**, 012302, 2013.

[190] Wang, D- Y et al., *Benijing: Chin. Phys. Lett.* 242, 1998.

[191] Wang, D- Y., and Huang G. L., *Chin. Phys. Lett.* **18**, 4, 553, 2001.

[192] Washimi, H. and Taniuti, T., *Phys. Rev. Lett.* **17**, 996, 1966.

[193] Watanabe, S. J., *J. Phys. Soc. Jpn.* **44**, 611, 1978.

[194] Yadav, L. L. and Sharma, S. R., *Phys. Lett. A* **150**, 397, 1990.

[195] Yadav, L. L., Tiwari, R. S., Maheshwari, K. P. and Sharma, S. R., *Phys. Rev. E* **52**, 3045, 1995.

[196] Yu, M. *Plasma Phys.* **18**, 139, 1977.

[197] Zabusky, N. J. and Krushkal, M. D., *Phys. Rev. Lett.* **15**, 240, 1965.

[198] Zakharov, V. E. *Sov. Phys. JETP* **35**, 908, 1972.